Synthesis of Cationic Nanoparticles *via* Polymerisation-Induced Self-Assembly

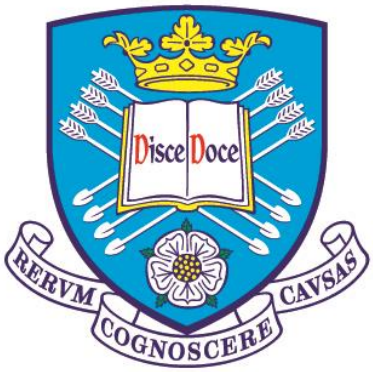

The University Of Sheffield.

Nicholas Jonathan William Penfold

Submitted to the University of Sheffield in partial fulfilment of the requirements for the degree of Doctor of Philosophy

University of Sheffield

Department of Chemistry

June 2017

Declaration

The work described in this thesis was undertaken at the University of Sheffield under the supervision of Professor Steven P. Armes between October 2013 and June 2017 and has not been submitted, either wholly or in part, for this or any other degree. All the work is the original work of the author, except where acknowledged.

Signature: _____

Nicholas Jonathan William Penfold

June 2017

Acknowledgements

I am extremely grateful to so many people for their support over not only the last four years, but for all of their help in the four years of my MChem degree preceding my postgraduate studies. First of all, I am indebted to my supervisor Prof. Steven Armes, FRS. Thank you for taking a punt on me and giving me the opportunity to undertake research in your group. Thank you for your meticulous proof reading and for the opportunity to attend numerous international and national conferences. Your dedication and attention to detail is unrivalled, while the scientific idea pipeline never stops flowing. This thesis is only a small testament to that. To the EPSRC and Procter and Gamble (P&G), thank you for providing financial support during my industrial CASE studentship. Thank you to my industrial contacts Dr. Pierre Verstraete and Dr. Johan Smets at P&G for their advice, ideas, informative scientific discussions and encouragement during our telecom meetings.

A huge thank you to all of the staff in the Chemistry department, whose help and advice has been gratefully appreciated over the years. In particular, a special thank you to the Pauline Boulding and Sharon Curl in the Common Room, to Denise Richards and Louise Brown-Leng in the finance department and to the Pete and Nick in Stores. The Chemistry department wouldn't be what it is today without your service. To Dr. Chris Hill and Dr. Svet Tzokov, thank you for all of your support with TEM imaging. Thank you to Dr. Yin Ning and Dr. Andy Parnell for your help with SEM and ellipsometry measurements.

It has been an absolute privilege to work with an amazing bunch of fun, helpful, supportive and friendly chemists in the Armes group. To Lizzy, thank you for introducing me into the world of worms. Thank you to Nick Warren, Mark Williams, Lee Fielding, Andrew Morse and Pengcheng Yang (Simon) for helping me to find my feet in the lab. Thank you to Kate Kirkham, Carlo Gonzato, Andreas Hanisch, Fiona Hatton, Dave Growney, Liam Ratcliffe, Joe Lovett, Matt Derry, Vicki Cunningham, Charlotte Mable, Amy Cockram, Matt Rymaruk, Sarah Byard and all of the past and present members of the Armes group for the great memories. Thank you to my summer student Marta Molina for all of your hard work.

Sport has been a key part of my university life. Thank you to everyone The Wednesday Cricket Club and Richmond Cricket Club for keeping my feet on the ground outside of the lab. I must thank everyone I have played football with including the numerous ChemSoc teams, Wednesday Pitch B guys, Sex Panthers, Armes Animals and last but not least the famous Bayer Neverlosen. It's an honour to call you gentlemen my friends and all of our European away days have been a blast.

I owe an enormous amount of gratitude and thanks to (soon to be Dr.) Lyndsey Benson. Thank you for all your support, advice and great friendship since 2009. I'm indebted to you for teaching me the art of storytelling and for always making time to listen to my woes. Your delicious bakes have kept me fuelled and I have had the best time travelling the world on our fun adventures home and abroad. To Will Clarke, James (Gwen) Holland and everyone else back home, thank you for your continued friendship since the TGS days and making it feel like I never left.

Last and by no means last, thank you to all of my family members, especially to Mum and Dad. No words will ever do justice to your generosity and how grateful I am for you unconditional support, love, advice and encouragement. I hope I have made you proud. This thesis is dedicated to you both.

Primary Publications

(1) N. J. W. Penfold, J. R. Lovett, N. J. Warren, P. Verstraete, J. Smets and S. P. Armes, 'pH-Responsive non-ionic diblock copolymers: protonation of a morpholine end-group induces an order-order transition,' *Polymer Chemistry*, **2016**, *7*, 79-88.

(2) N. J. W. Penfold, Y. Ning, P. Verstraete, J. Smets and S. P. Armes, 'Cross-linked cationic diblock copolymer worms are superflocculants for micrometer-sized silica particles,' *Chemical Science*, **2016**, *7*, 6894-6904

(3) N. J. W. Penfold, J. R. Lovett, N. J. Warren, P. Verstraete, J. Smets and S. P. Armes, 'Stimulus-responsive non-ionic diblock copolymers: protonation of a tertiary amine end-group induces vesicle-to-worm or vesicle-to-sphere transitions,' *Polymer Chemistry*, **2017**, *8*, 272-282.

(4) N. J. W. Penfold, A. J. Parnell, M. Molina, P. Verstraete, J. Smets and S. P. Armes, 'Layer-by-layer self-assembly of charged block copolymer worms onto planar surfaces', *manuscript submitted*

Secondary Publications

(5) Y. Ning, L. A. Fielding, K. E. B. Doncom, N. J. W. Penfold, A. N. Kulak, H. Matsuoka and S. P. Armes, 'Incorporating diblock copolymer nanoparticles into calcite crystals: do anionic carboxylate groups alone ensure efficient occlusion?,' *ACS Macro Letters*, **2016**, *5*, 311-315.

(6) M. Williams, N. J. W. Penfold, J. R. Lovett, N. J. Warren, C. W. I. Douglas, N. Doroshenko, P. Verstraete, J. Smets and S. P. Armes, 'Bespoke cationic nano-objects *via* RAFT aqueous dispersion polymerisation,' *Polymer Chemistry*, **2016**, *7*, 3864-3873.

(7) M. Williams, N. J. W. Penfold and S. P. Armes, 'Cationic and reactive primary amine-stabilised nanoparticles *via* RAFT aqueous dispersion polymerisation,' *Polymer Chemistry*, **2016**, *7*, 384-393.

(8) R. Deng, Y. Ning, E. R. Jones, V. J. Cunningham, N. J. W. Penfold and S. P. Armes, 'Stimulus-responsive block copolymer nano-objects and hydrogels *via* dynamic covalent chemistry,' *Polymer Chemistry*, **2017**, Advance Article, DOI: 10.1039/C7PY01242J.

Other Publications

(9) M. Semsarilar, N. J. W. Penfold, E. R. Jones and S. P. Armes, 'Semi-crystalline diblock copolymer nano-objects prepared *via* RAFT alcoholic dispersion polymerization of stearyl methacrylate,' *Polymer Chemistry*, **2015**, *6*, 1751-1757.

Conference Attendance

July 2014 *Poster Presentation* at Young Researchers Meeting, Durham (UK)

August 2015 *Oral Presentation* at 250th ACS National Meeting & Exposition, Boston (USA)

April 2016 *Poster Presentation* at Young Researchers Meeting, Liverpool (UK)

June 2016 *Oral Presentation* at 90th ACS Colloids & Surface Science Symposium, Boston (USA)

July 2016 *Poster Presentation* at The Polymer Conference, Warwick (UK)

April 2017 *Session Chair and Oral Presentations* at 253th ACS National Meeting & Exposition, San Francisco (USA)

May 2017 *Poster Presentation* at Advanced Polymers *via* Macromolecular Engineering, Ghent (Belgium)

June 2017 *Poster Presentation and Prize* at Young Researchers Meeting, Edinburgh (UK)

July 2017 *Oral Presentation* at UK Colloids 2017, Manchester (UK)

Abstract

Reversible addition-fragmentation chain transfer (RAFT) polymerisation has been utilised to prepare cationic block copolymer nanoparticles *via* polymerisation-induced self-assembly (PISA) in aqueous solution. In the first half of this thesis, a new morpholine-functionalised trithiocarbonate-based RAFT agent (MPETTC) was synthesised and used to prepare poly(glycerol monomethacrylate)-poly(2-hydroxypropyl methacrylate) ($PGMA_{50}$-$PHPMA_{140}$) diblock copolymer worm gels pH 7.0 – 7.5. Acidification of the morpholine end-groups resulted in a *reversible* worm-to-sphere morphological transition at pH 3, with concomitant degelation. The original gel strength was regained on returning to pH 7. In control experiments, pH-independent behaviour was observed for similar $PGMA_{58}$-$PHPMA_{160}$ worms prepared using an ester-functionalised RAFT agent.

This end-group protonation strategy for driving morphological transitions was extended by investigating the pH-responsive behaviour of morpholine-functionalised $PGMA_{43}$-$PHPMA_y$ *vesicles*. When the PHPMA DP_n is short (y = 190 or 200) an irreversible vesicle-to-worm morphological transition is observed. Moreover, the time scale for this transition is far longer (48 h) than that required for the corresponding worm-to-sphere transition (1 h). No morphology transition at all occurs when the PHPMA DP_n is too long (y = 220 or 230). Nevertheless, a vesicle-to-sphere transition was observed when cooling the acidified vesicular dispersions to 4 °C. However, the pH-responsive behaviour of PGMA-PHPMA worms and vesicles is suppressed in the presence of either excess acid (pH 1) or salt (100 mM KCl) as a result of charge screening effects.

In the second half of this thesis, a series of linear cationic diblock copolymer nanoparticles are prepared by the RAFT aqueous dispersion polymerisation of HPMA using a binary mixture of non-ionic poly(ethylene oxide) (PEO_{113}) and cationic ([2-(methacryloyloxy)ethyl] trimethylammonium chloride) ($PQDMA_{125}$) macromolecular chain transfer agents. A detailed phase diagram was constructed to determine the maximum amount of $PQDMA_{125}$ stabiliser block that could be incorporated while still allowing access to a pure worm phase. Aqueous electrophoresis studies indicated that pH-independent zeta potentials of +35 mV could be achieved for these worms. Core cross-linked worms were prepared *via* statistical copolymerisation of glycidyl methacrylate (GlyMA) with HPMA using a slightly modified PISA formulation, followed by reacting the epoxy groups of the GlyMA residues located within the worm cores with 3-aminopropyl triethoxysilane (APTES). Importantly, these cross-linked cationic worms are shown to be much more effective bridging flocculants for 1.0 μm silica particles at pH 9 than the corresponding linear cationic worms *via* laser diffraction and scanning electron microscopy (SEM) studies. Furthermore, these cross-linked worms are shown to be superflocculants because they outperform various commercial high molecular weight water-soluble polymers. It was found that flocculation was insensitive to the order of addition (i.e. addition of worms to silica spheres or *vice versa*). In addition, flocculation was observed when increasing the silica particle diameter to 4 μm, as judged by laser diffraction.

Finally, oppositely-charged cross-linked polyelectrolytic worms were synthesised and then successively deposited onto a planar surface *via* a layer-by-layer protocol. These worms mimic the rigid rod behaviour of water-soluble polyelectrolyte chains in salt-free solution. Furthermore, the dimensions of these worms allow direct imaging by SEM. The formation of worm multilayers was confirmed by SEM and ellipsometry measurements. Furthermore, surface charge reversal was confirmed *via* surface zeta potential measurements. The kinetics of electrostatic adsorption of these worms was shown to be extremely fast at 20 °C.

Common Abbreviations

AIBA	2,2′-azobis(2-methylpropionamidine) dihydrochloride
APTES	(3-aminopropyl)triethoxysilane
A_s	specific surface area
ATRP	atom transfer radical polymerisation
BzMA	benzyl methacrylate
CGT	critical gelation temperature
CTA	chain transfer agent
CTAB	cetyltrimethylammonium bromide
D	translational diffusion coefficient
$D_{[4/3]}$	volume-average diameter
DCC	*N*,*N*'-dicyclohexylcarbodiimide
DLS	dynamic light scattering
DMAP	4-dimethylaminopyridine
DMF	dimethylforamide
DP	degree of polymerisation
FRP	free radical polymerisation
G′	storage modulus
G″	loss modulus
GlyMA	glycidyl methacrylate
GMA	glycerol monomethacrylate
GPC	gel permeation chromatography
HPMA	2-hydroxypropyl methacrylate
KSPMA	potassium 3-sulfopropyl methacrylate
LAM	less activated monomer
LAP	living anionic polymerisation
L-b-L	layer-by-layer

Abbreviations

LCST	lower critical solution temperature
macro-CTA	macromolecular chain transfer agent
MAM	more activated monomer
M_n	number-average molecular weight
MPTES	(3-mercaptopropyl)trimethoxysilane
M_w	weight-average molecular weight
NMP	nitroxide-mediated polymerisation
NMR	nuclear magnetic resonance
P	packing parameter
PA	poly(acrylic acid)
PDADMAC	poly(diallyldimethylammonium chloride)
PDI	polydispersity index
PEM	polyelectrolyte multilayer
PEO	poly(ethylene oxide)
PETTC	4-cyano-4-(2-phenylethane sulfanyl thiocarbonyl) sulfanylpentanoic acid
PISA	polymerisation-induced self-assembly
PMMA	poly(methyl methacrylate)
$P_n^{\bullet}$	propagating polymer radical
PNVP	poly(*n*-vinylpyrrolidone)
PRE	persistent radical effect
QDMA	2-methacryloyloxyethyl trimethylammonium chloride
RAFT	reversible addition-fragmentation chain transfer
RDRP	reversible deactivation radical polymerisation
SEM	scanning electron microscopy
TEM	transmission electron microscopy
THF	tetrahydrofuran
UCST	upper critical solution temperature
VA-044	2,2'-azobis[2-(2-imidazolin-2-yl)propane] dihydrochloride

Table of Contents

Chapter 1

Introduction

1.1 General Concepts in Polymer Science

Polymers are long chain molecules made from the multiple repetition of chemically-linked monomer repeat units.[1, 2] The essential prerequisite for a small molecule to be a monomer is the possession of two or more bonding sites, to enable linking to other monomer units.[2] Many everyday items such as plastic bags, Teflon® non-stick frying pans, Gore-Tex® waterproof clothing and the new British £5 note compromise various types of polymers. Life itself would not be possible without polymers. Deoxyribonucleic acid (DNA), proteins and carbohydrates such as collagen and polysaccharides are all important examples of naturally occurring polymers.

Carothers categorised polymers into two types: addition and condensation polymers. The former only adds monomer units to a growing polymer chain while the latter also releases a small molecule, such as water on addition of a monomer unit.[3] However, these classifications lead to some difficulties regarding polymer nomenclature. Flory introduced the new terms step and chain polymerisation to address this confusion, instead classifying polymers in terms of their polymerisation mechanism.[4] Step polymerisation involves the step-wise reaction between monomers to initially form dimers. These dimers react further with monomer to form trimers, or with one another to form tetramers so on and so forth. On the other hand, chain polymerisation proceeds *via* chain reaction, with multiple monomer units being added to form a chain. Free radical and ionic polymerisations proceed *via* the latter mechanism, which is relevant to this thesis.

Chain polymerisation results in a distribution in the average number of monomer units per polymer chain. Thus, polymers do not have a precise molecular weight but rather have a molecular weight distribution (MWD), which can be described using different statistical

averages such as the number-average molecular weight (M_n) and weight-average molecular weight (M_w), see equations 1.1 and 1.2 below.

$$\boldsymbol{M_n = \frac{\Sigma n_i M_i}{\Sigma n_i}} \qquad \textbf{1.1}$$

$$\boldsymbol{M_w = \frac{\Sigma n_i M_i^2}{\Sigma n_i M_i}} \qquad \textbf{1.2}$$

$$\textbf{Đ or PDI} = \boldsymbol{\frac{M_w}{M_n}} \qquad \textbf{1.3}$$

Here, n_i is the number of chains consisting of i units and M_i is the molar mass of these chains. As recommended by IUPAC in 2009,[5] the breadth of the MWD is now termed the molar-mass dispersity, Đ which is given by the ratio of M_w to M_n as shown in equation 1.3. It should be noted that the term polydispersity index (PDI) has been historically used in the literature. To avoid any discrepancy in this thesis, M_w / M_n will be used instead of Đ. If every single polymer chain in a sample had an identical molecular weight then the M_w/M_n would be equal to unity and the polymer is said to be monodisperse.[6] Such M_w/M_n values remain the holy grail for synthetic polymer chemists, who are yet to achieve the monodisperse nature of proteins. Polymers are considered to have a broad MWD if their M_w/M_n is greater than 2.0 but a narrow MWD if their M_w/M_n is less than 1.5.[7]

1.2 Polymerisation Techniques

1.2.1 Free Radical Polymerisation (FRP)

Free radical polymerisation (FRP) is a long-established method of chain polymerisation, which has gained fame through its high versatility and ability to polymerise a wide range of functional vinyl monomers. Furthermore, FRP is tolerant to both protic and aprotic solvents and occurs *via* three main steps: initiation, propagation and termination, with the mechanism shown in Figure 1.1. Chain transfer mechanisms are also depicted.

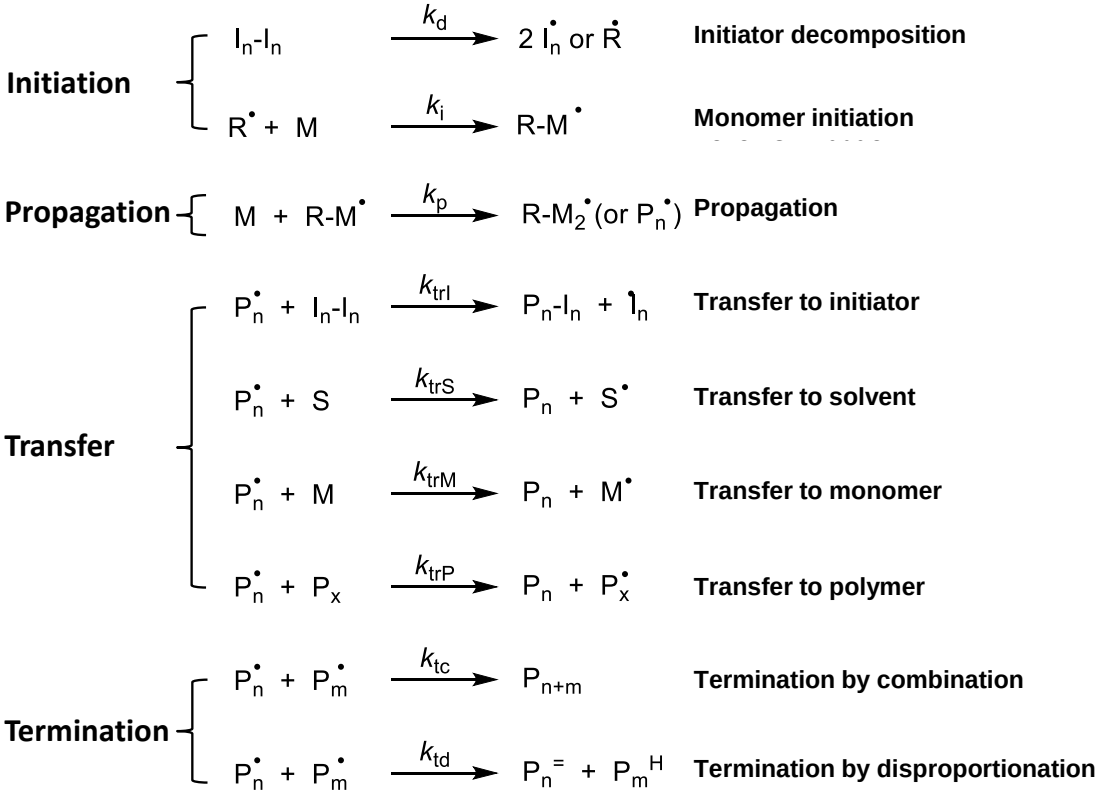

Figure 1.1 Reaction mechanism and rate constants for free radical polymerisation showing the three fundamental steps: initiation, propagation and termination. Radical transfer side reactions are also shown. I_n-I_n = initiator molecule, $I_n^{\bullet}$ = initiator radical, M = monomer, $P^{\bullet}$ = propagating polymer radical, P = dead polymer and S = solvent.

Firstly, a suitable initiator is selected for the monomer to be polymerised. Effective free radical initiators undergo decomposition *via* homolytic fission to form two radicals by exposure to heat, electromagnetic radiation or *via* redox reactions. Solely thermal azo initiators have been used in this thesis so only these types of radical initiators will be discussed. Polymerisation temperatures are normally selected to be approximately equal to the 10 h half-life temperature of the initiator to ensure a constant supply of free radicals. Homolytic cleavage of a symmetrical initiator, I_n-I_n, occurs with a rate constant, k_d, to form two identical initiator radicals, $I^{\bullet}$, that react with monomer to form an active radical centres, R-$M^{\bullet}$ or $P_n^{\bullet}$. One important factor to consider is the initiator efficiency, *f*, which is the ratio of propagating polymer radicals to primary radicals. This ratio equals unity when each initiator radical reacts to produce two propagating chains. However, in practice *f* is rarely equal to unity due to various side reactions. Radical recombination is possible both inside and outside the solvent cage, but predominately occurs inside the solvent cage because of very low relative monomer concentration and also the slow diffusion of $I_n^{\bullet}$ outside the solvent cage. Values of *f* typically range between 0.3 and 0.8.[2] Generally, k_d values ($\approx 10^{-5}$ M^{-1} s^{-1}) are much lower than k_i values ($\approx 10^{4}$ M^{-1} s^{-1}) so the overall rate of initiation, R_i, can be simplified as described in equation 1.4. A numerical factor of 2 is introduced because two polymer radicals can be formed from a single initiator molecule.

$$\boldsymbol{R_i = \frac{-d[I_n - I_n]}{dt} = 2fk_d[I_n - I_n]} \qquad \textbf{1.4}$$

Once the radical active centre, $P_n^{\bullet}$, is formed, propagation rapidly occurs *via* sequential monomer addition. The propagation rate equation is shown in equation 1.5. Typical values of k_p range from 10^2 to 10^4 M^{-1} s^{-1} depending on the monomer types and are much greater than k_d.[8] Throughout the reaction, radical transfer to unreacted initiator radicals, solvent, monomer or polymer can occur (Figure 1.1).

$$R_p = \frac{-d[M]}{dt} = k_p[P_n^{\bullet}][M] \qquad \textbf{1.5}$$

These reactions result in transfer (not annihilation) of the radical, resulting in an unreactive, non-propagating polymer chain. However, the activation energy for transfer reactions in radical polymerisations is higher compared to propagation, so the former are usually only important at high temperatures. Such transfer reactions result in MWD broadening by branching.[2] In contrast, the annihilation of radicals is achieved by termination reactions. Such diffusion-controlled bimolecular processes can occur *via* two mechanisms: combination and disproportionation. The former involves two propagating polymer radicals reacting to form a non-propagating polymer chain with a molar mass equal to the sum of the two individual chains. This mechanism is typical for styrene and acrylic monomers. In contrast, termination by disproportionation occurs when a hydrogen atom is abstracted from a second propagating chain to yield two non-propagating polymer chains containing unsaturated and saturated chain ends. Methacrylates undergo this mechanism due to steric crowding of tertiary radicals. Termination is a very fast, diffusion-controlled process with k_t values of approximately 10^8 M^{-1} s^{-1}. The rate of termination is the sum of the rate of termination by combination, k_{tc}, and that of disproportionation, k_{td}, as shown in equation 1.6.

$$R_t = k_t = 2(k_{tc} + k_{td})[P_n^{\bullet}]^2 = 2k_t[P_n^{\bullet}]^2 \qquad \textbf{1.6}$$

The overall rate of polymerisation depends on the polymer radical concentration, $[P_n^{\bullet}]$. However, in practice it is difficult to measure this quantity. Thus, the steady-state approximation is applied such that the rates of initiation and termination are assumed to be equal, as shown in equation 1.7.

$$2fk_d[I_n - I_n] = 2k_t[P_n^{\bullet}]^2 \qquad \textbf{1.7}$$

To a good approximation, the rate of polymerisation is assumed to be equal to the rate of propagation. Rearrangement of equation 1.7 to make $[P_n^{\bullet}]$ the subject, followed by insertion into the rate equation for propagation (equation 1.5) results in a rate equation for polymerisation (equation 1.8).

$$R_{polymerisation} = k_p[M]\sqrt{\frac{fk_d[I_n - I_n]}{k_t}} \qquad \textbf{1.8}$$

Thus, the rate of FRP is proportional to [M] and $[I_n\text{-}I_n]^{1/2}$ but only if *f* is high. For low initiator efficiencies, *f* becomes a function of M and the rate is proportional to $[M]^{3/2}$.[2] However, increasing both the monomer and initiator concentration increases the rate of polymerisation. Two important parameters can be extracted from this kinetic analysis: the kinetic chain length (D_k) and the number average degree of polymerisation (DP_n). D_k is the average number of monomer units consumed per active radical centre and is given by the ratio of the rate of propagation to the rate of termination, calculated using equation 1.9.

$$D_k = \frac{R_p}{R_t} = \frac{k_p[M]}{2k_t[P_n^{\bullet}]^2} = \frac{k_p[M]}{2\sqrt{fk_dk_t[I_n - I_n]}} \qquad \textbf{1.9}$$

Analysis of equation 1.9 shows that D_k is proportional to [M] and $[I_n\text{-}I_n]^{-1/2}$. Therefore, large D_k values (and hence high molecular weights) can be obtained by ensuring high monomer concentration and/or low initiator concentrations. Termination is prevalent in FRP and dramatically affects DP_n. For example, if termination occurs exclusively by combination then $DP_n = 2D_k$, but if termination occurs exclusively by disproportionation then $DP_n = D_k$.

FRP is one of the most popular polymerisation technique used for the industrial manufacture of vinyl polymers. This is because it offers remarkable versatility for polymerising a wide range of functional monomers. However, as has been shown, the lack of control over molecular weight, DP_n and MWD means that FRP is unsuitable for preparing well-defined, functional diblock copolymers. Polymerisation techniques that allow access to such polymers are now discussed.

1.2.2 Living Anionic Polymerisation (LAP)

While FRP is synthetically undemanding, its various termination and radical transfer side reactions prevent the production of polymers with narrow MWDs. In principle, preventing intrinsic termination and extending the lifetime of each propagating chain should result in polymers with narrower dispersities. Such polymerisations are said to be living because if monomer is continually introduced then the polymerisation proceeds indefinitely. Living polymerisations are characterised by: rapid initiation, a linear evolution of polymer molecular weight vs monomer conversion and predetermined molecular weights. Moreover, quantitative chain-end functionalisation enables polymeric products to be reactivated for further chain extension and while low M_w/M_n values approach those of a Poisson distribution.[9-11]

In 1956 Szwarc and co-workers used a sodium-naphthalene initiator to polymerise styrene in dry tetrahydrofuran: this was the first report of living anionic polymerisation (LAP).[12, 13] LAP is a chain polymerisation technique whereby electrostatic repulsion of the anionic reactive centres prevents intrinsic termination. Suitable monomers have electron-withdrawing substituents and no protic functionality, thus a major restriction of LAP is the relative lack of appropriate building blocks. Only aliphatic or aromatic hydrocarbons and THF or dioxane are suitable solvents; halogenated solvents are unsuitable because they undergo nucleophilic substitution reactions with carbanions.[1] However, rigorous purification of all components is required as any protic impurities result in the premature termination of the polymerisation.

Initiator type can influence the type of propagating anion. For example, an *n*-butyllithium initiator produces a monoanion whereas initiators that undergo electron transfer (such as sodium naphthalene) generate bifunctional, two-ended anions.[1] As initiators are already in their anionic form, initiation occurs faster than to any propagation ($k_i >> k_p$). Consequently, all polymer chains start to grow simultaneously at the same rate, and the concentration of active centres is constant, leading to a linear evolution of molecular weight with conversion (Figure 1.2) and relatively narrow MWDs.

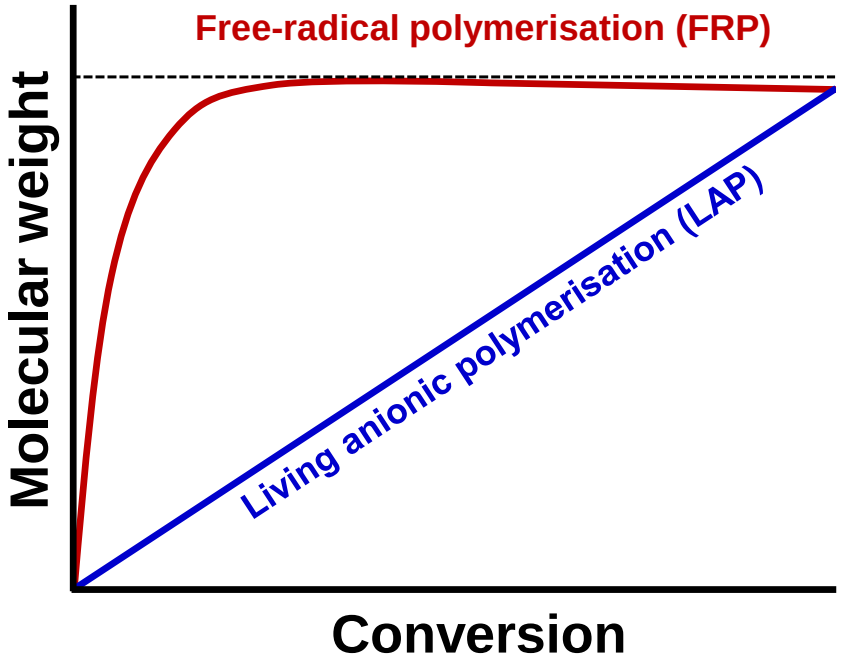

Figure 1.2 Evolution of polymer molecular weight with monomer conversion for a typical free radical polymerisation (FRP, red line) and living anionic polymerisations (LAP, blue line).

In contrast high molecular weights are obtained even at low conversions in FRP. Hence, propagation is the rate-limiting step in LAP and therefore the rate of polymerisation is equal to the rate of propagation. This gives equation 1.10, where $[P_n^-]$ is the concentration of propagating

anionic chains. The integrated rate equation is shown in equation 1.11, where $[M]_o$ is the initial monomer concentration at zero time.

$$R_p = \frac{-d[M]}{dt} = k_p[P_n^-][M] \quad \textbf{1.10}$$

$$[M] = [M]_o e^{(-k_p[P_n^-]t)} \quad \textbf{1.11}$$

Therefore, D_k can be calculated at any given time using equation 1.12. Assuming there is no termination during the lifetime of the polymerisation, the DP_n (after full monomer conversion) can be calculated using equation 1.13.

$$D_k = \frac{[M]_o - [M]}{[I_n - I_n]} \quad \textbf{1.12}$$

$$DP_n = \frac{[M]_o}{[I_n - I_n]} \quad \textbf{1.13}$$

In LAP, the target DP_n can be adjusted by simply altering the monomer to initiator molar ratio. Termination is achieved by adding a terminating reagent, typical an acid, alcohol or water to give the desired polymer end-group. Other living polymerisation techniques are also known such as living cationic polymerisation,[14, 15] group transfer polymerisation[16] and living ring-opening metathesis polymerisation.[17-19] However, such methods lie outside the scope of this thesis and as such, will not be discussed further. In addition, recent advances in polymer synthesis have led to the advent of so-called pseudo-living radical polymerisation techniques. These methods combine the versatility of FRP with the control offered by LAP and will now be discussed in detail.

1.2.3 Reversible Deactivation Radical Polymerisation (RDRP)

Over the past few decades, new methods of radical-based polymerisation have become extremely popular within the synthetic polymer chemistry community. These techniques have become known as 'controlled/living polymerisation.' However, in 2010 IUPAC recommended use of the term 'reversible deactivation radical polymerisation' (RDRP), which is defined[20] as a "chain polymerisation, propagated by radicals that are deactivated reversibly, bringing them into active-dormant equilibria of which there might be more than one." The extent of RDRP research has dramatically increased over the last decade as it combines the advantages of LAP and FRP, while minimising their inherent disadvantages. LAP allows the synthesis of well-defined homopolymers and diblock copolymers with narrow MWDs and predetermined molecular weights, but requires the rigorous removal of protic impurities and cannot be used to polymerise most functional monomers. On the contrary, FRP is compatible with many functional vinyl monomers and solvents. Moreover, it can be used under various physical conditions such as suspension, solution, emulsion and dispersion polymerisation conditions, but termination is prevalent. The RDRP methods discussed in this section allow access to polymers with varying degrees of complexity in their architecture (Figure 1.3).

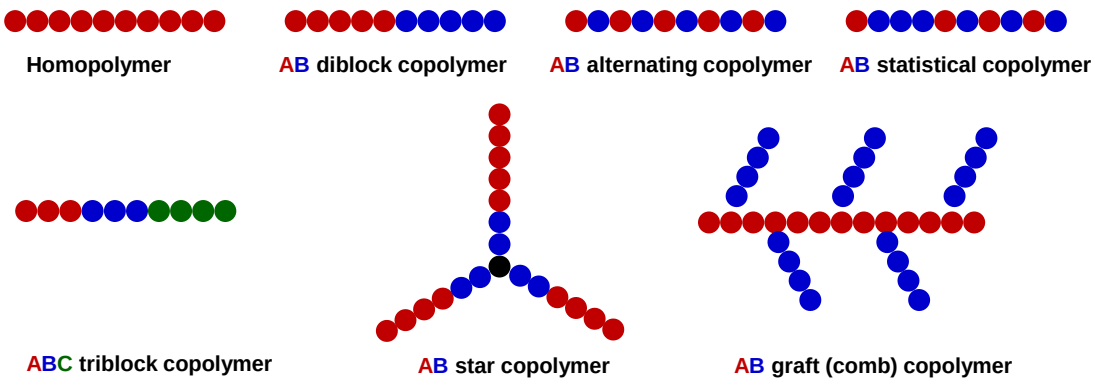

Figure 1.3 Cartoon of the some of the various types of polymer architectures accessible *via* RDRP techniques.[21]

The simplest architecture is a homopolymer, comprised of a single type of repeat unit. AB diblock copolymers comprise two distinct sections that are covalently joined together. As shown in Figure 1.3, more complex architectures such as alternating, statistical, multi-block, star and graft copolymers are accessible.

All RDRP methods rely on the rapid exchange of propagating polymer radicals between active and dormant states, which is achieved by the addition of a suitable moderating species.[22] Two types of equilibria exist: polymer radicals are involved in either a reversible deactivation/activation[23] (Scheme 1.1) or a reversible transfer (Scheme 1.2) process.[24]

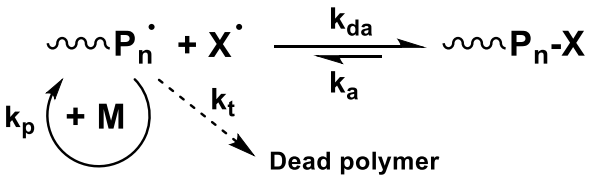

Scheme 1.1 Reversible deactivation/activation of propagating polymer radicals with a stable radical species, $X^{\bullet}$.[22]

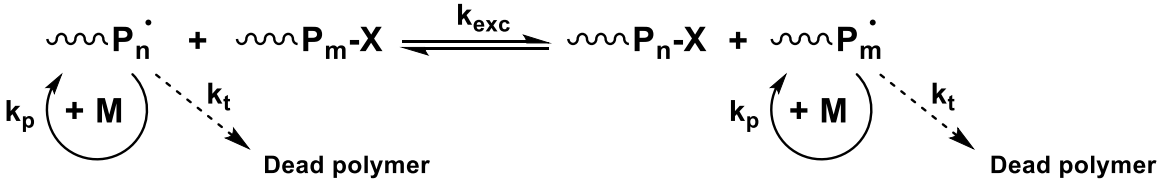

Scheme 1.2 Reversible transfer mechanism of propagating polymer radical chains.[22]

Both mechanisms reduce the instantaneous concentration of propagating polymer radicals, $[P_n^{\bullet}]$, and hence suppresses the rate of termination relative to that of propagation. Reversible deactivation/activation is the fundamental concept underpinning two popular RDRP techniques: nitroxide-mediated polymerisation (NMP) and atom transfer radical-polymerisation (ATRP). These two polymerisation techniques are based on the persistent radical effect (PRE).[25] A

propagating polymer radical is formed and reacts with a species, $X^{\bullet}$, with a rate constant of k_{da}. $X^{\bullet}$ is a persistent radical, such as a nitroxide species, which exhibits enhanced stability *via* steric hindrance.[26] Importantly, such species can only react with propagating radicals and not with themselves. Activation of the dormant species occurs with a rate constant k_a to yield the polymer radical species which is capable of both propagation and termination. It is vital that $k_{da} > k_a$ to ensure that the polymer chains remain predominantly in their dormant state and hence reduce $[P_n^{\bullet}]$. When termination occurs, there is an irreversible accumulation of $X^{\bullet}$; this shifts the equilibrium to the right, thus reducing the probability of termination. Conversely, reversible (degenerative) transfer is not based on PRE.[22] Instead, an initiator is required to form propagating polymer radicals. Therefore, the kinetics of reversible transfer are similar to FRP and initiation is the rate-determining step. Polymerisation is moderated by an additional species, termed a transfer agent that enables rapid rates of exchange (k_{exc}). Typically, the concentration of the transfer agent is greater compared to that of the initiator. Reversible addition-fragmentation chain transfer (RAFT) polymerisation is based on this method and is discussed in more detail in section 1.2.3.3.

1.2.3.1 Nitroxide-Mediated Polymerisation (NMP)

NMP, sometimes known as stable free radical polymerisation, was developed in the early 1980s at the Commonwealth Scientific and Industrial Research Organisation (CSIRO).[27] It can be argued that NMP is the most enviromentally-friendly RDRP technique as it does not require the use of a transition metal catalyst (ATRP) or malodorous sulphur compounds (RAFT). NMP proceeds *via* a reversible deactivation/activation mechanism, and as such, relies on the PRE. Initiation can occur by either addition[28] or by *in situ* formation[29] of alkoxyamines. The popularity of NMP was boosted by seminal work by Georges *et al.*,[29] who prepared polystyrene with a relatively narrow MWD using the 2,2,6,6-tetramethylpiperidinyl-1-oxy (TEMPO). Dynamic exhange of nitroxides between propagating polymer radicals is essential to control the

polymerisation and ensure pseudo-living character (Scheme 1.3). NMP is a versatile polymerisation method that has been successfully used under homogeneous (e.g. bulk or soluion), emulsion and miniemulsion conditions.[30] Like FRP, functional monomer classes (styrene, dienes, acrylates and acrylamides), functional groups and protic solvents are tolerated.[31]

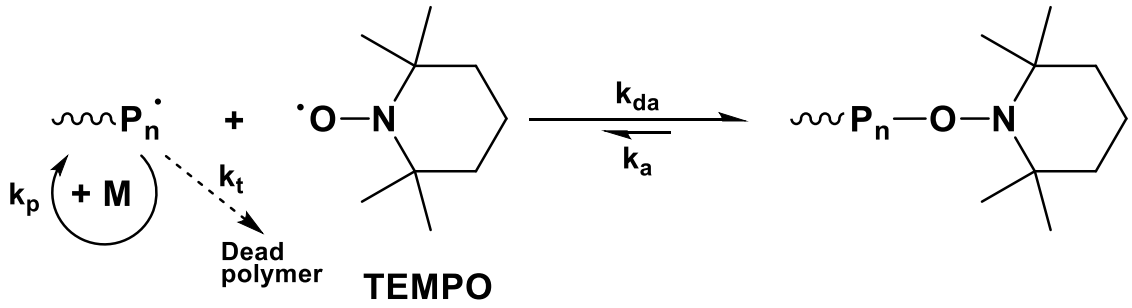

Scheme 1.3 Main deactivation/activation equilibrium mechanism for nitroxide-mediated polymerisation (NMP) using 2,2,6,6-tetramethyl-l-piperidinylox (TEMPO) as the stable radical species.[32]

Unfortunately TEMPO forms a relatively strong C-O (P_n-O) bond. Hence its equilibrium constant K_{eq} (where $K_{eq} = k_a / k_{da}$) is relatively low so elevated temperatues (120 °C) are required for the polymerisation of monomers such as styrene. Nevertheless, reduction of the C-O bond strength can be achieved by adjusting the electronic and steric nature of the nitroxide substituents, resulting in polymerisation temperatures below 100 °C.[33] However, a significant drawback of NMP is its incompatibility with methacrylic monomers. Steric stabilisation of the tertiary radical adduct results in very slow deactivation (k_{da}) and therefore prevents well-controlled polymerisations, thereby increasing the probability of termination by disproportionation. Although statistical copolymerisation with styrene can allieviate this problem,[34] the controlled homopolymerisation of methacrylates remains problematic.

1.2.3.2 Atom Transfer Radical Polymerisation (ATRP)

A new method of RDRP that is suitable for methacrylic monomers was reported by Sawamoto and Matyjaszewski in 1995, named ATRP.[35, 36] It is suitable for a wide range of monomers such as (meth)acrylates, (meth)acrylamides, vinylpyridines and substituted styrenes. Its versatility under various reaction conditions has been demonstrated by its successful application for bulk, solution, (mini)emulsion, suspension, dispersion and precipitation polymerisations.[37] ATRP requires selection of a suitable alkyl halide initiator (RX) and transition metal catalyst (Mt^n-L). Cleavage of an R-X bond by the transition metal catalyst liberates an alkyl radical, $R^{\bullet}$ which reacts with monomer to form propagating polymer radicals ($P_n^{\bullet}$). This results in a halide-based transition metal complex with a higher oxidation state (X-Mt^{n+1}-L). Thus, ATRP requires reducing conditions and is not tolerant of oxidising species such as oxygen. $P_n^{\bullet}$ can be reversibly deactivated (k_{da}) to form a dormant, halide-capped chain. This allows equilibrium between the active propagating radicals and the dormant halide-capped species to be established (Scheme 1.4).

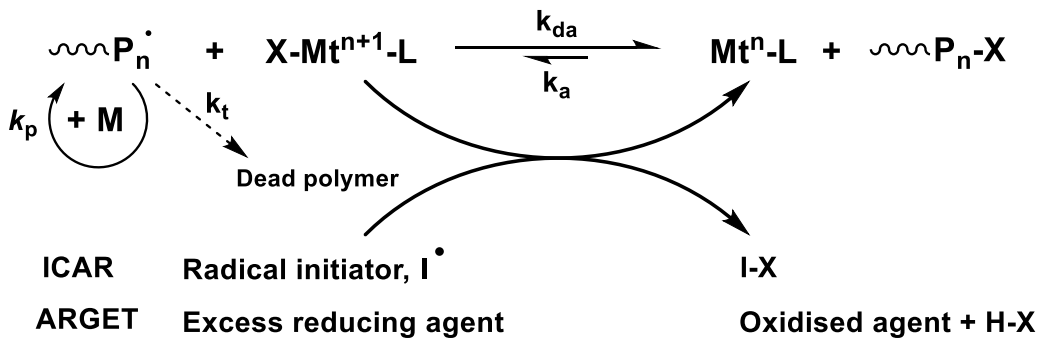

Scheme 1.4 Reversible deactivation/activation equilibrium obtained for a transition metal-mediated ATRP synthesis. Transition metal regeneration can be achieved by initiator for continuous activation regeneration (ICAR) or activators regenerated by electron transfer (ARGET).[22, 37]

The DP_n of polymers prepared using ATRP is determined by the monomer initiation molar ratio (see equation 1.13), but is independent of the transition metal catalyst concentration. The rate of polymerisation by ATRP is given by equation 1.14. This equation must lie in favour of the halide-capped species to provide pseudo-living character. For example, k_{da} can be optimised to be up to 10^7 times greater than k_a for the ATRP synthesis of polystyrene.[38, 39]

$$\boldsymbol{R_p = \frac{-d[M]}{dt} = k_p[\mathrm{M}][P_n^{\bullet}] = k_p[M]\left(\frac{k_a[PX][Mt^nL]}{k_{da}[XMt^{n+1}L]}\right)} \qquad \textbf{1.14}$$

Initiators are activated alkyl halides with either α-phenyl, vinyl, α-carbonyl or cyano groups to ensure a weak C-X bond. The ATRP equilibrium constant K_{ATRP} (where $K_{ATRP} = k_a / k_{da}$) is dictated by selection of the monomer type and the RX initiator. Hence the electronic and steric properties of the transition metal catalyst must be optimised for efficient polymerisation of a given monomer. ATRP can be performed using many different transition metals including titanium,[40] rhodium,[41] iron[42, 43] and nickel.[44] Undoubtedly the most efficient transition metal is copper, as demonstrated by its successful application for polymerising a wide range of monomers under various conditions.[38, 45] Ligands are designed to ensure high solvent solubility for the transition metal catalyst and to moderate the relative deactivation/activation rates. The most versatile transition metal compounds for ATRP are copper complexes with polydentate, nitrogen-containing ligands.[46] Copper does not form complexes with polar monomers and hydrogen abstraction is disfavoured, while nitrogen-rich ligands promote solubility and moderate catalyst activity.

A significant disadvantage of conventional ATRP is that termination results in the build-up of the oxidised transition metal catalyst, capable of significantly reducing the polymerisation rate. Two methods have been devised to combat this: activators regenerated by electron transfer

(ARGET)[47] and initiator for continuous activation regeneration (ICAR).[48] In ARGET, the transition metal catalyst is added to the reaction mixture in its oxidised state along with excess reducing agent, such as tin(II) 2-ethylhexanoate or ascorbic acid, which acts to reduce $XMt^{n+1}L$ to $Mt^{n}L$. ICAR is conceptually similar to ARGET, but the reducing agent is replaced by a radical initiator such as azobisisobutyronitrile (AIBN), see (Scheme 1.4). Given the long half-lives of these thermal initiators, only rather small quantities are required. ATRP has been developed further by the advent of electrochemically-induced ATRP (eATRP) which uses electrons, rather than additional reagents, as the reducing agent.[49]

These techniques allow for a significant reduction in the quantity of transition metal catalyst required for ATRP, resulting in environmental and economic benefits.[50, 51] However, the main drawback of ATRP remains is the high cost associated with its transition metal catalyst. Furthermore, these catalysts can be difficult to remove from the reaction solution. Hence, for the aforementioned reasons ATRP, was not employed as the RDRP technique within this thesis.

1.2.3.3 Reversible Addition-Fragmentation chain Transfer Polymerisation (RAFT)

RAFT polymerisation was first reported by Chiefari *et al.* in 1998.[52] RAFT is fundamentally based on the degenerative chain transfer mechanism and does not rely on the PRE. RAFT requires an external radical source to start the polymerisation. Typical initiators required for RAFT polymerisations are those used in FRP. A RAFT polymerisation formulation is identical to FRP but with the addition of a chain transfer agent (or CTA), commonly referred to as a RAFT agent. RAFT agent chemical structures are discussed later, but the generic structure is shown in Scheme 1.5 as species (1), where atoms X and A may or may not be identical (typically X = S and A = S, N or O).

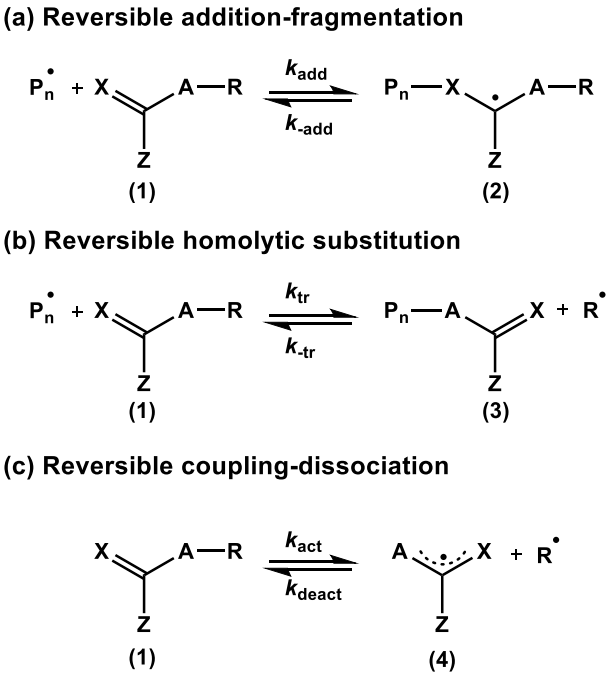

Scheme 1.5 Three mechanisms postulated to confer pseudo-living character in RAFT polymerisations: (a) reversible addition-fragmentation, (b) reversible homolytic substitution and (c) reversible coupling-dissociation. X and A represent different atoms, where X = S and A = S, O or N.[53]

Three mechanisms were initially considered to explain how RAFT agents reduce the propagating polymer radical concentration and hence confer control over the polymerisation: (a) reversible addition-fragmentation, (b) reversible homolytic substitution and (c) reversible coupling-dissociation (Scheme 1.5).

In the case of reversible addition-fragmentation (Scheme 1.5a), the activity of the C=X double bond in structure (1) is moderated by Z and A-R to enable polymer radical addition. The Z group provides stability to the radical adduct (2) while, R is a poor leaving group. Therefore, the RAFT agent is attached to the polymer chains agent only *via* X and never *via* atom A. It has been reported by Barner-Kowollik and co-workers that certain thioketones (Z and A-R = alkyl or aryl; X = sulphur) can exert control over the polymerisation of styrene[54] or *n*-butyl acrylate[55, 56] *via* this mechanism. The second postulated mechanism of reversible homolytic substitution is

shown in Scheme 1.5b. In this case, the propagating polymer radicals react with the weak A-R bond of species (1) to give species (3), releasing the R$^{\bullet}$ radical. Hence this is known as a chain transfer reaction. In this case, the polymer chain is always attached to atom A rather than atom X.

Frequently A and X are identical sulphur atoms, which makes it difficult to establish if this mechanism is prevalent. Iodine transfer polymerisation of styrene (in the presence of perfluorohexyl iodide)[57] and methyl acrylate (in the presence of iodine)[58] proceed *via* this mechanism. Reversible coupling-dissociation was the third and final mechanism considered (Scheme 1.5c). Homolytic cleavage of the weak A-R single bond occurs without any addition of external radicals, thus liberating R$^{\bullet}$ and species (4). However, most common RAFT agents are thermally stable at temperatures usually required for RAFT polymerisations ($\leq$ 150 °C) so this mechanism was discounted. While these three mechanisms cannot be completely disregarded, the volume of experimental and theoretical evidence suggests that addition-fragmentation chain transfer (Scheme 1.5a) is the dominant mechanism in controlling RAFT polymerisations.[53]

The overall RAFT mechanism that is widely accepted in the literature can be divided into five main stages: initiation, reversible chain transfer, reinitiation, chain equilibration/propagation and termination (Scheme 1.6)[59, 60] Like FRP, homolytic cleavage of an initiator leads to formation of propagating polymer radicals, $P_n^{\bullet}$. Moreover, $P_n^{\bullet}$ can react with the CTA species (5) by reversible chain transfer. This is known as pre-equilibrium step. For successful RAFT polymerisations, β-scission of species (6) must occur with a rate constant k_{β} to release the R$^{\bullet}$ and hence cap the propagating polymer radicals, species (7). The R$^{\bullet}$ species must be at least as a good a leaving group as that of $P_n^{\bullet}$ for efficient fragmentation, which is driven by a weak S-R bond.

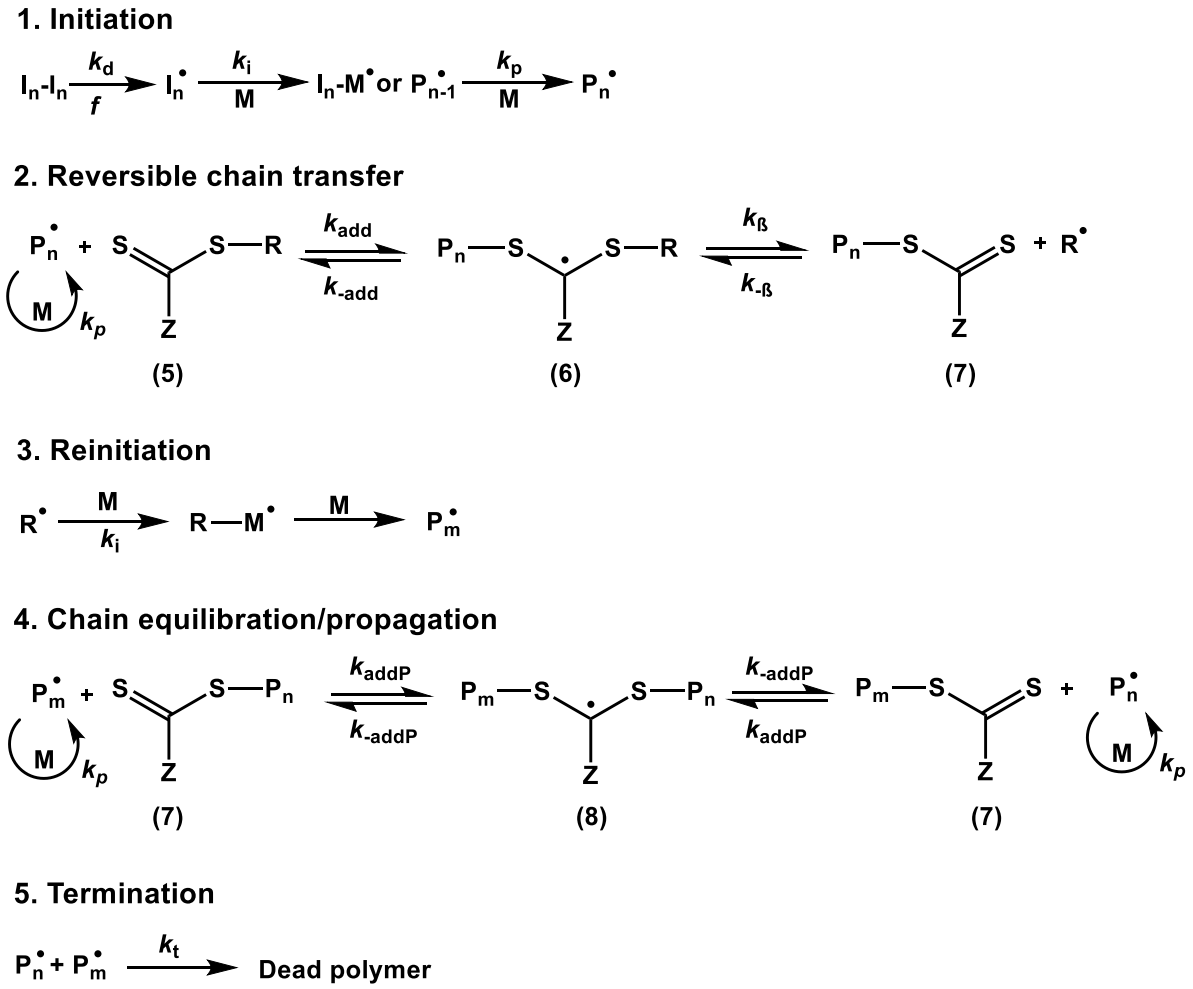

Scheme 1.6 The five main stages of RAFT polymerisation: initiation, reversible chain transfer, reinitiation, chain equilibration/propagation and termination.[61]

Therefore, k_{add} must be high for the formation of radical adduct (6), which must then fragment quickly ($k_{\beta} >> k_{-add}$)[62] If fragmentation is slow then species (6) is more likely to undergo chain transfer or irreversible radical-radical termination reactions, resulting in retardation. Furthermore, $R^{\bullet}$ must be able to reinitiate monomer (so $k_i > k_p$) creating another propagating polymer radical chain $P_m^{\bullet}$ in the third step known as reinitiation. These steps favour formation of the dormant, capped species (7). Chain equilibration/propagation (also referred to as the main equilibrium) is the critical step in the RAFT mechanism. Here, rapid and reversible transfer occurs between two propagating polymer radicals ($P_n^{\bullet}$ and $P_m^{\bullet}$) in their active and dormant states

occurs. This allows equal probability for the propagation of both chains, resulting in polymers with low M_w/M_n values. It should be noted that, in a well-designed RAFT polymerisation, the equilibria described in steps 2-4 do not generate or destroy radicals, thus they do not influence the rate of polymerisation (see equation 1.8). Finally, termination is not eliminated in RAFT polymerisation but merely suppressed relative to the rate of propagation. The probability of termination also increases at high monomer conversions (i.e. under monomer-starved conditions). When the polymerisation is stopped or completed, the majority of polymer chains should ideally retain their RAFT agent functionality. In 2008 Moad *et al.* published a review article 'Towards Living Radical Polymerization,' which provided a schematic representation of the various end-groups produced by RAFT polymerisation (Figure 1.4). [63]

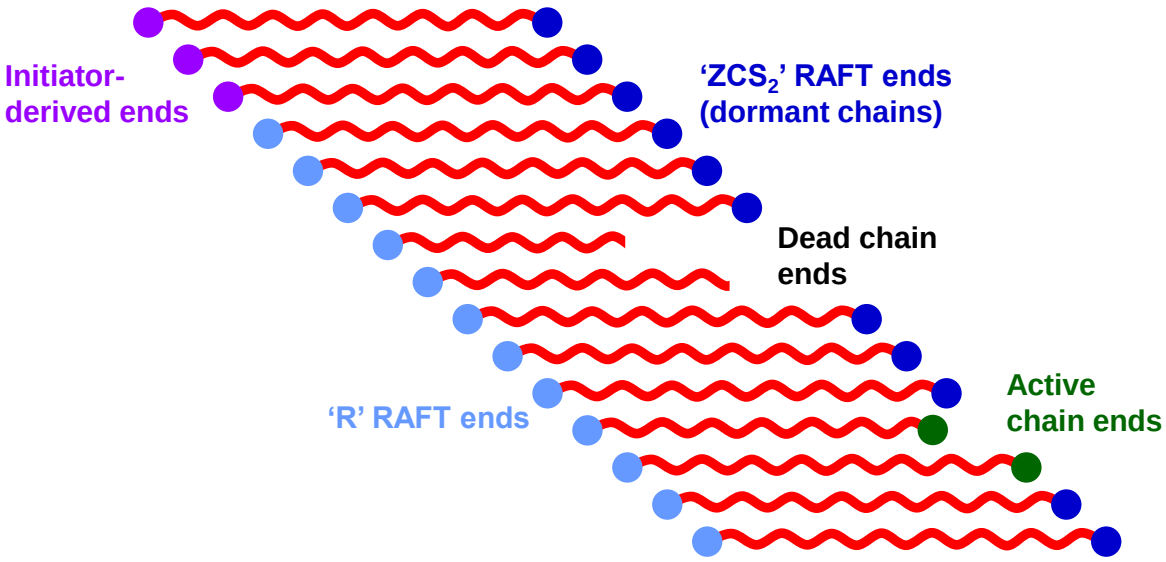

Figure 1.4 A schematic representation of the various end-groups during a RAFT polymerisation according to Moad *et al.*[63] The proportion of active, dormant end-groups and dead chains is not accurate but serves to act as an illustration. Ideally, the proportion of initiator-derived end-groups is much lower than that shown.

In an ideal situation, all polymer chains are initiated by the R group of the CTA but in practice a proportion of chains are initiator-derived. However, appropriate design of the RAFT agent can

result in identical initiator-derived and R end-groups (see later). The generic structure of a RAFT agent is shown in Figure 1.5.

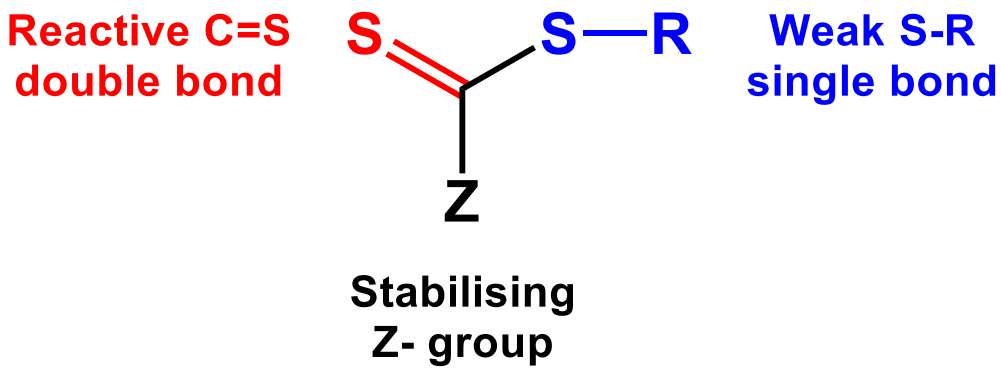

Figure 1.5 Structure of a thiocarbonylthio RAFT agent showing the R and Z groups. Note that if the Z group is *S*-alkyl then the RAFT agent is a trithiocarbonate.

As previously mentioned, the R group must be a good radical leaving group, but it also influences the probability of fragmentation by affecting the magnitude of k_{β}, $k_{-\beta}$ and k_{-add}. The Z group dictates the reactivity of C=S bond and hence influences the magnitude of k_{add} and k_{addP}. Moreover, the Z groups also confer stability on the radical adduct species (6) and (8). By adjusting the nature of the Z group, rates of addition can be tuned over five orders of magnitude.[53] Moad *et al.* published a set of guidelines for the appropriate selection of R and Z groups (Figure **1.6**) with respect to the class of monomer.[61] These were subdivided into two divisions: more-activated monomers (MAMs) or less-activated monomers (LAMs). MAMs are characterised by a conjugated carbon-carbon double bond and include styrenes, (meth)acrylates, (meth)acrylamides and acrylonitrile. These monomers are highlighted in green text in Figure **1.6**.[61] Keddie *et al.* suggested the further subdivision of MAMs into two groups where acrylates and acrylamides have k_p values > 10^3 M^{-1} s^{-1} but vinyl aromatics and methacrylates have k_p values < 10^3 M^{-1} s^{-1}.[64]

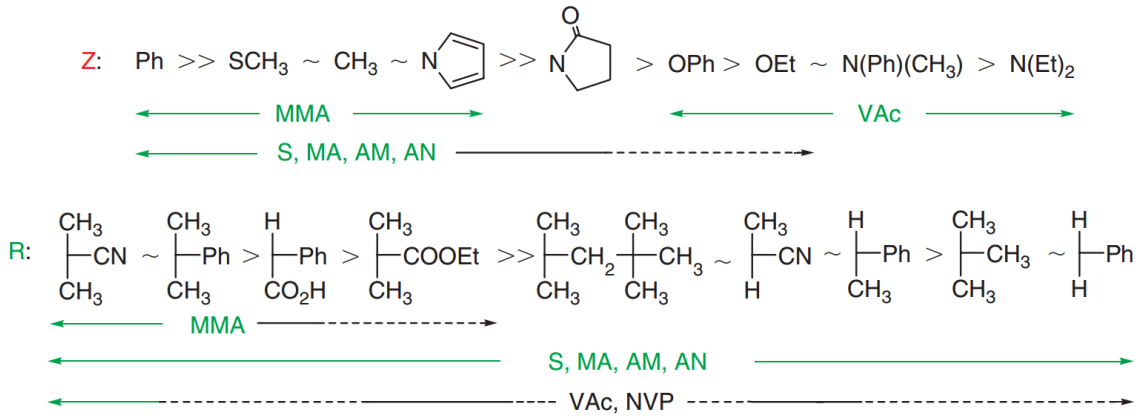

Figure 1.6 Guidelines for the appropriate selection of R and Z groups with respect to monomer class. For Z groups the rates of addition decrease and fragmentation increase from left to right. For R groups the rates of fragmentation decrease from left to right. Solid lines indicate good control while dashed lines indicate only control over target molecular weight but not over the molecular weight distribution. Abbreviations: AM = acrylamide, AN = acrylonitrile, MMA = methyl methacrylate, MA = methyl acrylate, VAc = vinyl acetate, NVP = *N*-vinylpyrrolidone, S = styrene.[61]

LAMs are characterised by a carbon-carbon double bond adjacent to a saturated carbon atom, oxygen or nitrogen with an available lone pair such as vinyl esters, vinyl acetate and vinyl amides. The appropriate choice of R and Z groups for MAMs and LAMs will now be discussed. In Figure 1.6, rate of addition for the Z group decreases and rate of fragmentation increases from left to right, as predicted by molecular orbital calculations.[9, 61] Propagating radicals for MAMs are less susceptible to radical addition (lower k_p, k_{add} and k_{addP}), hence a more activated RAFT agent is required. Hence, selecting Z groups with aromatic (dithiobenzoates) or *S*-alkyl (trithiocarbonates) functionality is necessary to control the RAFT polymerisation of MAMs.[63] Furthermore, aryl groups provide more radical stability relative to sp^3 carbon, oxygen, sulphur or nitrogen, thus reducing the rate of fragmentation.[64] There is some debate over whether the rate of fragmentation of dithiobenzoates is slow enough to directly cause retardation, or whether the rate of fragmentation is sufficiently slow enough so that termination reactions are more likely.[55, 56] Conversely, LAM propagating radicals are very susceptible to radical addition

(higher k_p, k_{add} and k_{addP}) thus less reactive RAFT agents are required for high levels of control. Furthermore, as the propagating radicals for LAMs are poor leaving groups, the radical intermediates (6) and (8) are inherently more stable (lower k_{-addP}). Consequently, the high relative reactivities of the C=S bonds in dithiobenzoates and trithiocarbonates render them unsuitable. These RAFT agents strongly inhibit the RAFT polymerisation of LAMs. To address this problem, the reactivity of the C=S bond is reduced by using nitrogen (*N,N'*-dialkyldithiocarbamates or *N*-alkyl-*N*-aryldithiocarbamates) or oxygen atoms (*O*-alkylxanthates) in the Z groups. Lone pair conjugation with C=S reduces the double bond character and stabilises the dormant, capped chains (species (7)) relative to the intermediate radical adduct (species (6) and (8)).[65] It should be noted that if the lone pair is already part of a conjugated system (such as pyrrole moieties or a neighbouring an α-carbonyl group) then the reactivity is more similar to that of trithiocarbonates.

Consideration of the fragmentation and reinitiation steps is crucial when determining the suitability of R groups for RAFT polymerisations. Fragmentation must occur to release $R^{\bullet}$ species, otherwise retardation is likely. Furthermore, the rate of reinitiation must be rapid relative to propagation. For MAMs such as methacrylates and methacrylamides, the best R groups are tertiary cyanoalkyl or cumyl. These electron-withdrawing functionalities reduce the rate of addition but increase the rate of fragmentation. Nevertheless, these R groups are not suitable for LAMs due to their very high k_p values ($> 10^3$ M^{-1} s^{-1}) rendering reinitiation slow relative to propagation. Therefore primary and secondary R groups are considered more suitable.

From the above discussion, it follows that it is very difficult to prepare diblock copolymers of poly(MAM)-*b*-poly(LAM) by RAFT polymerisation because MAMs and LAMs require RAFT agents with opposing properties. However, the design of so-called universal RAFT agents such

as (*N*-(4-pyridinyl)-*N*-methyldithiocarbamate) has attempted to address this problem (Scheme 1.7).[66]

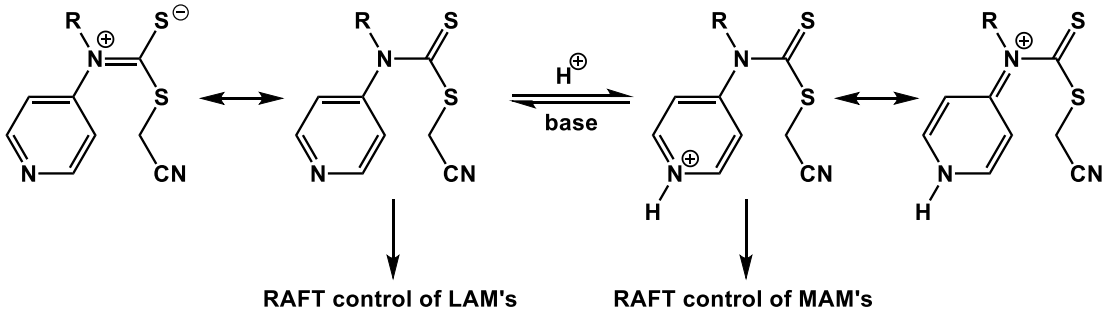

Scheme 1.7 Universal (switchable) RAFT agents based on cyanomethyl *N*-(aryl)(pyridine-4-yl)carbamodithioate RAFT agents. This schematic has been adapted from refs. [64, 67]

When the pyridine group is in its neutral form, the RAFT agent is capable of polymerising LAMs. On protonation of the pyridine group, the lone pair from the carbamate nitrogen is not available to conjugate with C=S, increasing the double bond reactivity and hence allowing the polymerisation of MAMs. More recently, it has been demonstrated that ensuring the R group on the universal RAFT agents has cyanomethyl functionality (e.g. cyanomethyl *N*-(aryl)(pyridine-4-yl)carbamodithioate) leads to a narrower MWD for poly(MAM)-*b*-poly(LAM) diblock copolymers.[67]

RAFT agents are typically low molecular weight, sulphur-rich small molecules. Many synthetic routes have been reported by numerous research groups.[64] An excellent perspective on the synthesis of effective RAFT agents has been published by Keddie *et al.* (Figure 1.7).[64] The authors critically examine numerous synthetic protocols for RAFT agents, outlining their various benefits and disadvantages. Common methods involve reactions of carbodithioate salts with alkylating agents,[68, 69] thiol exchange,[70, 71] reactions of radicals with bis(thio) disulphides (radical-induced decomposition)[72-74] and nucleophilic substitution reactions.

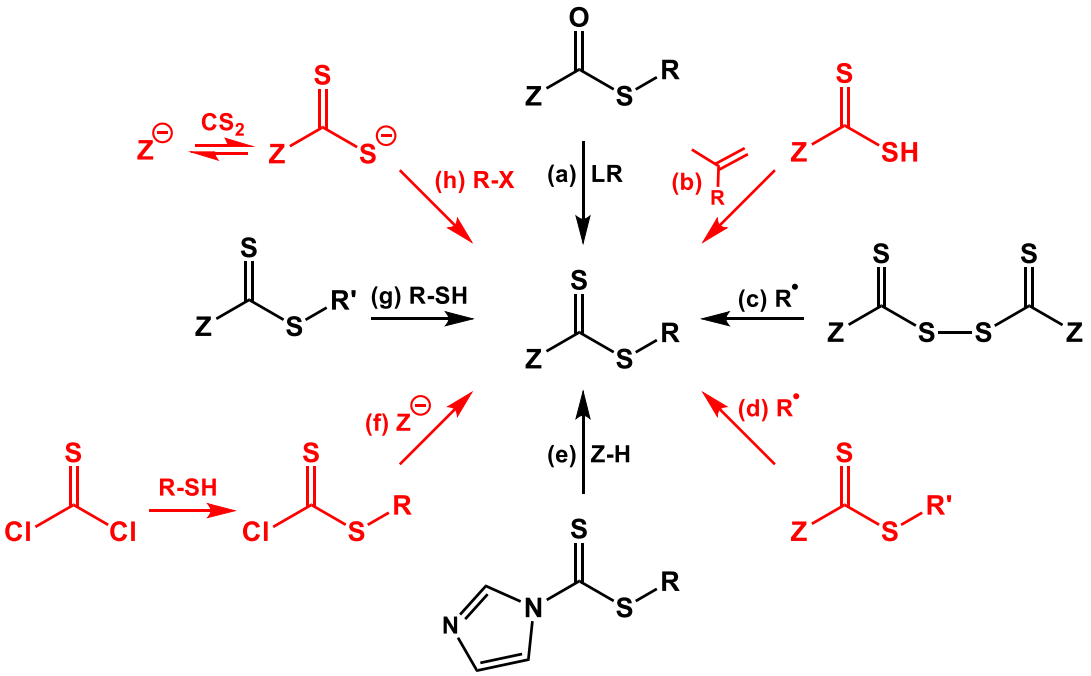

Figure 1.7 Main synthetic strategies used for synthesising RAFT agents: (a) thiolation using Lawesson's reagent, (b) Markovnikov addition, (c) radical-induced decomposition, (d) radical-induced R group exchange, (e) and (f) nucleophilic substitution, (g) thiol exchange and (h) alkylation of carbodithioate salts. Abbreviations: RX = alkylating agent, LR = Lawesson's reagent.[64]

The chemistry used to synthesise RAFT agents is dictated by the desired R and Z groups. In this thesis RAFT agents have been synthesised by radical-induced decomposition. Jones and co-workers reported the synthesis of the trithiocarbonate RAFT agent, 4-cyano-4-(2-phenylethanesulfanylthiocarbonyl) sulfanylpentanoic acid (PETTC) (Scheme 1.8).[75] Optimisation of the synthesis of PETTC has subsequently been undertaken in-house by the Armes research group, allowing as much as up to 100 g to be prepared in up to 80% yield. It should be noted that the PETTC R group is chemically identical to the initiator-derived end group when using 4,4′-azobis(4-cyanovaleric acid) (ACVA). PETTC allows the efficient preparation of various methacrylic homopolymers in either aqueous, polar solvents or non-polar media.[76-78]

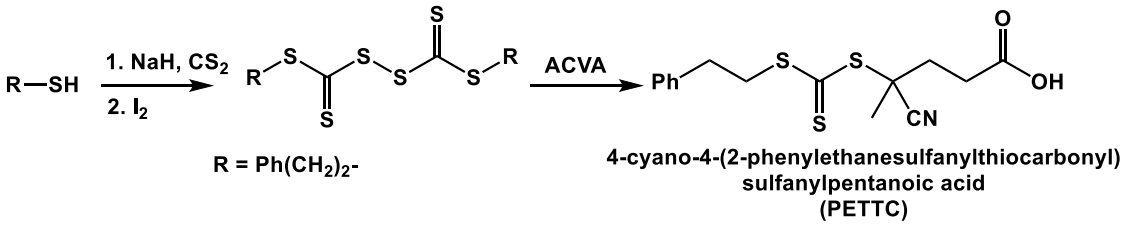

Scheme 1.8 Synthesis of the trithiocarbonate RAFT agent 4-cyano-4-(2-phenylethanesulfanylthiocarbonyl) sulfanylpentanoic acid (PETTC) by radical-induced decomposition. Abbreviations: ACVA = 4,4′-azobis(4-cyanopentanoic acid).[75]

As mentioned previously, one key disadvantage for RAFT polymerisation is the intrinsic colour and malodorous nature of RAFT agents. Several chemistries have been designed to remove or modify the RAFT end-groups, which is highly desirable for certain applications (Scheme 1.9). Further research in this area could be important for future successful industrial implementation of RAFT polymerisation.

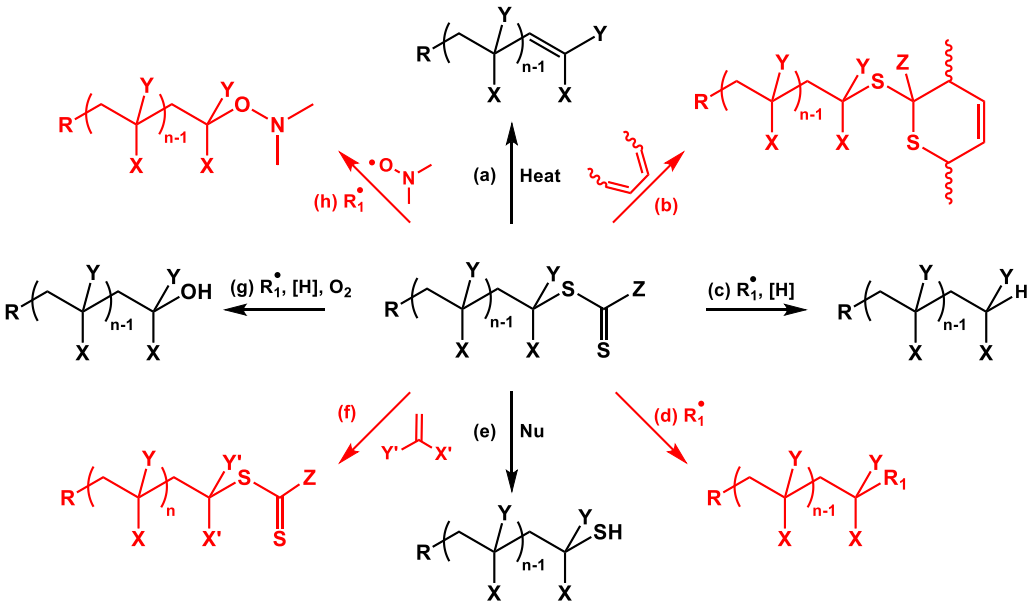

Scheme 1.9 Common techniques for RAFT end-group modification/removal reactions: (a) thermolysis, (b) hetreo-Diels-Alder, (c) radical-induced reduction, (d) addition-fragmentation coupling, (e) nucleophilic substitution, (f) chain extension to prepare diblock copolymers, (g) radical induced-oxidation and (f) radical-induced nitroxylation. [64, 79] Abbreviations: Nu = nucleophile, [H] = hydrogen atom donor, $R_1^{\bullet}$ = radical initiator such as AIBN.

End-group removal techniques include thermolysis, radical-induced reduction, addition-fragmentation coupling, nucleophilic substitution and radical-induced oxidation.[79] These methods remove the dithioester or trithiocarbonate functionality (and hence the colour and potential odour) while producing hydrogen, thiol, hydroxyl or alkyl end-groups. However, if further reactions are warranted that do *not* involve RAFT polymerisation, then functional group interconversion reactions can be undertaken to remove the CTA end-group, such as hetero-Diels-Alder, thermolysis to liberate alkene functionality or radical nitroxylation to enable subsequent NMP polymerisations.[64, 79]

A homopolymer containing thiocarbonyl end-groups is denoted as a macromolecular chain transfer agent (macro-CTA). Such macro-CTAs are capable of undergoing chain extension reactions to prepare well-defined block copolymers *via* RAFT polymerisation by sequential monomer addition. The partial RAFT polymerisation mechanism for the chain extension of macro-CTA 'A' (9) with monomer B is shown in Scheme 1.10. While this mechanism is very similar to RAFT homopolymerisation (Scheme 1.6), certain criteria require further discussion. In the reversible chain transfer step, the fragmentation of the radical adduct (10) must occur in favour of species (11), releasing the macro-radical, $A_n^{\bullet}$. Fragmentation must occur in preference to $A_n^{\bullet}$ to prevent contamination with homopolymer B. Furthermore, $A_n^{\bullet}$ must act as a reinitiation radical (akin to $R^{\bullet}$ in Scheme 1.6) to form the propagating diblock radical $A_nB_m^{\bullet}$. In chain equilibration/propagation, the propagating diblock radical $A_nB_m^{\bullet}$ can react with either the original macro-CTA species (9) or homopolymer B (11) to form the radical adduct (12) or radical adduct (14), respectively. In this context, it is vital that fragmentation must occur in preference to $A_nB_m^{\bullet}$ to prevent homopolymer contamination. Given the importance of the relative fragmentation rates in the preparation of diblock copolymers, it is essential to polymerise methacrylates *before* chain extension with styrenes or acrylates, if such hybrid diblocks are desired.

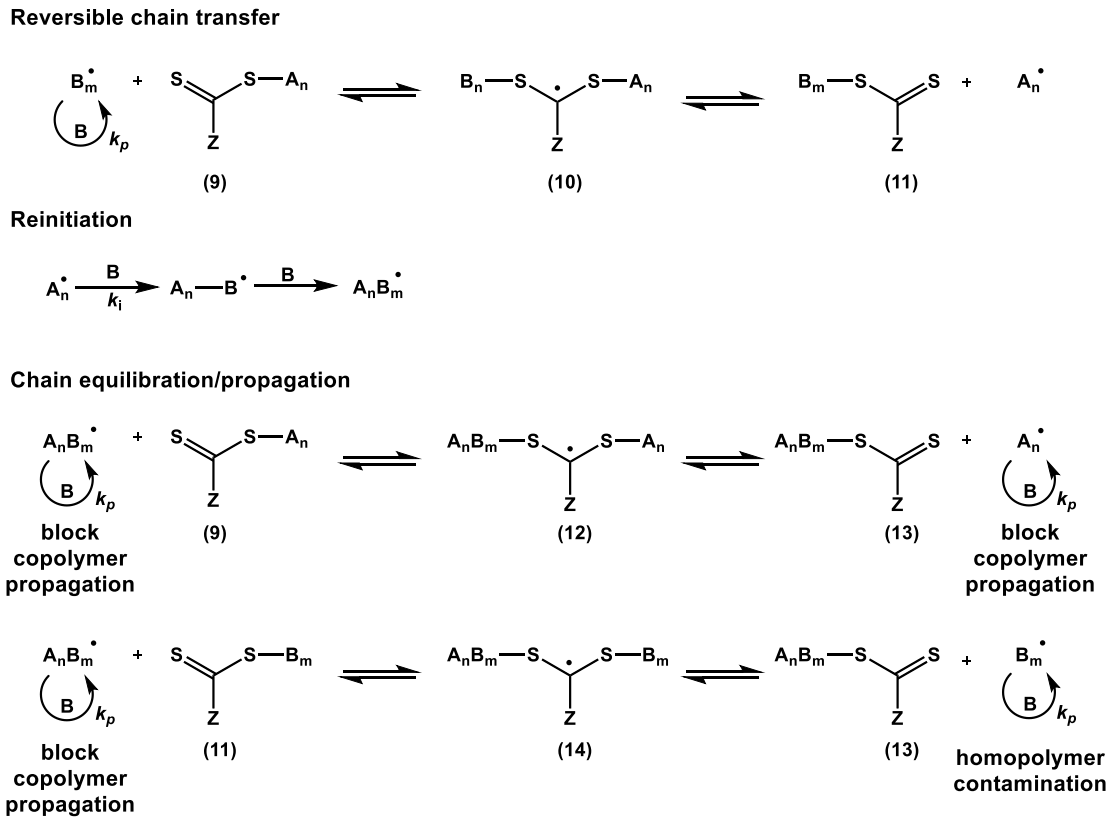

Scheme 1.10 Partial RAFT mechanism showing the reversible chain transfer, reinitiation and chain equilibration/propagation steps in the chain extension of macromolecular chain transfer agent A with monomer B to form AB diblock copolymers.[53]

In summary, for the effective RAFT polymerisation of methacrylates the Z group should contain either aryl or *S*-alkyl functionality while the R group should contain a tertiary cyanoalkyl moiety. Furthermore, if such polymerisations are to be carried out in water, then it is recommended to use trithiocarbonates instead of dithiobenzoates as the former are less susceptible to hydrolysis and decomposition by Lewis acids.[80]

However, the major drawback of RAFT polymerisation is the highly coloured and malodorous nature of the sulphur-based CTA. In principle, this problem can be addressed by post-polymerisation modification or removal of the RAFT agent. Selecting R and Z group with low volatilities helps minimise malodour.[72] It has been demonstrated that the RAFT polymerisation

technique is highly versatile with regard to monomer functionality, insensitive to protic impurities and useful for the preparation of *functional diblock copolymers*. Hence RAFT was the RDRP technique chosen for the work described in this thesis. The diblock copolymers prepared have been designed to self-assemble *in situ* to form nanoparticles with a range of morphologies.

1.3 Self-Assembly

Although no official IUPAC definition exists, Whitesides and Grzybowski describe 'self-assembly' as the spontaneous organisation of pre-existing components into structures or patterns without human involvement.[81] Self-assembly is prevalent across all length scales from solar systems and galaxies, to planetary weather patterns,[82] and the nanometer domain.[83] Examining the conditions required for efficient self-assembly at the nanoscale, polymer chemists have begun to mimic some of the naturally-occurring morphologies that can be found here.[84]

1.3.1 Properties of Water and the Hydrophobic Effect

Water is the most abundant molecule on earth and life could not exist without it. An understanding of the underlying principles of block copolymer self-assembly requires consideration of the remarkable behaviour of water. Water comprises a central oxygen atom with two lone pairs and two hydrogen atoms; it adopts a tetrahedral structure with an H-O-H bond angle of 104.5° (Scheme 1.11). Considering the other Group 16 chalcogen hydride properties, it would be expected that water is a gas at room temperature and pressure. However water is a liquid under ambient conditions as a result of extensive intermolecular hydrogen bonding, and it exhibits anomalously high melting (0 °C) and boiling (100 °C) points. Hydrogen bonding occurs when a hydrogen atom is covalently bonded to an electronegative atom such as nitrogen, oxygen or fluorine.[85] This difference in electronegativity results in partial negative

charge on the heteroatom and positive charge on the hydrogen atom, resulting in a strong electrostatic attraction between adjacent molecules (Scheme 1.11). For neutral molecules, the strength of hydrogen bonds typically lies between 10 and 65 kJ mol^{-1}, much greater than the 8 kJ mol^{-1} bond strength of van der Waals forces.[86] When one component of the hydrogen bond is ionic, the hydrogen bond strength can be up to 40 – 190 kJ mol^{-1}. Analysis by Aakeröy and Seddon showed that certain hydrogen bond strengths are comparable to weak covalent σ-bonds.[86]

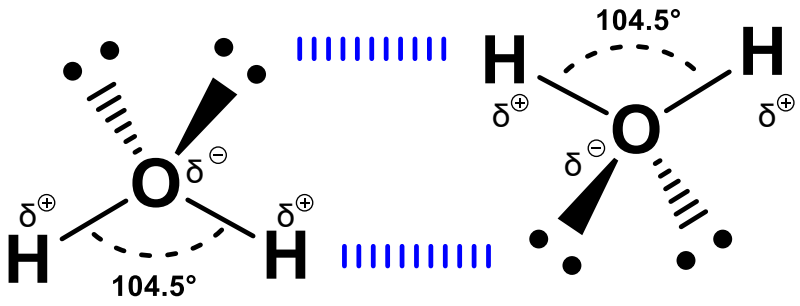

Scheme 1.11 The distorted tetrahedral structure of water, showing the H-O-H bond angle of 104.5° and the blue dashed line representing hydrogen bonding between the lone pairs on the oxygen and hydrogen atom of two neighbouring water molecules.

Water is frequently described as the universal solvent for its ability to solubilise many ionic and polar compounds.[87] One prerequisite for aqueous dissolution of a solute is it forms hydrogen bonds with water molecules, but other external factors such as temperature and solution pH may also influence its aqueous solubility. On the molecular scale, if a solute has no hydrogen bonding capability then at least one dipole of neighbouring water molecules must face the solute, resulting in the loss of at least one intermolecular water hydrogen bond. In an attempt to maintain the original number of hydrogen bonds, water molecules reorient to form a cage around the solute.[88, 89] This is known as the hydrophobic effect.[90] The significant increase in

molecular order around the solute is entropically unfavourable, thus an increase in the surface area of the solute results in an escalation of water molecule restructuring, cumulating in a larger entropic penalty. The result is that hydrophobic liquids are immiscible with water and hydrophobic solids will not dissolve. Nevertheless, when molecules possessing *both* hydrophobic and hydrophilic components (i.e. amphiphiles) are placed in water, then interesting complex molecular reorientation occurs. For instance, cell membranes are composed of phospholipid bilayers while surface-active agents (surfactants), the active ingredient in washing-up and laundry detergent formulations, form micelluar structures in aqueous solution.

1.3.2 Self-Assembly of Surfactants: The Packing Parameter

Surfactants are small amphiphilic molecules with two chemically distinct environments comprising a hydrophobic tail and a polar hydrophilic head-group. The emergence of surfactants as essential ingredients in both personal and home care products led to the huge expansion of companies with multi-billion dollar turnovers such as Unilever, Procter & Gamble and Johnson and Johnson. Furthermore, food science heavily relies on the ability of naturally-occurring surfactants to stabilise droplets of oil (or fat) in an aqueous continuous phase.[91] Hence structure-property relationships are crucial for understanding and optimising surfactant formulations.

A common characteristic of surfactants is their self-assembly behaviour in water. Considering the thermodynamics of surfactant self-assembly, such behaviour only occurs when the entropic penalty associated with forming higher order aggregates is less than the energy required for the amphiphiles to remain in solution. These self-assembled structures are collectively referred to as complex fluids or association colloids[92] and undergo rapid aggregate-monomer exchange, as shown in Figure 1.8. The mean lifetime of unimers within a surfactant micelle is typically very short, approximately 10^{-5} to 10^{-3} seconds.[92]

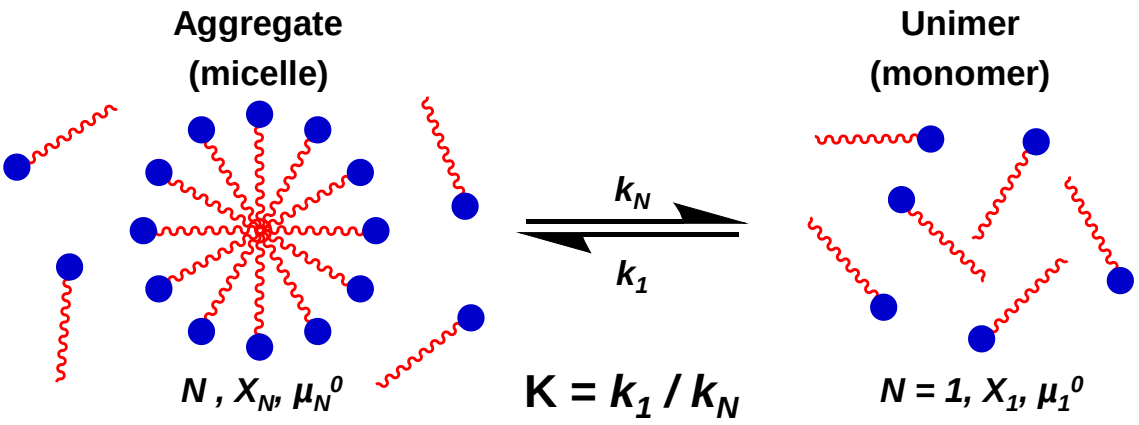

Figure 1.8 Schematic representation of the dynamic equilibrium between unimers (monomers) and their respective aggregates (micelles). The terms *N*, *X* and μ denote the aggregation number, activity/concentration and chemical potential, respectively.

The equilibrium constant K is defined as the ratio of the rate constant of association (k_1) to the rate constant of dissociation (k_N) and can be mathematically described as shown in equation 1.15, where k_B is the Boltzmann constant, T is the absolute temperature, μ_N^0 is the chemical potential of the aggregate in solution with an aggregation number N and μ_1^0 is the chemical potential of a single surfactant molecule in solution.[92]

$$K = \frac{k_1}{k_N} = e^{\left[-\frac{N(\mu_N^0 - \mu_1^0)}{k_B T}\right]} \qquad \textbf{1.15}$$

K must be positive for aggregation to occur, thus analysis of equation 1.15 shows that the chemical potential of the aggregates must be less than that for a single surfactant ($\mu_N^0 < \mu_1^0$). The self-assembly behaviour of surfactants has been studied for many decades. Multiple aggregate morphologies have been identified, such as spheres, worm-like micelles, vesicles and bilayers (Figure 1.9).[93] These equilibrium structures are usually soft and fluid-like and will exhibit a size distribution.

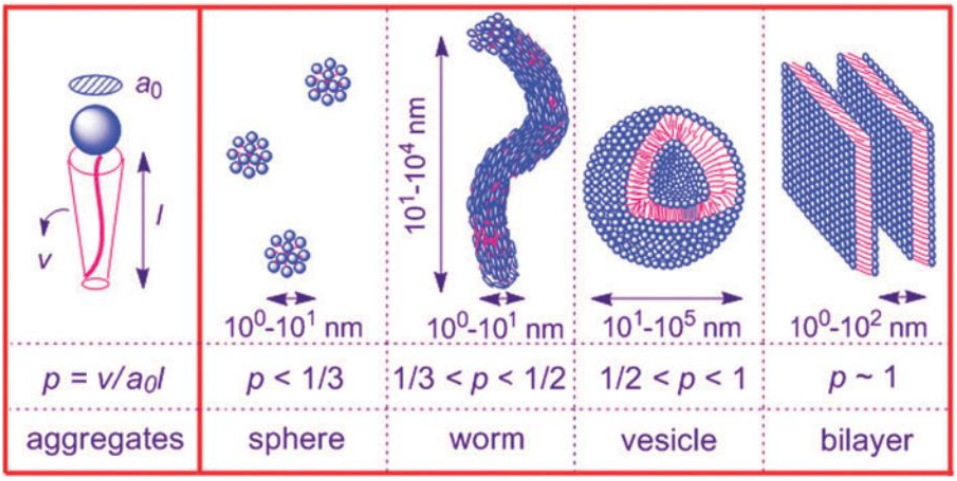

Figure 1.9 Schematic illustration of four (spheres, worms, vesicles and bilayers) self-assembled surfactant aggregate morphologies, showing their approximate dimensions and relation to the packing parameter,[93] as described by Israelachvili.[92]

Two forces primarily dictate the self-assembly behaviour of surfactants: (i) the hydrophobic attraction between the essentially fluid-like hydrophobic surfactant tails of at the hydrocarbon-water interface and (ii) the repulsion between neighbouring hydrophilic head-groups. While the first force is attractive, the latter is repulsive and the balance between them gives rise to the concept of 'opposing forces' occurring mainly at the interfacial region.[94] Hydrophobic attraction tends to reduce and head-group repulsion tends to increase the interfacial area per molecule (a), which essentially is the effective head-group area exposed to the aqueous phase.[94] Attractive interactions arise from both the interfacial tension and the hydrophobic effect. These forces act at the essentially fluid hydrocarbon-water interface resulting in a positive interfacial free energy per unit area (γ) of $\gamma \approx 50$ mJ m^{-2}. However, the γ value is likely to be lower (≈ 20 mJ m^{-2}) for surfactants owing to electrostatic head-group repulsion forces.

To a first reasonable approximation (ignoring the liquid-like nature of hydrocarbon chains) the attractive interfacial free energy contribution to the chemical potential of an aggregate with an aggregation number of N (μ_N^0) can be simply written as γa.[92] However, the repulsive forces of

the hydrophilic head-group arising from steric effects and ionic repulsions are difficult to formulate explicitly.[95] Nevertheless, the precise individual contributions are not essential as these factors are simply inversely proportional to the surface area occupied per head-group (K/a).[92] Thus the total interfacial free energy per molecule in an aggregate is mathematically described in equation 1.16, where K is a constant of proportionality for head-group repulsion.[92]

$$\mu_N^0 = \gamma a + \frac{K}{a} \qquad \textbf{1.16}$$

If it is assumed that both the attractive hydrophobic and repulsive hydrophilic interactions act in the same plane as the hydrophobic-hydrophilic interface, then a minimum in the interaction energy occurs when $\delta\mu_N{}^0/\delta a = 0$. At this point, $a = a_o$ where a_o is the optimum head-group area per molecule at the hydrophilic-hydrophobic interface, as illustrated in Figure 1.10.

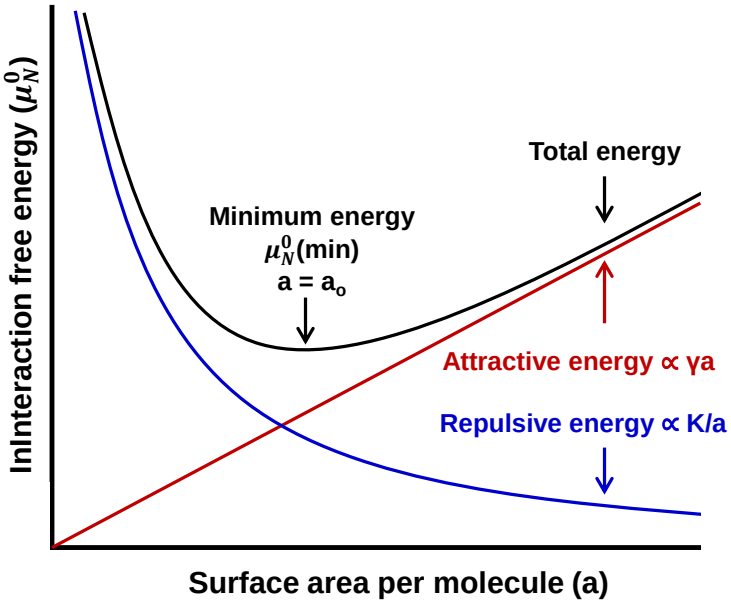

Figure 1.10 Schematic illustration of the relationship between the opposing forces of hydrophobic attraction and hydrophilic head-group repulsion, resulting in a minimum energy at the optimum head-group area, a_o, for self-assembled surfactant aggregates.

This can be mathematically expressed in equation 1.17.

$$\boldsymbol{\mu_N^0(min) = 2\gamma a_o \text{ where } a_o = \sqrt{K/\gamma}} \qquad \textbf{1.17}$$

This allows the unknown constant K to be eliminated, so the interfacial energy per molecule can be expressed in a more convenient form (equation 1.18).[96]

$$\boldsymbol{\mu_N^0 = 2\gamma a_o + \frac{\gamma}{a}(a - a_o)^2} \qquad \textbf{1.18}$$

Thus, the attractive and repulsive forces inside the aggregate are balanced, leading to a minimum in the interfacial free energy. This model is a first approximation and excludes important factors such as head-group ionic bridging, the effect of surface curvature on μ_N^0 and specific chain-chain interactions (as the hydrocarbon chains are in practice, never truly fluid). Aggregate formation is characterised by a small positive change in enthalpy but a surprisingly large change in entropy, which is explained by the release of unbound water into the bulk solution.[97] The concept of a_o is critical in introducing the geometric packing arrangement of surfactant molecules in an aggregate. Before discussing this concept, two parameters for the hydrophobic component must be considered: the volume of the hydrocarbon chain, v, (which is assumed to be fluid and incompressible) and the critical chain length, l_c, which is the *maximum* effective length that the hydrocarbon chain can extend. If a_o, v and l_c are known, then the morphology of the aggregate can be estimated using the dimensionless packing parameter, P, which relates to the curvature of the aggregate (Figure 1.11).[96]

Israelachvili[96] demonstrated that high curvature results in a low value of $P \leq {}^1/_3$, which corresponds to spherical micelles. In such cases, the mean diameter of the spherical micelle

cannot exceed $2l_c$. When P is such that $^1/_3 < P \leq {}^1/_2$, cylindrical micelles (commonly termed worms) are geometrically preferred. When $^1/_2 < P \leq 1$, the low curvature results in the formation of bilayers, that can wrap up into vesicles. When P = 1, planar bilayers are preferred and finally when P exceeds unity then so-called 'inverted' structures are formed. It should be noted that a_o can adopt a wide range of values depending on the local environmental conditions such as pH, salt type, concentration and temperature. Therefore, the predictive power of the packing parameter concept should treated with some caution.[98] Although specific values of v, a_0 and l_c are difficult to predict, the packing parameter is still a very useful qualitative concept for explaining morphology transitions observed for diblock copolymer aggregates (as discussed in Chapters 2 and 3). First, the self-assembly of diblock copolymers in the bulk and in solution is discussed.

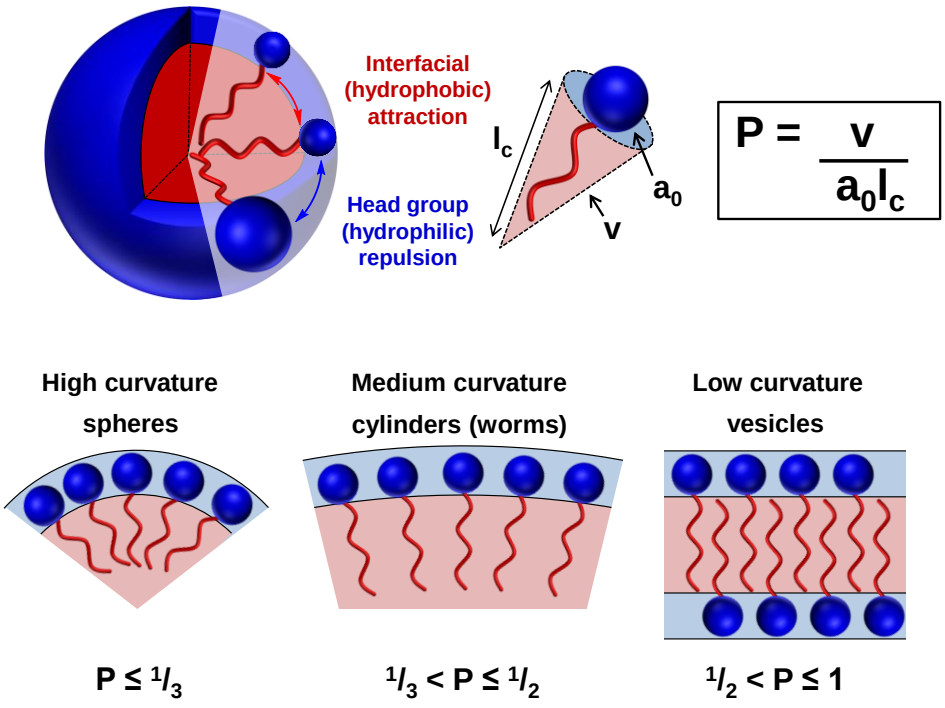

Figure 1.11 Schematic representation of the packing of surfactant molecules in an aggregate, showing the two balancing forces of interfacial hydrophobic attraction and head-group hydrophilic repulsion. The equation for the dimensionless packing parameter, P, is shown and the characteristic values of P for spheres, cylindrical (worm-like) micelles and vesicles are stated.

1.3.3 Self-Assembly of Diblock Copolymers

The second law of thermodynamics states that, in a closed system, a spontaneous process takes place when the change in the Gibbs free energy is negative ($\Delta G = \Delta H - T\Delta S$). This Gibbs free energy equation can be related to the mixing of two solvents or solvent plus polymer molecules ($\Delta G_{mix} = \Delta H_{mix} - T\Delta S_{mix}$). If small molecules behave ideally on mixing then $\Delta H_{mix} = 0$, hence the increase in entropy results in a negative ΔG_{mix}.[2] However, the mixing of amorphous polymers in solution leads to non-ideal behaviour (ΔH_{mix} and $\Delta S_{mix} \neq 0$), owing to the large difference in size between solvent and polymer molecules.

In the 1940s both Flory[99] and Huggins[100] independently developed a lattice model theory to describe the incompatibility of two polymers in the bulk or for a polymer in solution. From a theoretical point of view, only diblock copolymers in the bulk will be considered. The extent of microphase separation of blocks was found to depend on three factors: (i) the volume fraction of each block, φ, (ii) the DP_n, N and (iii) the Flory-Huggins interaction parameter, χ. Equation 1.19 describes both the entropic and enthalpic contributions to ΔG_{mix} where k_B is the Boltzmann constant, T is the absolute temperature, φ is the volume fraction of species 1 and 2, N is the DP_n and χ is the Flory-Huggins interaction parameter.

$$\frac{\Delta G_{mix}}{k_B T} = \left(\frac{\varphi_1 ln \varphi_1}{N_1}\right) + \left(\frac{\varphi_2 ln \varphi_2}{N_2}\right) + \varphi_1 \varphi_2 \chi_{12} \qquad \textbf{1.19}$$

The small combinatorial entropic terms depend on the volume fraction and DP_n of the two polymer blocks. The enthalpic contribution depends on the relative volume fractions of the polymer blocks and χ. Analysis of equation 1.19 shows that χ_{12} should be negative for the spontaneous mixing of two species, where χ is defined in equation 1.20.

$$\chi_{12} = \left(\frac{Z}{k_B T}\right)\left[\varepsilon_{12} - \frac{\varepsilon_{11} + \varepsilon_{22}}{2}\right] \qquad \textbf{1.20}$$

In contrast, positive values of χ_{12} indicate net repulsion between species 1 and 2, which can result in demixing. Here Z is the lattice coordination number (the number of nearest neighbours per repeat unit as a lattice model is assumed) and $\varepsilon_{12,}$ ε_{11} and ε_{22} are the interaction mean interaction energies per monomer unit between components 1-2, 1-1 and 2-2, respectively.[101] Typically, for unlike polymers, where there are no strong interactions (such as hydrogen bonding), χ_{12} is actually small and positive. For example the χ value of styrene and isoprene is approximately 0.1[101] while χ = 0.032 has been reported for polystyrene-poly(methyl methacrylate) blends.[102] Almost all polymers undergo microphase separation due to enthalpic incompatibility between the two blocks. When two polymer chains are linked together by covalent bonds (i.e. diblock copolymers), microphase separation is observed, rather than macrophase separation (as observed for oil and water mixtures). The separation product (χN) determines the degree of microphase separation and typically decreases with temperature. For low χN values, the compatibility between the two polymer chains increases, thus promoting mixing. Increasing χN results in greater microphase separation.

Analysis of equation 1.20 also shows that χ_{12} is inversely proportional to temperature, thus most polymer mixtures exhibit an order-disorder transition (ODT) at a specific temperature (T_{ODT}). Furthermore, such diblock copolymers may undergo an order-order transition (OOT). Swann and Topham described how varying both χN and the relative volume fraction (f_A) of diblock copolymers leads to various morphologies (Figure 1.12).[103] Huang and Lodge reported how the addition of solvent to a diblock copolymer increases the complexity, because interactions between each polymer block and the solvent must now also be considered.[104] It is well known that amphiphilic diblock copolymers undergo self-assembly in a solvent that is selective for one

block.[84, 105, 106] Such micelles consist of a polymer/solvent corona and a desolvated core, although the degree of solvation depends on the core polymer/solvent interactions. These diblock copolymer micelles are often compared to surfactant aggregates but they exhibit much slower unimer/aggregate exchange because the thermodynamic barrier to dissociation is greater, resulting in kinetically stable structures.[107] Traditionally, such block copolymers are prepared in a good solvent for both blocks using the synthetic techniques described earlier in this thesis. Following this, post-polymerisation processing methods are required to induce particle formation. The simplest method is to dissolve a diblock copolymer in a selective solvent followed by ageing for equilibrium to be achieved.[110]

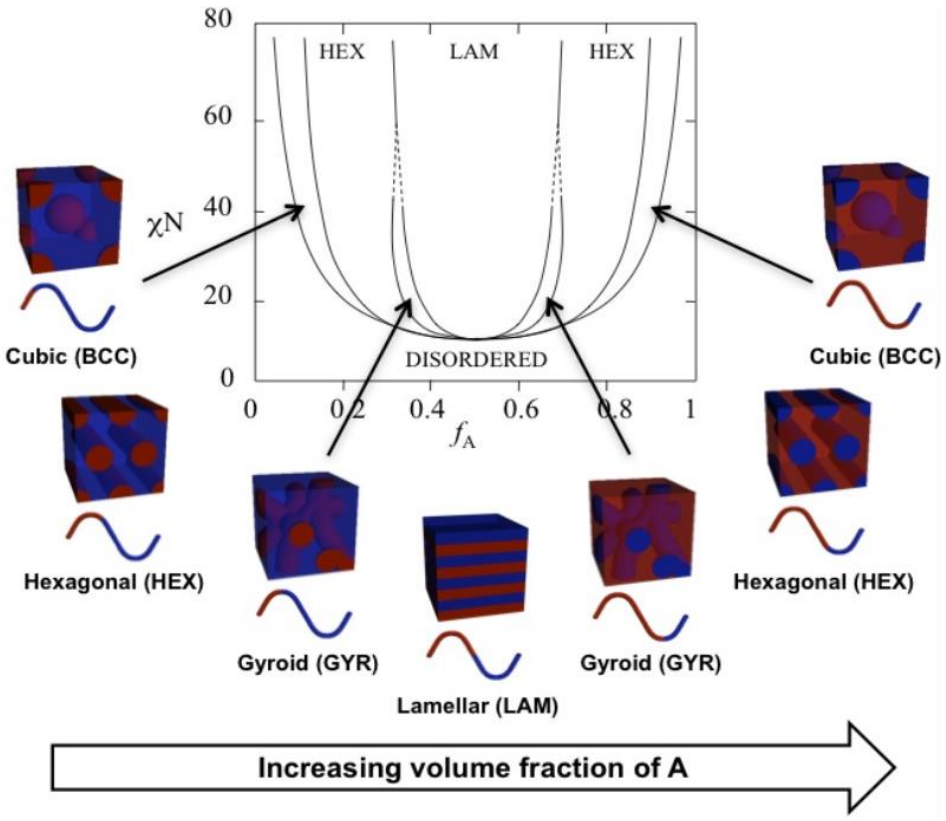

Figure 1.12 Theoretical morphology with the corresponding particle morphologies for diblock copolymers. N is total degree of polymerisation, χ is the Flory-Huggins interaction parameter and f_A is the volume fraction of polymer block A. Abbreviations: BCC = body centred cubic, HEX – hexagonal cylinders, GYR = gyroid and LAM = lamellar.[103, 108, 109]

Other techniques include thin film rehydration,[111] solvent[84, 112-114] and pH switching and pH switching.[115-118] While such techniques have been extensively examined for a wide range of block copolymer compositions under various conditions, all suffer the same significant disadvantage of requiring dilute conditions (< 1% w/w), thus limiting their potential industrial importance.

1.4 Conventional Aqueous Dispersion Polymerisation

Dispersion polymerisation is a modified precipitation polymerisation where the addition of a suitable stabilising agent enables the formation of microscopic sterically-stabilised latex particles.[110] A typical dispersion polymerisation formulation consists of a soluble monomer, initiator and stabiliser, which is typically surfactants, homopolymers and block copolymers.[111] A prerequisite for a dispersion polymerisation is that, while the monomer is soluble in the solvent of interest, the resulting polymer *must* be insoluble. Free radical dispersion polymerisation was first reported in 1962 by Imperial Chemical Industries.[112] Sterically-stabilised (meth)acrylate or styrenic latexes were prepared in both organic and non-polar solvents. Since this seminal report, dispersion polymerisation has received wide interest from the coatings industry and academia alike. A free radical dispersion polymerisation consists of six main steps (Figure 1.13). In stage one, all of the reaction components are mixed together and form a homogeneous solution. Thermal decomposition of the initiator occurs in stage two, followed by reaction with monomer to form propagating oligomeric radical chains *via* free radical polymerisation. At a certain critical molecular weight the oligomeric radical becomes insoluble and forms nascent particles (stage three). Note that, in the absence of any polymeric stabiliser, an unstable precipitate would form *via* precipitation polymerisation. In contrast, the polymeric stabiliser either physically adsorbs or is grafted onto the particle by hydrogen abstraction in stage four.[113]

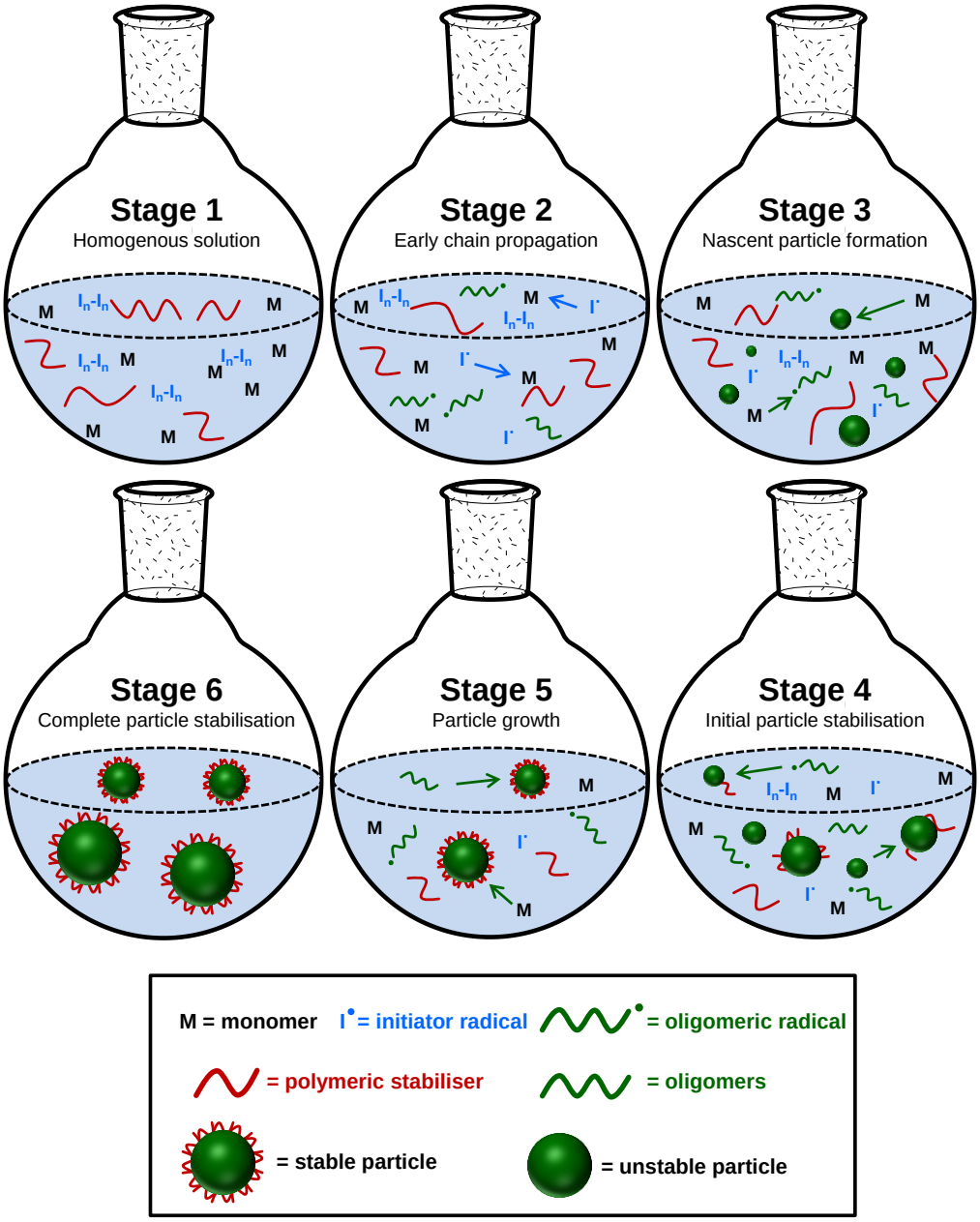

Figure 1.13 Schematic illustration describing the main six stages of free radical dispersion polymerisation.[114]

Particle diameters tend to increase as oligomer and monomer enter the particle, while particle-particle coalescence also occurs. At stage five, all particles become fully sterically-stabilised and residual monomer and oligomers enter these stabilised particles. Stage six depicts only sterically-stabilised latex particles present in solution. It is well known that well-defined latexes

can be prepared by non-aqueous dispersion polymerisation.[110, 115, 116] However, of particular relevance to this thesis is free radical aqueous dispersion polymerisation. The volume of literature on conventional aqueous dispersion polymerisation is somewhat less than that for non-aqueous dispersion polymerisation. This can be attributed to the fact that only a limited number vinyl monomers exhibit the correct solubility characteristics required for the former formulations. Two relatively expensive speciality monomers that meet the requirements for aqueous dispersion polymerisation are *N*-isopropylacrylamide[117] and *N*,*N*′-diethylacrylamide.[118] A much cheaper alternative is 2-hydroxypropyl methacrylate (HPMA). At room temperature the water solubility of HPMA is approximately 13% w/w while the resulting PHPMA is insoluble at all temperatures.[119] Ali *et al.* published the first report of the aqueous dispersion polymerisation of HPMA using non-ionic poly(*N*-vinylpyrrolidone) (PNVP) as a steric stabiliser (Figure 1.14).[119] The effect of PNVP concentration, additional comonomer or surfactant and initiator functionality on the mean particle diameters and polydispersity was examined.

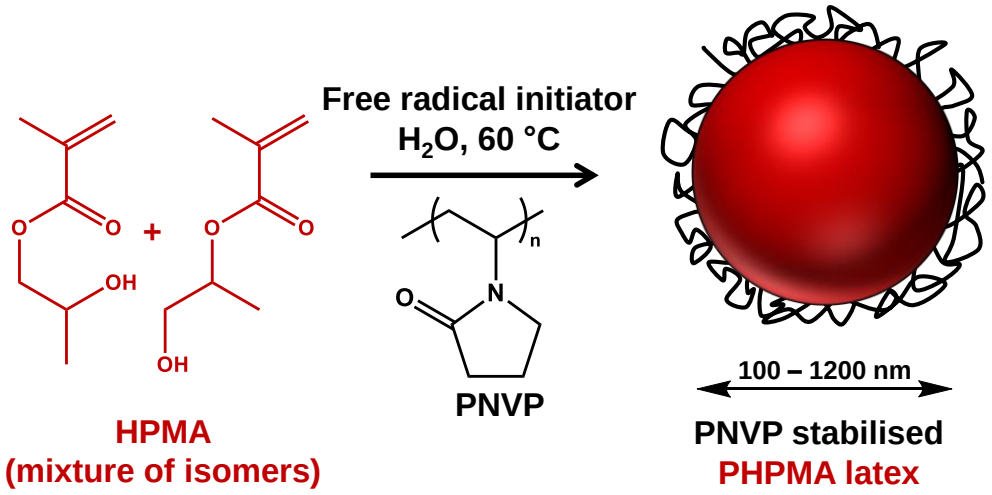

Figure 1.14 Schematic representation of the free radical aqueous dispersion polymerisation of 2-hydroxypropyl methacrylate (HPMA) using a poly(*N*-vinylpyrrolidone) as the stabiliser.[119]

By varying these parameters, mean particle diameters ranging from 100 to 1200 nm could be obtained. HPLC analysis of the HPMA batch used by Ali *et al* found the dimethacrylate content to be 0.1-0.2 mol%. As a result of this light cross-linking, these PHPMA latexes exhibited high degrees of swelling when diluted in methanol, which is a good solvent for both the PNVP and PHPMA chains.

The extent of research into conventional aqueous emulsion polymerisation is far greater than that for dispersion polymerisation, as the library of vinyl monomers that fulfil emulsion polymerisation conditions is far greater. Although aqueous emulsion polymerisation is prevalent in the scientific literature,[120] it lies outside the scope of this thesis and will not be discussed further.

1.5 Polymerisation-Induced Self-Assembly (PISA)

Polymerisation-induced self-assembly (PISA) is simplistic in concept, straightforward to implement but a nevertheless remarkably versatile method for accessing functional diblock copolymer nanoparticles (Figure 1.15). The basis of PISA is the chain extension of a soluble homopolymer with a second monomer to yield an insoluble polymer, driving *in-situ* self-assembly to form polymeric nanoparticles. Since the first report in 2002 by Ferguson *et al*,[121] the remarkable upsurge in popularity of PISA has been demonstrated by the rapidly growing volume of literature now available.[76, 122-127] One reason that PISA has gained such attention is that it overcomes the problem of high dilution, as syntheses can be conducted at high solids (up to 50% w/w). This is orders of magnitude greater than those allowed by traditional post-polymerisation processing techniques.[128] Furthermore, highly atom-efficient one-pot reactions have been reported, further enhancing the industrial utility of PISA.[78, 129-131]

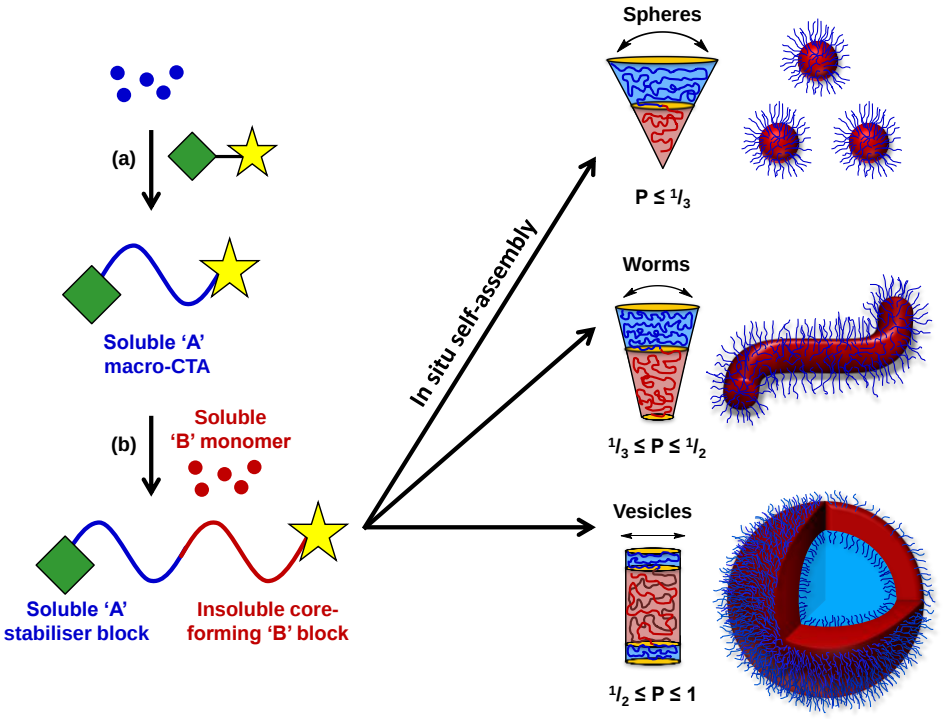

Figure 1.15 Schematic representation of a typical PISA synthesis: (a) RAFT solution polymerisation of monomer A to form a soluble macro-CTA followed by (b) soluble monomer in a RAFT dispersion polymerisation formulation to form block copolymer nanoparticles *in situ*. The green diamond and yellow star represent RAFT agent chain-ends.

In a dispersion polymerisation the monomer is soluble in the chosen solvent but the resulting polymer becomes insoluble, thus driving the *in situ* formation of nanoparticles. It should be noted that the initial soluble homopolymer employed in PISA syntheses becomes the steric stabiliser of the resulting nanoparticles. Unlike conventional aqueous dispersion (or emulsion) polymerisation, no additional stabilising agent (e.g. macromonomer or surfactant) is required. In principle, any of the RDRP techniques discussed in Section 1.2.3 can be used to prepare functional nanoparticles by PISA. However, in conventional ATRP, low levels of cross-linker are copolymerised at the start of the polymerisation to allow contaminant metal catalyst removal *via* dialysis, but this hinders the particle morphologies accessible.[132, 133] Advances in lowering the metal catalyst concentrations *via* ICAR-ATRP[133] are currently being examined in ATRP-mediated PISA. NMP has been seldom used in PISA syntheses but some examples of preparing

spheres,[134, 135] fibres[136] and vesicles[137] have been reported. In these NMP-mediated PISA examples, the block copolymer composition has unfortunately comprised a methacrylate-styrene statistical copolymer for reasons explained in section 1.2.3.1. A purely methacrylic NMP PISA formulation is yet to be reported.

By far the most popular and well-researched PISA technique is RAFT-mediated PISA.[138] As discussed in section 1.2.3.3, RAFT polymerisation allows the facile polymerisation of functional monomers (including methacrylates) in various solvents. Furthermore, it is straightforward to prepare multi-block copolymers.[139-142] RAFT-mediated PISA allows the preparation of spheres, worms and vesicles and can be conducted under a wide range of conditions such as dispersion polymerisation in aqueous media,[77, 143-153] lower alcohols,[154-158] *n*-alkanes[76, 159-163] and ionic liquids.[164, 165] RAFT-mediated aqueous emulsion polymerisation tends to result in the formation of spherical nanoparticles.[128, 166-168] Exceptionally, Charleux and co-workers have managed to prepare "nanofibers" (worms)[169] and vesicles.[170, 171] More recently, Cockram *et al.* reported a new, remarkable 'monkey-nut' morphology.[172] Research is currently being undertaken to investigate the effect of monomer solubility on the particle morphology. RAFT aqueous emulsion, alcoholic and *n*-alkane dispersion polymerisations are outside of the scope of this thesis. Chapters 2, 3, 4 and 5 are based solely on RAFT aqueous dispersion polymerisation so this topic warrants further discussion.

1.5.1 PISA by RAFT Aqueous Dispersion Polymerisation

In principle, any water soluble macro-CTA can act as a stabiliser during a PISA synthesis if steric and/or electrostatic stabilisation is conferred. Since 2002, numerous PISA publications have described the use of various non-ionic,[124, 145] cationic,[147, 173, 174] anionic[148, 175] and zwitterionic[144, 176] stabiliser blocks in RAFT-meditated aqueous dispersion polymerisation (Figure 1.16a).

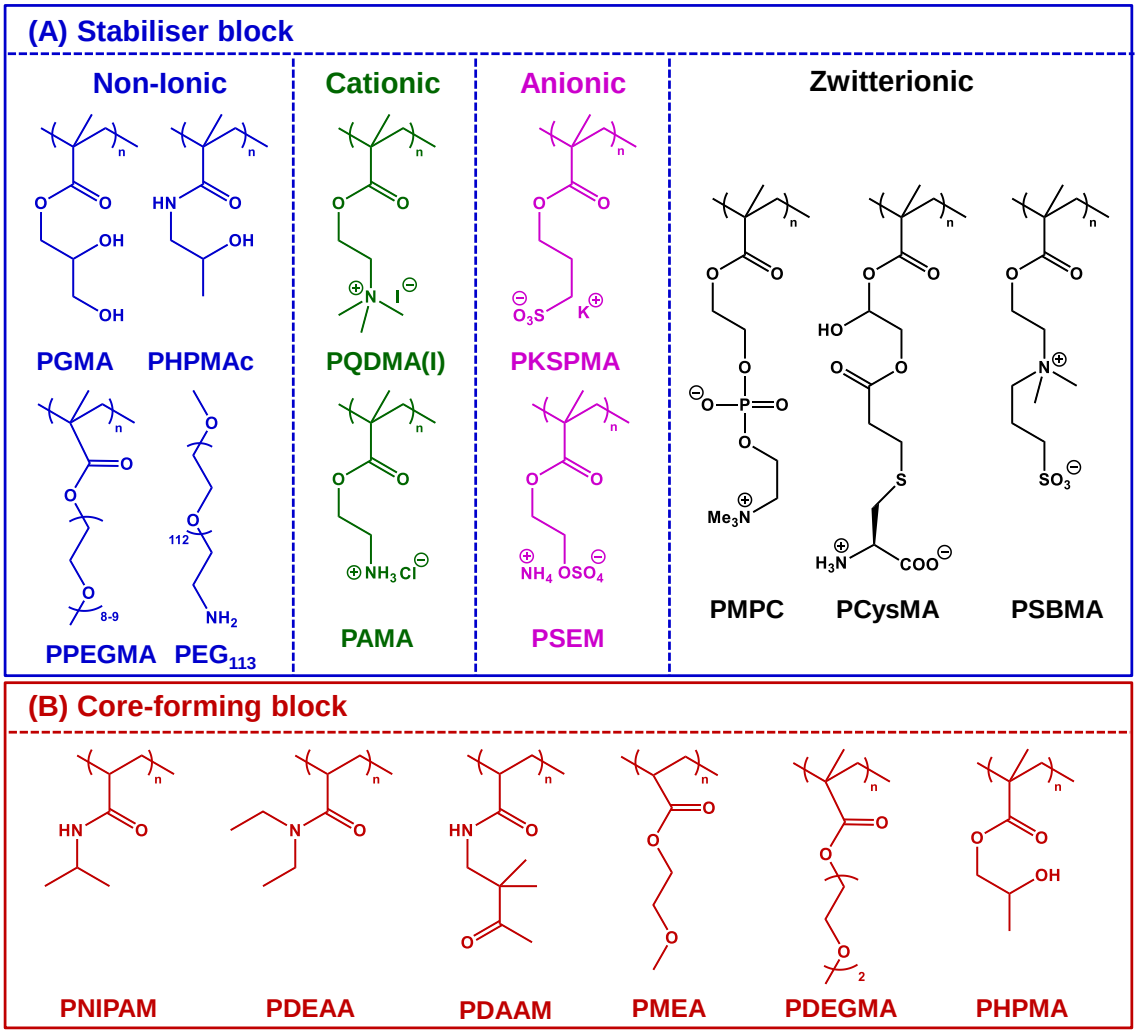

Figure 1.16 Chemical structures of various stabiliser and core-forming blocks that have been employed in RAFT aqueous dispersion polymerisation to form block copolymer nanoparticles *via* PISA. (A) Stabiliser blocks: poly(2-aminoethyl methacrylate) (PAMA),[173] poly(L-cysteine-based methacrylate) (PCysMA),[176] poly(ethylene glycol mono-amine) (PEG_{113}),[145] poly(glycerol monomethacrylate) (PGMA),[146] poly(2-hydroxypropyl methacrylamide) (PHPMAC),[177] poly(potassium 3-sulfopropyl methacrylate) (PKSPMA),[148] poly(2-(methacryloyloxy)ethyl phosphorylcholine) (PMPC),[144] poly(poly(ethylene glycol) methyl ether methacrylate) (PPEGMA),[178, 179] poly(2-(methacryloyloxy)ethyl)trimethylammonium iodide (PQDMA(I)),[147] poly(2-(methacryloyloxy)ethyl dimethyl-(3-sulfopropyl)ammonium hydroxide) (PSBMA),[180] poly(ammonium 2-sulfatoethyl methacrylate) (PSEM).[181] (B) Core-forming blocks: (poly(diacetone acrylamide) (PDAAM),[177, 182] poly(*N*,*N*′-diethyl acrylamide) (PDEAA),[183] poly(di(ethylene glycol) methyl ether methacrylate (PDEGMA),[178] poly(2-methoxyethyl acrylate) (PMEA),[179] poly(2-hydroxypropyl) methacrylate) (PHPMA),[146, 151, 152] poly(*N*-isopropylacrylamide) (PNIPAM)[117]

In contrast, there are relatively few core-forming monomers that satisfy the criteria for aqueous dispersion polymerisation. To date only six monomers have been reported (Figure 1.16b). [182] PDAAM is a particularly interesting core-forming block as it possesses latent reactive ketone functionality. Introducing such functionality into the core of the nanoparticles should enable post-PISA reactions such as core cross-linking to be conducted. The literature PISA examples that are most relevant to the work described in this thesis, particularly those employing PHPMA as the core forming block, will be discussed in the next section.

1.5.1.1 Non-Ionic Stabiliser Nanoparticles

In 2007 the first report of RAFT aqueous dispersion polymerisation was published by An *et al*.[117] Poly(*N*,*N*′-dimethylacrylamide)-poly(*N*-isopropylacrylamide) (PDMAAM-PNIPAM) diblock copolymer spheres were prepared using microwave irradiation at 70 °C (Figure 1.17).

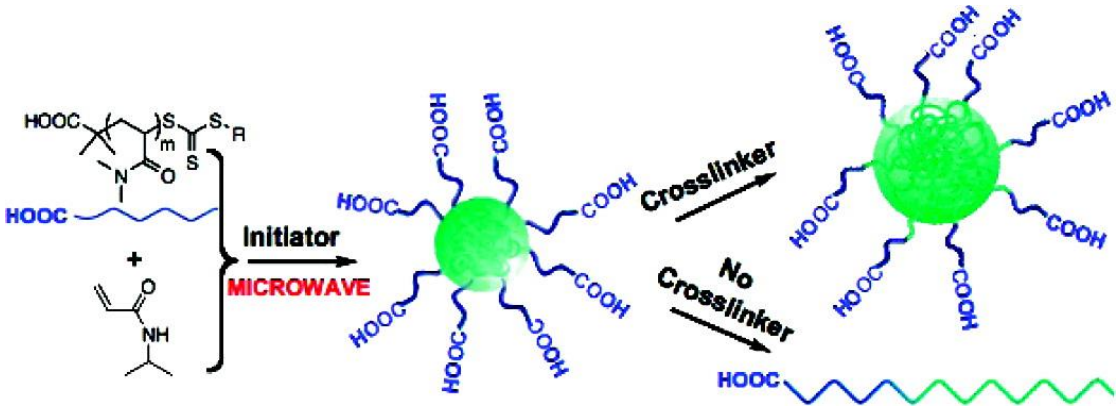

Figure 1.17 Schematic representation of the synthesis of poly(*N*,*N*′-dimethylacrylamide)-poly(*N*-isopropylacrylamide) (PDMAAM-PNIPAM) diblock copolymer spheres by the RAFT aqueous dispersion polymerisation of *N*-isopropylacrylamide at 70 °C. Sphere stabilisation was achieved by addition of a bisacrylamide cross-linking agent at 70 °C. Reproduced with permission from reference 117.

However, when these aqueous dispersions were cooled from 70 °C to room temperature, molecular dissolution of the copolymer chains occurred as PNIPAM exhibits inverse

temperature solubility. When synthesised by FRP, PNIPAM homopolymer has a lower critical solution temperature (LCST) of approximately 32 °C.[184] However, for PNIPAM prepared by RDRP techniques, its LCST temperature has been shown to be dependent on both molecular weight[185] and end-group functionality.[186] Nevertheless, addition of the diacrylamide cross-linker *N*,*N*′-methylenebisacrylamide at 70 °C enabled sufficient cross-linking to be achieved such that sterically-stabilised spheres were stable at room temperature in the form of nanogels. In 2010, Li and Armes[146] reported that the chain extension of a poly(glycerol monomethacrylate) ($PGMA_{65}$) macro-CTA with a mean degree of polymerisation (DP_n of 65, with HPMA led to the formation of exclusively spherical nanoparticles at 10% w/w solids (Figure 1.18a).

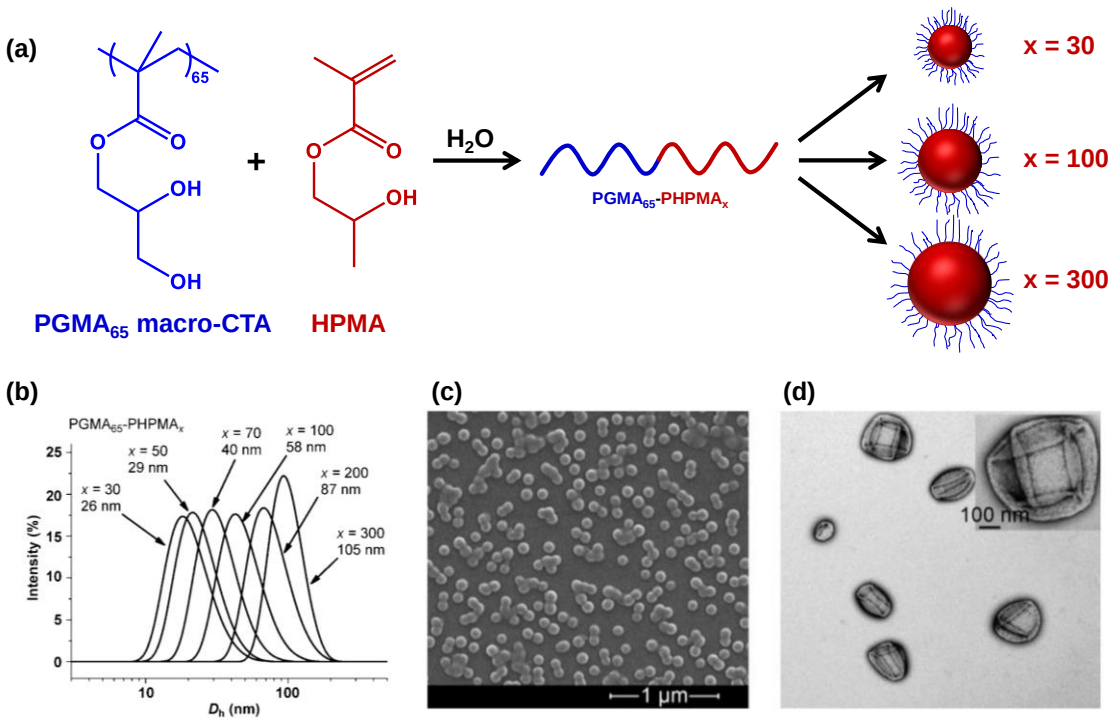

Figure 1.18 (a) Schematic cartoon representing the synthetic route for preparing $PGMA_{65}$-$PHPMA_x$ diblock copolymer spheres by RAFT aqueous dispersion polymerisation of HPMA in the presence of a $PGMA_{65}$ macro-CTA at 10% w/w solids. (b) Dynamic light scattering particle size distributions obtained for these spherical nanoparticles. Representative electron microscopy images obtained for $PGMA_{65}$-$PHPMA_{300}$ diblock copolymer (c) spheres and (d) vesicles prepared at 10% and 20% w/w solids, respectively.[146]

Moreover, by systematically increasing the target PHPMA block DP_n from 30 to 300, a monotonic increase in spherical hydrodynamic diameter from 26 nm to 105 nm was observed, as judged by dynamic light scattering (DLS), see Figure 1.18b. Moreover, the PISA synthesis of $PGMA_{65}$-$PHPMA_{300}$ at higher solids (20% w/w) resulted in the formation of polydisperse vesicles rather than near-monodisperse spheres (Figure 1.18c and d). This observation was important because it demonstrated that the diblock copolymer morphology depends on the synthesis conditions. Revisiting this aqueous dispersion formulation, Blanazs *et al.* published three phase diagrams using PGMA macro-CTAs with DP_ns of 47, 78 and 112, respectively (Figure 1.19).[151] These phase diagrams are constructed by preparing a series of PGMA-PHPMA diblock copolymers with varying PHPMA DP_n and copolymer concentrations, then assigning a morphology to each formulation based on post-polymerisation transmission electron microscopy (TEM) analysis. Assuming that dilution has no effect on the nanoparticle morphology, this approach enables the relationship between the block copolymer morphology, the synthesis concentration and the core-forming DP_n to be explored. Thus each phase diagram is constructed for a particular macro-CTA DP_n. Each macro-CTA is synthesised on a sufficiently large scale to allow construction of a detailed phase diagram. This approach minimises the experimental uncertainty that would be introduced if different macro-CTA batches were employed.[77]

The $PGMA_{47}$ phase diagram is shown in Figure 1.19a. Firstly, there is no concentration dependence for the copolymer morphology. Secondly, on increasing the core-forming PHPMA DP_n, the morphology evolves from spheres to linear worms, to branched worms and finally to vesicles. Increasing the core-forming DP_n, while keeping the stabiliser block DP_n constant, results in an increase in the relative volume fraction of the core-forming block. Hence, the packing parameter *P* increases with the PHPMA DP, which favours the formation of higher order morphologies (worms or vesicles).

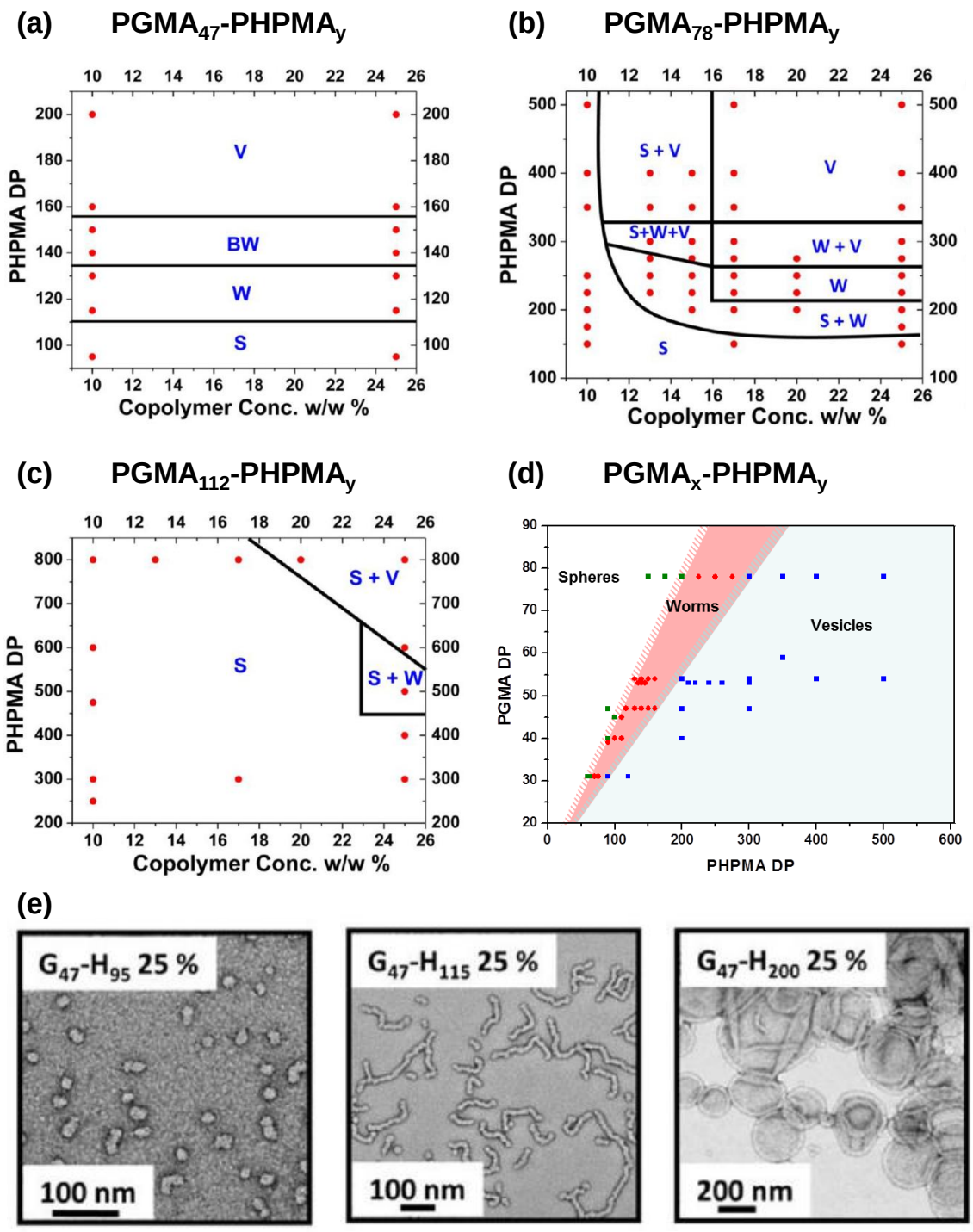

Figure 1.19 Three $PGMA_x$-$PHPMA_y$ phase diagrams constructed by Blanazs *et al*. where the $PGMA_x$ macro-CTA DP_n is varied such that x = (a) 47, (b) 78 and (c) 112. (d) A master phase diagram of PGMA DP_n vs PHPMA DP_n is also shown. (e) Representative transmission electron microscopy images obtained for $PGMA_{47}$-$PHPMA_y$ spheres (Y = 95), worms (Y = 115) and vesicles (Y = 200) prepared at 25% w/w solids.[151]

Conversely, in the case of the $PGMA_{78}$ phase diagram (Figure 1.19b) only spherical nanoparticles are obtained at a copolymer concentration of 10% w/w, regardless of the PHPMA DP_n. Blanazs *et al.*[151] argued that for a longer stabiliser block, a longer core-forming PHPMA block is required for the same molecular curvature. However, longer core-forming blocks are more hydrophobic and dehydrated, thus reducing their mobility during PISA synthesis and potentially inhibiting evolution in morphology. Thus, the $PGMA_{78}$-$PHPMA_{500}$ spheres prepared at 10% w/w are kinetically-trapped. Importantly, this problem can be overcome by increasing the initial HPMA concentration. At intermediate monomer conversions, unreacted HPMA monomer migrates into the core of the particles and plasticises the PHPMA chains, increasing chain mobility and allowing morphology evolution.

This is shown in the $PGMA_{78}$ phase diagram by the presence of three pure phase spaces corresponding to spheres, worms and vesicles at solids concentrations above 17% w/w. In PISA formulations, the worm phase is typically quite narrow relative to the sphere and vesicle phase space. For the $PGMA_{47}$ phase diagram the width of the worm phase is approximately 50 units of HPMA while the sphere and vesicular phases are much larger. The phase diagram for $PGMA_{112}$ is far simpler than the $PGMA_{47}$ and $PGMA_{78}$ phase diagrams (Figure 1.19c). Only spherical micelles are observed up to a PHPMA DP_n of 800 and for copolymer concentrations of 15% w/w, although higher order morphologies are accessible as mixed phases at or above 20% w/w and above. As stated earlier, kinetic trapping of the spheres prevents the formation of worms and vesicles. By collating all the data from these phase diagrams (and other PISA syntheses not reported by Blanazs *et al.*) a master phase diagram can be constructed (Figure 1.19d). This phase diagram shows the relationship of stabiliser DP_n and core-forming block DP_n on particle morphology. Together, these four phase diagrams show how to reproducibly target spheres, worms or vesicles for the PGMA-PHPMA formulation.

Blanazs *et al* extended their work with this PISA formulation by examining the kinetics and mechanism of vesicle formation.[152] $PGMA_{47}$-$PHPMA_{200}$ vesicles was prepared at 70 °C and 10% w/w solids. Aliquots were removed during the PISA synthesis and analysed by ^{1}H nuclear magnetic resonance (NMR) spectroscopy and TEM to calculate monomer conversion and assign copolymer morphology, respectively (Figure 1.20). During the first 60 min the reaction proceeds by RAFT aqueous solution polymerisation, resulting in molecularly-dissolved copolymer chains. However, at a conversion of ≈ 45% (corresponding to a PHPMA DP_n of 90) micellar nucleation is observed, denoted by the nascent spheres (Figure 1.20a). A five-fold rate increase is observed (Figure 1.20a inset) as unreacted HPMA monomer enters the micelle cores and acts as a co-solvent for the growing PHPMA chains, leading to a relatively high local monomer concentration. Almost complete monomer conversion is achieved after 2 h at 70 °C, resulting in a pure vesicular phase. The most interesting aspect of this report is the suggested mechanism of vesicle formation. Nascent spherical micelles are initially formed that then undergo sphere-sphere fusion to form dimers, trimers etc. Eventually short worms are formed that subsequently develop branch points as shown in Figure 1.20b, which ultimately transform into vesicles *via* transient bilayer octopuses and jellyfish intermediates. Such jellyfish structures have also been observed during the post-polymerisation processing of PMPC-PDPA diblock copolymers, suggesting that this is a generic mechanism of vesicle formation and not an unusual feature that is unique to PISA.[77]

Blanazs and co-workers prepared similar $PGMA_{54}$-$PHPMA_{140}$ diblock copolymers that self-assemble into worm-like micelles. At sufficiently high copolymer concentrations (typically > 4% w/w) these worm dispersions form soft free-standing gels at room temperature due to multiple inter-worm contacts[149, 150] Somewhat counterintuitively, these soft gels undergo a gel-sol transition to produce a free-flowing liquid on cooling to 4 °C (Figure 1.21a).

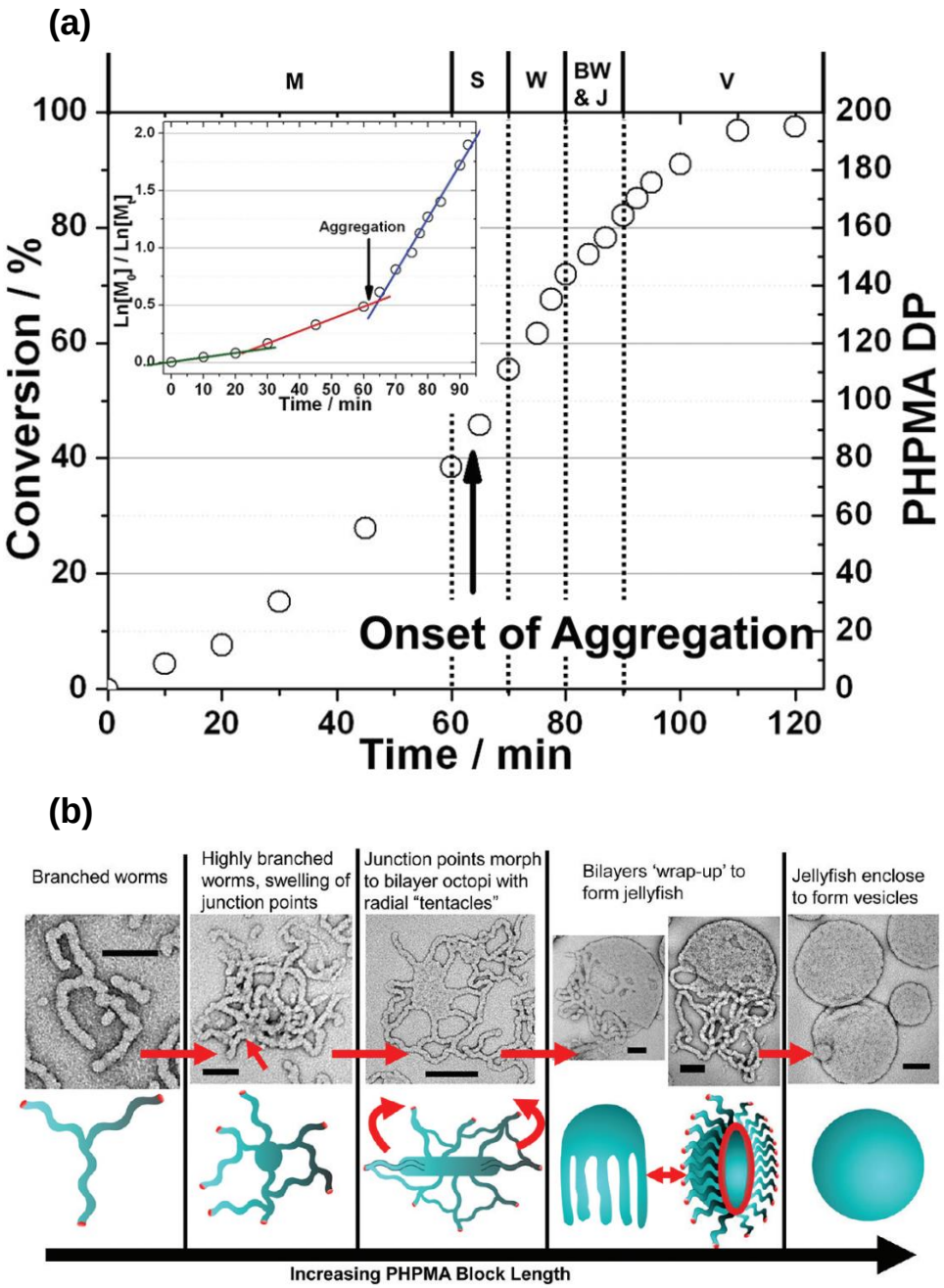

Figure 1.20 (a) Monomer conversion (and the corresponding effective PHPMA DP_n for a given conversion) vs time plot for the synthesis of $PGMA_{47}$-$PHPMA_{200}$ vesicles by the RAFT aqueous dispersion polymerisation of HPMA at 10% w/w solids and 70 °C. Five morphology regions are shown as determined by TEM studies. The inset is the semi-logarithmic vs time plot. (b) Suggested mechanism for the *in situ* worm-to-vesicle morphological transition through jellyfish intermediates. Abbreviations: M = molecularly dissolved chains, S = spheres, W = worms, BW = branched worms, J = jellyfish, V = vesicles.

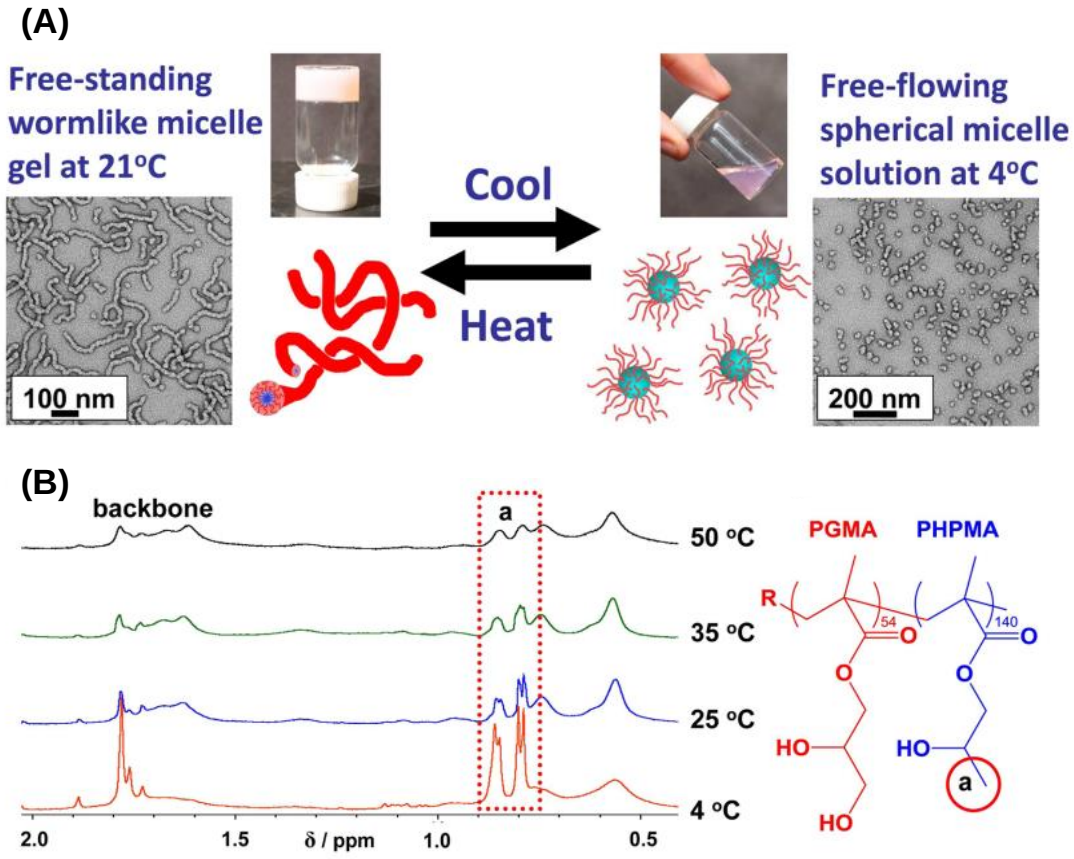

Figure 1.21 (a) Digital photograph, schematic cartoon and TEM images for 10% w/w $PGMA_{54}$-$PHPMA_{140}$ diblock copolymer worm gel undergoing a reversible worm-to-sphere transition on cooling from 25 °C to 4 °C. (b) Partial temperature dependent ^{1}H NMR spectra recorded as a function of temperature for the same diblock copolymer between 4 °C and 50 °C.[149]

TEM studies at this temperature indicated that a worm-to-sphere morphology transition occurred (Figure 1.21a). On returning to 25 °C, a sphere-to-worm and thus a sol-gel transition occurred. Variable temperature ^{1}H NMR studies were conducted on this worm gel at 10% w/w solids (Figure 1.21b). At lower temperatures, an increase in the intensity of the pendent methyl protons of the HPMA residues (highlighted by the red dashed rectangle) indicated a greater degree of hydration. If equal hydration across the whole PHPMA block occurred, the result would be in an increase in *P* and a worm-to-vesicle transition, but this is not observed experimentally. Instead, applying the packing parameter argument, surface plasticisation near

the PGMA-PHPMA block junction must occur, thus increasing the volume fraction of the stabiliser block, while reducing the volume fraction of the core and reducing so the value of *P*. This explanation accounts for the observed worm-to-sphere transition. Armes and co-workers have published numerous reports on the PGMA-PHPMA formulation[78, 187] with the most interesting applications including the cryopreservation of red blood cells[188] and the unexpected ability of worm hydrogels to induce stasis in human pluripotent stem cells.[189]

Another water-soluble macro-CTA that has been successfully chain-extended with HPMA under RAFT aqueous dispersion conditions is poly(ethylene oxide) (PEO).[145] PEO is an attractive polymer to use because of its biocompatibility, commercial availability, viability to industry and low cost. Furthermore, monomethoxy-terminated PEO (MeO-PEO-OH) can be purchased with predefined molecular weights of 2 kg mol^{-1}, 5 kg mol^{-1} or 10 kg mol^{-1}, corresponding to DP_ns of 45, 113 and 226, respectively. Although RAFT polymerisation allows the preparation of copolymers with predefined DP_ns, in practise it is actually quite difficult to prepare two macro-CTAs with an identical DP_n. Therefore, converting well-defined PEO into a RAFT agent is an attractive route for ensuring the same molecular weight when preparing several different batches of the same macro-CTA. Warren *et al.*[145] functionalised monomethoxy PEO_{113} (MeO-PEO_{113}-OH) into monoaminated PEO_{113} (MeO-PEO_{113}-NH_2) and reacted this with the succinimide ester of the RAFT agent 4-cyano-4-(phenylcarbonothioylthio) pentanoic acid (CPADB) to yield a PEO_{113} macro-CTA (Figure **1.22**).

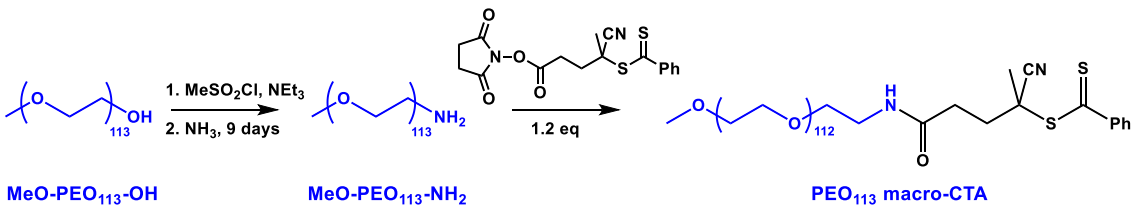

Figure 1.22 Synthetic route used by Warren *et al*. to prepare a PEO_{113} macro-CTA.[145]

A relatively high end-group functionality of 95% was achieved. Chain-extension with HPMA produced amphiphilic PEG_{113}-$PHPMA_y$ diblock copolymers (Figure 1.23 a) *via* RAFT-mediated PISA and a phase diagram was constructed (Figure 1.23 b) in a similar fashion to the PGMA-PHPMA examples discussed earlier.

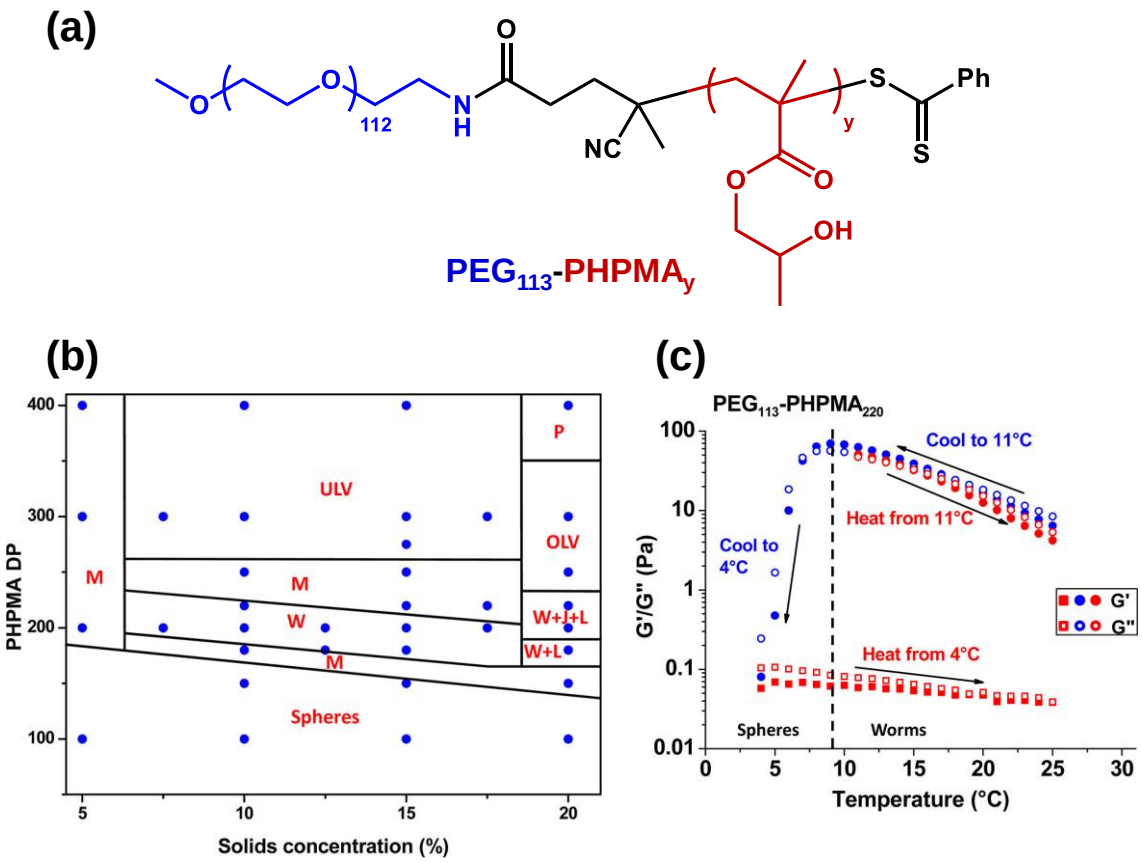

Figure 1.23 (a) Generic chemical structure of a PEG_{113}-$PHPMA_y$ diblock copolymer. (b) Phase diagram constructed for such copolymers prepared by the RAFT aqueous dispersion of HPMA. (c) Temperature-dependent oscillatory rheological studies for PEG_{113}-$PHPMA_{220}$ worm gels at 10% w/w showing the irreversible gel-sol transition that occurs on cooling from 25 °C to 4 °C and returning to 25 °C. Abbreviations: W = worms, M = mixed phase, ULV = unilamellar vesicles, J = jellyfish, L = lamella, OLV = oligolamellar vesicles and P = precipitate.

Pure phases of spheres, worms and unilamellar vesicles are obtained by increasing the target PHPMA DP_n, as expected. Either side of the pure phases are mixed phases, comprising either

spheres and worms or worms and vesicles. It should be noted that the worm phase is, again, rather narrow. A new oligolamellar vesicular phase was also identified at high copolymer concentrations.

Unlike the thermoreversible behaviour exhibited by the PGMA-PHPMA worm gels, PEG_{113}-$PHPMA_{220}$ worm gels undergo an irreversible worm-to-sphere transition at 10% w/w solids upon cooling from 25 °C to 4°C, as shown by the temperature-dependent rheological studies shown in Figure 1.23c. No explanation was offered as to why this transition is irreversible. However, Warren *et al.* did report that a reduction in vesicle polydispersity could be achieved by cooling PEG_{113}-$PHPMA_{300}$ vesicles at 10% w/w to 2 °C then heating at 50°C for 24 h.[145]

1.5.1.2 Polyelectrolyte Stabiliser Nanoparticles

In 2012 Semsarilar *et al.* published two complementary PISA papers detailing the synthesis of polyelectrolyte-stabilised nanoparticles.[147, 148] A cationic poly[2-(methacryloyloxy)ethyl] trimethylammonium iodide (PQDMA(I)) macro-CTA with a DP_n of 32 and an anionic poly(potassium 3-sulfopropyl methacrylate) macro-CTA with a DP_n of 34 were prepared by RAFT aqueous solution polymerisation. However, only spherical micelles were produced on chain-extension of either polyelectrolytic macro-CTA using HPMA in water, regardless of PHPMA DP_n or solids concentration. This was attributed to the strong lateral electrostatic repulsion between neighbouring stabiliser chains hindering the formation of higher order morphologies. Addition of 0.3 M NaCl to the reaction solution resulted in the formation of less polydisperse spheres, but worms and vesicles were still not accessible. The authors examined two strategies to reduce the charge density of the stabiliser block in order access higher order charged morphologies: (i) copolymerisation of a non-ionic monomer with the electrolyte monomer to generate a statistical macro-CTA or (ii) using a binary mixture of a non-ionic

macro-CTA with the polyelectrolytic PQDMA(I)$_{32}$ (Figure 1.24a) or PKSPMA$_{34}$ stabiliser block.

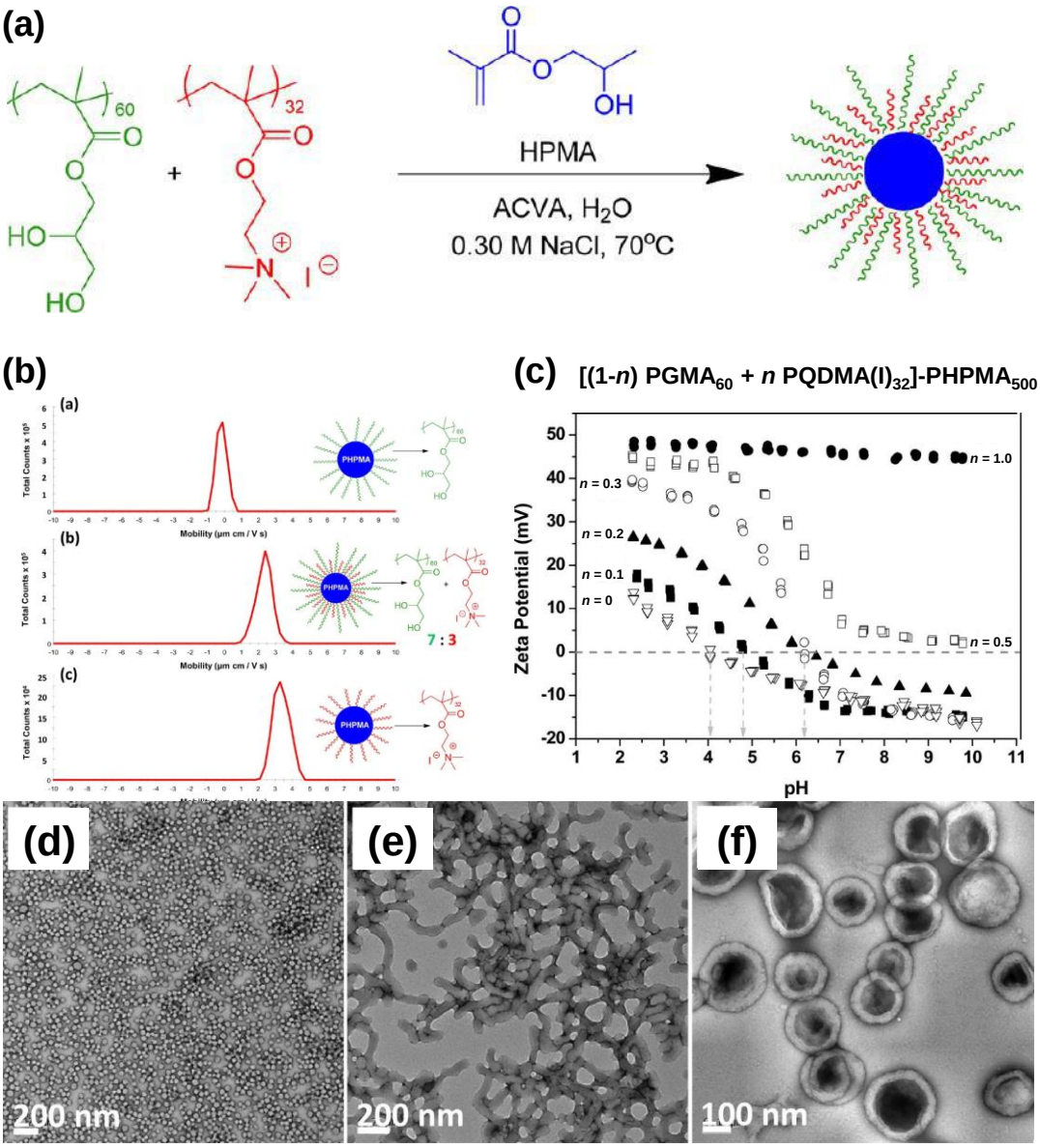

Figure 1.24 (a) Reaction scheme for the RAFT aqueous dispersion polymerisation of HPMA to afford cationic nanoparticles using a non-ionic PGMA$_{60}$ and cationic PQDMA(I)$_{32}$ macro-CTA in the presence of 0.3 M NaCl. (b) Electrophoretic mobility traces obtained for PGMA$_{50}$-PHPMA$_{500}$, (0.7 PGMA$_{60}$ + 0.3 PQDMA(I)$_{32}$)-PHPMA$_{500}$ and PQDMA(I)$_{32}$-PHPMA$_{500}$ nanoparticles. (c) Aqueous electrophoresis vs pH curves obtained for [(1-*n*) PGMA$_{60}$ + *n* PQDMA(I)$_{32}$]-PHPMA$_{500}$ nanoparticles. Representative TEM images obtained for (d) (0.5 PQDMA$_{32}$ + 0.5 PGMA$_{60}$)-PHPMA$_{500}$ spheres, (e) (0.2 PQDMA$_{32}$ + 0.8 PGMA$_{60}$)-PHPMA$_{500}$ worms and (f) (0.1 PQDMA$_{32}$ + 0.9 PGMA$_{60}$)-PHPMA$_{500}$ vesicles. All nanoparticles were prepared at 10% w/w solids in the presence of 0.3M NaCl.[147]

Both approaches allowed access to higher order morphologies but the binary mixture approach has offered added benefit of being able to fine-tune the molar ratio of the ionic/non-ionic macro-CTAs and hence the aqueous electrophoretic behaviour of the nanoparticles.

To confirm entropic mixing of the types of two macro-CTAs in the corona, aqueous electrophoretic mobility studies were undertaken at pH 4 (Figure 1.24b). The following example is for cationic nanoparticles. As a control, purely non-ionic $PGMA_{60}$-$PHPMA_{500}$ nanoparticles were prepared and exhibited essentially zero electrophoretic mobility. In contrast, $PQDMA(I)_{32}$-$PHPMA_{500}$ nanoparticles exhibit a high electrophoretic mobility of approximately + 3.5 μm cm/V s. Crucially, nanoparticles comprising (0.7 $PGMA_{60}$ + 0.3 $PQDMA(I)_{32}$)-$PHPMA_{500}$ exhibit an intermediate mobility of + 2.5 μm cm/V s, thus indicating entropic mixing. The binary macro-CTA mixture approach is particularly attractive as it provides a simple method for controlling the electrophoretic footprint of nanoparticles by simply adjusting the ionic/non-ionic stabiliser molar ratio. However, adjusting the dispersion pH to above 7, such nanoparticles surprisingly lose all of their cationic character and, in most cases, become weakly anionic. Although no explanation was offered by the authors, it seems likely that the terminal carboxylic acid group on the $PQDMA(I)_{32}$ stabiliser chain-end contributed to this weakly anionic character

1.6 Thesis Outline

This thesis focuses exclusively on the PISA synthesis of diblock copolymer nano-objects by RAFT aqueous dispersion polymerisation. There are two themes in this thesis. Firstly, essentially non-ionic PGMA-PHPMA diblock copolymer worms (Chapter 2) and vesicles (Chapter 3) are prepared at pH 7 using a new morpholine-functionalised RAFT agent. The morpholine group is located at the terminus of the stabiliser block and confers pH-responsive behaviour on these nanoparticles. Furthermore, in Chapter 3 the dual stimulus-responsive

behaviour of diblock copolymer vesicles with respect to pH and temperature is investigated. The second theme in this thesis is the synthesis of polyelectrolyte-stabilised diblock copolymer worms. In Chapter 4 the cationic-stabilised nanoparticles reported by Semsarilar *et al.*[147] are revisited, and this approach is combined with the work of Warren *et al.*[145] on PEG-PHPMA nanoparticles to prepare new, pH-independent cationic worms. Core cross-linking of the cationic worms is explored to ensure colloidal stability in a common solvent for the constituent copolymers and in the presence of a cationic surfactant. Furthermore, both the non-cross-linked and core cross-linked cationic worms are examined as effective bridging flocculants for model micron-sized silica particles. Their flocculation ability is compared to a number of commercial flocculants. Chapter 5 describes the synthesis of complementary core cross-linked anionic worms. Again, these worms are expected to exhibit pH-independent anionic character. The preparation of oppositely-charged worms gives rise to the opportunity to investigate and visualise the layer-by-layer assembly of polyelectrolytic worms onto planar surfaces.

1.7 References

1. G. Odian, *Principles of Polymerization*, Wiley, New Jersey, 4th edn., 2004.
2. J. M. G. Cowie, *Polymers: Chemistry & Physics of Modern Materials*, Nelson Thornes, Cheltenham, 2nd edn., 2001.
3. W. H. Carothers, *Journal of the American Chemical Society*, 1929, **51**, 2548.
4. P. J. Flory, *Principles of Polymer Chemistry*, Cornell University Press, Ithaca and London, 1st edn., 1953.
5. R. G. Gilbert, M. Hess, A. D. Jenkins, R. G. Jones, P. Kratochvil, R. F. T. Stepto, M. Baron, T. Kitayama, G. Allegra, T. Chang, C. dos Santos, A. Fradet, K. Hatada, J. He, K. H. Hellwich, R. C. Hiorns, P. Hodge, K. Horie, J. I. Jin, J. Kahovec, P. Kubisa, I. Meisel, W. V. Metanomski, V. Meille, I. Mita, G. Moad, W. Mormann, C. Ober, S. Penczek, L. P. Rebelo, M. Rinaudo, I. Schopov, M. Schubert, F. Schue, V. P. Shibaev, S. Slomkowski, D. Tabak, J. P. Vairon, M. Vert, J. Vohlidal, E. S. Wilks and W. J. Work, *Pure and Applied Chemistry*, 2009, **81**, 351.
6. S. R. Holding and E. Meehan, *Molecular Weight Characterisation of Synthetic Polymers*, Rapra Technology Ltd, Shrewsbury, 1995.
7. P. C. Hiemenz and T. P. Lodge, *Polymer Chemistry*, CRC Press, New York, 2nd edn., 2007.
8. W. A. Braunecker and K. Matyjaszewski, *Progress in Polymer Science*, 2007, **32**, 93.
9. J. Chiefari, R. T. A. Mayadunne, C. L. Moad, G. Moad, E. Rizzardo, A. Postma and S. H. Thang, *Macromolecules*, 2003, **36**, 2273.

10. T. P. Le, G. Moad, E. Rizzardo and S. H. Thang, *Polymerization with living characteristics with controlled dispersity, polymers prepared thereby, and chain-transfer agents used in the same*, WO9801478A1, 1998.
11. R. P. Quirk and B. Lee, *Polymer International*, 1992, **27**, 359.
12. M. Szwarc, M. Levy and R. Milkovich, *Journal of the American Chemical Society*, 1956, **78**, 2656.
13. M. Szwarc, *Nature*, 1956, **178**, 1168.
14. T. Higashimura, M. Mitsuhashi and M. Sawamoto, *Macromolecules*, 1979, **12**, 178.
15. M. Miyamoto, M. Sawamoto and T. Higashimura, *Macromolecules*, 1984, **17**, 265.
16. O. W. Webster, W. R. Hertler, D. Y. Sogah, W. B. Farnham and T. V. RajanBabu, *Journal of the American Chemical Society*, 1983, **105**, 5706.
17. R. R. Schrock, J. Feldman, L. F. Cannizzo and R. H. Grubbs, *Macromolecules*, 1987, **20**, 1169.
18. C. W. Bielawski and R. H. Grubbs, *Progress in Polymer Science*, 2007, **32**, 1.
19. P. Schwab, R. H. Grubbs and J. W. Ziller, *Journal of the American Chemical Society*, 1996, **118**, 100.
20. A. D. Jenkins, R. G. Jones and G. Moad, *Pure and Applied Chemistry*, 2010, **82**, 483.
21. N. Hadjichristidis, H. Iatrou, M. Pitsikalis and J. Mays, *Progress in Polymer Science*, 2006, **31**, 1068.
22. Krzysztof Matyjaszewski, Yvs Gnanou and L. Leibler, *Macromolecular Engineering: Precise Synthesis, Materials Properties, Applications*, Wiley-VCH Verlag GmbH & Co. KGaA, Weinheim, Germany, Volume 1: Synthetic Techniques edn., 2007.
23. D. Greszta, D. Mardare and K. Matyjaszewski, *Macromolecules*, 1994, **27**, 638.
24. A. Goto and T. Fukuda, *Progress in Polymer Science*, 2004, **29**, 329.
25. H. Fischer, *Chemical Reviews*, 2001, **101**, 3581.
26. C. J. Hawker, A. W. Bosman and E. Harth, *Chemical Reviews*, 2001, **101**, 3661.
27. D. H. Solomon, E. Rizzardo and P. Cacioli, *Free radical polymerization and the produced polymers*, EP135280A2, 1985.
28. C. J. Hawker, G. G. Barclay, A. Orellana, J. Dao and W. Devonport, *Macromolecules*, 1996, **29**, 5245.
29. M. K. Georges, R. P. N. Veregin, P. M. Kazmaier and G. K. Hamer, *Macromolecules*, 1993, **26**, 2987.
30. J. Nicolas, B. Charleux, O. Guerret and S. Magnet, *Macromolecules*, 2005, **38**, 9963.
31. J. Qiu, B. Charleux and K. Matyjaszewski, *Progress in Polymer Science*, 2001, **26**, 2083.
32. J. Nicolas, Y. Guillaneuf, C. Lefay, D. Bertin, D. Gigmes and B. Charleux, *Progress in Polymer Science*, 2013, **38**, 63.
33. N. R. Cameron, O. Lagrille, P. A. Lovell and B. Thongnuanchan, *ACS Macro Letters*, 2012, **1**, 1262.
34. J. Nicolas, C. Dire, L. Mueller, J. Belleney, B. Charleux, S. R. A. Marque, D. Bertin, S. Magnet and L. Couvreur, *Macromolecules*, 2006, **39**, 8274.
35. M. Kato, M. Kamigaito, M. Sawamoto and T. Higashimura, *Macromolecules*, 1995, **28**, 1721.
36. J.-S. Wang and K. Matyjaszewski, *Journal of the American Chemical Society*, 1995, **117**, 5614.
37. K. Matyjaszewski, *Macromolecules*, 2012, **45**, 4015.
38. K. Matyjaszewski, T. E. Patten and J. Xia, *Journal of the American Chemical Society*, 1997, **119**, 674.
39. K. Ohno, A. Goto, T. Fukuda, J. Xia and K. Matyjaszewski, *Macromolecules*, 1998, **31**, 2699.

40. Y. A. Kabachii, S. Y. Kochev, L. M. Bronstein, I. B. Blagodatskikh and P. M. Valetsky, *Polymer Bulletin*, 2003, **50**, 271.
41. V. Percec, B. Barboiu, A. Neumann, J. C. Ronda and M. Zhao, *Macromolecules*, 1996, **29**, 3665.
42. K. Matyjaszewski, M. Wei, J. Xia and N. E. McDermott, *Macromolecules*, 1997, **30**, 8161.
43. M. Teodorescu, S. G. Gaynor and K. Matyjaszewski, *Macromolecules*, 2000, **33**, 2335.
44. G. Moineau, M. Minet, P. Dubois, P. Teyssie, T. Senninger and R. Jerome, *Macromolecules*, 1999, **32**, 27.
45. V. Coessens, T. Pintauer and K. Matyjaszewski, *Progress in Polymer Science*, 2001, **26**, 337.
46. J. Xia and K. Matyjaszewski, *Macromolecules*, 1997, **30**, 7697.
47. W. Jakubowski and K. Matyjaszewski, *Angewandte Chemie International Edition*, 2006, **45**, 4482.
48. K. Matyjaszewski, W. Jakubowski, K. Min, W. Tang, J. Huang, W. A. Braunecker and N. V. Tsarevsky, *Proceedings of the National Academy of Sciences of the United States of America*, 2006, **103**, 15309.
49. A. J. D. Magenau, N. C. Strandwitz, A. Gennaro and K. Matyjaszewski, *Science*, 2011, **332**, 81.
50. N. V. Tsarevsky and K. Matyjaszewski, *Chemical Reviews*, 2007, **107**, 2270.
51. T. Pintauer and K. Matyjaszewski, *Chemical Society Reviews*, 2008, **37**, 1087.
52. J. Chiefari, Y. K. Chong, F. Ercole, J. Krstina, J. Jeffery, T. P. T. Le, R. T. A. Mayadunne, G. F. Meijs, C. L. Moad, G. Moad, E. Rizzardo and S. H. Thang, *Macromolecules*, 1998, **31**, 5559.
53. C. Barner-Kowollik, *Handbook of RAFT Polymerisation*, Wiley-VCH Verlag CMBh & Co. KGaA, Weinheim, 2008.
54. A. A. Toy, H. Chaffey-Millar, T. P. Davis, M. H. Stenzel, E. I. Izgorodina, M. L. Coote and C. Barner-Kowollik, *Chemical Communications*, 2006, 835.
55. T. Junkers, M. H. Stenzel, T. P. Davis and C. Barner-Kowollik, *Macromolecular Rapid Communications*, 2007, **28**, 746.
56. T. Junkers, G. Delaittre, R. Chapman, F. Guenzler, E. Chernikova and C. Barner-Kowollik, *Macromolecular Rapid Communications*, 2012, **33**, 984.
57. M. Lansalot, C. Farcet, B. Charleux, J.-P. Vairon and R. Pirri, *Macromolecules*, 1999, **32**, 7354.
58. P. Lacroix-Desmazes, R. Severac and B. Boutevin, *Macromolecules*, 2005, **38**, 6299.
59. T. Junkers, *Journal of Polymer Science Part A: Polymer Chemistry*, 2011, **49**, 4154.
60. B. Klumperman, E. T. A. van den Dungen, J. P. A. Heuts and M. J. Monteiro, *Macromolecular Rapid Communications*, 2010, **31**, 1846.
61. G. Moad, E. Rizzardo and S. H. Thang, *Australian Journal of Chemistry*, 2006, **59**, 669.
62. G. Moad, E. Rizzardo and S. H. Thang, *Australian Journal of Chemistry*, 2009, **62**, 1402.
63. G. Moad, E. Rizzardo and S. H. Thang, *Accounts of Chemical Research*, 2008, **41**, 1133.
64. D. J. Keddie, G. Moad, E. Rizzardo and S. H. Thang, *Macromolecules*, 2012, **45**, 5321.
65. G. Moad, J. Chiefari, Y. K. Chong, J. Krstina, R. T. A. Mayadunne, A. Postma, E. Rizzardo and S. H. Thang, *Polymer International*, 2000, **49**, 993.
66. M. Benaglia, J. Chiefari, Y. K. Chong, G. Moad, E. Rizzardo and S. H. Thang, *Journal of the American Chemical Society*, 2009, **131**, 6914.
67. D. J. Keddie, C. Guerrero-Sanchez, G. Moad, R. J. Mulder, E. Rizzardo and S. H. Thang, *Macromolecules*, 2012, **45**, 4205.
68. J. Skey and R. K. O'Reilly, *Chemical Communications*, 2008, 4183.

69. B. V. K. J. Schmidt, M. Hetzer, H. Ritter and C. Barner-Kowollik, *Macromolecules*, 2011, **44**, 7220.
70. R. Severac, P. Lacroix-Desmazes and B. Boutevin, *Polymer International*, 2002, **51**, 1117.
71. A. Favier, M.-T. Charreyre, P. Chaumont and C. Pichot, *Macromolecules*, 2002, **35**, 8271.
72. G. Moad, Y. K. Chong, A. Postma, E. Rizzardo and S. H. Thang, *Polymer*, 2005, **46**, 8458.
73. G. Bouhadir, N. Legrand, B. Quiclet-Sire and S. Z. Zard, *Tetrahedron Letters*, 1999, **40**, 277.
74. S. H. Thang, Y. K. Chong, R. T. A. Mayadunne, G. Moad and E. Rizzardo, *Tetrahedron Letters*, 1999, **40**, 2435.
75. E. R. Jones, M. Semsarilar, A. Blanazs and S. P. Armes, *Macromolecules*, 2012, **45**, 5091.
76. M. J. Derry, L. A. Fielding and S. P. Armes, *Progress in Polymer Science*, 2016, **52**, 1.
77. N. J. Warren and S. P. Armes, *Journal of the American Chemical Society*, 2014, **136**, 10174.
78. L. P. D. Ratcliffe, A. J. Ryan and S. P. Armes, *Macromolecules*, 2013, **46**, 769.
79. G. Moad, E. Rizzardo and S. H. Thang, *Polymer International*, 2011, **60**, 9.
80. E. Rizzardo, M. Chen, B. Chong, G. Moad, M. Skidmore and S. H. Thang, *Macromolecular Symposia*, 2007, **248**, 104.
81. G. M. Whitesides and B. Grzybowski, *Science*, 2002, **295**, 2418.
82. D. Philp and J. F. Stoddart, *Angewandte Chemie International Edition*, 1996, **35**, 1155.
83. C. De Rosa, C. Park, E. L. Thomas and B. Lotz, *Nature*, 2000, **405**, 433.
84. L. Zhang and A. Eisenberg, *Science*, 1995, **268**, 1728.
85. E. Arunan, G. R. Desiraju, R. A. Klein, J. Sadlej, S. Scheiner, I. Alkorta, D. C. Clary, R. H. Crabtree, J. J. Dannenberg, P. Hobza, H. G. Kjaergaard, A. C. Legon, B. Mennucci and D. J. Nesbitt, *Pure and Applied Chemistry*, 2011, **83**, 1619.
86. C. B. Aakeroy and K. R. Seddon, *Chemical Society Reviews*, 1993, **22**, 397.
87. L. Slade and H. Levine, *Critical Reviews in Food Science and Nutrition*, 1991, **30**, 115.
88. D. Chandler, *Nature*, 2005, **437**, 640.
89. H. Schober, H. Itoh, A. Klapproth, V. Chihaia and W. F. Kuhs, *European Physics Journal E*, 2003, **12**, 41.
90. C. Tanford, *Science*, 1978, **200**, 1012.
91. E. Dickinson, *Soft Matter*, 2006, **2**, 642.
92. J. N. Israelachvili, *Intermolecular & Surface Forces*, Academic Press, London, 2nd edn., 1991.
93. Z. Chu, C. A. Dreiss and Y. Feng, *Chemical Society Reviews*, 2013, **42**, 7174.
94. C. Tanford, *The Hydrophobic Effect*, Wiley, New York, 1980.
95. S. Puvvada and D. Blankschtein, *Journal of Chemical Physics*, 1990, **92**, 3710.
96. J. N. Israelachvili, D. J. Mitchell and B. W. Ninham, *Journal of the Chemical Society, Faraday Transactions 2: Molecular and Chemical Physics*, 1976, **72**, 1525.
97. J. Eastoe, *Colloid Science: Principles, Methods and Applications*, John Wiley & Sons Ltd., Chippenham, 2010.
98. S. Svenson, *Current Opinion in Colloid & Interface Science*, 2004, **9**, 201.
99. P. J. Flory, *Journal of Chemical Physics*, 1942, **10**, 51.
100. M. L. Huggins, *Journal of the American Chemical Society*, 1942, **64**, 1712.
101. F. S. Bates and G. H. Fredrickson, *Physics Today*, 1999, **52**, 32.
102. T. P. Russell, R. P. Hjelm, Jr. and P. A. Seeger, *Macromolecules*, 1990, **23**, 890.
103. J. M. Swann and P. D. Topham, *Polymers*, 2010, **2**, 454.
104. C.-I. Huang and T. P. Lodge, *Macromolecules*, 1998, **31**, 3556.

105. K. Yu and A. Eisenberg, *Macromolecules*, 1996, **29**, 6359.
106. H. Shen, L. Zhang and A. Eisenberg, *Journal of Physical Chemistry B*, 1997, **101**, 4697.
107. Y. K. Vihik Krikorian, Edwim L. Thomas, *Macromolecular Engineering*, Wiley-VCH, Weinheim, Germany, 2007.
108. A. K. Khandpur, S. Foerster, F. S. Bates, I. W. Hamley, A. J. Ryan, W. Bras, K. Almdal and K. Mortensen, *Macromolecules*, 1995, **28**, 8796.
109. M. W. Matsen and F. S. Bates, *Macromolecules*, 1996, **29**, 1091.
110. F. L. Baines, S. Dionisio, N. C. Billingham and S. P. Armes, *Macromolecules*, 1996, **29**, 3096.
111. A. P. Richez, H. N. Yow, S. Biggs and O. J. Cayre, *Progress in Polymer Science*, 2013, **38**, 897.
112. D. W. J. Osmond and H. H. Thompson, *Dispersion polymerization*, GB893429, 1962.
113. A. J. Paine, Y. Deslandes, P. Gerroir and B. Henrissat, *Journal of Colloid and Interface Science*, 1990, **138**, 170.
114. S. Kawaguchi and K. Ito, *Advances in Polymer Science*, 2005, **175**, 299.
115. Y. Almog and M. Levy, *Journal of Polymer Science. Polymer Chemistry Edition*, 1981, **19**, 115.
116. Y. Almog, S. Reich and M. Levy, *British Polymer Journal*, 1982, **14**, 131.
117. Z. An, Q. Shi, W. Tang, C.-K. Tsung, C. J. Hawker and G. D. Stucky, *Journal of the American Chemical Society*, 2007, **129**, 14493.
118. J. Rieger, C. Grazon, B. Charleux, D. Alaimo and C. Jerome, *Journal of Polymer Science Part A: Polymer Chemistry*, 2009, **47**, 2373.
119. A. M. I. Ali, P. Pareek, L. Sewell, A. Schmid, S. Fujii, S. P. Armes and I. M. Shirley, *Soft Matter*, 2007, **3**, 1003.
120. C. S. Chern, *Progress in Polymer Science*, 2006, **31**, 443.
121. C. J. Ferguson, R. J. Hughes, B. T. T. Pham, B. S. Hawkett, R. G. Gilbert, A. K. Serelis and C. H. Such, *Macromolecules*, 2002, **35**, 9243.
122. P. B. Zetterlund, S. C. Thickett, S. Perrier, E. Bourgeat-Lami and M. Lansalot, *Chemical Reviews*, 2015, **115**, 9745.
123. B. Charleux, G. Delaittre, J. Rieger and F. D'Agosto, *Macromolecules*, 2012, **45**, 6753.
124. S. L. Canning, G. N. Smith and S. P. Armes, *Macromolecules*, 2016, **49**, 1985.
125. J. Rieger, *Macromolecular Rapid Communications*, 2015, **36**, 1458.
126. J.-T. Sun, C. Y. Hong and C.-Y. Pan, *Soft Matter*, 2012, **8**, 7753.
127. M. J. Rymaruk, K. L. Thompson, M. J. Derry, N. J. Warren, L. P. D. Ratcliffe, C. N. Williams, S. L. Brown and S. P. Armes, *Nanoscale*, 2016, **8**, 14497.
128. V. J. Cunningham, A. M. Alswieleh, K. L. Thompson, M. Williams, G. J. Leggett, S. P. Armes and O. M. Musa, *Macromolecules*, 2014, **47**, 5613.
129. H. Xu, F. Meng and Z. Zhong, *Journal of Materials Chemistry*, 2009, **19**, 4183.
130. I. Chaduc, M. Girod, R. Antoine, B. Charleux, F. D'Agosto and M. Lansalot, *Macromolecules*, 2012, **45**, 5881.
131. W.-M. Wan, C.-Y. Hong and C.-Y. Pan, *Chemical Communications*, 2009, 5883.
132. S. Sugihara, K. Sugihara, S. P. Armes, H. Ahmad and A. L. Lewis, *Macromolecules*, 2010, **43**, 6321.
133. G. Wang, M. Schmitt, Z. Wang, B. Lee, X. Pan, L. Fu, J. Yan, S. Li, G. Xie, M. R. Bockstaller and K. Matyjaszewski, *Macromolecules*, 2016, **49**, 8605.
134. A. Darabi, P. G. Jessop and M. F. Cunningham, *Macromolecules*, 2015, **48**, 1952.
135. G. Delaittre, J. Nicolas, C. Lefay, M. Save and B. Charleux, *Chemical Communications*, 2005, 614.
136. E. Groison, S. Brusseau, F. D'Agosto, S. Magnet, R. Inoubli, L. Couvreur and B. Charleux, *ACS Macro Letters*, 2012, **1**, 47.

137. G. Delaittre, C. Dire, J. Rieger, J.-L. Putaux and B. Charleux, *Chemical Communications*, 2009, 2887.
138. A. B. Lowe, *Polymer*, 2016, **106**, 161.
139. H. Gemici, T. M. Legge, M. Whittaker, M. J. Monteiro and S. Perrier, *Journal of Polymer Science Part A: Polymer Chemistry*, 2007, **45**, 2334.
140. G. Gody, T. Maschmeyer, P. B. Zetterlund and S. Perrier, *Macromolecules*, 2014, **47**, 3451.
141. L. Martin, G. Gody and S. Perrier, *Polymer Chemistry*, 2015, **6**, 4875.
142. G. Gody, R. Barbey, M. Danial and S. Perrier, *Polymer Chemistry*, 2015, **6**, 1502.
143. S. Sugihara, S. P. Armes, A. Blanazs and A. L. Lewis, *Soft Matter*, 2011, **7**, 10787.
144. S. Sugihara, A. Blanazs, S. P. Armes, A. J. Ryan and A. L. Lewis, *Journal of the American Chemical Society*, 2011, **133**, 15707.
145. N. J. Warren, O. O. Mykhaylyk, D. Mahmood, A. J. Ryan and S. P. Armes, *Journal of the American Chemical Society*, 2014, **136**, 1023.
146. Y. Li and S. P. Armes, *Angewandte Chemie International Edition*, 2010, **49**, 4042.
147. M. Semsarilar, V. Ladmiral, A. Blanazs and S. P. Armes, *Langmuir*, 2013, **29**, 7416.
148. M. Semsarilar, V. Ladmiral, A. Blanazs and S. P. Armes, *Langmuir*, 2012, **28**, 914.
149. A. Blanazs, R. Verber, O. O. Mykhaylyk, A. J. Ryan, J. Z. Heath, C. W. Douglas and S. P. Armes, *Journal of the American Chemical Society*, 2012, **134**, 9741.
150. R. Verber, A. Blanazs and S. P. Armes, *Soft Matter*, 2012, **8**, 9915.
151. A. Blanazs, A. J. Ryan and S. P. Armes, *Macromolecules*, 2012, **45**, 5099.
152. A. Blanazs, J. Madsen, G. Battaglia, A. J. Ryan and S. P. Armes, *Journal of the American Chemical Society*, 2011, **133**, 16581.
153. J. Tan, H. Sun, M. Yu, B. S. Sumerlin and L. Zhang, *ACS Macro Letters*, 2015, **4**, 1249.
154. E. R. Jones, M. Semsarilar, P. Wyman, M. Boerakker and S. P. Armes, *Polymer Chemistry*, 2016, **7**, 851.
155. M. Semsarilar, N. J. W. Penfold, E. R. Jones and S. P. Armes, *Polymer Chemistry*, 2015, **6**, 1751.
156. C. Gonzato, M. Semsarilar, E. R. Jones, F. Li, G. J. P. Krooshof, P. Wyman, O. O. Mykhaylyk, R. Tuinier and S. P. Armes, *Journal of the American Chemical Society*, 2014, **136**, 11100.
157. M. Semsarilar, E. R. Jones, A. Blanazs and S. P. Armes, *Advanced Materials*, 2012, **24**, 3378.
158. Y. Pei, N. C. Dharsana and A. B. Lowe, *Australian Journal of Chemistry*, 2015, **68**, 939.
159. M. J. Derry, L. A. Fielding and S. P. Armes, *Polymer Chemistry*, 2015, **6**, 3054.
160. L. A. Fielding, J. A. Lane, M. J. Derry, O. O. Mykhaylyk and S. P. Armes, *Journal of the American Chemical Society*, 2014, **136**, 5790.
161. L. A. Fielding, M. J. Derry, V. Ladmiral, J. Rosselgong, A. M. Rodrigues, L. P. D. Ratcliffe, S. Sugihara and S. P. Armes, *Chemical Science*, 2013, **4**, 2081.
162. Y. Pei, O. R. Sugita, L. Thurairajah and A. B. Lowe, *RSC Advances*, 2015, **5**, 17636.
163. Y. Pei, L. Thurairajah, O. R. Sugita and A. B. Lowe, *Macromolecules*, 2015, **48**, 236.
164. Q. Zhang and S. Zhu, *ACS Macro Letters*, 2015, **4**, 755.
165. B. Zhang, X. Yan, P. Alcouffe, A. Charlot, E. Fleury and J. Bernard, *ACS Macro Letters*, 2015, **4**, 1008.
166. W. Zhang, F. D'Agosto, P.-Y. Dugas, J. Rieger and B. Charleux, *Polymer*, 2013, **54**, 2011.
167. I. Chaduc, A. Crepet, O. Boyron, B. Charleux, F. D'Agosto and M. Lansalot, *Macromolecules*, 2013, **46**, 6013.
168. I. Chaduc, M. Lansalot, F. D'Agosto and B. Charleux, *Macromolecules*, 2012, **45**, 1241.

169. S. Boisse, J. Rieger, K. Belal, A. Di-Cicco, P. Beaunier, M.-H. Li and B. Charleux, *Chemical Communications*, 2010, **46**, 1950.
170. W. Zhang, F. D'Agosto, O. Boyron, J. Rieger and B. Charleux, *Macromolecules*, 2012, **45**, 4075.
171. S. Boisse, J. Rieger, G. Pembouong, P. Beaunier and B. Charleux, *Journal of Polymer Science Part A: Polymer Chemistry*, 2011, **49**, 3346.
172. A. A. Cockram, T. J. Neal, M. J. Derry, O. O. Mykhaylyk, N. S. J. Williams, M. W. Murray, S. N. Emmett and S. P. Armes, *Macromolecules*, 2017, **50**, 796.
173. M. Williams, N. J. W. Penfold and S. P. Armes, *Polymer Chemistry*, 2016, **7**, 384.
174. M. Williams, N. J. W. Penfold, J. R. Lovett, N. J. Warren, C. W. I. Douglas, N. Doroshenko, P. Verstraete, J. Smets and S. P. Armes, *Polymer Chemistry*, 2016, **7**, 3864.
175. Y. Ning, L. A. Fielding, K. E. B. Doncom, N. J. W. Penfold, A. N. Kulak, H. Matsuoka and S. P. Armes, *ACS Macro Letters*, 2016, **5**, 311.
176. V. Ladmiral, A. Charlot, M. Semsarilar and S. P. Armes, *Polymer Chemistry*, 2015, **6**, 1805.
177. Y. Jiang, N. Xu, J. Han, Q. Yu, L. Guo, P. Gao, X. Lu and Y. Cai, *Polymer Chemistry*, 2015, **6**, 4955.
178. W. Shen, Y. Chang, G. Liu, H. Wang, A. Cao and Z. An, *Macromolecules*, 2011, **44**, 2524.
179. G. Liu, Q. Qiu, W. Shen and Z. An, *Macromolecules*, 2011, **44**, 5237.
180. K. E. B. Doncom, N. J. Warren and S. P. Armes, *Polymer Chemistry*, 2015, **6**, 7264.
181. Y. Ning, L. A. Fielding, L. P. D. Ratcliffe, Y.-W. Wang, F. C. Meldrum and S. P. Armes, *Journal of the American Chemical Society*, 2016, **138**, 11734.
182. S. J. Byard, M. Williams, B. E. McKenzie, A. Blanazs and S. P. Armes, *Macromolecules*, 2017, **50**, 1482.
183. C. Grazon, J. Rieger, N. Sanson and B. Charleux, *Soft Matter*, 2011, **7**, 3482.
184. C. Wu and X. Wang, *Physical Review Letters*, 1998, **80**, 4092.
185. Y. Xia, X. Yin, N. A. D. Burke and H. D. H. Stöver, *Macromolecules*, 2005, **38**, 5937.
186. S. Furyk, Y. Zhang, D. Ortiz-Acosta, P. S. Cremer and D. E. Bergbreiter, *Journal of Polymer Science Part A: Polymer Chemistry*, 2006, **44**, 1492.
187. M. K. Kocik, O. O. Mykhaylyk and S. P. Armes, *Soft Matter*, 2014, **10**, 3984.
188. D. E. Mitchell, J. R. Lovett, S. P. Armes and M. I. Gibson, *Angewandte Chemie International Edition*, 2016, **55**, 2801.
189. I. Canton, N. J. Warren, A. Chahal, K. Amps, A. Wood, R. Weightman, E. Wang, H. Moore and S. P. Armes, *ACS Central Science*, 2016, **2**, 65.

Chapter 2

pH Responsive Non-Ionic Diblock Copolymer Worms

Reproduced in full with permission from:

[N. J. W. Penfold, J. R. Lovett, N. J. Warren, P. Verstraete, J. Smets, S. P. Armes, *Polymer Chemistry*, **2016**, **7**, 79-88.]

2.1 Introduction

Block copolymer self-assembly has become one of the most important fields in polymer chemistry over the last few decades.[1-20] The synthesis of functional block copolymers is not trivial by classical living ionic polymerisation techniques, since many functional groups (OH, COOH, NH_2) etc. lead to premature termination *via* proton abstraction. However, the development of pseudo-living radical polymerisation techniques, such as ATRP[21, 22] and RAFT[23-26] has revolutionised the design and synthesis of functional block copolymers over the past two decades.

The development of robust RAFT-mediated PISA formulations offers a highly convenient route for the preparation of a wide range of well-defined amphiphilic diblock copolymer nano-objects directly in aqueous media.[27] Initially, a macro-CTA is synthesised and then this soluble precursor is chain-extended *via* aqueous dispersion (or aqueous emulsion) polymerisation. Self-assembly occurs *in situ* as the growing second block becomes insoluble.[28] Depending on the precise reaction conditions, this enables the reproducible formation of spheres, worms or vesicles at relatively high solids (25–50% w/w).[29, 30] In the case of RAFT aqueous emulsion polymerisation, kinetically-trapped spheres[31-33] are often obtained when the targeted diblock copolymer composition might be expected to favour worms or vesicles.[33-35] In contrast, RAFT aqueous dispersion polymerisation usually provides access to all three copolymer morphologies, provided that the stabiliser macro-CTA is not so long as to impede sphere–sphere fusion.[36] Moreover, phase diagrams can be constructed for any given macro-CTA to enable pure copolymer phases to be consistently targeted for these latter formulations. Warren and Armes have summarised recent PISA syntheses *via* RAFT aqueous dispersion polymerisation.[37] The final block copolymer morphology can be somewhat qualitatively described by using the surfactant based dimensionless packing parameter, *P*, which depends on the relative volume

fractions of the solvophilic stabiliser and solvophobic core-forming blocks.[28, 38] When $P \leq {}^{1}/_{3}$, a spherical micelle morphology is favoured. If P lies in the range between ${}^{1}/_{3} < P \leq {}^{1}/_{2}$ then worms (i.e. cylinders) are produced, and vesicles are obtained when ${}^{1}/_{2} < P \leq 1$. The diblock copolymer worms are of particular interest, because they typically form free-standing gels as a result of multiple inter-worm contacts.[39, 40]

Stimulus-responsive polymers[41] are defined as polymers that undergo large physical or chemical changes in response to a change in temperature,[42] pH,[43] light[44] or redox[44] chemistry. Adjusting the solution pH is a very convenient trigger for stimulus-responsive block copolymer composed of weak polyacids or polybases. The mildly acidic nature of the extra cellular environment of cancerous tumours[45] has inspired the application of pH-responsive copolymer micelles for the delivery of anti-cancer drugs.[46, 47] So-called 'schizophrenic' pH-responsive block copolymers have also been designed that are capable of forming two (or even three) nano-objects in aqueous solution. [48-51]

The field of stimulus-responsive nanoparticles prepared *via* RAFT-mediated PISA has recently been reviewed by Pei *et al.*[52] While there are numerous reports of reversible thermoresponsive nanoparticles in aqueous,[40, 53-55] alcoholic[56-58] and non-polar[59-62] media, there is a surprising lack of literature reporting pH-induced morphology transitions. In 2015, Lovett *et al.* utilised a carboxylic acid-based RAFT agent to prepare $PGMA_{56}$-$PHPMA_{155}$ diblock copolymer worms (Figure 2.1). On switching the solution pH from 3.5 to 7.0, these ostensibly non-ionic diblock copolymer worms undergo a reversible worm-to-sphere transition, with concomitant degelation.[63] DLS, aqueous electrophoresis, TEM and rheological studies confirm that ionisation of a single carboxylic acid group located at the end of each PGMA stabiliser chain is responsible for this unusual pH-responsive behaviour.

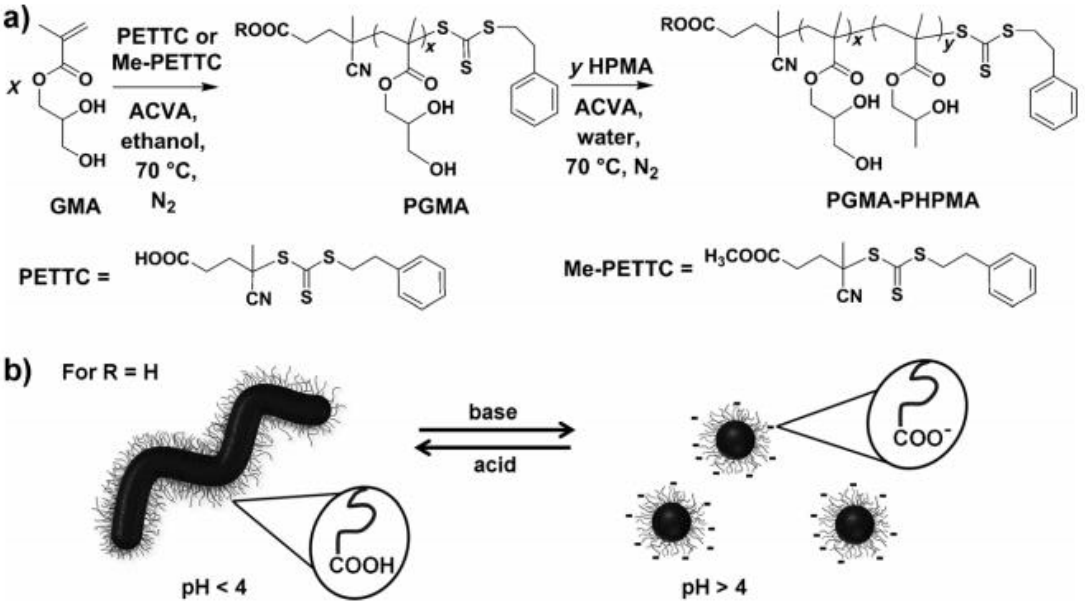

Figure 2.1 (a) Synthetic route to preparing carboxylic acid terminated $PGMA_{56}$-$PHPMA_{155}$ diblock copolymer worms by the RAFT aqueous dispersion of HPMA at 70 °C using a $PGMA_{56}$ macro-CTA. (b) Schematic of the reversible worm-to-sphere transition that occurs upon ionisation of carboxylic-acid terminated $PGMA_{56}$-$PHPMA_{155}$.[63]

The packing parameter, *P*, is reduced as the carboxylic acid end-group becomes ionised, thus inducing a worm-to-sphere transition that results in complete degelation. More specifically, the gel storage modulus (*G'*) is dramatically reduced from ≈ 102 Pa at pH 3.7 to ≈ 0.02 Pa at pH 6.9. Returning to pH 3.7 leads to reprotonation of the anionic carboxylate end-groups; this induces a sphere-to-worm transition that results in regelation, with the reconstituted worm gel possessing a comparable modulus to that of the original worm gel. In this Chapter, the synthesis of a new morpholine-functional trithiocarbonate-based RAFT chain transfer agent (MPETTC) is described and used to prepare morpholine-functionalised PGMA-PHPMA diblock copolymer worms (Scheme 2.1). These essentially non-ionic, tertiary-amine functionalised worms are expected to exhibit a similar pH response to the carboxylic acid terminated worms. Furthermore, the effect of salt on end-group charge is examined. These hypotheses are examined by TEM, DLS, aqueous electrophoresis and oscillatory rheology experiments.

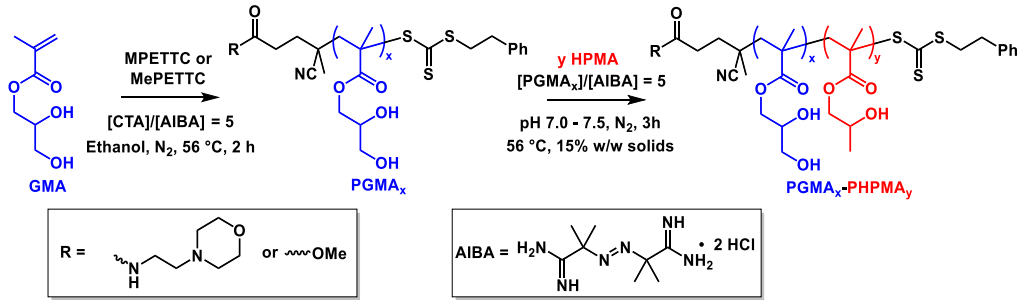

Scheme 2.1 Reaction scheme for the synthesis of $PGMA_x$ by RAFT alcoholic solution polymerisation of GMA using either MPETTC or MePETTC RAFT agents. These $PGMA_x$ macro-CTAs were subsequently chain extended with HPMA at pH 7.0 – 7.5 to produce $PGMA_x$-$PHPMA_y$ diblock copolymer nanoparticles.

2.2 Experimental

2.2.1 Materials

Glycerol monomethacrylate (GMA; 99.8%; < 0.06 mol % dimethacrylate impurity) was kindly donated by GEO Specialty Chemicals (Hythe, UK) and used without further purification. 2-Hydroxypropyl methacrylate (HPMA; 97%), 2,2'-azobis(2-methylpropionamidine) dihydrochloride (AIBA; 99%), *N*-hydroxyl succinimide (98%), *N*,*N*'-dicyclohexylcarbodiimide (99%) and 4-(dimethylamino)pyridine (DMAP, 99%) were purchased from Sigma Aldrich and were used as received. VA-044 was purchased from Wako Chemicals Ltd. 4-(2-Aminoethyl)morpholine (99%) was purchased from Sigma Aldrich (UK) and distilled under vacuum before use. All other chemicals and solvents were purchased from either VWR Chemicals or Sigma Aldrich and were used as received, unless otherwise stated. Anhydrous dichloromethane and chloroform were obtained from an in-house Grubbs purification system.

2.2.2 Synthesis of PETTC RAFT Agent

2-Phenylethanethiol (21.0 g, 151 mmol) was gradually added over 20 min to a stirred suspension of sodium hydride (60% w/w in oil, 6.26 g, 156 mmol) in diethyl ether (600 mL). Vigorous evolution of hydrogen gas was observed, and the gray suspension was slowly

transformed into a white viscous slurry of sodium phenylethanethiolate over 1 h. The reaction mixture was cooled to 0 °C, and carbon disulfide (11.9 g, 156 mmol) was gradually added to produce a thick yellow precipitate of sodium 2-phenylethanetrithiocarbonate, which was collected by vacuum filtration after 2 h and used without further purification. Solid iodine (17.6 g, 69 mmol) was gradually added to a suspension of 2-phenylethanetrithiocarbonate (31.0 g, 131 mmol) and diethyl ether (600 mL) and this reaction mixture was stirred at room temperature for 2 h. The insoluble white precipitate of sodium iodide was removed by filtration. The yellow-brown filtrate was washed with a saturated aqueous solution of sodium thiosulfate (4 x 250 mL) to remove excess iodine, dried over sodium sulfate, and then evaporated to yield bis(2-phenylethanesulfanylthiocarbonyl) disulfide. 4,4′-Azobis(4-cyanopentanoic acid) (ACVA) (50.0 g, 178 mmol) was added to a solution of ethyl acetate (500 mL) and bis(2-phenylethanesulfanylthiocarbonyl) disulfide (49.8 g, 116 mmol) and this solution was degassed under nitrogen for 40 min at room temperature. The solution was refluxed at 77 °C under a dry nitrogen atmosphere for 18 h. After concentration by rotary evaporation, the crude product was washed with water (4 x 250 mL), dissolved in a minimal volume of ethyl acetate: hexane (4:1 v/v) at 65 °C, then placed into a -25 °C freezer to induce recrystallisation of PETTC as yellow crystals (72% yield). ^{1}H NMR (400 MHz, CD_2Cl_2, 25 °C): δ 1.90 (s, 3H, -CN)C***H*****$_3$**), 2.41–2.61 (m, 2H, -(CH_3)(CN)C***H*****$_2$**CH_2COOH), 2.65–2.75 (t, 2H, -(CH_3)(CN)CH_2C***H*****$_2$**COOH), 2.95–3.05 (t, 2H, -PhC***H*****$_2$**CH_2S(C=S)S), 3.56–3.64 (t, 2H, PhCH_2C***H*****$_2$**S(C=S)S), 7.20 - 7.50 (m, 5H, -***Ph***CH_2CH_2S(C=S)S). ^{13}C NMR (400 MHz, $CDCl_3$, 25 °C): δ 25.0 (*C*H_3), 29.5 (CH_2*C*H_2COOH), 33.6 (Ph***C***H_2CH_2S), 34.1 (***C***H_2CH_2COOH), 38.1 (PhCH_2***C***H_2S), 46.5 (S***C***(CH_3)(CN)CH_2), 118.9 SC(CH_3)(***C***N)CH_2), 127.0, 128.6, 128.8, 139.3 (***Ph***CH_2), 167.2 (***C***=O), 216.4 (***C***=S).

2.2.3 Synthesis of SPETTC RAFT Agent

All glassware was dried in a 150 °C oven overnight and then flame-dried under vacuum before use to remove trace water. A 50 mL, one-neck round-bottom flask was charged with PETTC (1.60 g, 4.71 mmol) and *N*-hydroxyl succinimide (0.54 g, 4.71 mmol) which were then dissolved in anhydrous dichloromethane (20.0 g, 15.0 mL). *N,N′*-dicyclohexylcarbodiimide (0.97 g, 4.71 mmol) was added and then stirred in the dark for 16 h. The insoluble *N,N′*-dicyclohexylurea was removed by vacuum filtration. The organic solution was washed with water (4 x 10 ml), dried with $MgSO_4$, concentrated under vacuum and purified by recrystallisation from a 4:1 (v/v) ethyl acetate/hexane mixture at 60 °C to yield 4-cyano-4-(2-phenylethanesulfanylthiocarbonyl) sulfanyl pentanoic succinimide ester (SPETTC, 1.90 g, 92% yield). ^{1}H NMR (400 MHz, CD_2Cl_2, 25 °C): δ 1.89 (s, 3H, -(CN)C***H*****$_3$**), 2.51–2.68 (m, 2H, -(CH_3)(CN)C***H*****$_2$**CH_2C(=O)O), 2.81 (s, 4H, -(C=O)(C***H*****$_2$**$)_2$(C=O), 2.90–2.96 (t, 2H, -(CH_3)(CN)CH_2C***H*****$_2$**C(=O)), 2.97–3.03 (t, 2H, -PhC***H*****$_2$**CH_2S(C=S)S), 3.56–3.64 (t, 2H, PhCH_2C***H*****$_2$**S(C=S)S), 7.20-7.36 (m, 5H, -***Ph***CH_2CH_2S(C=S)S). ^{13}C NMR (400 MHz, $CDCl_3$, 25 °C): δ 24.8 (***C***H_3), 25.7 (C(=O)(***C***$H_2$$)_2$C(=O)), 26.9 ($CH_2$***C***$H_2$C(=O)ON), 33.2 (Ph***C***H_2CH_2S), 34.1 (***C***H_2CH_2C(=O)O), 38.1 (PhCH_2***C***H_2S), 46.2 (S***C***(CH_3)(CN)CH_2), 118.7 SC(CH_3)(***C***N)CH_2), 126.9, 128.6, 128.8, 139.2 (***Ph***CH_2), 167.2 (***C***=O), 168.9 (***C***(=O)$(CH_2)_2$C(=O)), 216.4 (***C***=S). HR-MS (ES^+) m/z calcd: 437.0658 Found: 437.0658 Anal. Calcd for $C_{19}H_{20}N_2O_4S_3$: C, 52.27; H, 4.62; N, 6.42; S, 22.03 Found: C, 52.65; H, 4.72; N, 6.39; S, 21.93.

2.2.4 Synthesis of MPETTC RAFT Agent

All glassware was dried in a 150 °C oven overnight, then flame-dried under vacuum before use to remove traces of water. A 500 ml one-neck round-bottom flask containing a magnetic stirrer bar was charged with SPETTC (5.35 g, 12.3 mmol), which was dissolved in anhydrous chloroform (250 mL). In a separate 50 ml one-neck round-bottom flask, freshly distilled 4-(2-

aminoethyl)morpholine (1.52 g, 1.53 mL, 11.7 mmol) was dissolved in anhydrous chloroform (25 mL), then added in one portion to the solution of SPETTC. The yellow reaction mixture was heated at 30 °C for 90 min, filtered and washed with saturated $NaHCO_3$ solution (3 x 400 mL) to remove residual *N*-hydroxysuccinimide, before being dried with $MgSO_4$. After solvent removal, the yellow oil was purified to remove any residual SPETTC *via* column chromatography using silica gel 60 (Merck) as the stationary phase and a 95:5: v/v dichloromethane/methanol mixed eluent, followed by drying in a vacuum oven overnight to isolate a viscous yellow oil (MPETTC, 4.75 g, 86%). ^{1}H NMR (400 MHz, CD_2Cl_2, 25 °C): δ 1.89 (s, 3H, -(CN)C***H*****$_3$**), 2.31–2.56 (m, 10H, see Figure 2.2 for assignment), 2.96–3.03 (t, 2H, -PhC***H*****$_2$**CH_2S(C=S)S), 3.27–3.34 (q, 2H, C(=O)NHC***H*****$_2$**CH_2), 3.56–3.62 (t, 2H, PhCH_2C***H*****$_2$**S(C=S)S), 3.64–3.71 (t, 4H, -CH_2NCH_2C***H*****$_2$**O) 5.98–6.13 (s, 1H, CON***H***), 7.20-7.36 (m, 5H, -***Ph***CH_2CH_2S(C=S)S). ^{13}C NMR (400 MHz, $CDCl_3$, 25 °C): δ 25.1 (***CH*****$_3$**), 31.8 (CH_2***CH*****$_2$**CONH), 34.6 (Ph***CH*****$_2$**CH_2S), 34.5 (***CH*****$_2$**CH_2CONH), 35.7 (CONH***CH*****$_2$**CH_2N), 37.9 (PhCH_2***CH*****$_2$**S), 46.8 (S***C***$(CH_3)(CN)CH_2$), 53.3 (-N***CH*****$_2$**CH_2O), 56.9 (CONHCH_2***CH*****$_2$**N), 66.9 (-NCH_2***CH*****$_2$**O), 119.2 (SC(CH_3)(***CN***)CH_2), 126.8, 128.5, 128.7, 139.1 (***Ph***CH_2), 170.1 (***C=O***), 216.8 (***C=S***). HR-MS (ES^+) *m/z* calcd: 452.1495 Found: 452.1495. Anal. Calcd for $C_{21}H_{29}N_3O_2S_3$: C, 55.85; H, 6.47; N, 9.30; S, 21.29. Found: C, 55.47; H, 6.48; N, 9.08; S, 21.09.

2.2.5 Synthesis of MPETTC-PGMA$_{50}$ macro-CTA by RAFT Solution Polymerisation in Ethanol

A 100 ml round-bottom flask was charged with a magnetic stirrer bar, glycerol monomethacrylate (GMA, 18.9 g, 118 mmol), MPETTC RAFT agent (0.76 g, 1.70 mmol; target DP_n = 70), AIBA (92.0 mg, 0.34 mmol; [MPETTC]/[AIBA] molar ratio = 5.0) and ethanol (24.2 g, 30.6 mL) to afford a 45% w/w orange solution. The flask was sealed, placed in an ice bath and degassed under N_2 for 30 min at 0 °C, before being placed in a preheated oil bath set at 56 °C for 2 h. Polymerisation was quenched by exposure to air while cooling to 20

°C. ^{1}H NMR studies indicated 61% monomer conversion by comparison of the integrated methacrylic backbone signals at 3.70–4.30 ppm to that of the GMA vinyl signals at 6.14–6.20 ppm. Purification was achieved by precipitation into a twenty-fold excess of dichloromethane to remove unreacted GMA monomer, followed by filtration. The crude PGMA was redissolved in the minimum amount of methanol and precipitated a second time using a ten-fold excess dichloromethane, with isolation *via* filtration. Purified PGMA macro-CTA was dissolved in water, placed on a rotary evaporator to remove residual dichloromethane, and then freeze-dried for 48 h to afford a pale yellow powder. ^{1}H NMR studies indicated no residual GMA monomer and a mean degree of polymerisation of 50 was determined *via* end-group analysis, with a RAFT agent efficiency of 85%. DMF gel permeation chromatography (GPC) studies indicated an M_n of 12,800 g mol^{-1} and an M_w / M_n of 1.20 vs near-monodisperse poly(methyl methacrylate) standards.

2.2.6 Synthesis of MPETTC-PGMA$_{50}$-PHPMA$_{140}$ Diblock Copolymer Worms by RAFT Aqueous Dispersion Polymerisation

A typical protocol for the synthesis of PGMA$_{50}$-PHPMA$_{140}$ diblock copolymers by RAFT aqueous dispersion polymerisation was conducted as follows. PGMA$_{50}$ macro-CTA (0.80 g, 94.7 µmol), HPMA monomer (1.90 g, 13.2 mmol; target DP$_n$ = 140), AIBA (5.10 mg, 18.8 µmol; PGMA$_{50}$ macro-CTA/AIBA molar ratio = 5.0) and H_2O (15.3 mL) were added to a 50 mL round-bottomed flask to afford a 15% w/w solution. The solution pH was adjusted from pH 6.5 to pH 7.0-7.5 using 0.1 M KOH. The sealed reaction flask was placed in an ice bath and degassed under N_2 for 30 min at 0 °C, then placed in a preheated oil bath set at 56 °C for 3 h. The HPMA polymerisation was quenched by exposure to air while cooling to 20 °C. The resulting diblock copolymer worm gel was characterised by ^{1}H NMR, DLS, DMF GPC, TEM and oscillatory rheology experiments.

2.2.7 Synthesis of MePETTC

MePETTC was synthesised according to a previous protocol.[61] A 25 mL round-bottomed flask was flame-dried under vacuum and cooled to 20 °C, then charged with a magnetic stirrer bar, PETTC RAFT agent (0.56 g, 1.65 mmol) and anhydrous dichloromethane (5.60 g, 4.20 mL). The flask was immersed in an ice bath to 0 °C for 5 min. DMAP (45.0 mg, 0.37 mmol) and excess methanol (0.28 g, 8.74 mmol) were added and then *N,N′*-dicyclohexylcarbodiimide (0.36 g, 1.73 mmol) was gradually added over 5 min. The reaction was stirred overnight at 20 °C. *N,N'*-Dicyclohexylurea was isolated *via* filtration and the crude product was purified by column chromatography (silica gel 60, using dichloromethane eluent) and dried in a vacuum oven overnight to isolate a viscous yellow oil (MePETTC, 4.75 g, 89%). ^{1}H NMR (400 MHz, CD_2Cl_2, 25 °C) δ 1.86 (s, 3H, -(CN)C***H*****$_3$**), 2.32–2.61 (m, 2H, -(CH_3)(CN)C***H*****$_2$**CH_2COOMe), 2.64–2.74 (t, 2H, -(CH_3)(CN)CH_2C***H*****$_2$**COOMe), 2.96–3.05 (t, 2H, -PhC***H*****$_2$**CH_2S(C=S)S)**,** 3.56–3.63 (t, 2H, PhCH_2C***H*****$_2$**S(C=S)S), 3.68 (s, 3H, -COOC***H*****$_3$**), 7.20–7.36 (m, 5H, -***Ph***CH_2CH_2S(C=S)S). HRMS (ES^+) *m/z* calcd: 354.0651 Found: 354.0651. Anal. Calcd for $C_{16}H_{19}NO_2S_3$: C, 54.36; H, 5.42; N, 3.96; S, 27.21. Found: C, 53.92; H, 5.21; N, 3.34; S, 27.40.

2.2.8 Synthesis of MePETTC-PGMA$_{58}$ macro-CTA by RAFT Solution Polymerisation

A 25 mL round-bottomed flask was charged with GMA (4.65 g, 29.0 mmol), MePETTC (0.146 g, 0.416 mmol), AIBA (22.3 mg, 82.4 μmol) and ethanol (5.90 g, 7.47 mL) to afford a 45% w/w orange solution (target DP_n = 70, [MePETTC]/[AIBA] molar ratio = 5.0). The flask was sealed, placed in an ice bath and degassed under N_2 for 30 min at 0 °C. The flask was placed in a preheated oil bath set at 56 °C for 2 h. The GMA polymerisation was quenched by exposure to air and cooling to 20 °C. ^{1}H NMR indicated 58% monomer conversion by comparison of the integrated methacrylic backbone signals at 3.70-4.30 ppm to that of the GMA

vinyl signals at 6.14 – 6.20 ppm. Purification was achieved by precipitation into a twenty-fold excess of dichloromethane to remove unreacted GMA monomer, followed by filtration. The isolated crude PGMA was redissolved in the minimum amount of methanol, precipitated using a ten-fold excess of dichloromethane and again isolated *via* filtration. The purified macro-CTA was dissolved in water, residual dichloromethane was removed under reduced pressure using a rotary evaporator and then freeze-drying was conducted for 48 h to afford a yellow powder. ^{1}H NMR studies indicated no residual GMA monomer and end-group analysis indicated a mean degree of polymerisation of 58, with a RAFT agent efficiency of 70%. DMF GPC studies indicated an M_n of 14,600 g mol^{-1} and an M_w / M_n of 1.23 against a series of ten near-monodisperse poly(methyl methacrylate) calibration standards.

2.2.9 Synthesis of MePETTC-PGMA$_{58}$-PHPMA$_{160}$ Diblock Copolymer Worms by RAFT Aqueous Dispersion Polymerisation

A typical protocol for the synthesis of a PGMA$_{58}$-PHPMA$_{160}$ diblock copolymer by RAFT aqueous dispersion polymerisation was conducted as follows. PGMA$_{58}$ macro-CTA (0.10 g, 10.4 µmol), HPMA monomer (0.24 g, 1.66 mmol; target DP$_n$ = 160), AIBA (0.56 mg, 2.07 µmol; PGMA$_{58}$ macro-CTA/AIBA molar ratio = 5.0) and H_2O (1.95 mL) were added to a 10 mL round-bottom flask to afford a 15% w/w solution. The solution pH was adjusted from pH 6.5 to pH 7.0-7.5 with 0.1 M KOH and stirred for 5 minutes. The sealed reaction flask was placed in an ice bath and degassed under N_2 for 20 minutes at 0 °C, then placed in a preheated oil bath set at 56 °C for 3 h. Polymerisation was quenched by cooling to room temperature while exposing to air. Diblock copolymer worm gels were characterised by ^{1}H NMR, DMF GPC, DLS, TEM and oscillatory rheology experiments.

2.2.10 Copolymer Characterisation

Dynamic light scattering

DLS and aqueous electrophoresis measurements were conducted at 20 °C using a Malvern Instruments Zetasizer Nano series instrument equipped with a 4 mW He−Ne laser (λ = 633 nm) and an avalanche photodiode detector. Scattered light was detected at 173°. Copolymer dispersions were diluted using an aqueous solution of 1 mM KCl to a final concentration of 0.1% w/w solids and the pH was adjusted using 1 M or 0.1 M HCl or KOH, as required. Intensity-average hydrodynamic diameters were calculated *via* the Stokes-Einstein equation. Zeta potentials were calculated from the Henry equation using the Smoluchowski approximation.

Oscillatory Rheology

An AR-G2 rheometer equipped with a variable temperature Peltier plate and a 40 mm 2° aluminium cone was used for all rheological experiments. Percentage strain and angular frequency sweeps were conducted at pH 7 and 20 °C. The storage modulus (*G′*) and loss modulus (*G″*) were determined at 15% w/w and 20 °C as a function of dispersion pH at an applied strain of 1.0 % and an angular frequency of 1.0 rad s^{-1}.

^{1}H/^{13}C NMR Spectroscopy

^{1}H and ^{13}C NMR spectra were recorded at ambient temperature using a 400 MHz Bruker AV3-HD spectrometer in either CD_3OD (for calculation of monomer conversions and mean degrees of polymerisation, or CD_2Cl_2 and $CDCl_3$ (for RAFT agent synthesis).

DMF Gel permeation chromatography

0.50% w/w copolymer solutions were prepared in DMF containing DMSO (10 μL mL^{-1}) as a flow rate marker. GPC measurements were conducted using HPLC-grade DMF eluent

containing 10 mM LiBr at 60 °C at a flow rate of 1.0 mL min^{-1}. A Varian 290-LC pump injection module was connected to two Polymer Laboratories PL gel 5 μm Mixed-C columns connected in series and a Varian 390-LC multi-detector suite (refractive index detector). Sixteen near-monodisperse poly(methyl methacrylate) standards ranging from M_p = 645 g mol^{-1} to 2,480,000 g mol^{-1} were used for column calibration and used to calculate molecular weight data.

Transmission electron microscopy

Copper/palladium grids were surface-coated in-house to produce a thin film of amorphous carbon and then plasma glow-discharged for 20 seconds to produce a hydrophilic surface. Droplets (10 μL) of freshly-prepared 0.1% w/v aqueous copolymer dispersions of the desired solution pH were placed on the hydrophilic grid for 30 seconds, blotted to remove excess solution and then negatively stained with uranyl formate solution (0.75% w/v) for a further 30 seconds. Excess stain was removed by blotting and each grid was carefully dried with a vacuum hose. TEM grids were imaged using a FEI Tecnai Spirit microscope fitted with a Gatan 1kMS600CW CCD camera operating at 80 kV.

2.3 Results & Discussion

2.3.1 Synthesis of MPETTC RAFT Agent

In order to prepare diblock copolymer worms with peripheral tertiary amine functionality, the R and Z groups of the RAFT agent must be carefully considered. In a RAFT-mediated PISA formulation, the final location of the Z group is within the particle core while the R group remains at the particle surface. Therefore, in this case the R group must contain tertiary amine functionality in order to prepare particles with an appropriate surface functionality. Bathfield *et al.*[64] reported reacting various primary amines with a succinimidyl-activated RAFT agent precursors. Amine groups preferentially react with succinimidyl groups rather than with the

dithioester or trithiocarbonate groups of RAFT agents, providing that the amine to succinimidyl molar ratio is less than unity.[65] It is also well known that trithiocarbonate-based RAFT agents exhibit greater thermal and hydrolytic stability than dithiobenzoate-based RAFT agents.[66, 67] Hence, the trithiocarbonate RAFT agent PETTC was synthesised according to previous reports and used in this work.[68] Functional group modification was performed as follows: the carboxylic acid R group of PETTC was coupled with *N*-hydroxyl succinimide to give a succinimidyl group, yielding SPETTC (Scheme 2.2a). Next, this succinimide was reacted with 4-(2-aminoethyl)morpholine to generate the MPETTC RAFT agent, with the desired morpholine moiety located at the terminal end of the R group (Scheme 2.2b).

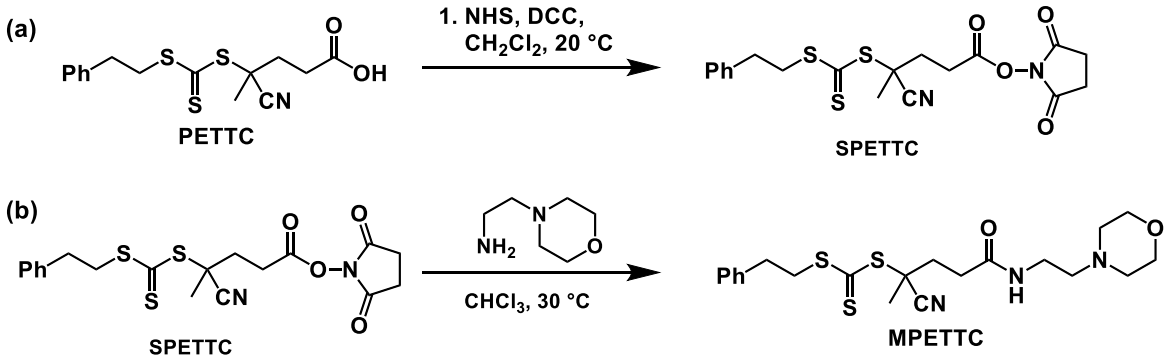

Scheme 2.2 Two-step synthesis of the MPETTC RAFT agent: (a) PETTC is converted into the corresponding succinimide ester, SPETTC: (b) this intermediate is then reacted with 4-(2-aminoethyl)morpholine to produce the desired MPETTC. Other reagents: NHS = *N*-hydroxylsuccinimide, DCC = *N*,*N*′-dicyclohexylcarbodiimide.

^{1}H NMR (Figure 2.2) and ^{13}C NMR (Figure 2.3) spectroscopy were used to monitor the end-group derivatisation of PETTC. Spectra were recorded in CD_2Cl_2 for ^{1}H NMR experiments, but $CDCl_3$ was required for ^{13}C NMR experiments to avoid any residual solvent signal overlapping with the RAFT agent signals.

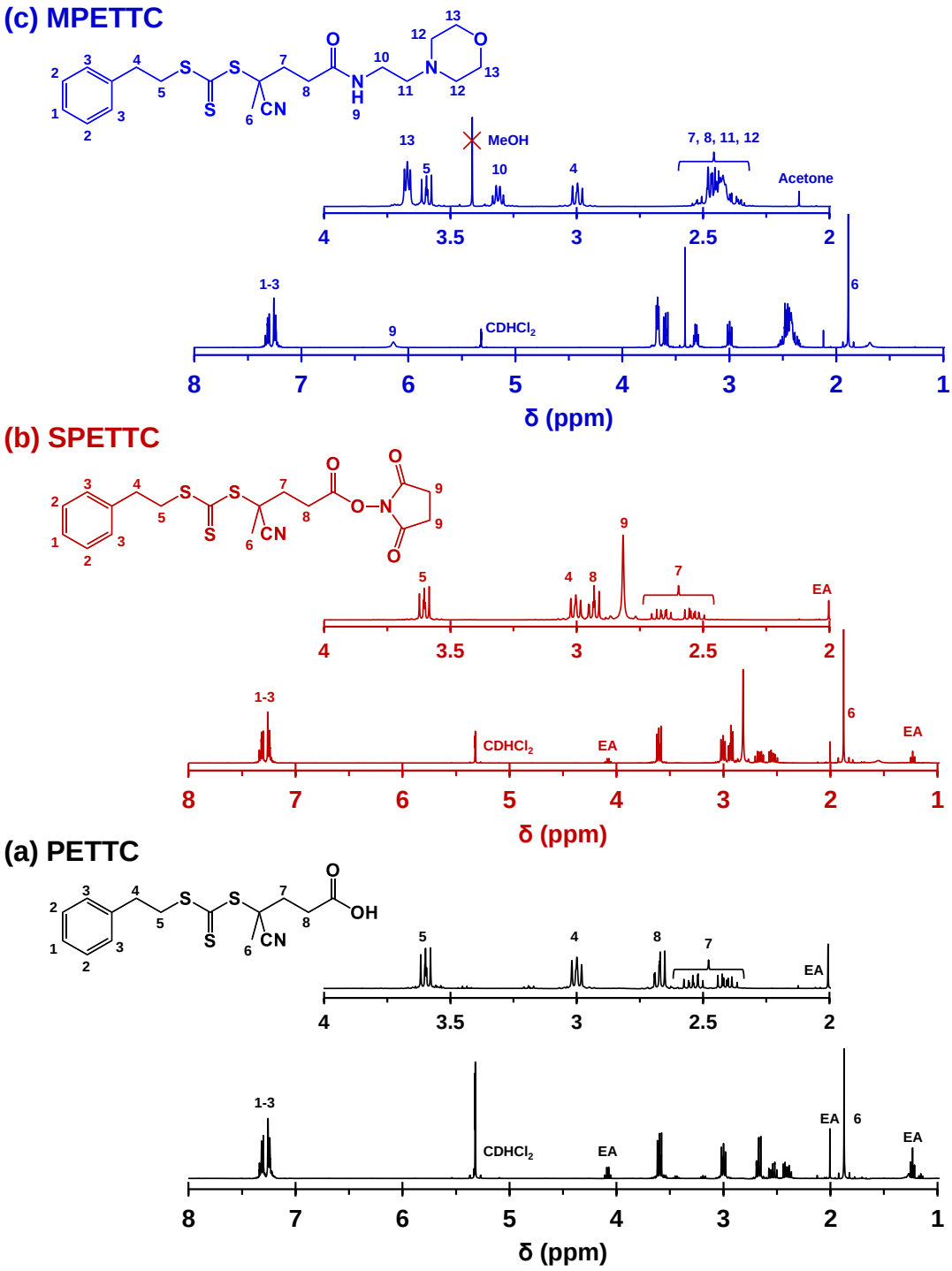

Figure 2.2 ^{1}H NMR spectra recorded for PETTC (a, black trace), SPETTC (b, red trace) and MPETTC (c, blue trace) RAFT agents in CD_2Cl_2. The 2 – 4 ppm region is expanded to indicate proton splitting patterns. 'EA' and 'MeOH' denotes traces of ethyl acetate and methanol, respectively.

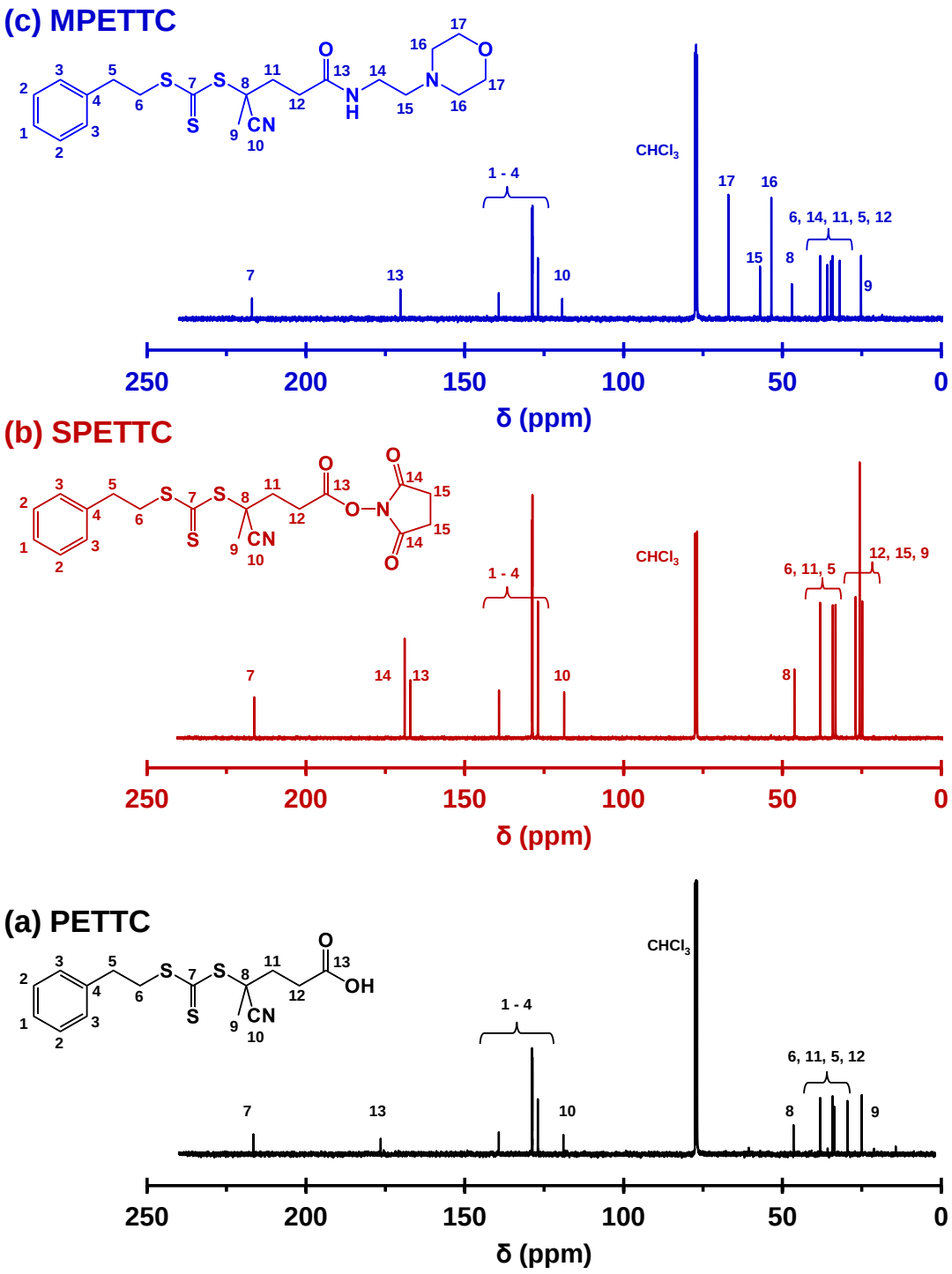

Figure 2.3 ^{13}C NMR spectra recorded for PETTC (a, black trace), SPETTC (b, red trace) and MPETTC (c, blue trace) RAFT agents in $CDCl_3$.

PETTC precursor has six distinct proton environments in its ^{1}H NMR spectra. The multiplet at 7.20–7.40 ppm represents the five aromatic protons (Figure 2.2a, black trace, signals 1-3) that remain unchanged in chemical shift before and after R group derivatisation. As such, these signals conveniently act as a suitable internal standard. Four distinct proton environments exist between 2.0 and 4.0 ppm, associated with the four methylene protons (Figure 2.2a, black trace, signals 4, 5, 7, 8), with the methyl protons (Figure 2.2a, black trace, signal 6) at 1.86 ppm. ^{13}C NMR (Figure 2.3a, black trace) reveals that PETTC has 13 carbon environments, as expected. Attachment of the succinimide group was performed in a 92% yield and confirmed by the presence of a new singlet corresponding to the four new methylene protons at 2.82 ppm (Figure 2.2b, red trace, signal 9). A small downfield shift in signals 7 and 8 are observed due to the attachment of the electron-withdrawing succinimide group. 4-(2-Aminoethyl)morpholine was reacted with SPETTC under the same conditions as used by Bathfield *et al.*,[64] with yield of 87% after purification by column chromatography. Attachment of 4-(2-aminoethyl)morpholine was confirmed by the appearance of a triplet between 3.64 – 3.73 ppm (Figure 2.2c, blue trace signal 13), a quartet at 3.27 – 3.34 ppm (Figure 2.2c, blue trace, signal 10) and a multiplet between 2.31 – 2.55 ppm (Figure 2.2c, blue trace, signals 7, 8 11, 12). Time of flight electrospray mass spectroscopy confirmed the expected 452 m/z ion, with no PETTC or SPETTC precursors. ^{13}C NMR confirmed 4-(2-aminoethyl)morpholine attachment by the appearance of peaks 14, 15, 16 and 17 in (Figure 2.3c, blue trace).

It is well known that the nature of the substituents on amino compounds dictate the pK_a values of the conjugate acid, through inductive effects.[69] For example, the pK_a value of the conjugate acid of morpholine is 8.5, *n*-methylmorpholine is 7.4 and *n*-ethylmorpholine is 7.7.[70, 71] Furthermore, poly(tertiary amine methacrylates) such as poly(2-(diethylamino)ethyl methacrylate) or poly(2-(diisopropylamino)ethyl methacrylate) are insoluble at around neutral pH but dissolution occurs on protonation.[72] Therefore, it was prudent to examine whether the

MPETTC RAFT agent exhibited pH-dependent solubility. A 0.5% w/w aqueous yellow slurry of MPETTC was prepared at pH 7.5. 0.1M HCl was added until this suspension dissolved at pH 4.5, owing to protonation of the morpholine group (Figure 2.4).

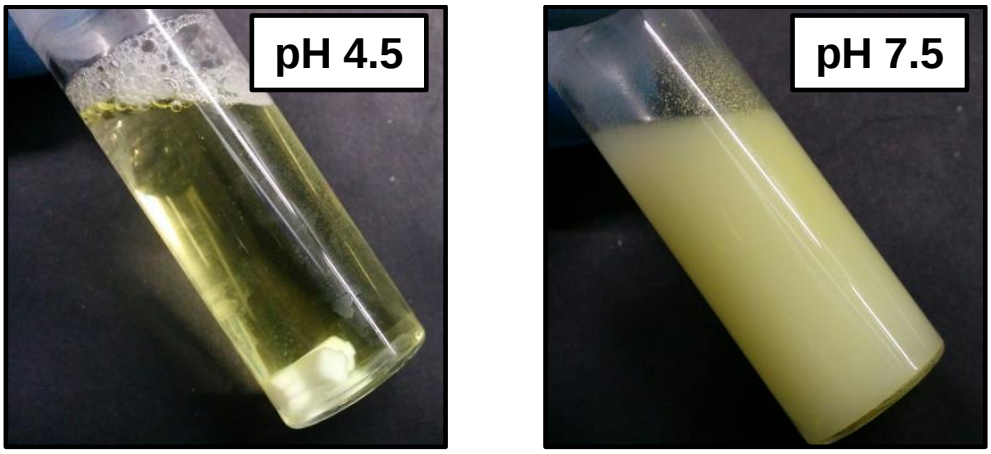

Figure 2.4 Digital images of a 0.5% w/w aqueous slurry of MPETTC at pH 7.5 and after dissolution owing to morpholine protonation on addition of 0.1M HCl to pH 4.5 to produce a clear, yellow solution.

This is a relatively rare example of a trithiocarbonate RAFT agent that is water-soluble.[73] Previous reports of RAFT aqueous solution polymerisations typically recommend that the RAFT agent is initially dissolved in the monomer, which acts as a co-solvent for the RAFT agent. Alternatively, addition of a small volume of a miscible organic solvent, such as dioxane, is required for solubility of the RAFT agent.[32, 74-76]

2.3.2 Synthesis of MPETTC-PGMA$_{50}$ and MePETTC-PGMA$_{58}$ Macro-CTAs

In view of the pH-dependent water solubility of MPETTC, the RAFT aqueous solution polymerisation of GMA was attempted using this RAFT agent. This polymerisation serves as a useful examination of the effectiveness of MPETTC as a RAFT agent. The reaction scheme for the RAFT aqueous solution polymerisation of GMA is shown in Figure 2.5a.

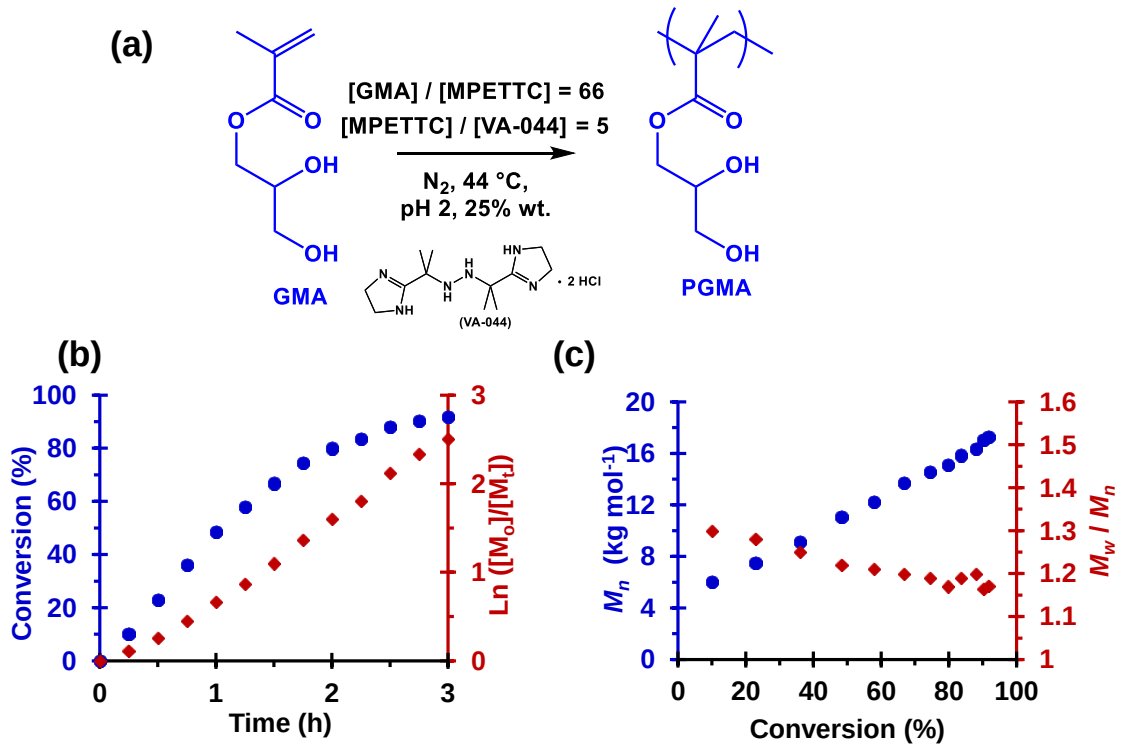

Figure 2.5 (a) Reaction scheme, (b) monomer conversion and semi-log plot vs. time and (c) number-average molecular weight (M_n) and polydispersity (M_w / M_n) vs. monomer conversion for the RAFT aqueous solution polymerisation of GMA. Polymerisation conditions: [GMA] / [MPETTC] = 66, [MPETTC] / [VA-044] = 5, 25% w/w solids, 44 °C. M_n and M_w values were calculated by aqueous GPC acidified to pH 2 and calibrated with near-monodisperse poly(ethylene oxide) standards.

A DP_n of 66 was targeted at 25% w/w solids, and the pH was adjusted with 1 M HCl to pH 2.0 to ensure full solubility of the RAFT agent. A water soluble initiator, VA-044, was used at a molar ratio of 0.2 relative to MPETTC. The polymerisation was conducted at 44 °C (10 h half-life of VA-044 in water) for 3 hours. Samples were taken from the reaction approximately every 15 minutes for 3 hours and immediately analysed by ^{1}H NMR to calculate monomer conversion and construct a monomer conversion *vs* time plot (Figure 2.5b). Aliquots were also analysed by DMF GPC to calculate the M_n and M_w / M_n vs. monomer conversion plot (Figure 2.5c). Monomer conversion was calculated by comparison of the integrated aromatic signals of MPETTC at 7.2–7.4 ppm against the vinyl signal of GMA monomer at 5.6 and 6.1 ppm. After

2 h monomer conversion was 80% with an increase to 92% after 3h. A linear semi-logarithmic vs. time plot indicated first order kinetics with respect to monomer concentration. Furthermore, DMF GPC shows the linear evolution of M_n with monomer conversion and M_w / M_n reducing to less than 1.20. These characteristics are typical of pseudo-living polymerisation and provide strong evidence that this polymerisation proceeds under RAFT control.

One drawback of preparing a PGMA macro-CTA by this method is that the terminal morpholine group is isolated in its protonated state. Given that the main hypothesis of this Chapter is to examine the effect of end-group charge on copolymer morphology, isolation of the morpholine group in its neutral deprotonated form is essential. Therefore, switching the solvent to ethanol was required to prepare a PGMA macro-CTA with a neutral morpholine end-group. A similar kinetics study was performed where a DP_n of 70 was targeted using AIBA initiator at a molar ratio of 0.2 relative to MPETTC RAFT agent. The reaction was performed at 45% w/w and 56 °C (Figure 2.6a). Samples were taken approximately every 15 minutes for 4 h. ^{1}H NMR was used to monitor GMA conversion by comparison of the integrated aromatic signal of the MPETTC RAFT agent at 7.2 – 7.4 ppm against the GMA vinyl signals at 5.6 and 6.1 ppm (Figure 2.6b). The linear relationship of the semi-logarithmic plot indicates first order kinetics with respect to monomer concentration. After 2 h monomer conversion was calculated to be 74%, with 94% conversion achieved after 4 h. These samples were analysed by DMF GPC, which revealed the linear evolution of M_n with monomer conversion and a decrease in M_w / M_n (Figure 2.6c). The non-zero intercept is a common artefact in RAFT homopolymerisation[77, 78] and can be attributed to slow chain initiation[79] or poor resolution of the GPC columns employed.

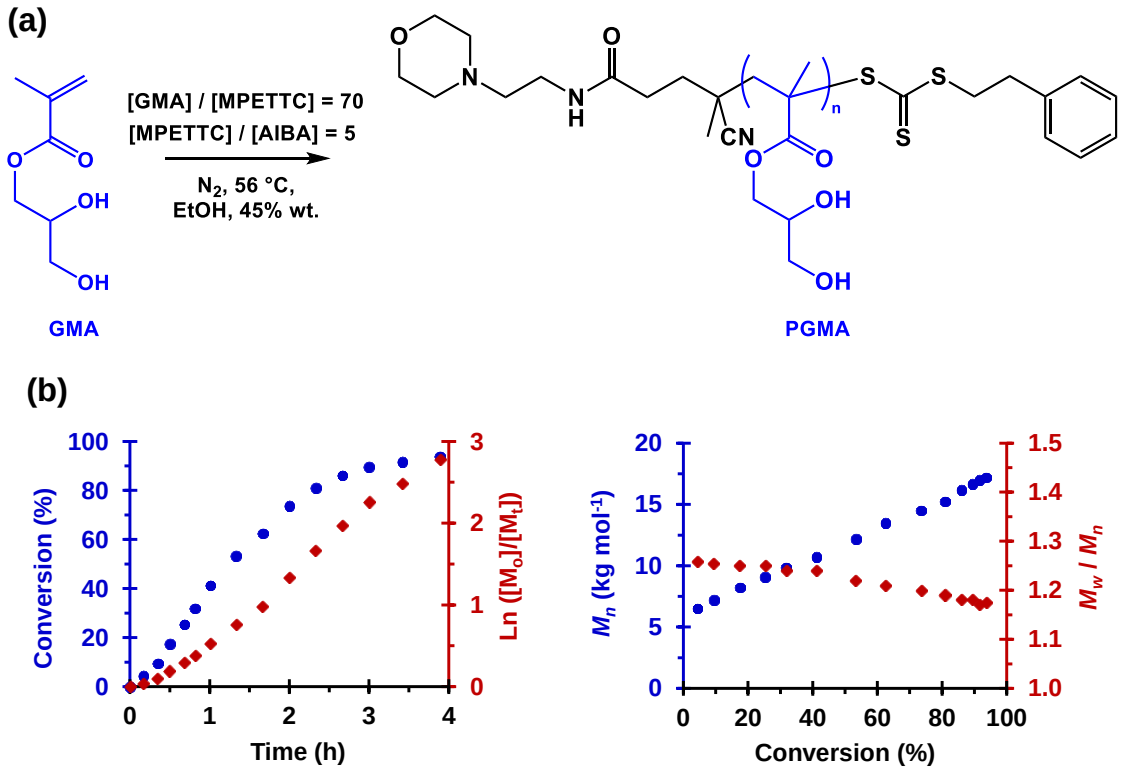

Figure 2.6 (a) Reaction scheme, (b) monomer conversion and semi-log plot vs. time and (c) number-average molecular weight (M_n) and polydispersity (M_w / M_n) vs. monomer conversion for the RAFT ethanolic solution polymerisation of GMA. Conditions: [GMA] / [MPETTC] = 70, [MPETTC] / [AIBA] = 5, 45% w/w solids, 56 °C. M_n and M_w values were calculated using DMF GPC calibrated with a series of near-monodisperse poly(methyl methacrylate) standards.

Having established the kinetics for the RAFT ethanolic homopolymerisation of GMA, a large batch (15 g) of PGMA macro-CTA was synthesised. ^{1}H NMR (Figure 2.7) was used to calculate the PGMA DP_n of 50 by comparison of the integrated aromatic signal at 7.2 – 7.4 ppm vs. the polymer backbone at 0.5 – 2.5 ppm. DMF GPC analysis indicated an M_n of 12,800 g mol^{-1} with a relatively low M_w / M_n of 1.20, relative to PMMA standards (Figure 2.8a). Acid titration studies were conducted on this MPETTC-$PGMA_{50}$ macro-CTA, revealing a pK_a of 6.27 (Figure 2.8b). This value is somewhat lower than previously reported for a similar *N*-methylmorpholine of 7.41 by Hall.[70]

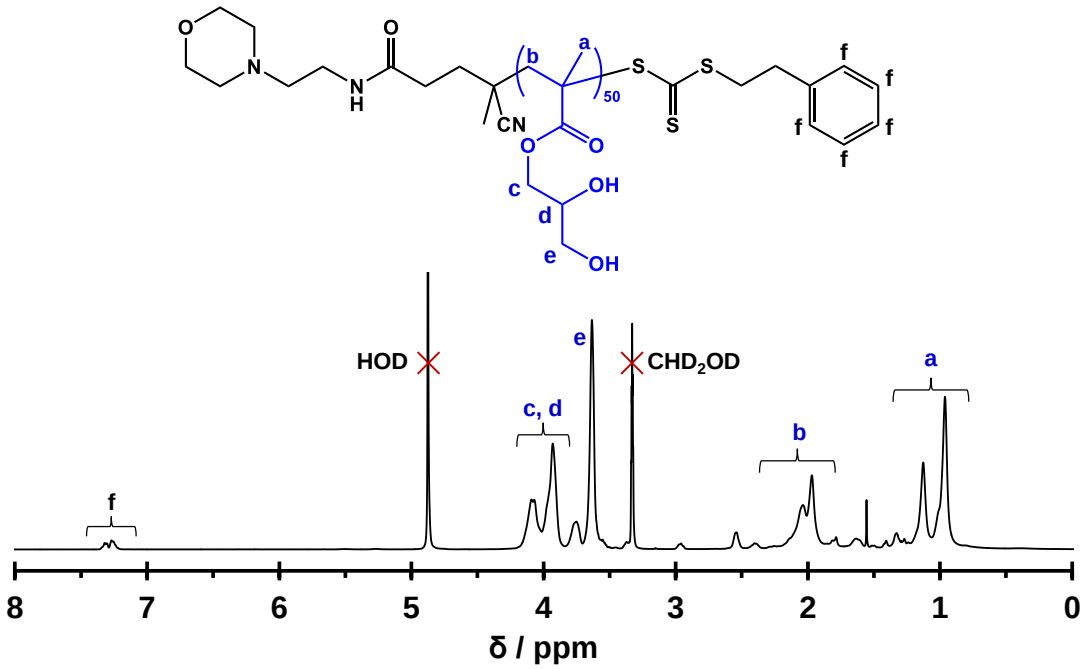

Figure 2.7 Partially assigned ^{1}H NMR spectra recorded in CD_3OD and at 298 K of MPETTC-PGMA$_{50}$ macro-CTA . Labelled are the major polymeric backbone and side groups, as well as the aromatic end-group in (a) used to calculate the DP_n of the MPETTC-PGMA macro-CTA.

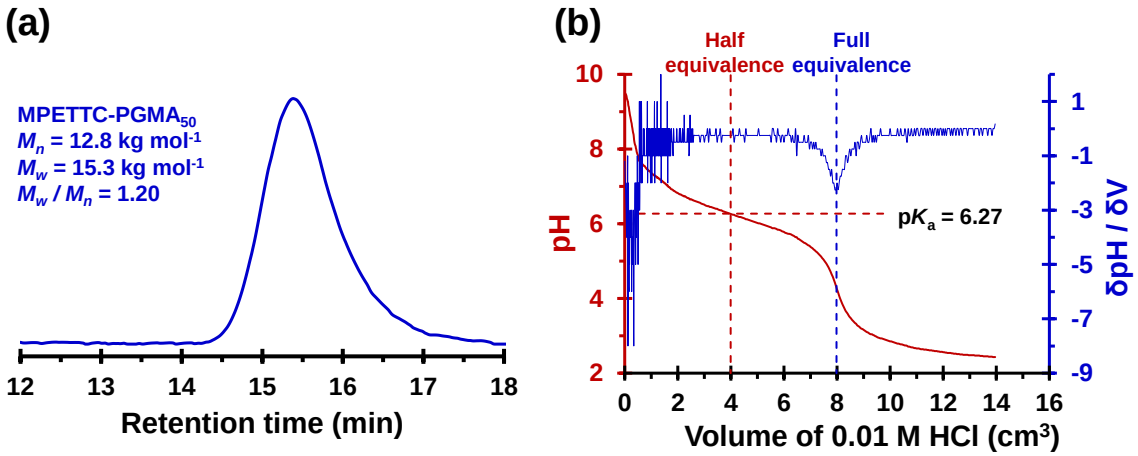

Figure 2.8 (a) Number-average (M_n) and weight-average (M_w) molecular weight data obtained for MPETTC-PGMA$_{50}$ macro-CTA. Data was obtained by DMF GPC calibrated with sixteen near-monodisperse poly(methyl methacrylate) standards. (b) Acid titration curves for a 0.5% w/w aqueous solution of MPETTC-PGMA$_{50}$ macro-CTA. Aqueous solution pH was adjusted with 0.01 M HCl.

2.3.3 Synthesis of MPETTC-PGMA-PHPMA and MePETTC-PGMA-PHPMA Diblock Copolymer Worms

Using the PGMA-PHPMA master phase diagram shown in Chapter 1 (see Figure 1.19d) as a guide, the MPETTC-PGMA$_{50}$ macro-CTA was chain-extended *via* RAFT aqueous dispersion polymerisation of HPMA at 56 °C for 4 h. The conditions selected were 15% w/w total solids with a MPETTC-PGMA$_{50}$ to AIBA molar ratio of 5.0, targeting a PHPMA DP$_n$ of 140. Importantly, the pH was adjusted prior to polymerisation to pH 7.0 – 7.5, ensuring the morpholine end-group remained mainly in its neutral, free amine form. After heating for 4 h, the polymerisation was quenched by exposure to air followed by cooling to room temperature. ^{1}H NMR studies indicated more than 99% HPMA conversion when comparing the integrated signal of the methacrylic backbone at 0 – 2.5 ppm to that of the monomer vinyl signal at 6.1 ppm (Figure 2.9).

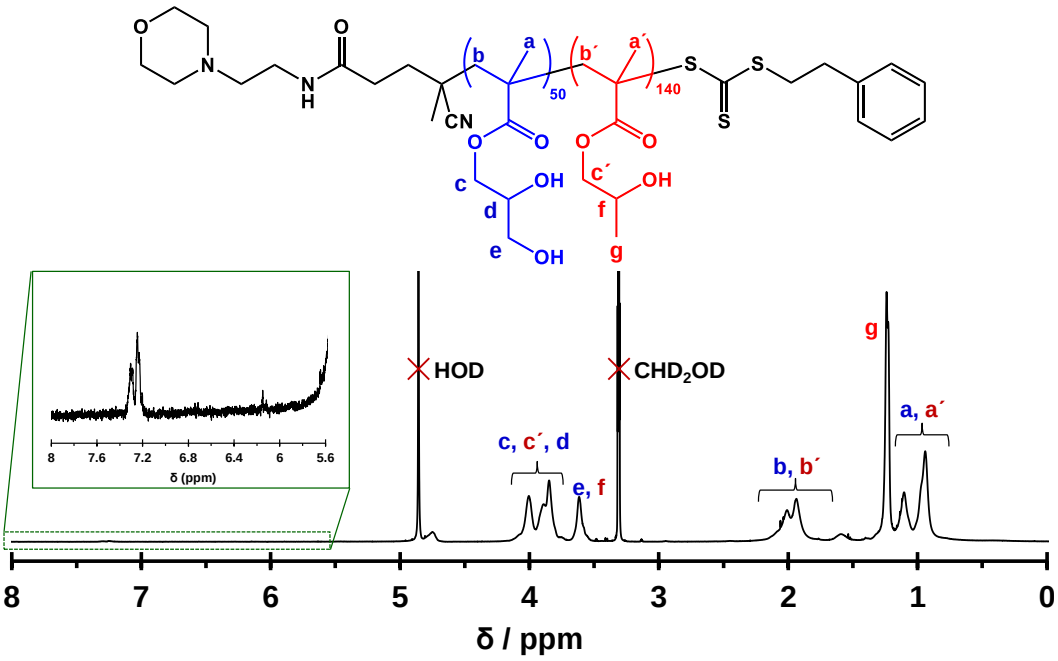

Figure 2.9 Partial assigned ^{1}H NMR spectrum recorded in CD_3OD and at 298 K of MPETTC-PGMA$_{50}$-PHPMA$_{140}$ diblock copolymer. The green inset magnifies the 5.6 to 8.0 ppm region to show the aromatic end-group and the lack of any detectable HPMA monomer vinyl signal.

DMF GPC studies (Figure 2.10) studies indicated clean blocking of the $PGMA_{50}$ macro-CTA with a M_n of 33,000 g mol^{-1} with a relatively low final M_w / M_n of 1.14 relative to PMMA standards.

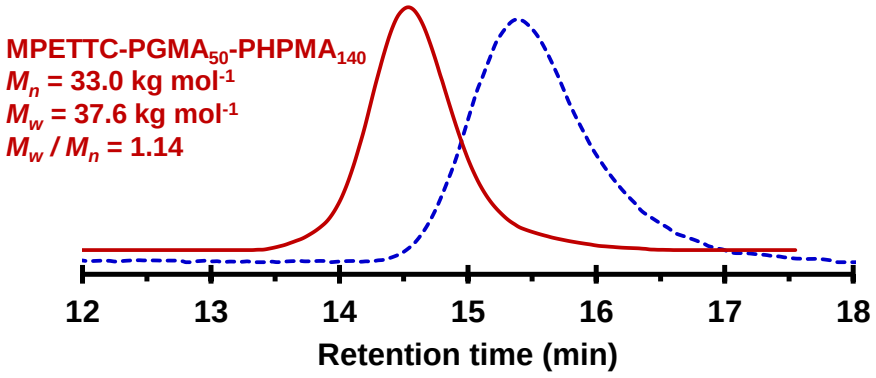

Figure 2.10 Number-average (M_n) and weight-average (M_w) molecular weight data obtained for a MPETTC-$PGMA_{58}$-$PHPMA_{140}$ diblock copolymer. Data was obtained by DMF GPC calibrated with sixteen near-monodisperse poly(methyl methacrylate) standards. The MPETTC-$PGMA_{50}$ macro-CTA is shown by the blue-dotted line to allow for easy comparison.

In control experiments, the carboxylic acid group of PETTC was exhaustively methylated to produce a non-ionic RAFT agent, termed MePETTC. ^{1}H NMR confirmed full methylation by comparison of the integrated aromatic signal a 7.2 – 7.4 ppm (Figure 2.11, peaks 1-3) with that of the newly formed methyl ester $–CH_3$ group (Figure 2.11, peak 9) at 3.67 ppm. Elemental analysis was in extremely good agreement with theoretical values and time of flight mass spectroscopy confirmed a m/z ion of 354. MePETTC RAFT agent was used to prepare a MePETTC-$PGMA_{58}$ macro-CTA by RAFT solution polymerisation in ethanol. DMF GPC studies indicated a M_n of 13,800 g mol^{-1} with an M_w / M_n of 1.20 relative to PMMA standards (Figure 2.12). Chain-extension was performed with 160 units of HPMA *via* RAFT aqueous dispersion polymerisation at pH 7.0 – 7.5 and 15% w/w solids. ^{1}H NMR studies indicated >99% HPMA conversion and DMF GPC studies showed high blocking efficiency of the MePETTC-$PGMA_{58}$ macro-CTA with a M_n of 35,700 g mol^{-1} and a low M_w / M_n of 1.15 .

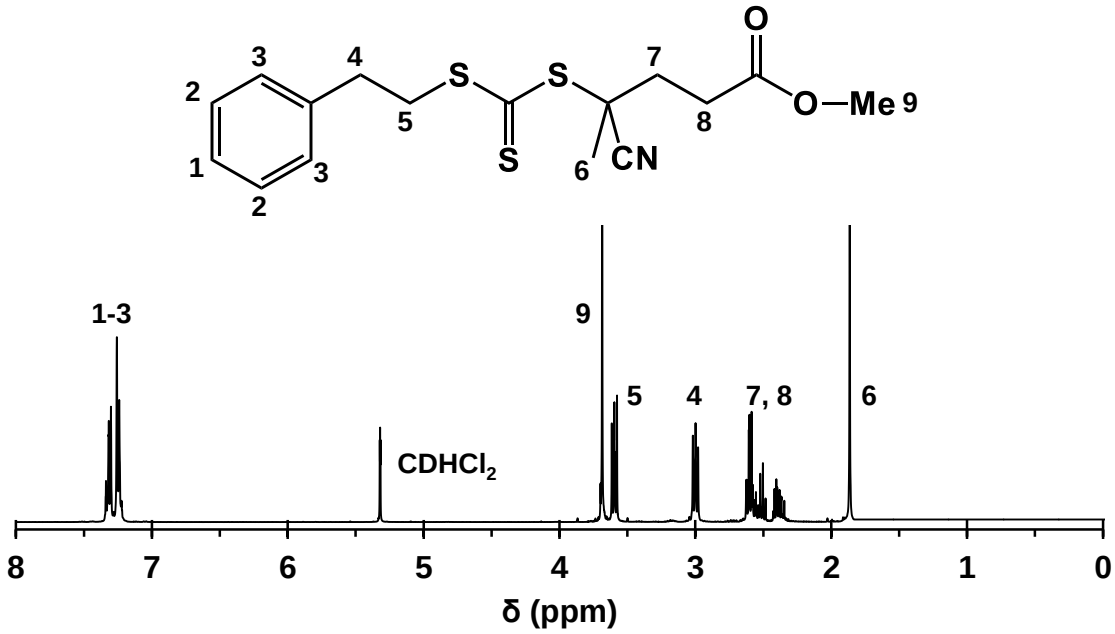

Figure 2.11 Fully assigned ^{1}H NMR spectra recorded in CD_2Cl_2 and at 298 K for MePETTC RAFT agent.

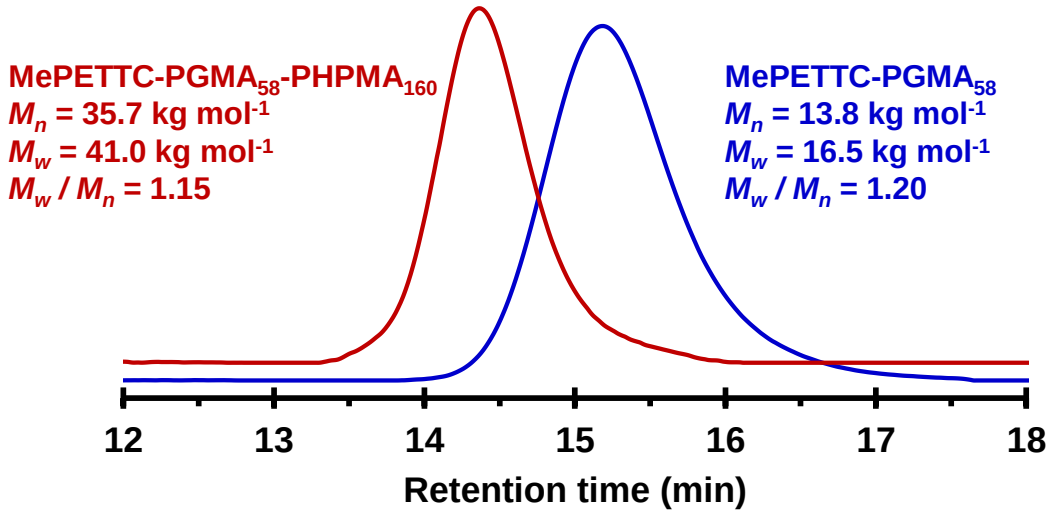

Figure 2.12 Number-average (M_n) and weight-average (M_w) molecular weight data obtained for MePETTC-PGMA$_{58}$ macro-CTA and MePETTC-PGMA$_{58}$-PHPMA$_{160}$ diblock copolymer. Data was obtained by DMF GPC and molecular weight data was calculated relative to sixteen near-monodisperse poly(methyl methacrylate) standards.

Both the morpholine terminated MPETTC-PGMA$_{50}$-PHPMA$_{140}$ and MePETTC-PGMA$_{58}$-PHPMA$_{160}$ diblock copolymer nanoparticles formed soft, free-standing gels at 15% w/w solids and pH 7.0 – 7.5. TEM analysis at pH 7 confirmed that both MPETTC-PGMA$_{50}$-PHPMA$_{140}$ and MePETTC-PGMA$_{58}$-PHPMA$_{160}$ block copolymer compositions formed worms, as expected (Figure 2.13). Interestingly, a significant amount of branching was observed. The degrees of worm branching and mean worm-contour length are difficult parameters to control in PISA formulations, although Figg *et al.* have begun to examine this problem.[80]

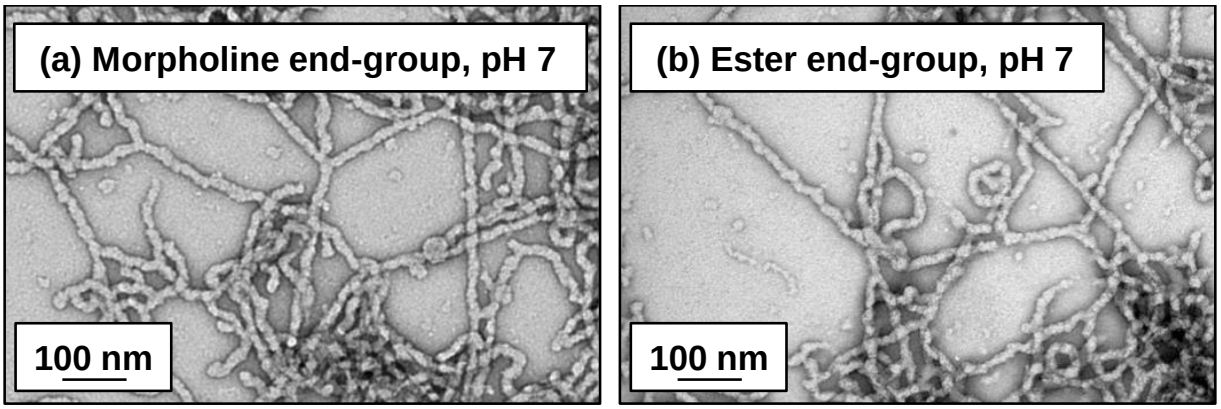

Figure 2.13 TEM images obtained for (a) MPETTC-PGMA$_{50}$-PHPMA$_{140}$ and (b) MePETTC-PGMA$_{58}$-PHPMA$_{160}$ diblock copolymer worms at pH 7.

2.3.4 Examination of pH-Responsive Behaviour

DLS is a well-established technique for relating the Brownian motion of spherical particles dispersed within a liquid to their diameter. Brownian motion is quantified *via* a translational diffusion coefficient (D) and particle sizes are calculated using the Stokes-Einstein equation (see equation 2.1) where k_b is the Boltzmann constant, T is absolute temperature and η is the viscosity.[81] Thus, DLS requires accurate knowledge of the liquids viscosity and temperature. Typically larger particles move slower in a liquid relative to smaller particles, hence they exhibit a lower value of D.

$$d_h = \frac{k_b T}{3\pi\eta D} \qquad \textbf{2.1}$$

In DLS a 633 nm laser is shone at a dilute dispersion of particles and analysis of the fluctuations in the intensity of the scattering pattern over extremely short timescales (ns or μs) yields a decay rate which can be linked to D. Although DLS is a very simple, quick and convenient technique for determining particle size distributions it does have certain limitations. Firstly the intensity of scattered light is highly dependent on particle sizes ($I \alpha r^6$), thus DLS is very sensitive to any large particle contaminant (i.e. dust) and reports an intensity-average particle diameter. Volume-average and number-average diameters can be calculated from the intensity-average diameter. Secondly DLS assumes only one scattering event per particle and must be conducted at low concentrations (typically 0.1% w/w). Finally DLS assumes that particles are spherical and non-interacting. Thus for non-spherical particles a 'sphere-equivalent' diameter is reported, whereby this diameter is equal to that of a sphere which exhibits same effective particle movement (i.e. same D value). While the 'sphere-equivalent' number is numerically meaningless (i.e. does not represent the actual mean worm length or width), it is affected by the rod/worm length more than width.[82] Notwithstanding these limitations, DLS can serve as a meaningful method for determining changes in particle size upon response to certain stimuli. Furthermore, aqueous electrophoresis experiments are conducted to determine the zeta potential of particles using the same instrument, thus suffer from similar limitations. Thus, DLS and aqueous electrophoresis experiments were performed to examine the effect of pH on both the apparent particle diameter and zeta potential of MPETTC-PGMA$_{50}$-PHPMA$_{140}$ and MePETTC-PGMA$_{58}$-PHPMA$_{160}$ diblock copolymer worms (Figure 2.14). Aqueous dispersions were initially prepared at 0.1% w/w and pH 7.2. Acidification was performed using either 0.1 M or 1 M HCl with approximately 20 minutes equilibration allowed between each measurement point.

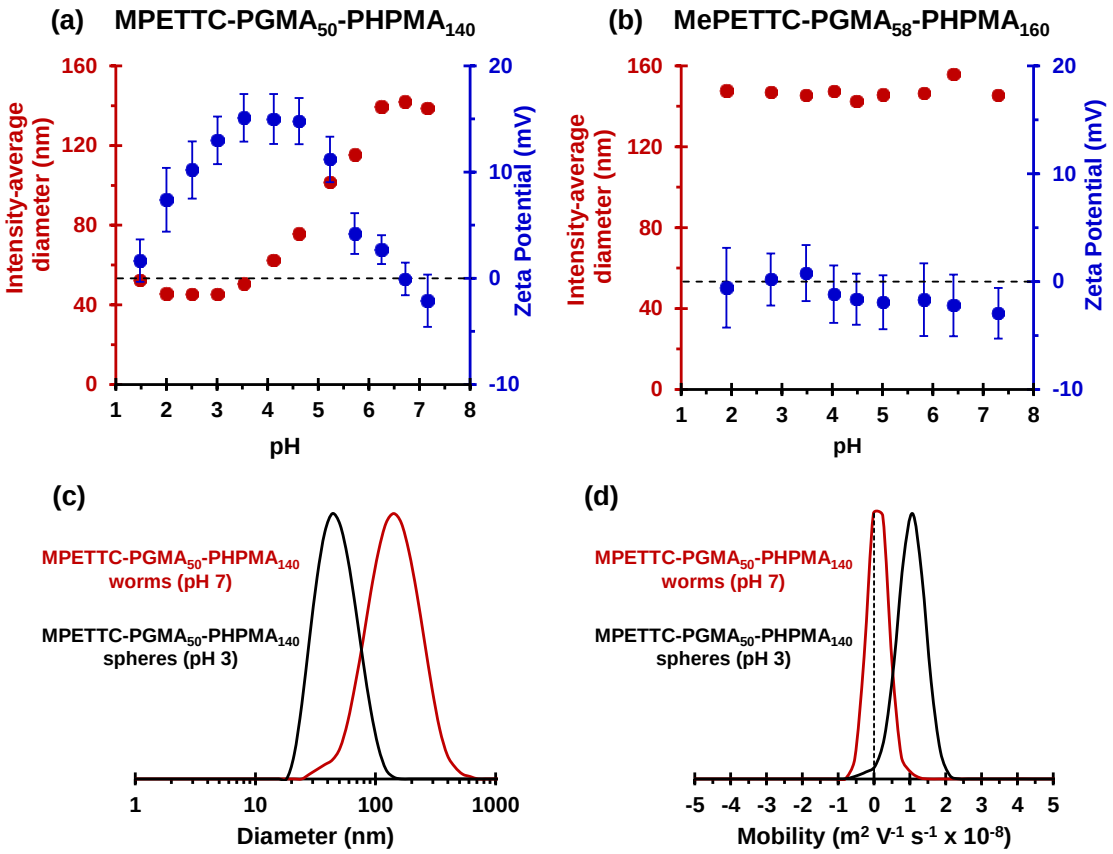

Figure 2.14 Intensity-average diameter and zeta potential vs. pH data obtained for either (a) MPETTC-PGMA$_{50}$-PHPMA$_{140}$ or (b) MePETTC-PGMA$_{58}$-PHPMA$_{160}$ diblock copolymer nanoparticles. Measurements were conducted on 0.1% w/w aqueous dispersions at 20 °C. Dispersion pH was adjusted with either 0.1 M or 1 M HCl to minimise particle dilution. Error bars are equivalent to 1 standard deviation. Representative (c) intensity-average diameter and (d) aqueous electrophoretic mobility traces for MPETTC-PGMA$_{50}$-PHPMA$_{140}$ worms at pH 7 (red traces) and corresponding spheres at pH 3 (black traces).

For morpholine-terminated MPETTC-PGMA$_{50}$-PHPMA$_{140}$ diblock copolymer worms (Figure 2.14a) a significant reduction in apparent particle diameter from 139 nm to 43 nm was observed on lowering the solution pH from 7.2 to 3.0. According to Liu and Xiao[83] the translational diffusion coefficient for high aspect ratio particles is typically much faster than their corresponding rotational diffusion coefficient. Thus a unimodal DLS trace is observed for the MPETTC-PGMA$_{50}$-PHPMA$_{140}$ worms at pH 7.2 (see Figure 2.14a). In addition, a representative

unimodal DLS trace is shown in Figure 2.14b for 43 nm cationic spheres at pH 3. It should be noted that a reduction in the derived count-rate from 43,700 kcps to 19,700 kcps was observed as the morphology transition proceeds. Considering that the initial volume of the pH titrations was 30 mL of 0.1% w/w aqueous worm dispersion, the additional volume of 1 M HCl required to induce the pH change (typically 100-300 μL) is not sufficient to cause a reduction in the derived count-rate. This reduction in hydrodynamic diameter is observed because the all of the morpholine end-groups become fully protonated below its pK_a of 6.27. Subsequently, this terminal cationic charge increases the degree of hydration of the PGMA stabiliser block and hence its volume fraction and reducing the packing parameter, *P*, resulting in a worm-to-sphere transition. TEM analysis of dried dispersions at pH 3 (Figure 2.15a) shows exclusively spheres and provides conclusive evidence of a worm-to-sphere transition.

In aqueous electrophoresis studies, the electrophoretic mobility of particles is measured and the zeta potential can be calculated from the Henry equation (see equation 2.2), assuming the Smoluchowski approximation. Here, U_e is the electrophoretic mobility, ε is the dielectric constant, ζ is the zeta potential, f(κa) is Henry's function and η is the viscosity.

$$\boldsymbol{U_e = \frac{2\varepsilon\zeta f(\kappa a)}{3\eta}} \qquad \textbf{2.2}$$

A concomitant increase in zeta potential from approximately 0 mV to +15 mV occurred when acidifying the aqueous worm dispersion from pH 7.2 to pH 3.0 due to protonation of the morpholine end-group. Representative aqueous electrophoretic mobility traces are unimodal for both the neutral worms (pH 7) and cationic spheres (pH 3), as shown in Figure 2.14d. Furthermore a reduction in apparent zeta potential to approximately 0 mV occurs upon lowering the dispersion pH to pH 1.5.

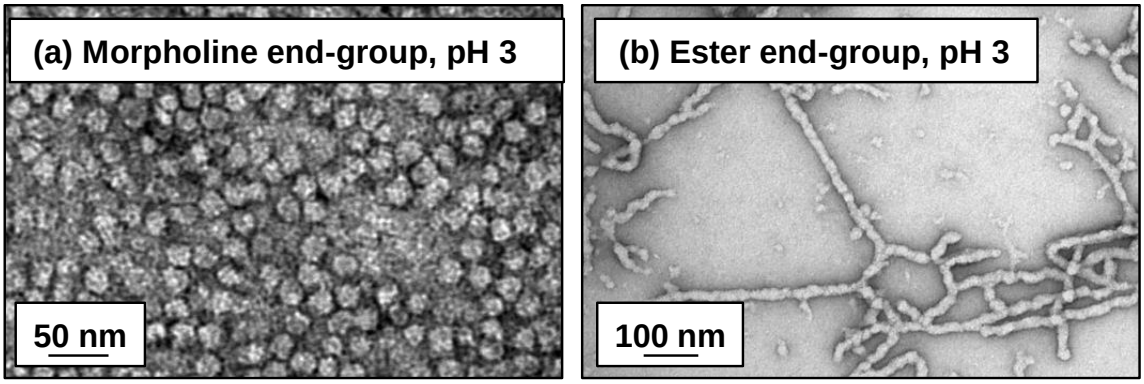

Figure 2.15 TEM images obtained for (a) MPETTC-PGMA$_{50}$-PHPMA$_{140}$ and (b) MePETTC-PGMA$_{58}$-PHPMA$_{160}$ diblock copolymer worms at pH 7.

Here, excess HCl is acting as a salt and screening the cationic charge arising from the protonated morpholine end-groups. This observation, together with a minor increase in apparent hydrodynamic diameter, suggests that worm reformation might be feasible. Nevertheless, efficient fusion of multiple spheres (the first step in worm formation)[36] is very unlikely to occur under both the high dilution (0.1% w/w required for DLS and aqueous electrophoresis) and normal experimental timescales (approximately 1-2 h). For MePETTC-PGMA$_{58}$-PHPMA$_{160}$ diblock copolymer worms no change in both apparent particle diameter (≈ 145 nm) and zeta potential (≈ 0 mV) is observed upon decreasing the dispersion pH from pH 7 to pH 2. TEM studies at pH 3 confirm an exclusive worm morphology (Figure 2.15b). This demonstrates that methyl ester terminated worms are *not* pH responsive, as expected.

Oscillatory rheological studies were conducted on both morpholine and methyl ester terminated worms at 20 °C to examine the effect of pH on gel strength. All measurements were conducted at 15% w/w solids content with a strain of 1% and at an angular frequency of 1 rad s^{-1}. Acidification of the nanoparticles was performed using 1M HCl to minimise the subtle change in copolymer concentration upon adding aqueous acid. Samples were left to incubate for a 24 h at 20 °C before analysis. MPETTC-PGMA$_{50}$-PHPMA$_{140}$ diblock copolymer worms exhibit a

maximum G' value of 342 Pa at pH 6.8 (Figure 2.16a). A gel is formed from the multiple inter-worm contacts.[40] Upon acidification of the aqueous dispersion to pH 3.0, a dramatic reduction in G' to just 0.4 Pa was observed. Degelation (as judged by the point where $G'' > G'$) occurs between pH 5.0 and pH 3.8. Furthermore, lowering the dispersion pH to below 3 had a significant effect on the gel strength. As seen in Figure 2.14, excess HCl acts as a salt, shielding the terminal cationic charge from the protonated morpholine end-groups. Low particle concentrations required for DLS experiments mean a sphere-to-worm transition is very unlikely. However, the possibility of efficient sphere-sphere fusion is significantly increased at the high concentrations (15% w/w *vs.* 0.1% w/w) required for oscillatory rheological experiments. An increase in G' is seen at pH 1.5 but here G'' still exceeds G'. Further acidification to pH 0.9 results in regelation but in this case G' is only 48 Pa (*vs.* original 342 Pa). TEM studies at pH 0.9 confirm that worms are the dominant morphology (Figure 2.16b).

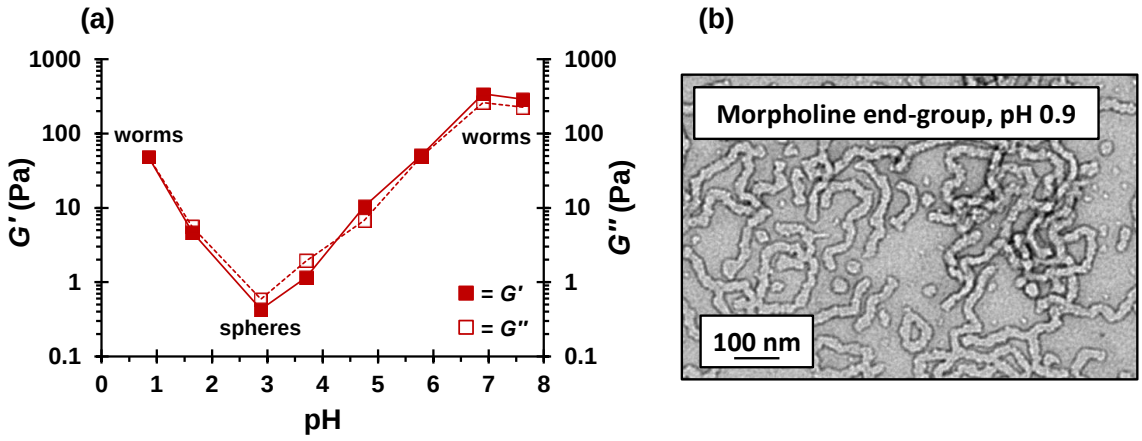

Figure 2.16 (a) Storage-modulus (G') and loss-modulus (G'') values obtained by oscillatory rheology for acidifying a 15% w/w aqueous dispersion of MPETTC-PGMA$_{50}$-PHPMA$_{140}$ diblock copolymer nanoparticles from pH 7.4 to pH 0.9. Storage and loss modulus values are obtained for 15 % w/w copolymer dispersions at an angular frequency of 1 rad s^{-1}, a strain of 1% and at a temperature of 20 °C. (b) Representative TEM image for the diblock copolymer worms obtained after acidification to pH 0.9.

There are two plausible reasons as to why the gel strength at pH 0.9 is more than an order of magnitude less than the original gel strength at pH 6.8. Firstly, the mean worm contour length of the reconstituted worms at pH 0.9 is shorter than the original worms at pH 6.8, reducing the number of inter-worm contacts. Secondly, the worms at pH 0.9 may regain the original mean worm contour length but the inter-worm attractive interactions may be weakened, as the worm end-groups possess residual cationic character. DLS studies at pH 0.9 revealed an intensity-average particle diameter of 161 nm, larger than the original 139 nm, suggesting formation of somewhat longer worms at pH 0.9. Therefore, the reduction in gel strength at pH 0.9 is most likely weaker because each worm possesses residual cationic character, which leads to inter-worm repulsion.

In contrast, the original gel strength can be regained *via* a pH sweep from pH 6.8 to pH 3.0 and back to pH 7.3 (Figure 2.17a). Deprotonation of the morpholine end-group occurs as the solution pH increases from 3.0 to 7.3, inducing a sphere-to-worm transition at high copolymer concentrations. DLS studies indicate a sphere-equivalent diameter of 140 nm for the reconstituted worms. This is nearly identical to that of the original diameter of 139 nm. Furthermore, a G' value of 321 Pa (vs. 342 Pa) is obtained suggesting comparable mean worm contour lengths and comparable number of inter-worm contacts. TEM studies confirm that worms are the exclusive morphology (Figure 2.17c). MePETTC-PGMA$_{58}$-PHPMA$_{160}$ diblock copolymer worms are somewhat stronger gels at the same copolymer concentration with G' of 360 Pa (Figure 2.17b). Here the gel strength remains unchanged with dispersion pH, as the methyl ester end-groups located on the PGMA chain-ends are pH-insensitive. Hence, no change in the packing parameter, *P*, occurs under these condition and consequently there is no worm-to-sphere transition.

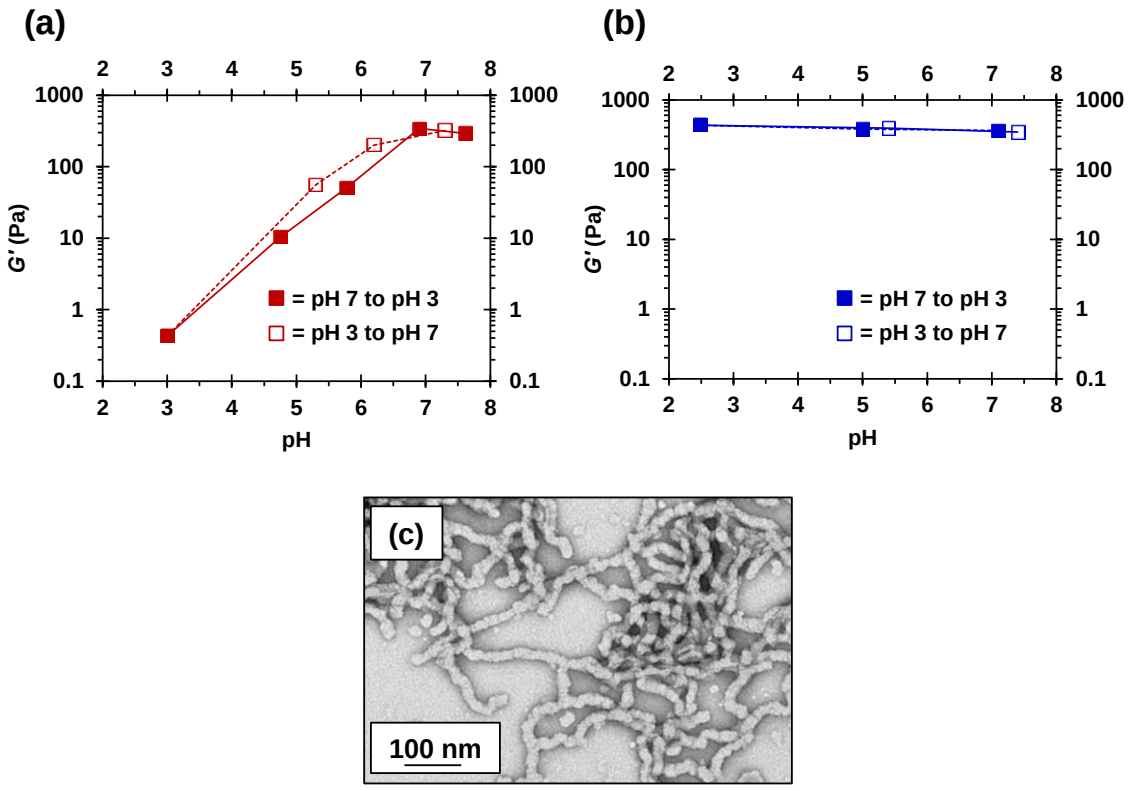

Figure 2.17 Variation in the storage modulus (*G'*) for (a) a 15% w/w aqueous dispersion of MPETTC-PGMA$_{50}$-PHPMA$_{160}$ diblock copolymer nanoparticles upon lowering dispersion pH from pH 6.8 to pH 3.0 (red solid line) then returning to pH 7.3 (red dotted line). The same experiment was performed on (b) a 15% w/w aqueous dispersion of MePETTC-PGMA$_{58}$-PHPMA$_{160}$ diblock copolymer nanoparticles undergoing a pH switch from pH 7.1 to pH 2.5 (blue solid line) and back to pH 7.8 (blue dotted line). (c) Representative TEM image obtained for MPETTC-PGMA$_{50}$-PHPMA$_{160}$ worms after a reversible pH switch from pH 7 to pH 3 and back to pH 7.

As excess acid can act as a salt and screen the end-group charge at very low dispersion pH, the effect of adding KCl on both particle morphology and gel strength was examined by TEM and oscillatory rheology studies (Figure 2.18). A 15% w/w dispersion of *exclusively* MPETTC-PGMA$_{50}$-PHPMA$_{140}$ cationic spheres at pH 3.0 was prepared and KCl was added so the final concentration ranges from 0 mM to 100 mM. At low KCl concentrations (20 mM KCl) there was over an order of magnitude increase in viscosity to 14 Pa.

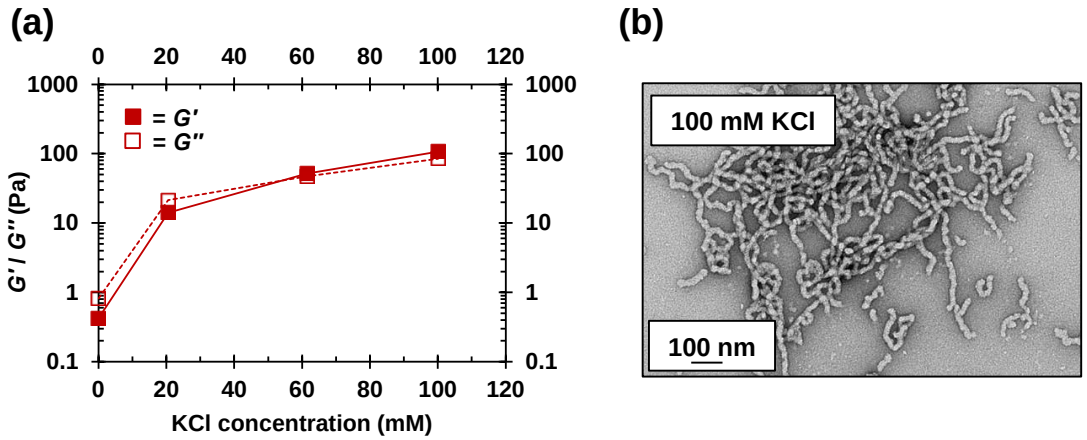

Figure 2.18 (a) Variation of storage-modulus (*G′*) and loss-modulus (*G″*) with KCl concentration for a 15 % w/w aqueous dispersion of MPETTC-PGMA$_{50}$-PHPMA$_{140}$ diblock copolymer nanoparticles acidified at pH 3. (b) Representative TEM image obtained for this block copolymer composition in the presence of 100 mM KCl.

However, *G″* exceeds *G′* so regelation has not occurred. Gelation is seen upon increasing the salt concentration to 60 mM KCl as *G′* (52 Pa) exceeds *G″* (47 Pa). Further increasing the salt concentration to 100 mM leads to a stronger gel with a *G′* value of 107 Pa, but the original gel strength of 342 Pa could not be regained. TEM analysis (Figure 2.18b) indicated exclusive worm morphology. We hypothesise that this is because the protonated cationic morpholine end-groups located at the worm periphery lead to weaker and/or fewer inter-worm contacts. These results agree with previous work by Geng *et al.* who found that the addition of salt to poly(acrylic acid)-polybutadiene diblock copolymer spheres leads to a sphere-to-worm morphology transition from 0 mM KCl to 100 mM KCl.[84]

2.4 Conclusions

In this Chapter, a new morpholine terminated RAFT agent, MPETTC, has been prepared in two steps by modification of the PETTC, with a total yield of 80%. MPETTC has been determined to be an effective RAFT agent by the solution polymerisation of GMA in either ethanol or water at pH 4. A PGMA$_{50}$ macro-CTA was prepared by RAFT solution polymerisation in ethanol to

maintain the neutral character of the morpholine end-group. Chain extension of this $PGMA_{50}$ macro-CTA was performed by RAFT aqueous dispersion polymerisation of HPMA at pH 7.0 – 7.5 to prepare MPETTC-$PGMA_{50}$-$PHPMA_{140}$ diblock copolymer worms. At this pH, such worms form free-standing gels as judged by both the tube inversion test and oscillatory rheological studies. Protonation of the morpholine end-group induced a worm-to-sphere transition with *in situ* degelation occurring at pH 3. Near full gel strength can be regained by returning to pH 7 with the corresponding sphere-to-worm and gelation taking place. However, upon acidification to pH < 3, excess acid can act as a salt, screening the effect of the end-group cationic charge leading to reformation of the worm gel. Furthermore, addition of KCl to a dispersion of cationic spheres at pH 3 can also cause a sphere-to-worm transition, but original gel modulus values cannot be recovered (see Figure 2.19). Such morphology transitions are solely driven by *end-group* protonation effects caused by a subtle increase in the relative volume fraction of the stabiliser compared to the particle core.

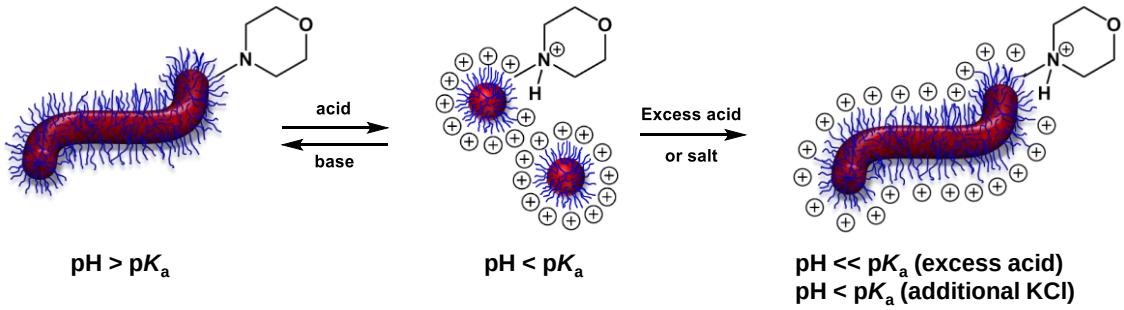

Figure 2.19 Schematic cartoon of the reversible worm-to-sphere transition that occurs when morpholine-functionalised $PGMA_{50}$-$PHPMA_{140}$ diblock copolymer worms prepared using MPETTC undergo a pH switch upon addition of acid or base. Addition of salt to a spherical dispersion at pH 3 can also induce the sphere-to-worm transition.

2.5 References

1. R. C. Hayward and D. J. Pochan, *Macromolecules*, 2010, **43**, 3577.
2. Z. Tuzar and P. Kratochvil, *Advances in Colloid and Interface science*, 1976, **6**, 201.

3. L. Zhang and A. Eisenberg, *Science*, 1995, **268**, 1728.
4. Z. Li, E. Kesselman, Y. Talmon, M. A. Hillmyer and T. P. Lodge, *Science*, 2004, **306**, 98.
5. D. J. Pochan, Z. Chen, H. Cui, K. Hales, K. Qi and K. L. Wooley, *Science*, 2004, **306**, 94.
6. H. Cui, Z. Chen, S. Zhong, K. L. Wooley and D. J. Pochan, *Science*, 2007, **317**, 647.
7. J. A. Zupancich, F. S. Bates and M. A. Hillmyer, *Macromolecules*, 2006, **39**, 4286.
8. S. Jain and F. S. Bates, *Macromolecules*, 2004, **37**, 1511.
9. H. Bermudez, A. K. Brannan, D. A. Hammer, F. S. Bates and D. E. Discher, *Macromolecules*, 2002, **35**, 8203.
10. S. Jain and F. S. Bates, *Science*, 2003, **300**, 460.
11. Y.-Y. Won, H. T. Davis and F. S. Bates, *Macromolecules*, 2003, **36**, 953.
12. J. A. Zupancich, F. S. Bates and M. A. Hillmyer, *Biomacromolecules*, 2009, **10**, 1554.
13. M. S. Donovan, A. B. Lowe, B. S. Sumerlin and C. L. McCormick, *Macromolecules*, 2002, **35**, 4123.
14. A. B. Lowe, B. S. Sumerlin, M. S. Donovan and C. L. McCormick, *Journal of the American Chemical Society*, 2002, **124**, 11562.
15. B. S. Sumerlin, A. B. Lowe, D. B. Thomas and C. L. McCormick, *Macromolecules*, 2003, **36**, 5982.
16. C. L. McCormick, B. S. Sumerlin, B. S. Lokitz and J. E. Stempka, *Soft Matter*, 2008, **4**, 1760.
17. R. K. O'Reilly, M. J. Joralemon, C. J. Hawker and K. L. Wooley, *Journal of Polymer Science Part A: Polymer Chemistry*, 2006, **44**, 5203.
18. J. Bang, S. H. Kim, E. Drockenmuller, M. J. Misner, T. P. Russell and C. J. Hawker, *Journal of the American Chemical Society*, 2006, **128**, 7622.
19. R. J. Amir, S. Zhong, D. J. Pochan and C. J. Hawker, *Journal of the American Chemical Society*, 2009, **131**, 13949.
20. S.-Y. Ku, M. A. Brady, N. D. Treat, J. E. Cochran, M. J. Robb, E. J. Kramer, M. L. Chabinyc and C. J. Hawker, *Journal of the American Chemical Society*, 2012, **134**, 16040.
21. J.-S. Wang and K. Matyjaszewski, *Journal of the American Chemical Society*, 1995, **117**, 5614.
22. M. Kato, M. Kamigaito, M. Sawamoto and T. Higashimura, *Macromolecules*, 1995, **28**, 1721.
23. J. Chiefari, Y. K. Chong, F. Ercole, J. Krstina, J. Jeffery, T. P. T. Le, R. T. A. Mayadunne, G. F. Meijs, C. L. Moad, G. Moad, E. Rizzardo and S. H. Thang, *Macromolecules*, 1998, **31**, 5559.
24. G. Moad, E. Rizzardo and S. H. Thang, *Australian Journal of Chemistry*, 2006, **59**, 669.
25. G. Moad, E. Rizzardo and S. H. Thang, *Australian Journal of Chemistry*, 2009, **62**, 1402.
26. G. Moad, E. Rizzardo and S. H. Thang, *Australian Journal of Chemistry*, 2012, **65**, 985.
27. Y. Li and S. P. Armes, *Angewandte Chemie International Edition*, 2010, **49**, 4042.
28. A. Blanazs, S. P. Armes and A. J. Ryan, *Macromolecular Rapid Communications*, 2009, **30**, 267.
29. A. Blanazs, A. J. Ryan and S. P. Armes, *Macromolecules*, 2012, **45**, 5099.
30. B. T. T. Pham, D. Nguyen, C. J. Ferguson, B. S. Hawkett, A. K. Serelis and C. H. Such, *Macromolecules*, 2003, **36**, 8907.
31. V. J. Cunningham, A. M. Alswieleh, K. L. Thompson, M. Williams, G. J. Leggett, S. P. Armes and O. M. Musa, *Macromolecules*, 2014, **47**, 5613.
32. I. Chaduc, A. Crepet, O. Boyron, B. Charleux, F. D'Agosto and M. Lansalot, *Macromolecules*, 2013, **46**, 6013.

33. X. Zhang, S. Boisse, W. Zhang, P. Beaunier, F. D'Agosto, J. Rieger and B. Charleux, *Macromolecules*, 2011, **44**, 4149.
34. S. Boisse, J. Rieger, K. Belal, A. Di-Cicco, P. Beaunier, M.-H. Li and B. Charleux, *Chemical Communications*, 2010, **46**, 1950.
35. W. Zhang, F. D'Agosto, O. Boyron, J. Rieger and B. Charleux, *Macromolecules*, 2012, **45**, 4075.
36. A. Blanazs, J. Madsen, G. Battaglia, A. J. Ryan and S. P. Armes, *Journal of the American Chemical Society*, 2011, **133**, 16581.
37. N. J. Warren and S. P. Armes, *Journal of the American Chemical Society*, 2014, **136**, 10174.
38. J. N. Israelachvili, D. J. Mitchell and B. W. Ninham, *Journal of the Chemical Society, Faraday Transactions 2: Molecular and Chemical Physics*, 1976, **72**, 1525.
39. Z. Chu, C. A. Dreiss and Y. Feng, *Chemical Society Reviews*, 2013, **42**, 7174.
40. R. Verber, A. Blanazs and S. P. Armes, *Soft Matter*, 2012, **8**, 9915.
41. E. S. Gil and S. M. Hudson, *Progress in Polymer Science*, 2004, **29**, 1173.
42. I. Dimitrov, B. Trzebicka, A. H. E. Mueller, A. Dworak and C. B. Tsvetanov, *Progress in Polymer Science*, 2007, **32**, 1275.
43. C. L. McCormick and A. B. Lowe, *Accounts of Chemical Research*, 2004, **37**, 312.
44. J. Du and R. K. O'Reilly, *Soft Matter*, 2009, **5**, 3544.
45. D. Lindner and D. Raghavan, *British Journal of Cancer*, 2009, **100**, 1287.
46. F. C. Giacomelli, P. Stepanek, C. Giacomelli, V. Schmidt, E. Jaeger, A. Jaeger and K. Ulbrich, *Soft Matter*, 2011, **7**, 9316.
47. N. Rapoport, *Progress in Polymer Science*, 2007, **32**, 962.
48. S. Liu and S. P. Armes, *Angewandte Chemie International Edition*, 2002, **41**, 1413.
49. J. Rodriguez-Hernandez and S. Lecommandoux, *Journal of the American Chemical Society*, 2005, **127**, 2026.
50. V. Bütün, S. Liu, J. V. M. Weaver, X. Bories-Azeau, Y. Cai and S. P. Armes, *Reactive and Functional Polymers*, 2006, **66**, 157.
51. A. E. Smith, X. Xu, S. E. Kirkland-York, D. A. Savin and C. L. McCormick, *Macromolecules*, 2010, **43**, 1210.
52. Y. Pei, A. B. Lowe and P. J. Roth, *Macromolecular Rapid Communications*, 2017, **38**, 1600528.
53. A. Blanazs, R. Verber, O. O. Mykhaylyk, A. J. Ryan, J. Z. Heath, C. W. Douglas and S. P. Armes, *Journal of the American Chemical Society*, 2012, **134**, 9741.
54. M. Williams, N. J. W. Penfold, J. R. Lovett, N. J. Warren, C. W. I. Douglas, N. Doroshenko, P. Verstraete, J. Smets and S. P. Armes, *Polymer Chemistry*, 2016, **7**, 3864.
55. N. J. Warren, O. O. Mykhaylyk, D. Mahmood, A. J. Ryan and S. P. Armes, *Journal of the American Chemical Society*, 2014, **136**, 1023.
56. Y. Pei, N. C. Dharsana, J. A. van Hensbergen, R. P. Burford, P. J. Roth and A. B. Lowe, *Soft Matter*, 2014, **10**, 5787.
57. Y. Pei, K. Jarrett, M. Saunders, P. J. Roth, C. E. Buckley and A. B. Lowe, *Polymer Chemistry*, 2016, **7**, 2740.
58. J. Yeow, J. Xu and C. Boyer, *ACS Macro Letters*, 2015, **4**, 984.
59. L. A. Fielding, J. A. Lane, M. J. Derry, O. O. Mykhaylyk and S. P. Armes, *Journal of the American Chemical Society*, 2014, **136**, 5790.
60. M. J. Derry, O. O. Mykhaylyk and S. P. Armes, *Angewandte Chemie International Edition*, 2017, **56**, 1746.
61. Y. Pei, L. Thurairajah, O. R. Sugita and A. B. Lowe, *Macromolecules*, 2015, **48**, 236.
62. Y. Pei, O. R. Sugita, L. Thurairajah and A. B. Lowe, *RSC Advances*, 2015, **5**, 17636.

63. J. R. Lovett, N. J. Warren, L. P. D. Ratcliffe, M. K. Kocik and S. P. Armes, *Angewandte Chemie International Edition*, 2015, **54**, 1279.
64. M. Bathfield, F. D'Agosto, R. Spitz, M.-T. Charreyre and T. Delair, *Journal of the American Chemical Society*, 2006, **128**, 2546.
65. G. W. Anderson, J. E. Zimmerman and F. M. Callahan, *Journal of the American Chemical Society*, 1964, **86**, 1839.
66. J.-F. Baussard, J.-L. Habib-Jiwan, A. Laschewsky, M. Mertoglu and J. Storsberg, *Polymer*, 2004, **45**, 3615.
67. D. B. Thomas, A. J. Convertine, R. D. Hester, A. B. Lowe and C. L. McCormick, *Macromolecules*, 2004, **37**, 1735.
68. E. R. Jones, M. Semsarilar, A. Blanazs and S. P. Armes, *Macromolecules*, 2012, **45**, 5091.
69. J. Clayden, N. Greeves, S. Warren and P. Wothers, *Organic Chemistry*, Oxford University Press, Oxford, 8th edn., 2009.
70. H. K. Hall, Jr., *Journal of the American Chemical Society*, 1957, **79**, 5441.
71. M. Morgenthaler, E. Schweizer, A. Hoffmann-Roder, F. Benini, R. E. Martin, G. Jaeschke, B. Wagner, H. Fischer, S. Bendels, D. Zimmerli, J. Schneider, F. Diederich, M. Kansy and K. Muller, *ChemMedChem*, 2007, **2**, 1100.
72. V. Bütün, S. P. Armes and N. C. Billingham, *Polymer*, 2001, **42**, 5993.
73. A. B. Lowe and C. L. McCormick, *Progress in Polymer Science*, 2007, **32**, 283.
74. I. Chaduc, M. Lansalot, F. D'Agosto and B. Charleux, *Macromolecules*, 2012, **45**, 1241.
75. M. Semsarilar, V. Ladmiral, A. Blanazs and S. P. Armes, *Langmuir*, 2012, **28**, 914.
76. M. Semsarilar, V. Ladmiral, A. Blanazs and S. P. Armes, *Langmuir*, 2013, **29**, 7416.
77. M. J. Derry, L. A. Fielding and S. P. Armes, *Polymer Chemistry*, 2015, **6**, 3054.
78. L. A. Fielding, M. J. Derry, V. Ladmiral, J. Rosselgong, A. M. Rodrigues, L. P. D. Ratcliffe, S. Sugihara and S. P. Armes, *Chemical Science*, 2013, **4**, 2081.
79. A. Favier and M.-T. Charreyre, *Macromolecular Rapid Communications*, 2006, **27**, 653.
80. C. A. Figg, R. N. Carmean, K. C. Bentz, S. Mukherjee, D. A. Savin and B. S. Sumerlin, *Macromolecules*, 2017, **50**, 935.
81. R. Pecora, *Journal of Nanoparticle Research*, 2000, **2**, 123.
82. Y. Boluk and C. Danumah, *Journal of Nanoparticle Research*, 2014, **16**, 2174/1.
83. T. Liu and Z. Xiao, *Macromolecular Chemistry and Physics*, 2012, **213**, 1697.
84. Y. Geng, F. Ahmed, N. Bhasin and D. E. Discher, *Journal of Physical Chemistry B*, 2005, **109**, 3772.

Chapter 3

Dual Stimulus-Responsive Diblock Copolymer Vesicles

Reproduced in full with permission from:

[N. J. W. Penfold, J. R. Lovett, P. Verstraete, J. Smets, S. P. Armes, *Polymer Chemistry*, 2017, **8**, 272-282]

3.1 Introduction

AB diblock copolymer self-assembly has been of considerable interest to many research groups over the last fifty years. Numerous copolymer morphologies have been reported in dilute solution with the most common being spheres, worms and vesicles.[1-10] In particular, block copolymer vesicles have found applications in numerous fields such as drug delivery,[11-14] medical diagnostics,[15] as nano-reactors[16, 17] and as Pickering emulsifiers.[18, 19] Most of these applications require the encapsulation of water-soluble payload within the vesicle lumen, which protects this cargo from the external environment. Moreover, stimulus-responsive vesicles have been designed to undergo morphological transformations (thus releasing the encapsulated payload) on exposure to external stimuli such as temperature,[20] solution pH,[21, 22] light irradiation[23, 24] or the addition of salt.[25] However, traditional vesicle preparation typically involves post-polymerisation processing. This is often time-consuming and usually results in rather low vesicle concentrations (< 1% w/w), which limits potential industrial applications.

As discussed in Chapter 1, RAFT-mediated PISA is a very convenient method for preparing block copolymer nanoparticles. Furthermore, stimulus-responsive behaviour can be designed into the final particles *via* selection of appropriate RAFT agents and/or monomer. Pei *et al.* have recently reviewed the field of stimulus-responsive nanoparticles prepared *via* RAFT-mediated PISA.[26] These authors describe how thermoresponsive block copolymer nanoparticles can be divided into either LCST-type or upper critical solution temperature (UCST)-type behaviour (Scheme 3.1). As discussed in Chapter 1, the rearrangement of water molecules to form ordered 'cages' around hydrophobic solutes is entropically unfavourable, resulting in insolubility of the dehydrated solute. Pei *et al.*[26] argued that similar hydration should occur at the junction between the hydrophilic and hydrophobic blocks of a self-assembled nanoparticle, and termed this phenomenon an "interfacial LCST."

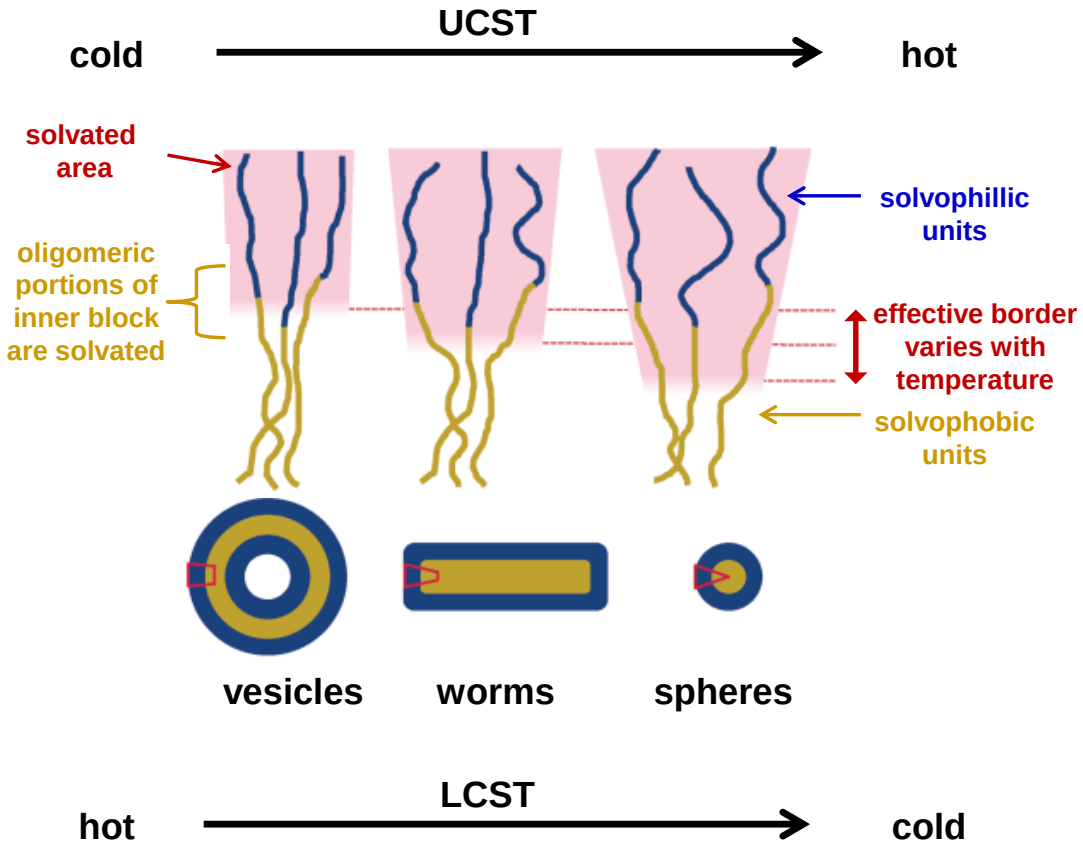

Scheme 3.1 Schematic representation of the subtle change in solvation that occurs near the block junction of thermo-responsive diblock copolymer nanoparticles. UCST-type behaviour is typically observed for block copolymer nanoparticles in organic solvents, while LCST-type behaviour is often observed for block copolymer nanoparticles in aqueous solution. In both cases, the arrow indicates the change in particle morphology from vesicles to worms to spheres. Adapted from ref. 26.

If such nanoparticles are prepared by RAFT aqueous dispersion polymerisation, the core-forming block is only weakly hydrophobic. The hydrophilic stabiliser block is highly solvated and surrounded by water molecules. However, the water molecules can penetrate the interfacial layer between the two blocks, with greater penetration occurring at lower temperatures. This leads to surface plasticisation of the nanoparticles, which causes a shift in the apparent block junction. An increase in core hydration on cooling block copolymer nanoparticles has been confirmed by variable temperature ^{1}H NMR studies of both PGMA-PHPMA[27] and PEO-

PHPMA[28] nanoparticles. Consequently, the effective core-shell boundary, relative volume fractions of the stabiliser and core blocks, fractional packing parameter and (perhaps) particle morphology are highly temperature dependent.[26] However in practice, particle morphology transitions are not always reversible or may not even occur. For example, in the case of RAFT aqueous emulsion polymerisation kinetically-trapped spheres are typically observed when using strongly hydrophobic core-forming blocks such as PMMA,[29] PBzMA,[30, 31] PS[32, 33] or PTFEMA.[34, 35] Even in the rare cases where block copolymer worms and vesicles can be obtained *via* RAFT aqueous emulsion polymerisation,[36-39] a morphology transition would not be expected. Water penetration of the core (or membrane) would be minimal even at relatively low temperatures as the monomer repeat units are extremely hydrophobic.[26] Nevertheless, morphology transitions can be induced by post-polymerisation addition of plasticisers such as solvent[40] or monomer.[41]

This Chapter is focused on the stimulus-responsive nature of vesicles prepared *via* RAFT aqueous dispersion polymerisation, so "interfacial UCST" behaviour will not be discussed in detail. Nevertheless, UCST behaviour is more common in organic solvents than aqueous solution.[42] For example, a reversible vesicle-to-worm transition has been recently reported by Derry *et al.* where the solvent is a non-polar mineral oil.[43] Lowe *et al.* also reported a partially vesicle-to-sphere transition in ethanol.[44]

There are surprisingly few reports of stimulus-responsive vesicles prepared *via* RAFT aqueous dispersion polymerisation.[45-47] Warren *et al.*[45] have described the thermoreversible vesicle-to-sphere transition that occurs for PEO_{113}-$PHPMA_{300}$ vesicles. Doncom *et al.*[47] reported the vesicle-to-vesicle/worm mixed phase transition that occurs on cooling zwitterionic $PSBMA_{38}$-$PHPMA_{310}$ diblock copolymers to 2 °C. In this case, a vesicle phase was formed on heating to 70 °C for 5 h, albeit with a minor population of worms remaining.

More recently, Lovett *et al.*[48] have reported the remarkable pH-responsive behaviour of essentially non-ionic $PGMA_{43}$-$PHPMA_z$ vesicles (Figure 3.1). The RAFT agent used in this work was PETTC (Chapter 1, Scheme 1.8). As the R group of PETTC has a carboxylic acid group, the resulting diblock copolymer vesicles have carboxylic acid end-groups at the PGMA stabiliser terminus (HOOC-$PGMA_{43}$-$PHPMA_z$). In this work, the vesicles were prepared below pH 4, thus the carboxylic acid end-groups were present in their non-ionised form. However, addition of an aqueous base to such vesicular dispersions causes deprotonation and hence formation of anionic carboxylate groups. A morphology transition from vesicles to either spheres or worms was observed, depending on the precise $PGMA_{43}$-$PHPMA_z$ composition.

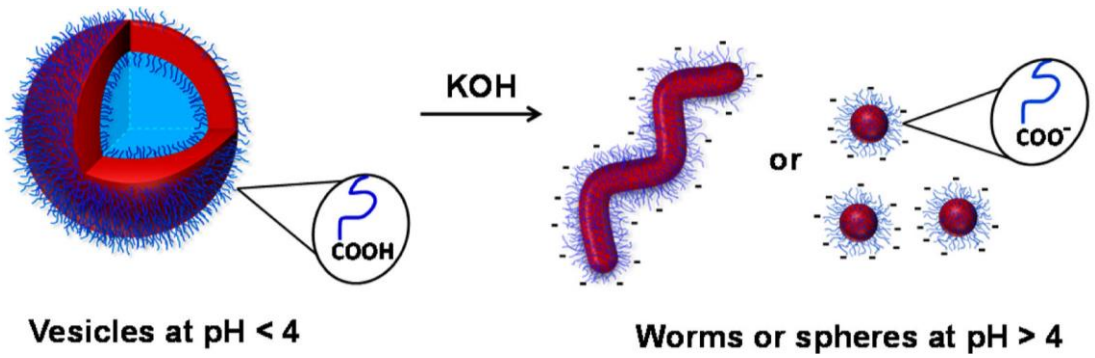

Figure 3.1 Schematic representation of the vesicle-to-worm or vesicle-to-sphere transition that occurs upon deprotonation of the carboxylic acid end-groups of HOOC-$PGMA_{43}$-$PHPMA_z$ vesicles.[48]

The work described in Chapter 2 is extended in the present Chapter to examine the pH-responsive behaviour of morpholine-terminated vesicles, rather than worms. A mini-series of four morpholine-terminated PGMA-PHPMA (MPETTC-PGMA-PHPMA) vesicles are synthesised by RAFT aqueous dispersion polymerisation of HPMA at pH 7.0 – 7.5 (see Scheme 3.2). The pH-responsive, thermo-responsive behaviour of these vesicles is examined.

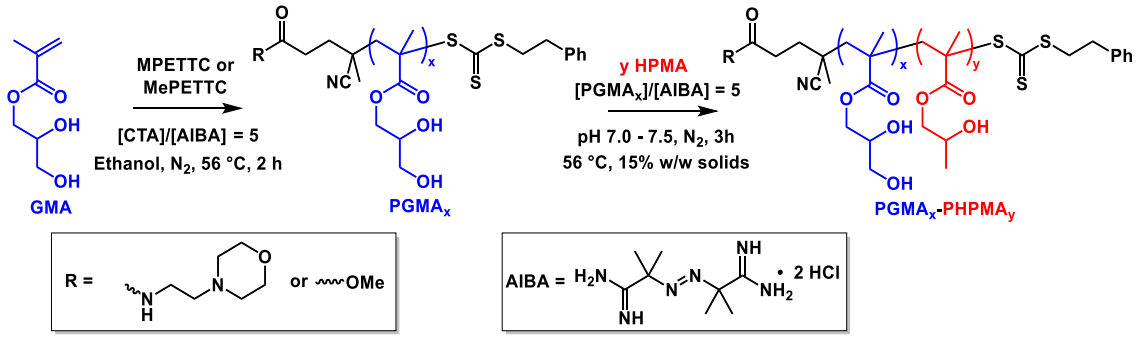

Scheme 3.2 Schematic representation of the synthesis of MPETTC-PGMA$_{43}$ macro-CTA by RAFT solution polymerisation of GMA and its subsequent chain extension with HPMA *via* RAFT aqueous dispersion polymerisation at pH 7.0 – 7.5 to produce MPETTC-PGMA$_{43}$-PHPMA$_y$ vesicles.

3.2 Experimental

3.2.1 Materials

Glycerol monomethacrylate (GMA, 99.8%, ~ 0.06 mol % dimethacrylate impurity) was kindly donated by GEO Specialty Chemicals (Hythe, UK) and used without further purification. 2-Hydroxypropyl methacrylate (HPMA; 97%) and 2,2′-azobisisobutyramide dihydrochloride (AIBA; 99%) were purchased from Sigma Aldrich and were used as received. Deionised water was obtained from an Elgastat Option 3A water purification unit and ultrafiltered using a 0.22 µm filter prior to use. All other chemicals and solvents were purchased from VWR Chemicals, Fischer Scientific or Sigma Aldrich and were used as received.

3.2.2 Synthesis of Morpholine-terminated poly(glycerol monomethacrylate) Macro-CTA by RAFT Solution Polymerisation in Ethanol

MPETTC RAFT agent was prepared as described in Chapter 2. A 100 ml round-bottom flask was charged with a magnetic stirrer bar, glycerol monomethacrylate (GMA, 18.5 g, 116 mmol), MPETTC RAFT agent (1.16 g, 2.57 mmol; [GMA] / [MPETTTC] = 45), AIBA (0.139 g, 0.51 mmol; [MPETTC]/[AIBA] = 5.0) and ethanol (24.2 g) to afford a 45% w/w orange

solution. The flask was sealed, placed in an ice bath and degassed under N_2 for 30 min, before being placed in a preheated oil bath set at 56 °C. The GMA polymerisation was allowed to proceed for 2 h at this temperature, and then quenched by cooling to 20 °C with concomitant exposure to air. ^{1}H NMR studies indicated 72% GMA conversion by comparison of the integrated aromatic end-group signals at δ 7.1 – 7.4 to that of the vinyl signals at δ 6.14 – 6.20. Purification was achieved by precipitation into a twenty-fold excess of dichloromethane to remove unreacted GMA monomer, followed by filtration. The crude PGMA was redissolved in the minimum amount of methanol and precipitated a second time using a ten-fold excess dichloromethane, with isolation achieved *via* filtration. The purified PGMA macro-CTA was dissolved in water, placed on a rotary evaporator to remove residual dichloromethane, and then freeze-dried for 48 h to afford a yellow powder. ^{1}H NMR studies confirmed the absence of residual GMA monomer and a DP_n of 43 was calculated by comparison of the integral values of the aromatic end-group at 7.2 – 7.5 ppm with that of the polymer backbone at 0 – 2.5 ppm. DMF GPC studies indicated an M_n of 12,700 g mol^{-1} and an M_w / M_n of 1.13 using a series of near-monodisperse poly(methyl methacrylate) calibration standards.

3.2.3 Synthesis of Morpholine-terminated poly(glycerol monomethacrylate)-poly(2-hydroxypropyl methacrylate) Diblock Copolymer Vesicles by RAFT Aqueous Dispersion Polymerisation of 2-Hydroxypropyl Methacrylate

A typical protocol for the synthesis of MPETTC-$PGMA_{43}$-$PHPMA_{200}$ diblock copolymer vesicles by RAFT aqueous dispersion polymerisation of HPMA was as follows. MPETTC-$PGMA_{43}$ macro-CTA (0.40 g, 54.5 μmol), HPMA monomer (1.57 g, 10.9 mmol; [HPMA] / [MPETTC-$PGMA_{43}$] = 200), AIBA (2.95 mg, 10.8 μmol; [$PGMA_{43}$]/[AIBA] molar ratio = 5.0) and H_2O (17.85 mL) were added to a 24 mL sample vial fitted with a suba-seal to afford a 10% w/w reaction solution. The solution pH was adjusted to pH 7.0-7.5 using 0.1 M KOH, if required. The reaction flask was sealed, placed in an ice bath and degassed using a N_2 gas

stream for 30 min, then placed in a preheated oil bath set at 56 °C. The HPMA polymerisation was allowed to proceed at this temperature for 4 h, and then quenched by exposure to air while cooling to 20 °C. Alternative DPs for the PHPMA block were targeted by simply varying the number of moles of HPMA in the formulation (adjusting the amount of water to maintain the same overall 10% w/w solids concentration) to produce additional diblock copolymer vesicle dispersions where the PHPMA DP_n = 190, 210, 220 and 230. The aqueous solution behaviour of these vesicles was assessed by ^{1}H NMR, DLS, DMF GPC, TEM, turbidimetry and rheological studies.

3.2.4 Copolymer Characterisation

^{1}H NMR Spectroscopy

^{1}H NMR spectra were recorded at 298 K using a 400 MHz Bruker AV3-HD spectrometer in CD_3OD. Sixty-four scans were averaged per spectrum and all chemical shifts are reported in ppm (δ).

Dynamic Light Scattering

DLS studies were conducted at 20 °C using a Malvern Instruments Zetasizer Nano series instrument equipped with a 4 mW He-Ne laser (λ = 633 nm) and an avalanche photodiode detector. Scattered light was detected at 173°. The same instrument was used for aqueous electrophoresis studies. Copolymer dispersions were diluted to 0.1% w/w using an aqueous solution of 1 mM KCl for particle sizing and aqueous electrophoresis measurements. The dispersion pH was adjusted using either 0.1 M or 1 M HCl, as required. Intensity-average hydrodynamic diameters were calculated *via* the Stokes-Einstein equation, while zeta potentials were determined *via* the Henry equation using the Smoluchowski approximation. Temperature sweeps were conducted at 1 °C intervals with 10 min being allowed for thermal equilibrium at each temperature.

DMF Gel permeation chromatography (GPC)

Aqueous copolymer dispersions were freeze-dried overnight to obtain pale yellow powders. 0.50% w/w copolymer solutions were prepared in DMF containing DMSO (1% v/v) as a flow rate marker. GPC studies were conducted using HPLC-grade DMF eluent containing 10 mM LiBr at 60 °C at a flow rate of 1.0 mL min^{-1}. The GPC set-up comprised an Agilent 1260 Infinity series degasser and pump, an Agilent PL-gel guard column, two Agilent PL-gel MIXED-C columns and a refractive index detector. Sixteen near-monodisperse poly(methyl methacrylate) standards ranging from M_p = 645 g mol^{-1} to 2,480,000 g mol^{-1} were used for column calibration and molecular weight data calculations.

Transmission electron microscopy (TEM)

Copper/palladium grids were coated with a thin film of amorphous carbon, then subjected to a plasma glow discharge for 30 seconds to produce a hydrophilic surface. Aqueous copolymer dispersions were diluted from 10% to 0.1% w/w solids at either pH 7, pH 3, pH 1 or pH 3 in the presence of 100 mM KCl. An aqueous droplet (10 μL) of a 0.1% w/w copolymer dispersion at the desired pH and temperature was placed on a hydrophilic grid for 40 seconds and blotted to remove excess solution. Each grid was negatively stained using uranyl formate (0.75% w/v) solution for 20 seconds. Excess stain was removed by blotting and each grid was carefully dried with a vacuum hose. TEM images were recorded using a FEI Tecnai Spirit instrument fitted with an Orius SC1000B camera operating at 80 kV.

Rheology

An AR-G2 rheometer equipped with a variable temperature Peltier plate and a 40 mm 2° aluminium cone was used for all rheological experiments. Percentage strain sweeps were conducted at an angular frequency of 1.0 rad s^{-1} and angular frequency sweeps were conducted at 1.0% strain; these conditions correspond to the viscoelastic regime. Both percentage strain

and angular frequency sweeps were conducted on diblock copolymer worm gels at pH 3 and 20 °C. The storage (G') and loss (G'') moduli were determined for a 10% w/w aqueous copolymer dispersion as a function of temperature using the above conditions, with 20 minutes equilibration time being allowed for each 1 °C increment.

Turbidimetry

The absorbance of 0.1% w/w aqueous diblock copolymer dispersions was recorded using a Shimadzu UV-1800 spectrometer operating at 450 nm and 20 °C. The solution pH was adjusted to pH 7, 3 or 1, with additional studies being performed at pH 3 in the presence of 100 mM KCl.

3.3 Results & Discussion

3.3.1 Synthesis of Morpholine-functionalised PGMA-PHPMA Vesicles

The morpholine-functionalised RAFT agent, MPETTC, was synthesised as according to the protocol described in Chapter 2. This RAFT agent was used to synthesise a PGMA macro-CTA by RAFT solution polymerisation in ethanol to isolate the morpholine end-group in its neutral, free amine form. ^{1}H NMR studies suggested a DP_n of 43, by comparison of the integrated aromatic signal at 7.2 – 7.4 ppm of the RAFT end-group to that of the polymer backbone at 0 – 2.5 ppm. Furthermore, DMF GPC studies indicated a M_n of 12,700 g mol^{-1} relative to PMMA standards with a M_w / M_n = 1.13 (Figure 3.2). Using the master PGMA-PHPMA phase diagram described in Chapter 1 as a guide, this MPETTC-$PGMA_{43}$ macro-CTA was chain extended with HPMA at 56 °C by RAFT aqueous dispersion polymerisation, to target a mini-series of MPETTC-$PGMA_{43}$-$PHPMA_y$ diblock copolymer vesicles at 10% w/w solids. As discussed in Chapter 2, the pK_a of the morpholine end-group for a near-identical MPETTC-$PGMA_{50}$ macro-CTA is approximately 6.3.

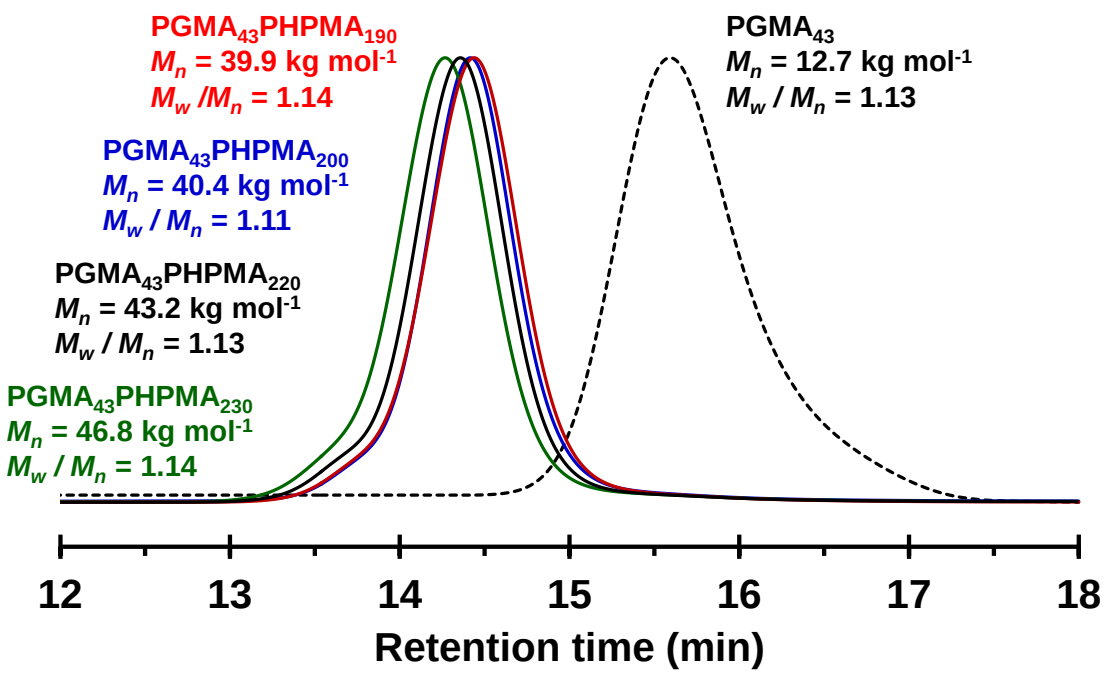

Figure 3.2 DMF chromatograms obtained for MPETTC-PGMA$_{43}$ macro-CTA (black dotted curve) and the corresponding MPETTC-PGMA$_{43}$-PHPMA$_y$ diblock copolymer vesicles (y = 190, 200, 220 and 230). M_n and M_w data are calculated relative to a series of near-monodisperse poly(methyl methacrylate) calibration standards.

Consequently, the pH was adjusted to lie between 7.0 – 7.5 prior to polymerisation to ensure that most of the morpholine end-groups were present in their neutral free amine form. Higher pH values were *not* investigated because it is well-known that such alkaline conditions can lead to hydrolysis of the RAFT CTA chain-ends, although trithiocarbonates are known to be less susceptible than dithiobenzoates.[49-51]

The target PHPMA DP$_n$ (y values) were y = 190, 200, 210, 220 and 230. Monomer conversions were calculated to be > 99% by ^{1}H NMR spectroscopy in all cases. The resulting MPETTC-PGMA$_{43}$-PHPMA$_y$ diblock copolymers were freeze-dried to remove water and analysed by DMF GPC. All chromatograms indicated high blocking efficiencies of the MPETTC-PGMA$_{43}$

macro-CTA and narrow final polydispersities of the final diblock copolymers were achieved, with M_w / M_n < 1.15 (Figure 3.2). TEM studies at pH 7 confirmed all diblock copolymer compositions gave a vesicular morphology (Figure 3.3) with particle diameters ranging from 150 – 450 nm. When targeting a diblock copolymer composition with a slightly lower PHPMA DP_n of 180 a mixed phase of worms and vesicles resulted. Thus the vesicles prepared in this Chapter lie very close to the vesicle/worm phase boundary.

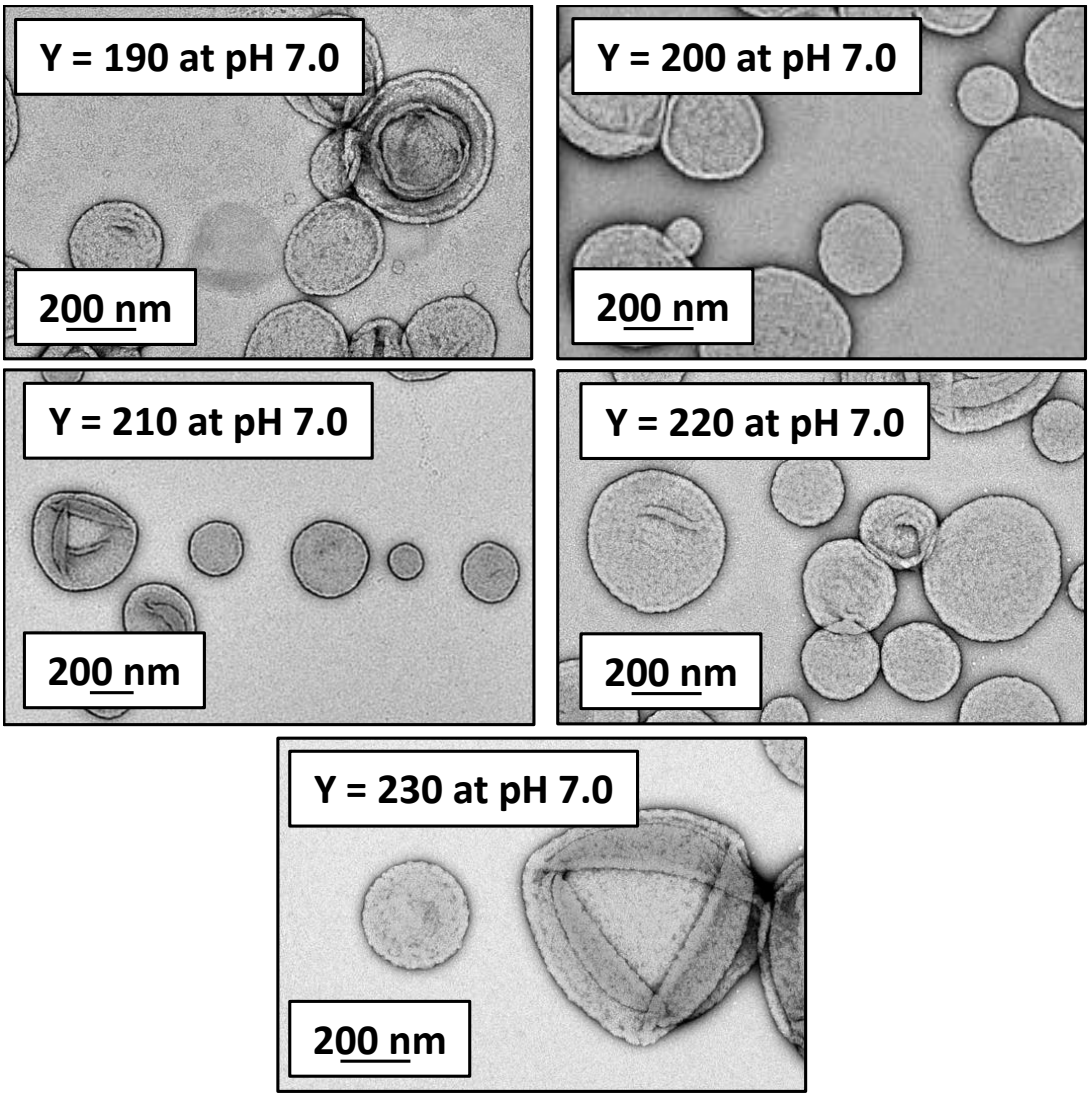

Figure 3.3 Representative TEM images obtained for dried dispersions of MPETTC-$PGMA_{43}$-$PHPMA_y$ vesicles (y = 190, 200, 210, 220 and 230) diblock copolymer nanoparticles at pH 7.0.

3.3.2 Examination of the pH-Responsive Behaviour of Morpholine-functionalised PGMA-PHPMA Vesicles

To examine the pH-responsive behaviour of MPETTC-PGMA$_{43}$-PHPMA$_y$ vesicles, the native 10% w/w aqueous dispersions were acidified to pH 3.0 with 1 M HCl at 20 °C. A change in physical appearance from turbid, free flowing liquids to a semi-translucent, free-standing gel was observed after 48 h when y = 190, 200 or 210 (Figure 3.4 a-b).

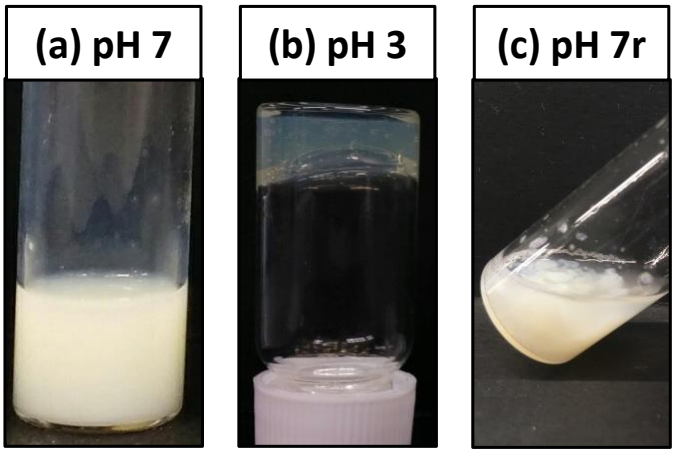

Figure 3.4 Digital photographs for a 10% w/w aqueous dispersion of MPETTC-PGMA$_{43}$-PHPMA$_{190}$ diblock copolymer (a) vesicles at pH 7.0 and (b) worms at pH 3.0. Upon returning to (c) pH 7 from pH 3 with syneresis occurring within minutes to give an inhomogeneous white paste. Photographs were obtained at 20 °C and 48 h after initial acidification.

However, there was no change in the physical appearance of the acidified aqueous dispersions when y = 220 or 230, which remained as free flowing, turbid dispersions. TEM analysis at pH 3 was performed after 48 h equilibration to examine the effect of acidification on particle morphology (Figure 3.5). The vesicle-to-worm transition when y = 190 or 200 is in good agreement with the results from Chapter 2. The morphological transition occurs because the morpholine group located on the periphery of the PGMA chain and hence the vesicles, becomes fully protonated at pH 3.0.

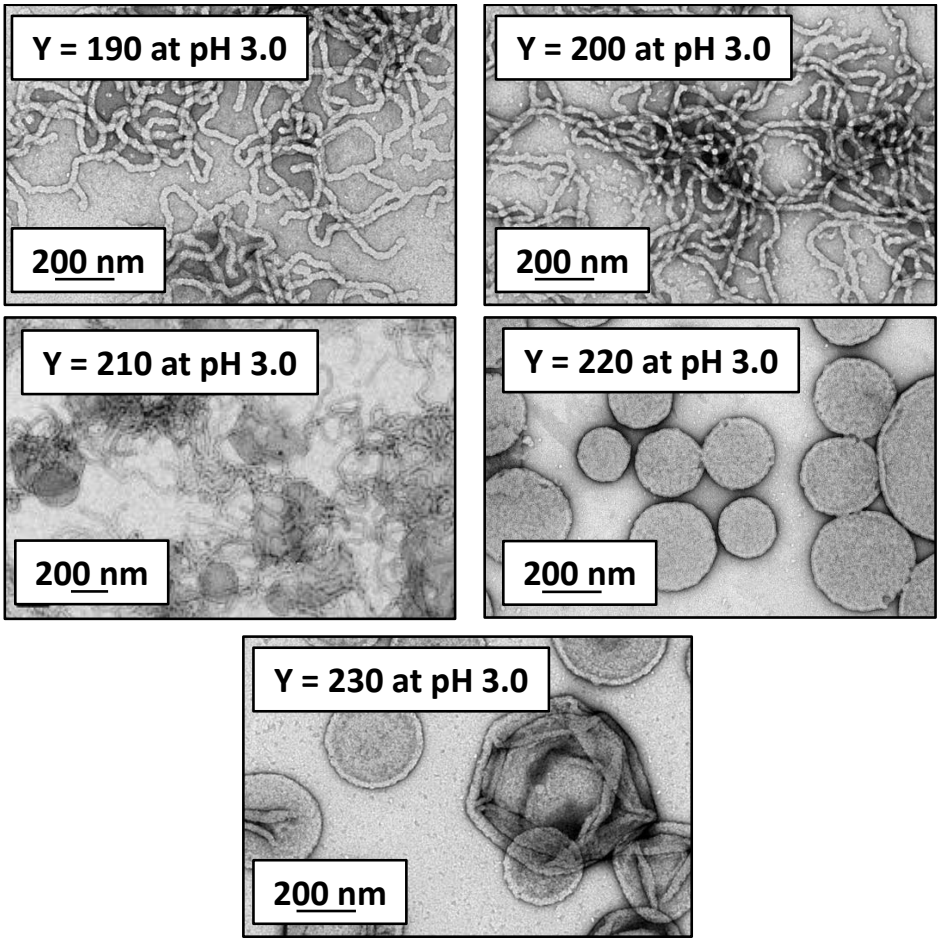

Figure 3.5 Representative TEM images obtained for dried dispersions of MPETTC-PGMA$_{43}$-PHPMA$_y$ nanoparticles (y = 190, 200, 210, 220 and 230) at pH 3.0.

This leads to a subtle increase in the end-group hydration and hence volume fraction of the hydrophilic, PGMA stabiliser block. In turn, as the volume fraction of the core remains constant, P decreases from the vesicle regime ($^1/_2 < P \leq 1$) to the worm regime ($^1/_3 < P \leq {}^1/_2$).[52] Note that on returning to pH 7 an inhomogeneous white paste is formed, which undergoes syneresis in minutes (Figure 3.4c). Even heating at 56 °C (reaction temperature) for 24 h at pH 7 did not lead to redispersion, confirming the irreversibility of this transition. It is suspected that the lack of HPMA monomer, which acts as a co-solvent for the PHPMA core during the initial PISA synthesis of the vesicles and enables high chain mobility, may explain the irreversibility of the transition. It is noteworthy that increasing the PHPMA DP$_n$ to 210 leads to a mixed phase

of worms and vesicles at pH 3 rather than a pure phase. Thus this diblock copolymer composition was not investigated further. When the core-forming block is further increased to a PHPMA DP_n of 220 or 230, protonation of the morpholine end-group is insufficient to induce a change in the packing parameter from the vesicle regime. This is expected, as increasing the PHPMA DP_n increases the packing parameter further to unity, so the vesicles lie further from the worm/vesicle boundary. Thus the modest increase in stabiliser volume fraction cannot induce a morphological transition (Figure 3.5 d and e). The observed vesicle-to-worm transition is significantly slower than the corresponding worm-to-sphere transition as described in Chapter 2. Interestingly, after 24 h jellyfish-like structures are observed by TEM (Figure 3.6a). These structures have been previously reported for both PISA[53-55] and non-PISA[56, 57] formulations, which suggest that this intermediate is a generic transient morphology and merely not a PISA artefact.

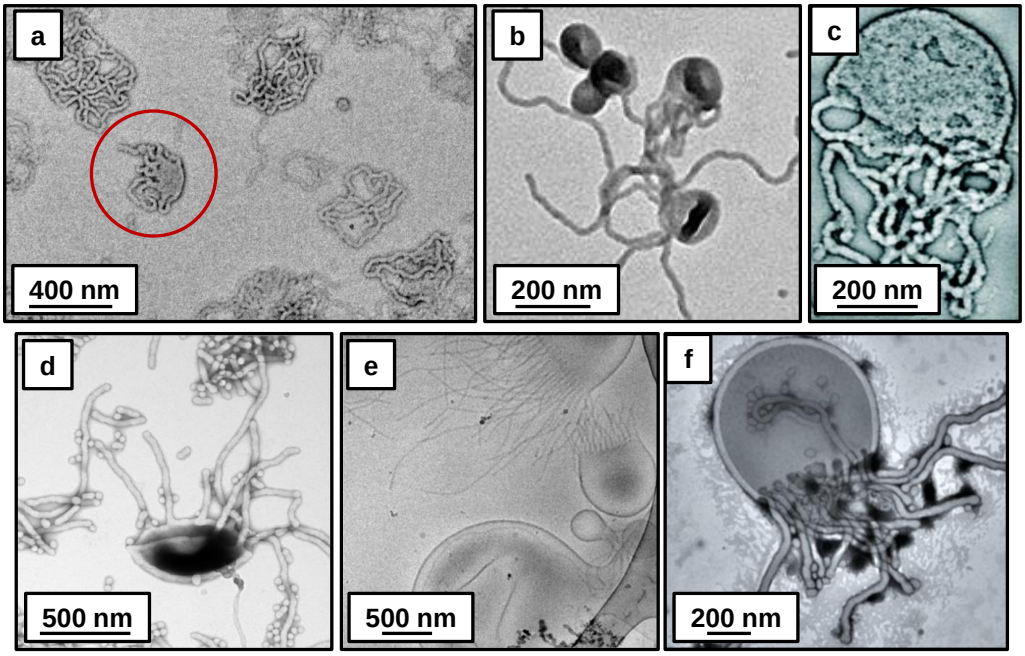

Figure 3.6 (a) TEM image obtained for transient 'jellyfish' intermediate structures formed by MPETTC-$PGMA_{43}$-$PHPMA_{190}$ diblock copolymer after 24 h at pH 3.0. Similar transient morphologies have been reported for both (b)-(d) PISA[53-55] and (e), (f) non-PISA[56, 57] formulations.

This provides strong evidence that the mechanism of the end-group driven vesicle-to-worm transition is simply the reverse of the worm-to-vesicle transition observed for the *in situ* PISA synthesis of similar PGMA-PHPMA vesicles (see Figure 1.20).[55] No morphology change was observed by TEM after a 48 h period. DLS and aqueous electrophoresis studies were performed on MPETTC-PGMA$_{43}$-PHPMA$_y$ vesicles at 20 °C to examine the effect of varying the solution pH on the mean particle diameter and zeta potential (Figure 3.7).

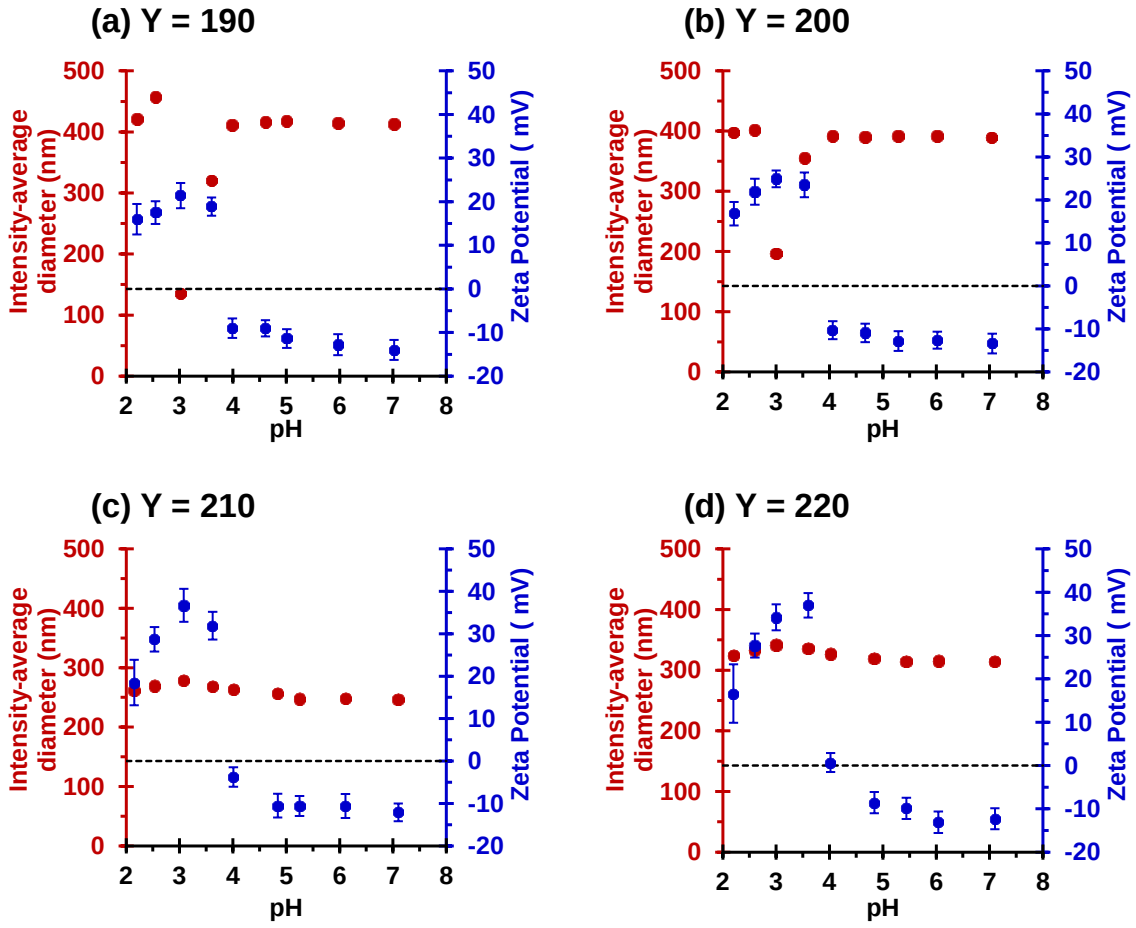

Figure 3.7 Intensity-average diameter and zeta potential vs. dispersion pH curves obtained for MPETTC-PGMA$_{43}$-PHPMA$_y$ diblock copolymer nanoparticles where y = (a) 190, (b) 200, (c) 220 and (d) 230. Aqueous dispersion pH was adjusted at 0.1% w/w with 48 h aging time at 20 °C to allow for morphological equilibrium. All measurements were made at 20 °C for 0.1% w/w dispersions prepared in the presence of 1 mM KCl background salt.

Diblock copolymer vesicles were diluted to 0.1% w/w and the pH was adjusted using 1 M or 0.1 M HCl. The diluted dispersions were left for 48 h in a 20 °C incubator to ensure that equilibrium morphologies were attained. For PHPMA DP_ns of 190 and 200 a significant reduction in apparent particle diameter was observed (from 415 nm to 135 nm (y = 190) or from 392 nm to 196 nm (y = 200)), with a corresponding increase in the apparent zeta potential from -14 mV to +22 mV (y = 190) and -13 mV to +25 mV (y = 200), on lowering the dispersion pH from 7.1 to 3.0 (Figure 3.7). It is noteworthy that intensity-average hydrodynamic diameters were calculated *via* the Stokes-Einstein equation; hence a 'sphere-equivalent' diameter is reported for the worms, which corresponds to neither the mean worm length nor the mean worm width. This reduction in nanoparticle dimensions and surface charge reversal is consistent with TEM studies and provides conclusive evidence that a pure phase of cationic worms is formed at pH 3.0. Below this pH, the apparent particle diameter increases further to 457 nm (y = 190) and 415 nm (y = 200), while the corresponding zeta potentials are reduced. It is likely that excess HCl screens the cationic surface charge arising from the protonated morpholine end-groups. Furthermore, according to TEM studies (see Figure 3.8) the initial vesicular morphology remains unperturbed under these conditions. The increase in the original vesicle diameter below pH 3.0 is the result of the protonated morpholine end-groups inducing an increase in hydration (and hence thickness) for the $PGMA_{43}$ stabiliser block. For block copolymer compositions for which no morphological transition was observed (i.e. where y = 220 or 230), a modest increase in hydrodynamic diameter of approximately 30 nm occurred on lowering the dispersion pH from 7.1 to 3.0. Once again, end-group protonation induces an increase the stabiliser hydration and volume, manifesting in an increase in the intensity-average particle diameter. A simultaneous change in zeta potential from approximately -10 mV to + 35 mV occurs (Figure 3.7). Furthermore, the zeta potential for these cationic vesicles is greater than that reported for the cationic worms at pH 3.0 (+35 mV vs. + 25 mV). Ohshima has recently published an approximate analytical expression for the electrophoretic mobility of cylindrical colloidal

particles.[58] However, this refinement has not been utilised in the present study. Like the two diblock copolymer compositions for which a vesicle-to-worm transition was observed, the zeta potential of these cationic vesicles was reduced below pH 3.0 because excess HCl acted as a salt, leading to charge screening effects.

Diblock copolymer vesicles typically appear turbid because they are relatively large and strongly scatter visible light. In contrast, worms scatter light rather less efficiently. Therefore turbidimetry study was conducted whereby the transmittance of light at an arbitrary wavelength of 450 nm was monitored over 20 h to examine the time scale required for the MPETTC-$PGMA_{43}$-$PHPMA_{190}$ vesicle-to-worm transition. Diblock copolymer dispersions were diluted to 0.1% w/w so the transmittance was within the appropriate range. Control experiments were performed at pH 7.0, where the transmittance recorded for the vesicles remained essentially unchanged over 20 h, as expected (Figure 3.8a, blue trace). However, when these vesicles were diluted to pH 3.0, a gradual increase in light transmittance was observed over time (Figure 3.8, red trace). This increase in transmittance (and hence reduction in particle scattering) is indicative of a vesicle-to-worm transition. As shown in Chapter 2, end-group protonation effects are very sensitive to the addition of salt. Essentially no change in transmittance occurred after 20 h at either pH 1.0 (where excess HCl acts as a salt, Figure 3.8 green trace) or pH 3.0 in the presence of 100 mM KCl (Figure 3.8 black trace); TEM studies confirmed the presence of a pure vesicle phase in both of these cases (Figure 3.8b). Conversely, if non-responsive MPETTC-$PGMA_{43}$-$PHPMA_{230}$ vesicles are examined at pH 3.0, the transmittance remains essentially unchanged over 20 h because protonation of the morpholine end-groups is not sufficient to induce a morphological transition owing to the relatively long core-forming block.

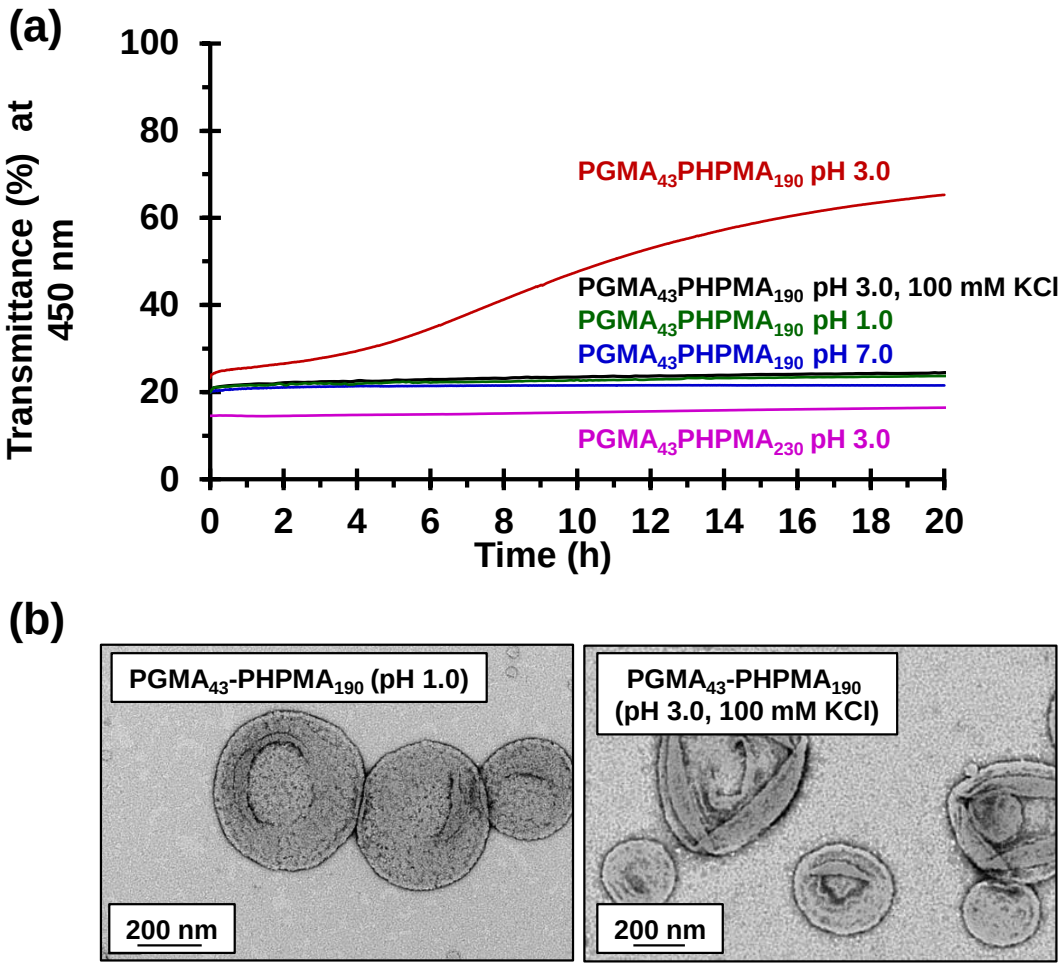

Figure 3.8 (a) Turbidimetric data at 450 nm obtained for MPETTC-PGMA$_{43}$-PHPMA$_{190}$ nanoparticles at either pH 7.0 (blue), pH 3.0 (red) or pH 1.0 (green), or at pH 3.0 in the presence of 100 mM KCl (black), or for (non-responsive) MPETTC-PGMA$_{43}$-PHPMA$_{230}$ vesicles at pH 3.0 (purple). All measurements were recorded over 20 h for 0.1% w/w dispersions at 20 °C. (b) TEM images obtained for MPETTC-PGMA$_{43}$-PHPMA$_{190}$ diblock copolymer vesicles after 20 h at either pH 1.0 in the absence of added salt or pH 3.0 in the presence of 100 mM KCl.

3.3.3 Examination of the Thermoresponsive Behaviour of Morpholine-functionalised PGMA-PHPMA Vesicles

The thermoresponsive behaviour of PGMA-PHPMA diblock copolymer worm gels has been studied in great detail by Armes and co-workers.[27, 59, 60] It is well-established that a thermo-reversible worm-to-sphere transition (with concomitant degelation) occurs on cooling to 4 °C as

the ingress of water results in surface plasticisation of the hydrophobic PHPMA chains. However, further cooling to -2 °C resulted in almost complete molecular dissolution of PGMA-PHPMA diblock copolymer chains.[60] In addition, Verber *et al.* found that the critical gelation temperature (CGT) of $PGMA_{54}$-$PHPMA_z$ worms (z = 130 to 170) could be lowered by targeting progressively longer PHPMA DP_ns.[59] This is because the increasingly hydrophobic core required a greater degree of hydration, and hence a lower temperature, in order to induce a morphological transition. Temperature-dependent studies conducted on carboxylic acid terminated $PGMA_{43}$-$PHPMA_y$ diblock copolymer vesicles have been reported by Lovett *et al.*[48] who only observe thermo-responsive behaviour for a PHPMA DP_n of 175. Upon cooling to 5 °C an irreversible vesicle-to-worm transition occurred, accompanied by a sol-gel transition. More recently, Mable *et al.* prepared $PGMA_{58}$-$PHPMA_{250}$ vesicles in the presence of a 18 nm silica sol.[46] Encapsulation was observed, as the silica nanoparticles can diffuse into the open-ended jellyfish during the initial vesicle synthesis. Importantly, when the silica-loaded vesicles were cooled at 0 °C for 30 min, a morphological transformation from silica-loaded vesicles to a mixture of spheres and short worms occurred, with the encapsulated silica cargo being released (Figure 3.9).

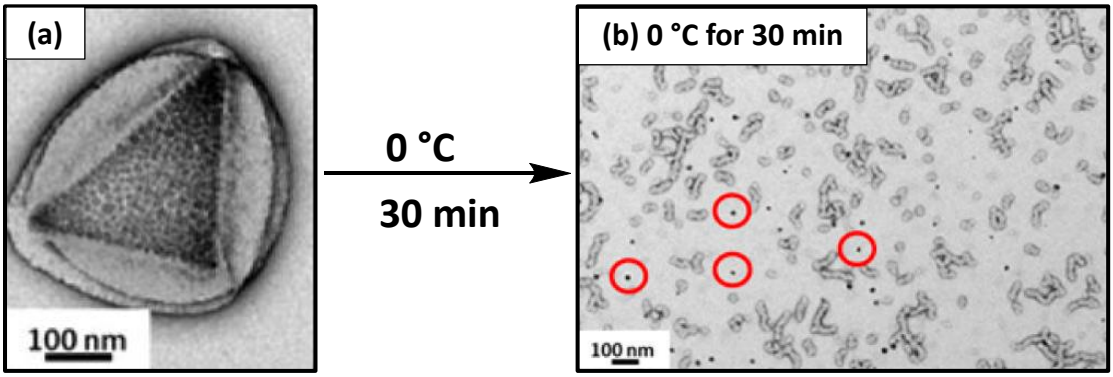

Figure 3.9 (a) Silica loaded $PGMA_{58}$-$PHPMA_{250}$ vesicles at 25 °C. (b) After cooling to 0 °C for 30 min, a change in morphology from vesicles to a mixed phase of worms and spheres was observed, along with the concomitant release of the silica nanoparticles, highlighted by the red circles.[46]

This concept was extended by the encapsulation and release of BSA protein, which demonstrates the potential application of such vesicles for the encapsulation of biologically-active species. In the light of these studies, it was prudent to examine the thermoresponsive nature of these morphology-terminated vesicles. In view of work by Kocik *et al.*,[60] the lower temperature limit was set to 4 °C. Temperature-dependent DLS experiments were conducted from 25 °C to 4 °C. TEM studies were immediately performed after the cooling cycle. These experiments occurred at 0.1% w/w copolymer and at pH 7 in order to exclude any effect of the morpholine end-group (Figure 3.10).

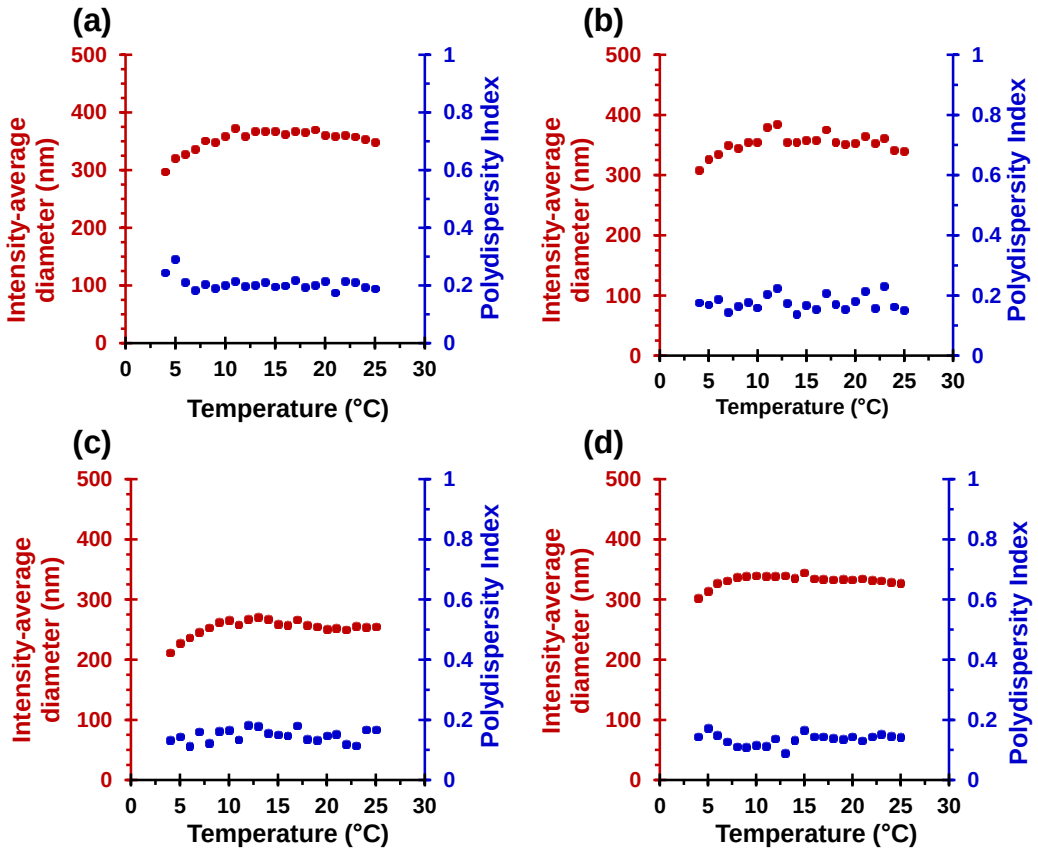

Figure 3.10 Variation of intensity-average particle diameter and polydispersity index vs. temperature upon cooling an aqueous dispersion of MPETTC-PGMA$_{43}$-PHPMA$_y$ diblock copolymer vesicles from 20 °C to 4 °C where (a) y = 190, (b) y = 200, (c) y = 220 and (d) y = 230. Measurements were conducted at pH 7.0, a concentration of 0.1% w/w with 10 minutes equilibration time between each 1 °C interval.

In all cases, no significant change in either the intensity-average diameter or polydispersity index was observed. If a vesicle-to-worm transition had occurred on cooling, a reduction in apparent particle diameter and a concomitant significant increase in polydispersity index would be expected. The timescale of these DLS experiments is approximately 4 h. Thus, to exclude any time effects the MPETTC-PGMA$_{43}$-PHPMA$_{190}$ vesicles were examined after cooling at 4 °C for a 24 h. However, no change in particle diameter was observed demonstrating the lack of thermoresponsive nature of these vesicles. In this case, the PHPMA DP_n is too long relative to the PGMA$_{43}$ stabiliser block such that the mild increase in core hydration isn't sufficient enough to induce a morphology transition. These results are in good agreement with TEM studies, which confirmed that no change in copolymer morphology occurred on cooling to 4 °C for 24 h (Figure 3.11). Thus, for this mini-series of MPETTC-PGMA$_{43}$-PHPMA$_y$ vesicles, end-group ionisation seems to be a more powerful stimulus for inducing a morphology transition than temperature.

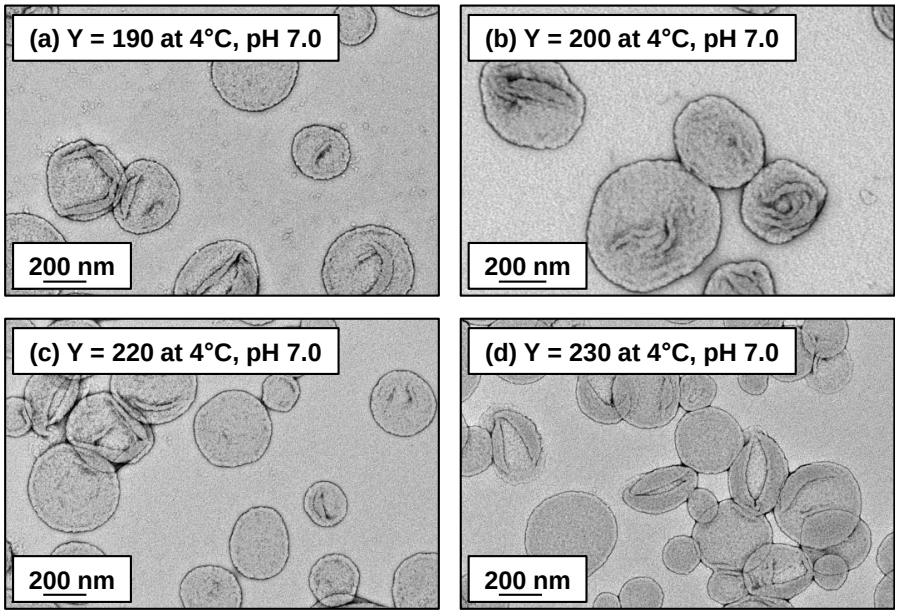

Figure 3.11 Representative TEM images of MPETTC-PGMA$_{43}$-PHPMA$_y$ diblock copolymer vesicles at pH 7.0 and 4 °C where y = (a) 190, (b) 200, (c) 220 and (d) 230. TEM grids were prepared after cooling the 10% w/w aqueous dispersions for 24 h, followed by dilution to 0.1% w/w with cold water

3.3.4 Examination of the Dual-Stimulus Responsive Behaviour of Morpholine-functionalised PGMA-PHPMA Vesicles

Finally, all four MPETTC-PGMA$_{43}$-PHPMA$_y$ diblock copolymer nanoparticles obtained at pH 3 (either worms or vesicles) were cooled from 25 °C to 4 °C so the dual stimulus effect of pH and temperature on the copolymer morphology could be examined. DLS temperature sweeps (Figure 3.12) were conducted at pH 3 from 25 °C to 4 °C with 10 min being allowed at each temperature for thermal equilibration to be achieved. TEM studies were immediately performed afterwards (Figure 3.13) on the 0.1% w/w dispersions. When the initial particle morphology at pH 3 is worms (y = 190 or 200; Figure 3.12 a and b), an initial intensity-average diameter of approximately 150 nm and 200 nm is reported at 25 °C, respectively.

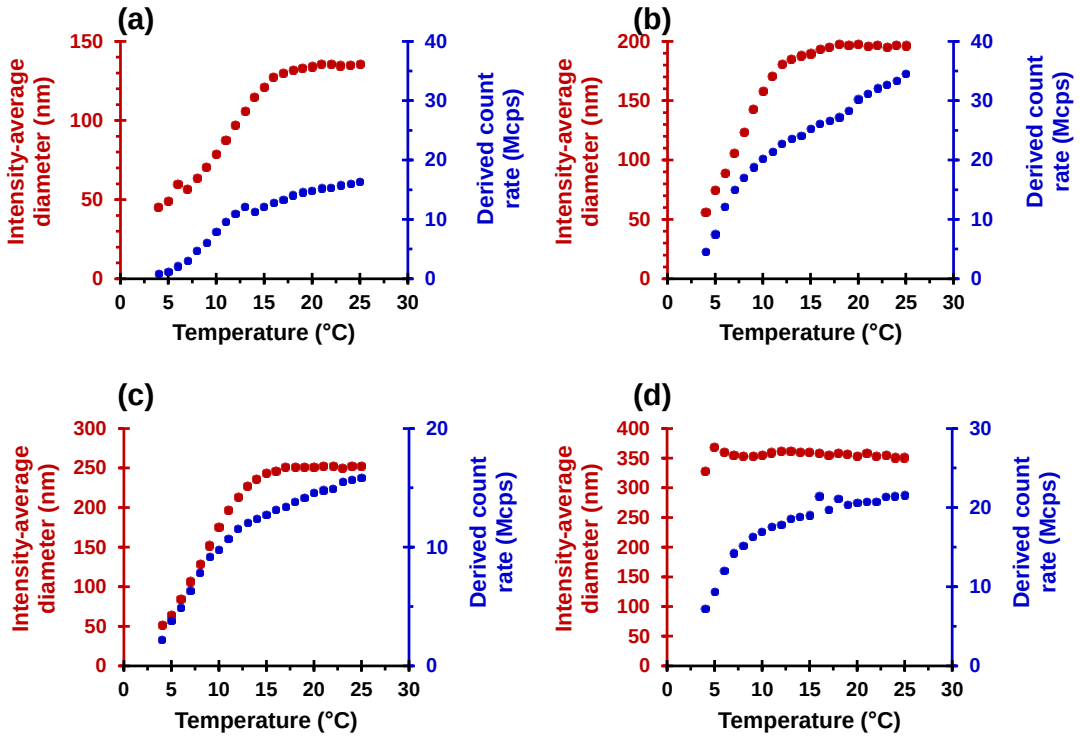

Figure 3.12 Variation of intensity-average particle diameter and derived count rate with temperature for MPETTC-PGMA$_{43}$-PHPMA$_y$ nanoparticles acidified to pH 3 on cooling from 25 °C to 4 °C where (a) y = 190, (b) y = 200, (c) y = 220 and (d) y = 230. Measurements were conducted on 0.1% w/w aqueous dispersions with 10 minutes equilibration time between each measurement point.

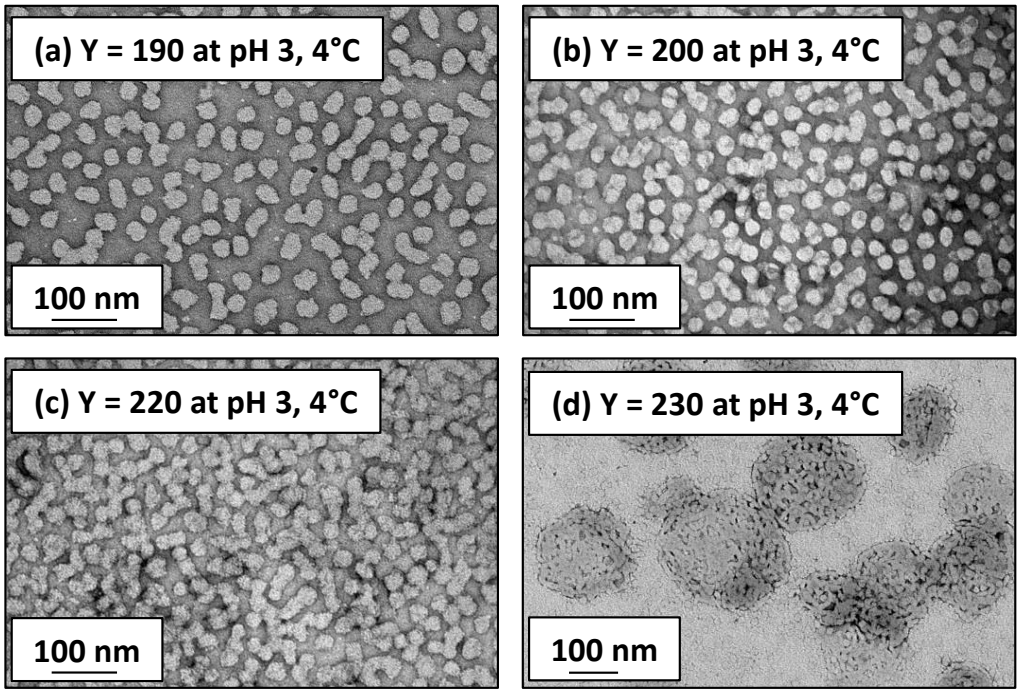

Figure 3.13 Representative TEM images obtained for MPETTC-PGMA$_{43}$-PHPMA$_y$ diblock copolymer nanoparticles immediately after cooling 0.1% w/w, pH 3 aqueous dispersions from 25 °C to 4 °C for 4 hours.

On cooling to 4 °C, a significant reduction in the intensity-average diameter to approximately 50 nm is observed in both cases. Furthermore, the reduction in the derived count rate (i.e. the amount of scattered light) is indicative of a reduction in particle diameter. TEM studies (Figure **3.13**a and b) conducted at 4 °C reveal spheres as the exclusive copolymer morphology. The mean zeta potential of these cold spheres at pH 3 is + 24 mV in the presence of 1 mM KCl. When the PHPMA DP$_n$ is equal to 220, the initial particle morphology at pH 3 is vesicles, with an intensity-average diameter of approximately 250 nm. Upon cooling to 4 °C a significant reduction in the intensity-average diameter to 50 nm and reduction in the derived count rate is observed (Figure 3.12c). Once again, spherical micelles are observed by TEM at 4 °C (Figure **3.13**c). Increasing the PHPMA DP$_n$ to 230 led to minimal reduction in the intensity-average diameter over the 4 h time scale of the experiment (Figure 3.13d). TEM analysis conducted immediately after the completing the cooling experiment revealed an extraordinary morphology of vesicle-like particles, comprising a distinctive worm-like surface texture. DLS studies

reported an intensity-average diameter of 328 nm. A similar morphology has been observed by Förster *et al.* for poly(ethylene oxide)-poly(2-vinylpyridine) PEO_{46}-$P2VP_{66}$ vesicles subject to cooling from 25 °C to 4 °C (Figure 3.14).[57]

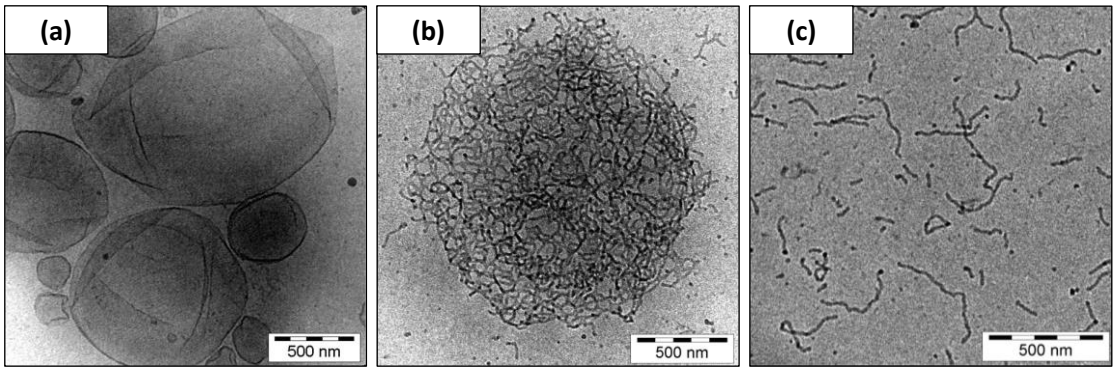

Figure 3.14 Cryogenic-TEM images of polydisperse poly(ethylene oxide)-poly(2-vinylpyridine) (PEO_{46}-$P2VP_{66}$) vesicles obtained at (a) 25 °C and after cooling to 4 °C for (b) 1 h and (c) 24 h. Adapted with permission from ref. 61

After cooling these PEO_{46}-$P2VP_{66}$ vesicles to 4 °C for 1 h, a change in particle morphology to "a spherical basketlike network of entangled linear and branched wormlike micelles" was observed.[61] Further cooling at 4 °C for 24 h resulted in the formation of mainly worms, with a small proportion of spheres. Inspired by this work, the acidified MPETTC-$PGMA_{43}$-$PHPMA_{230}$ nanoparticles at pH 3 were cooled to 4 °C for 24 h. TEM analysis indicated the break-up of these surface-textured vesicles to afford a mixed phase of worms and vesicles (Figure 3.15a). This mixed phase, rather than a pure phase composed of solely spheres, is a result of the greater hydrophobic nature of the longer PHPMA block. Moreover, when the original diblock copolymer vesicles were exposed to the dual stimuli of temperature and pH at a higher copolymer concentration of 10% w/w, a change in the physical appearance from a turbid, free-flowing dispersion to a translucent, soft gel was observed. Furthermore, TEM analysis (after immediate dilution from 10% w/w to 0.1% w/w) confirmed the same change in particle morphology. (Figure 3.15b). Thus, such transitions are not merely a dilution artefact.

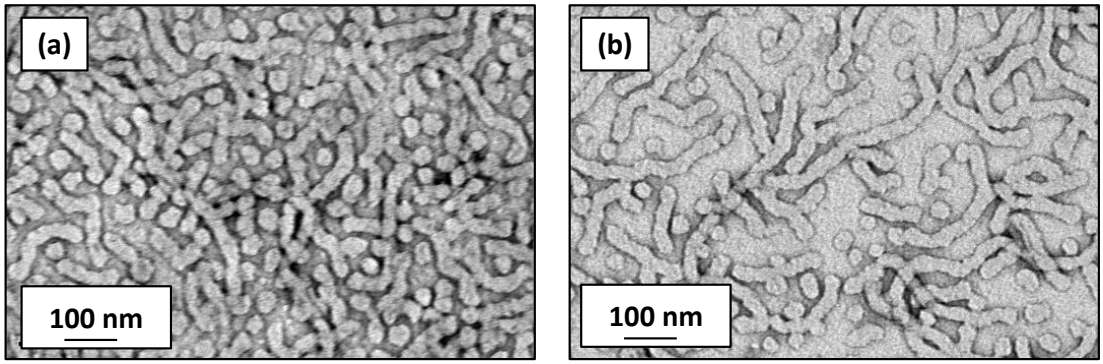

Figure 3.15 Representative TEM images obtained for MPETTC-PGMA$_{43}$-PHPMA$_{230}$ diblock copolymer nanoparticles after being stored at pH 3.0 and 4 °C for 24 h at (a) 0.1% w/w or (b) 10% w/w.

Temperature-dependent oscillatory rheology studies were performed on a 10% w/w aqueous dispersion of MPETTC-PGMA$_{43}$-PHPMA$_{190}$ worms at pH 3. Angular frequency and percentage strain sweeps indicated the formation of a viscoelastic gel at 20 °C using an angular frequency of 1.0 rad s^{-1} and an applied strain of 1.0% (Figure 3.16).[59] These conditions were then used to perform a reversible temperature sweep from 20 °C to 4 °C (see Figure 3.17a).

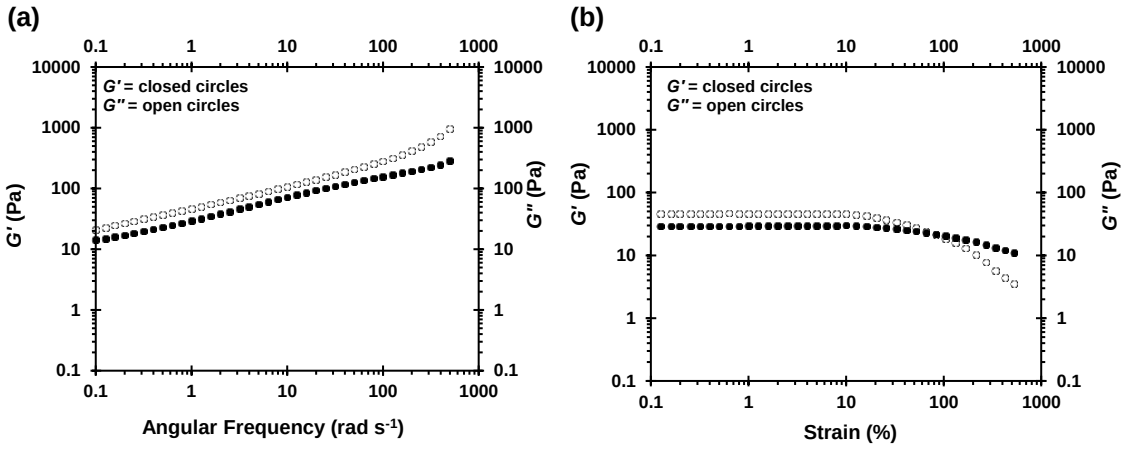

Figure 3.16 (a) Angular frequency sweeps conducted at 1.0% strain and (b) percentage strain sweeps conducted at 1.0 rad s^{-1} for MPETTC-PGMA$_{43}$-PHPMA$_{190}$ diblock copolymer worm gels at pH 3 and 20 °C. The open circles represent *G′* and the closed circles represent *G″*.

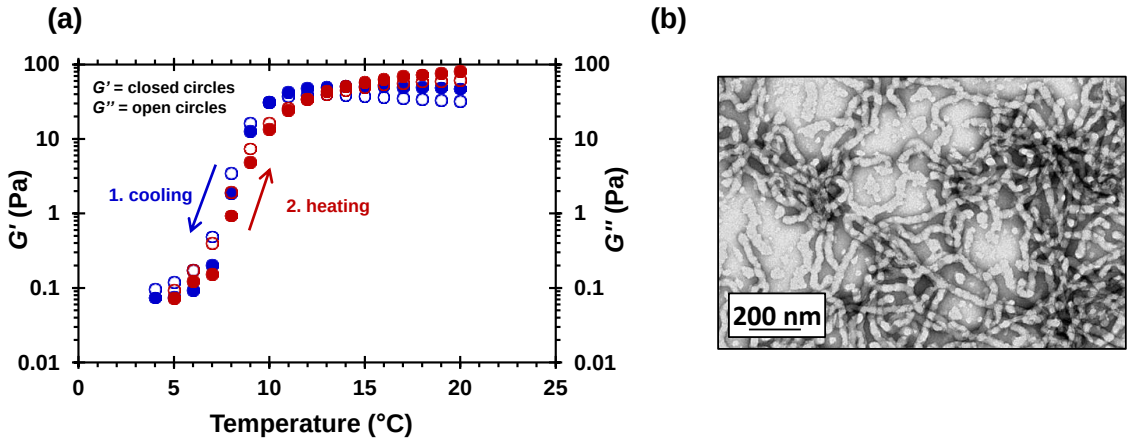

Figure 3.17 (a) Variation of storage modulus (*G′*, filled circles) and loss modulus (*G″*, open circles) with temperature for a 10% w/w aqueous dispersion of MPETTC-PGMA$_{43}$-PHPMA$_{190}$ diblock copolymer worms at pH 3. The blue circles represent a cooling cycle from 20 °C to 4 °C and the red circles represent a heating cycle from 4 °C to 20 °C. Measurements were conducted at an angular frequency of 1.0 rad s^{-1} and an applied strain of 1.0 %, with an equilibration time of 20 min at each temperature. (b) Representative TEM image obtained for this diblock copolymer after the temperature sweep.

An initial gel strength of 47 Pa was observed at 20 °C. This gel strength is lower than that indicated in previous reports for the same copolymer concentration.[27, 59] This is attributed to the cationic surface charge leading to weak electrostatic repulsion between neighbouring worms, thus reducing the number of inter-worm contacts. A worm-to-sphere transition occurs on cooling to 4 °C, which leads to *in situ* degelation (see Figure 3.13a). A CGT of 10 °C is observed, as judged by the cross-over temperature for the *G′* and *G″* curves. This is marginally higher than that reported by Verber *et al.*[59] for similar PGMA-PHPMA worms, which is attribute to the greater hydration of the cationic PGMA$_{43}$ stabiliser at pH 3 compared to the neutral PGMA$_{43}$ chains at pH 7. Regelation occurred at 12 °C during heating from 4 °C to 20 °C, with minimal hysteresis being observed. However, a somewhat stronger gel (*G′* = 80 Pa) was obtained on returning to 20 °C. TEM confirmed the presence of diblock copolymer worms under these conditions (Figure 3.17b). However, DLS studies indicated a sphere-equivalent diameter of 148 nm for the reconstituted worms after the temperature cycle, which is marginally

larger than that obtained before the thermal cycle (135 nm). Thus, the observed increase in gel strength can be somewhat attributed to a longer mean worm contour length and hence a greater number of inter-worm contacts. This observation is strikingly different to that reported by Lovett *et al.*,[48] who observed an irreversible worm-to-sphere for near-identical carboxylic acid-functionalised PGMA-PHPMA worms subjected to a similar thermal cycle.[48] However, this difference might be simply the result of the rather longer equilibration time of 20 min (vs. 2 min) employed for the gel rheology experiments.

Clearly, the stimulus-responsive behaviour of MPETTC-PGMA$_{43}$-PHPMA$_y$ vesicles is remarkably complex, as summarised in Table 3.1. This is depicted in a schematic cartoon in Figure 3.18. Protonation of a single morpholine end-group located at the end of the PGMA stabiliser block induces a subtle increase in its volume fraction. This in turn leads to a reduction in the packing parameter, which drives a vesicle-to-worm transition. Lowering the solution temperature increases the degree of hydration of the PHPMA core-forming block, which further reduces the packing parameter and hence leads to the formation of spheres.

Table 3.1 Summary of observations made for four MPETTC-PGMA$_{43}$-PHPMA$_y$ diblock copolymer vesicles illustrating their pH-responsive, thermo-responsive and dual stimulus-responsive behaviour. S = spheres, W = worms, V = vesicles.

Target PHPMA DP_n	M_n / kg mol^{-1} (M_w / M_n)[a]	Morphology observed by TEM under the stated conditions				Summary of stimulus-responsive behaviour		
		pH 7 [b]	pH 3 [b]	pH 3, 100 mM KCl or pH 1[b]	pH 3 [c]	pH-responsive	Thermo-responsive	pH- and thermo-responsive
190	39.9 (1.14)	V	W	V	S	Yes	No	Yes
200	40.4 (1.11)	V	W	V	S	Yes	No	Yes
220	43.2 (1.13)	V	V	V	S	No	No	Yes
230	46.8 (1.14)	V	V	V	S & W	No	No	Yes

[a] Determined by DMF GPC relative to PMMA standards. [b] Particle morphology determined by TEM at 20 °C. [c] Particle morphology determined by TEM at 20 °C.

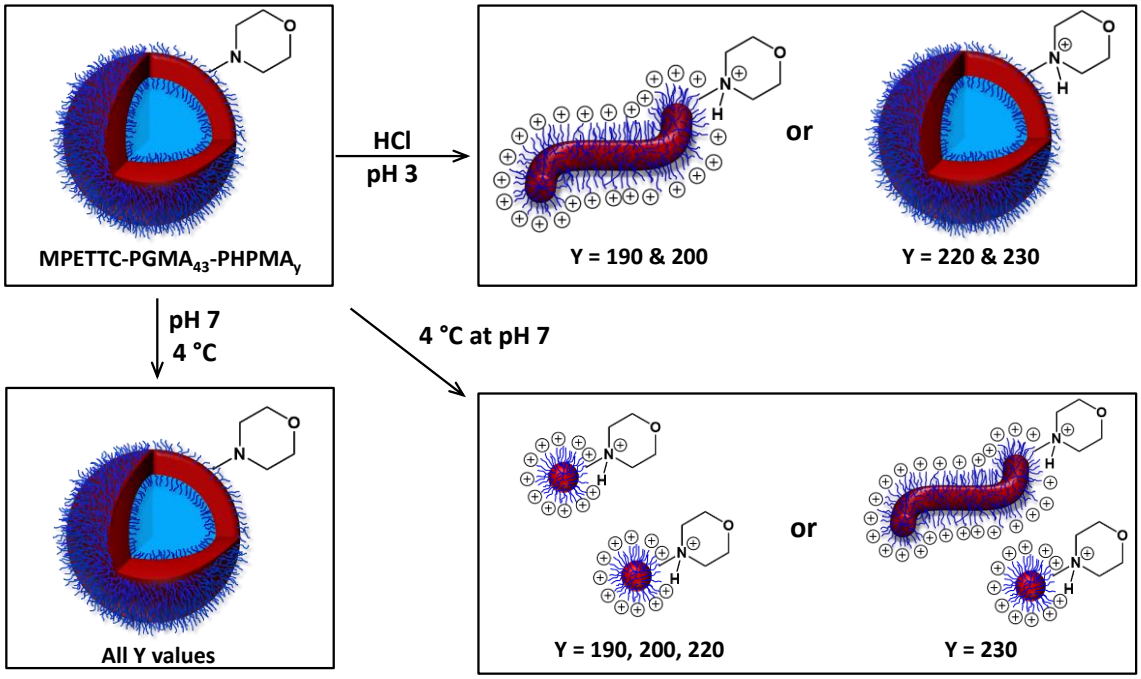

Figure 3.18 Schematic representation of the pH-responsive, thermoresponsive and dual pH- and thermo-responsive behaviour of MPETTC-PGMA$_{43}$-PHPMA$_y$ vesicles.

Warming these spheres induces a sphere-to-worm transition as the PHPMA core gradually becomes less solvated, hence increasing the packing parameter. However, if the PHPMA DP$_n$ is too high, then protonation of the morpholine end-group alone is not sufficient enough to drive a morphological transition. Nevertheless, application of both pH and temperature stimuli results in an overall vesicle-to-sphere (or vesicle-to-sphere/short worm) morphological transition by increasing both the PGMA stabiliser volume fraction and the degree of hydration of the core-forming PHPMA block.

3.4 Conclusions

In summary, a well-defined, water-soluble MPETTC-PGMA$_{43}$ macro-CTA was chain-extended with HPMA to form a series of four MPETTC-PGMA$_{43}$-PHPMA$_y$ diblock copolymer vesicles at 10% w/w solids at approximately neutral pH. Acidification to pH 3 leads to protonation of the

morpholine end-group and consequently induces a change in copolymer morphology from weakly anionic vesicles to a pure phase comprising cationic worms for y values of 190 or 200. The presence of added electrolyte (excess HCl at pH 1 or 100 mM KCl) causes charge-screening, which suppresses this morphological transition. Turbidimetry studies confirm that such vesicle-to-worm transitions are relatively slow compared to the worm-to-sphere transition described in Chapter 2. Moreover, no change in morphology is observed for higher PHPMA DP_ns, because this membrane-forming block becomes too hydrophobic to be affected by this rather subtle end-group effect. The series of four MPETTC-$PGMA_{43}$-$PHPMA_y$ vesicles reported herein did not exhibit thermoresponsive behaviour when cooled to 4 °C at neutral pH. However, lowering both the solution pH and temperature induced a vesicle-to-sphere transition (or a mixture of spheres and short worms, depending on the PHPMA DP_n). Nevertheless, vesicles comprising the longest PHPMA block (y = 230) responded much more slowly to this dual stimulus. Temperature-dependent gel rheology studies conducted on acidified MPETTC-$PGMA_{43}$-$PHPMA_{190}$ worms at pH 3 confirmed that the worm-to-sphere transition is fully reversible. In summary, the aqueous solution behaviour of MPETTC-$PGMA_{43}$-$PHPMA_y$ vesicles is rather complex and critically depends on the PHPMA DP_n, the solution pH and temperature. The work in this Chapter provides useful new insights regarding the pH-responsive behaviour of non-ionic vesicles modulated by morpholine end-groups located on the stabiliser block.

3.5 References

1. F. Liu and A. Eisenberg, *Journal of the American Chemical Society*, 2003, **125**, 15059.
2. B. M. Discher, Y.-Y. Won, D. S. Ege, J. C. M. Lee, F. S. Bates, D. E. Discher and D. A. Hammer, *Science*, 1999, **284**, 1143.
3. J. C. M. Lee, H. Bermudez, B. M. Discher, M. A. Sheehan, Y.-Y. Won, F. S. Bates and D. E. Discher, *Biotechnology and Bioengineering*, 2001, **73**, 135.
4. D. E. Discher and A. Eisenberg, *Science*, 2002, **297**, 967.
5. L. Zhang and A. Eisenberg, *Science*, 1995, **268**, 1728.
6. K. Yu and A. Eisenberg, *Macromolecules*, 1996, **29**, 6359.

7. D. J. Pochan, Z. Chen, H. Cui, K. Hales, K. Qi and K. L. Wooley, *Science*, 2004, **306**, 94.
8. H. Bermudez, A. K. Brannan, D. A. Hammer, F. S. Bates and D. E. Discher, *Macromolecules*, 2002, **35**, 8203.
9. R. C. Hayward and D. J. Pochan, *Macromolecules*, 2010, **43**, 3577.
10. N. J. Warren, O. O. Mykhaylyk, A. J. Ryan, M. Williams, T. Doussineau, P. Dugourd, R. Antoine, G. Portale and S. P. Armes, *Journal of the American Chemical Society*, 2015, **137**, 1929.
11. B. Surnar and M. Jayakannan, *Biomacromolecules*, 2013, **14**, 4377.
12. J. Du, L. Fan and Q. Liu, *Macromolecules*, 2012, **45**, 8275.
13. C. J. F. Rijcken, O. Soga, W. E. Hennink and C. F. van Nostrum, *Journal of Controlled Release*, 2007, **120**, 131.
14. C. G. Palivan, R. Goers, A. Najer, X. Zhang, A. Car and W. Meier, *Chemical Society Reviews*, 2016, **45**, 377.
15. N. A. Christian, M. C. Milone, S. S. Ranka, G. Li, P. R. Frail, K. P. Davis, F. S. Bates, M. J. Therien, P. P. Ghoroghchian, C. H. June and D. A. Hammer, *Bioconjugate Chemistry*, 2007, **18**, 31.
16. D. M. Vriezema, M. C. Aragones, J. A. A. W. Elemans, J. J. L. M. Cornelissen, A. E. Rowan and R. J. M. Nolte, *Chemical Reviews*, 2005, **105**, 1445.
17. P. Tanner, P. Baumann, R. Enea, O. Onaca, C. Palivan and W. Meier, *Accounts of Chemical Research*, 2011, **44**, 1039.
18. C. J. Mable, N. J. Warren, K. L. Thompson, O. O. Mykhaylyk and S. P. Armes, *Chemical Science*, 2015, **6**, 6179.
19. Z. Wang, M. C. M. van Oers, F. P. J. T. Rutjes and J. C. M. van Hest, *Angewandte Chemie International Edition*, 2012, **51**, 10746.
20. H. Xu, F. Meng and Z. Zhong, *Journal of Materials Chemistry*, 2009, **19**, 4183.
21. J. Du, Y. Tang, A. L. Lewis and S. P. Armes, *Journal of the American Chemical Society*, 2005, **127**, 12800.
22. K. E. B. Doncom, C. F. Hansell, P. Theato and R. K. O'Reilly, *Polymer Chemistry*, 2012, **3**, 3007.
23. E. Blasco, J. L. Serrano, M. Pinol and L. Oriol, *Macromolecules*, 2013, **46**, 5951.
24. J. He, P. Zhang, T. Babu, Y. Liu, J. Gong and Z. Nie, *Chemical Communications*, 2013, **49**, 576.
25. K. Yu and A. Eisenberg, *Macromolecules*, 1998, **31**, 3509.
26. Y. Pei, A. B. Lowe and P. J. Roth, *Macromolecular Rapid Communications*, 2017, **38**, 1600528.
27. A. Blanazs, R. Verber, O. O. Mykhaylyk, A. J. Ryan, J. Z. Heath, C. W. Douglas and S. P. Armes, *Journal of the American Chemical Society*, 2012, **134**, 9741.
28. K. Ren and J. Perez-Mercader, *Polymer Chemistry*, 2017, **8**, 3548.
29. F. L. Hatton, M. Ruda, M. Lansalot, F. D'Agosto, E. Malmstroem and A. Carlmark, *Biomacromolecules*, 2016, **17**, 1414.
30. V. J. Cunningham, A. M. Alswieleh, K. L. Thompson, M. Williams, G. J. Leggett, S. P. Armes and O. M. Musa, *Macromolecules*, 2014, **47**, 5613.
31. Y. Ning, L. A. Fielding, T. S. Andrews, D. J. Growney and S. P. Armes, *Nanoscale*, 2015, **7**, 6691.
32. J. Rieger, C. Grazon, B. Charleux, D. Alaimo and C. Jerome, *Journal of Polymer Science Part A: Polymer Chemistry*, 2009, **47**, 2373.
33. C. J. Ferguson, R. J. Hughes, B. T. T. Pham, B. S. Hawkett, R. G. Gilbert, A. K. Serelis and C. H. Such, *Macromolecules*, 2002, **35**, 9243.
34. L. Guo, Y. Jiang, T. Qiu, Y. Meng and X. Li, *Polymer*, 2014, **55**, 4601.

35. B. Akpinar, L. A. Fielding, V. J. Cunningham, Y. Ning, O. O. Mykhaylyk, P. W. Fowler and S. P. Armes, *Macromolecules*, 2016, **49**, 5160.
36. W. Zhang, F. D'Agosto, O. Boyron, J. Rieger and B. Charleux, *Macromolecules*, 2012, **45**, 4075.
37. X. Zhang, S. Boisse, W. Zhang, P. Beaunier, F. D'Agosto, J. Rieger and B. Charleux, *Macromolecules*, 2011, **44**, 4149.
38. S. Boisse, J. Rieger, K. Belal, A. Di-Cicco, P. Beaunier, M.-H. Li and B. Charleux, *Chemical Communications*, 2010, **46**, 1950.
39. S. Boisse, J. Rieger, G. Pembouong, P. Beaunier and B. Charleux, *Journal of Polymer Science Part A: Polymer Chemistry*, 2011, **49**, 3346.
40. N. P. Truong, M. R. Whittaker, A. Anastasaki, D. M. Haddleton, J. F. Quinn and T. P. Davis, *Polymer Chemistry*, 2016, **7**, 430.
41. N. P. Truong, J. F. Quinn, A. Anastasaki, D. M. Haddleton, M. R. Whittaker and T. P. Davis, *Chemical Communications*, 2016, **52**, 4497.
42. J. Seuring and S. Agarwal, *Macromolecular Rapid Communications*, 2012, **33**, 1898.
43. M. J. Derry, O. O. Mykhaylyk and S. P. Armes, *Angewandte Chemie International Edition*, 2017, **56**, 1746.
44. Y. Pei, N. C. Dharsana, J. A. van Hensbergen, R. P. Burford, P. J. Roth and A. B. Lowe, *Soft Matter*, 2014, **10**, 5787.
45. N. J. Warren, O. O. Mykhaylyk, D. Mahmood, A. J. Ryan and S. P. Armes, *Journal of the American Chemical Society*, 2014, **136**, 1023.
46. C. J. Mable, R. R. Gibson, S. Prevost, B. E. McKenzie, O. O. Mykhaylyk and S. P. Armes, *Journal of the American Chemical Society*, 2015, **137**, 16098.
47. K. E. B. Doncom, N. J. Warren and S. P. Armes, *Polymer Chemistry*, 2015, **6**, 7264.
48. J. R. Lovett, N. J. Warren, S. P. Armes, M. J. Smallridge and R. B. Cracknell, *Macromolecules*, 2016, **49**, 1016.
49. J.-F. Baussard, J.-L. Habib-Jiwan, A. Laschewsky, M. Mertoglu and J. Storsberg, *Polymer*, 2004, **45**, 3615.
50. M. Mertoglu, A. Laschewsky, K. Skrabania and C. Wieland, *Macromolecules*, 2005, **38**, 3601.
51. A. B. Lowe and C. L. McCormick, *RAFT polymerization in homogeneous aqueous media: initiation systems, RAFT agent stability, monomers and polymer structures*, Wiley-VCH Verlag GmbH & Co. KGaA, Weinheim, Germany, 2008.
52. A. Blanazs, S. P. Armes and A. J. Ryan, *Macromolecular Rapid Communications*, 2009, **30**, 267.
53. D. Zehm, L. P. D. Ratcliffe and S. P. Armes, *Macromolecules*, 2013, **46**, 128.
54. M. J. Derry, L. A. Fielding, N. J. Warren, C. J. Mable, A. J. Smith, O. O. Mykhaylyk and S. P. Armes, *Chemical Science*, 2016, **7**, 5078.
55. A. Blanazs, J. Madsen, G. Battaglia, A. J. Ryan and S. P. Armes, *Journal of the American Chemical Society*, 2011, **133**, 16581.
56. N. J. Warren and S. P. Armes, *Journal of the American Chemical Society*, 2014, **136**, 10174.
57. C. Fuerst, P. Zhang, S. V. Roth, M. Drechsler and S. Förster, *Polymer*, 2016, **107**, 434.
58. H. Ohshima, *Langmuir*, 2015, **31**, 13633.
59. R. Verber, A. Blanazs and S. P. Armes, *Soft Matter*, 2012, **8**, 9915.
60. M. K. Kocik, O. O. Mykhaylyk and S. P. Armes, *Soft Matter*, 2014, **10**, 3984.
61. A. Rank, S. Hauschild, S. Förster and R. Schubert, *Langmuir*, 2009, **25**, 1337.

Chapter 4

Cross-Linked Cationic Diblock Copolymer Worms are Superflocculants for Micrometer-sized Silica Particles

Reproduced in full with permission from:

[N. J. W. Penfold, Y. Ning, P. Verstraete, J. Smets, S. P. Armes, *Chemical Science*, 2016, **7**, 6894-6904.]

4.1 Introduction

The controlled aggregation of colloidal particles plays a vital role in many important industrial processes such as paper manufacture,[1, 2] mineral separation[3] and water purification.[4-6] Historically, silica suspensions have been used as models to assess the flocculation efficiency of various high molecular weight water-soluble polymers.[7, 8] Typically, soluble cationic (or non-ionic) polyelectrolytes[9-14] have been studied as effective flocculants for such anionic particles. This approach is well-established for nano-sized silica particles, since the length scales of the particles and the flocculant are comparable (see Figure 4.1a).

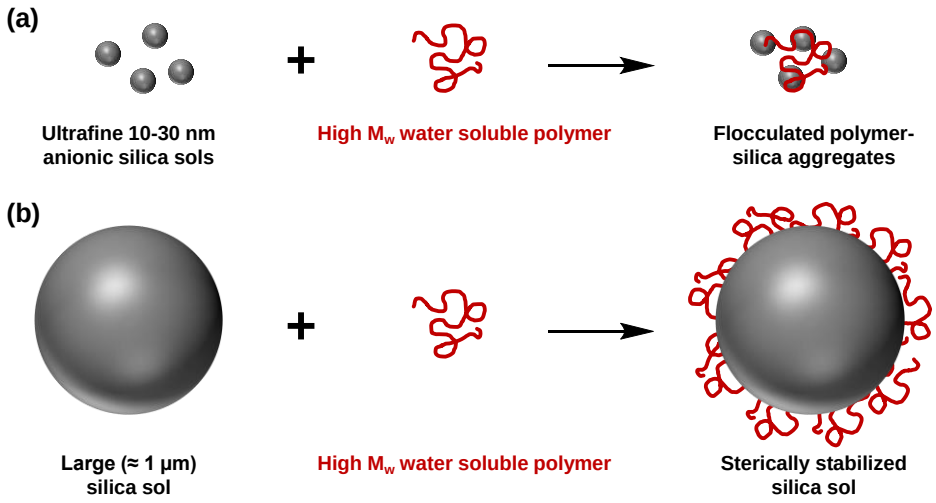

Figure 4.1 (a) Flocculation of nanometer-sized silica sols and (b) steric stabilisation of micrometer-sized silica sols on addition of a high molecular weight water-soluble polymer.

However, for micrometer-sized silica particles, this usually leads to steric stabilization rather than bridging flocculation (see Figure 4.1b). This qualitatively different behaviour is the result of the mismatch in length scales for the two components. However, polyelectrolytic block copolymer nanoparticles have not yet been evaluated as flocculants for relatively large silica particles. In particular, cylindrical or worm-like nanoparticles can be formed from various

diblock copolymers for a relatively narrow range of compositions.[15-26] The highly anisotropic nature of such nanoparticles leads to a much longer effective length scale, which should enable effective inter-particle bridging. More specifically, in the present Chapter it is hypothesized that cationic worms may act as efficient flocculants.

Over the last decade or so, various research groups have demonstrated the versatility of PISA for the design of bespoke functional AB diblock copolymer nanoparticles.[27-47] Such PISA formulations are based on either dispersion or emulsion polymerisation and can be conducted at relatively high copolymer concentrations (up to 50% w/w) in either polar (e.g. water or lower alcohols) or non-polar solvents (e.g. n-alkanes, mineral oil or poly(α-olefins)).[48-52] Briefly, a macro-CTA is used as a soluble stabiliser 'A' block and self-assembly occurs *in situ* as the growing second 'B' block gradually becomes insoluble in the polymerisation medium. Various nanoparticle morphologies can be accessed using this approach, including spheres, worms, unilamellar vesicles, oligolamellar vesicles, framboidal vesicles and platelet-like lamella sheets.[53-55] In particular, the worm morphology has received much recent attention since it offers interesting applications, such as sterilisable biocompatible hydrogels,[56] viscosity modifiers,[20, 57] 3D cell culture media,[58] efficient Pickering emulsifiers,[59] a cost-effective storage medium for stem cell transportation[60] or the effective cryopreservation of red blood cells.[61] Furthermore, certain diblock copolymer worms can undergo a morphology transition on exposure to external stimuli such as pH or temperature.[30, 62-67]

Several techniques have been developed for the preparation of cross-linked block copolymer nanoparticles.[16, 20, 68-74] *In situ* core cross-linking of nanoparticles prepared by PISA can be achieved by either (i) addition of a divinyl comonomer during the latter stages of the polymerisation[59, 71] or (ii) the post-polymerisation addition of a suitable cross-linking agent.[75]

The preparation of cross-linked spheres or vesicles is relatively straightforward.[59, 76-78] However, the preparation of cross-linked block copolymer worms is much more challenging. This is in part because of their tendency to form free-standing gels under the PISA synthesis conditions,[57] which makes the addition of cross-linker reagents somewhat problematic. Moreover, addition of a divinyl comonomer can sometimes lead to (partial) loss of the desired worm copolymer morphology, because this occupies relatively narrow phase space.[59] Nevertheless, Lovett *et al.*[75] have recently reported the preparation of core cross-linked worms *via* statistical copolymerisation of HPMA and glycidyl methacrylate (GlyMA) to form an epoxy-functional core-forming block. Post-polymerisation addition of 3-aminopropyl triethoxysilane (APTES) leads to an epoxy-amine reaction within the worm cores, with concomitant siloxane hydrolysis and condensation with secondary hydroxyl groups located on neighbouring HPMA residues, leading to extensive cross-linking. Such non-ionic cross-linked worms remained colloidally stable during a methanol challenge (which is a good solvent for both of the core-forming blocks) or on addition of anionic surfactant, whereas the linear worms do not.

Semsarilar and co-workers reported that using polyelectrolytic macro-CTAs in PISA formulations typically leads to purely spherical morphologies due to the strong lateral repulsion between the charged stabilizer chains.[79, 80] Even with the addition of salt to screen these unfavourable electrostatics, higher order morphologies such as worms and vesicles could not be observed. However, judicious dilution of the polyelectrolytic stabilizer blocks *via* addition of a non-ionic macro-CTA during the PISA synthesis allowed access to both worms and vesicles.[79] Unfortunately, such linear anionic or cationic worms rapidly dissociate to form individual copolymer chains in the presence of surfactant. Moreover, negative zeta potentials were observed above pH 7 as a result of the relatively short cationic macro-CTA (and perhaps also

the use of a carboxylic acid-based RAFT agent and azo initiator) employed in such PISA formulations.

This Chapter describes the synthesis of both linear and cross-linked cationic block copolymer worms using a binary macro-CTA approach *via* RAFT-mediated PISA. The two macro-CTAs employed in this approach are PEO and PQDMA. The colloidal stability of the resulting nano-objects in the presence of methanol or excess cationic surfactant is compared using DLS and TEM. Both types of cationic worms are evaluated as putative flocculants for aqueous dispersions of micrometer-sized silica particles using scanning electron microscopy (SEM) and laser diffraction studies. A critical comparison of their performance is made with various commercial soluble polymeric flocculants.

4.2 Experimental

4.2.1 Materials

[2-(Methacryloyloxy)ethyl] trimethylammonium chloride (80% w/w aqueous solution), poly(ethylene oxide) monomethyl ether (PEO, DP_n = 113), glycidyl methacrylate (GlyMA, 97%), 3-aminopropyl triethoxysilane (APTES, >98%), triethylamine (>99%), methanesulfonyl chloride (>99%), poly(*N*-vinylpyrrolidone) (M_w = 1,300 kg mol^{-1}) and poly(diallyldimethylammonium chloride) (M_w = 500 kg mol^{-1}) were all purchased from Sigma Aldrich (UK) and used as received. Deuterated methanol (CD_3OD; D, 99.8%) and dichloromethane (CD_2Cl_2; D, 99.9%) were purchased from Cambridge Isotopes Laboratories Ltd. 2-Hydroxypropyl methacrylate (HPMA; 97%) was purchased from Alfa Aesar (UK) and used as received. VA-044 was purchased from Wako Chemicals Ltd. All solvents were purchased from either VWR International or Sigma Aldrich and were HPLC-grade quality. Commercial polymers: Poly(ethylene glycol) (M_w = 4,000 kg mol^{-1}) and polyacrylamide

(M_w = 6,000 kg mol^{-1}) were purchased from Polysciences Inc., Warrington, PA, USA. Commercial silica particles: AngstromSphere silica particles of nominal 1.0 μm and 4.0 μm diameters were purchased from Fiber Optic Center Inc. (MA) and used as received. Bindzil 2040 silica particles of diameter 31 nm (measured by DLS) were kindly donated by AkzoNobel.

4.2.2 Synthesis of mono-aminated poly(ethylene oxide)$_{113}$-NH$_2$

Poly(ethylene glycol) monomethyl ether (50.0 g, 10.0 mmol, M_n = 5000 g mol^{-1}) was dissolved in toluene (500 ml) and this solution was azeotropically distilled to remove approximately 300 ml of solvent. After cooling to room temperature, anhydrous dichloromethane (200 ml) was added, and then triethylamine (6.00 g, 59.3 mmol) was added dropwise. Subsequently, methanesulfonyl chloride (6.79 g, 59.3 mmol) was added dropwise and the reaction solution was stirred under N_2 for 18 hours. The white ammonium chloride salt was removed by filtration and the organic layer was concentrated under vacuum, then precipitated into diethyl ether. The off-white precipitate was collected by filtration and dried in a 30 °C vacuum oven to yield PEO$_{113}$-OMs (48.8 g, 9.76 mmol) which was dissolved in 2 L of 35% aqueous ammonia over a 7 h period. The lid was sealed and the solution was stirred at 20 °C for 6 days. The lid was removed and stirred for a further 3 days to remove excess ammonia. The pH was increased to pH 13 using NaOH and the polymer was extracted into dichloromethane (3 x 150 ml). The organic layers were washed with brine and dried over magnesium sulfate. After concentration under vacuum, the polymer was precipitated into diethyl ether and PEO$_{113}$-NH$_2$ (45.1 g, 9.02 mmol) was isolated by filtration and dried under vacuum, with a yield of 90%. The primary amine end-group was confirmed by ^{1}H NMR spectroscopy as the triplet signal of the methylene protons adjacent to the amine was observed at δ 2.9 ppm. Comparison of this integrated triplet signal, relative to that of the methyl ether end group, indicated an end-group functionality of 96%.

4.2.3 Synthesis of poly(ethylene oxide)$_{113}$ Macro-CTA

All glassware was dried in a 120 °C oven overnight then flame-dried under vacuum before use to remove trace water. SPETTC was synthesized according to Chapter 2. SPETTC (4.45 g, 10.2 mmol) was dissolved in anhydrous dichloromethane (20 ml) in a 250 ml two-necked round-bottomed flask equipped with a pressure-equalizing dropping funnel. PEO_{113}-NH_2 (45.1 g, 9.02 mmol) was dissolved in anhydrous dichloromethane (100 ml) and added to the dropping funnel via cannula transfer under N_2. The PEO_{113}-NH_2 solution was added dropwise to the yellow SPETTC solution over approximately 1 hour and stirred for 16 h at room temperature. The yellow polymer solution was precipitated into diethyl ether (1500 ml) and the yellowish polymer was isolated by vacuum filtration and dried in a 30 °C vacuum oven to yield PEO_{113}-PETTC (42.1 g, 7.88 mmol) in 87% yield. ^{1}H NMR spectroscopy confirmed conjugation of the RAFT agent to the mono-aminated PEO_{113} and comparison of the aromatic integrals at δ 7.1 – 7.4 ppm with the triplet at δ 2.9 ppm indicated a degree of PETTC functionality of 96%. UV spectroscopy indicated an end-group functionality of 94%. THF GPC indicated an M_n = 4,400 g mol^{-1}, M_w / M_n = 1.08 vs. PEO standards.

4.2.4 Synthesis of poly([2-(methacryloyloxy)ethyl]trimethylammonium chloride Macro-CTA by RAFT Aqueous Solution Polymerisation

MPETTC RAFT agent was synthesized according to Chapter 2. A 100 ml round-bottom flask was charged with MPETTC (0.237 g, 0.524 mmol) and ([2-(methacryloyloxy)ethyl] trimethylammonium chloride monomer (QDMA) (16.4 g of 80% aqueous solution, 13.1 g QDMA monomer, 63.0 mmol, target DP_n = 120) and stirred for 10 minutes. Then 2,2'-azobis[2-(2-imidazolin-2-yl)propane]dihydrochloride (VA-044, 34.0 mg, 0.105 mmol) and H_2O (27.9 g) were added to afford a 30% w/w cloudy yellow solution. The pH was lowered to 4.0 by the careful addition of 1 M HCl and the cloudy solution became transparent and was stirred for a

further 5 min. The yellow solution was degassed under N_2 for 30 min in an ice/water slurry. The sealed reaction vessel was immersed in a preheated oil bath set at 44 °C for 3 h. Polymerisation was quenched by exposure to air and cooling to room temperature. Monomer conversion was calculated to be 96% conversion by ^{1}H NMR. Purification and isolation of the polymer was achieved by precipitation into excess acetonitrile (3 x 500 mL), dissolution into deionised water, removal of residual acetonitrile under vacuum and then freeze-drying overnight. ^{1}H NMR spectroscopy confirmed a DP_n of 125 by comparison of the integral of the aromatic end-group signal at δ 7.1 – 7.4 ppm to that of the methacrylic backbone at δ 0.4 – 2.5 ppm, indicating a RAFT agent efficiency of 92%. Aqueous GPC analysis of the $PQDMA_{125}$ macro-CTA indicated an M_n = 31,800 g mol^{-1} and M_w/M_n = 1.19 against near-monodisperse PEO standards.

4.2.5 Synthesis of linear (poly(ethylene oxide) + poly([2-(methacryloyloxy)ethyl]trimethylammonium chloride))-poly(2-hydroxypropyl methacrylate) Diblock Copolymer Nanoparticles by RAFT Aqueous Dispersion Polymerisation of 2-Hydroxypropyl methacrylate

In a typical protocol for the synthesis of linear cationic nano-objects (0.9 PEO_{113} + 0.1 $PQDMA_{125}$)-$PHPMA_{225}$ at 20% solids: A 7 mL sample vial was charged with $PQDMA_{125}$ macro-CTA (77.7 mg, 2.94 μmol), PEO_{113}-PETTC macro-CTA (0.152 g, 26.4 μmol), VA-044 (3.17 mg, 9.80 μmol), HPMA (0.954 g, 6.62 mmol) and water (4.75 g) to afford a 20% w/w solution. The sealed vial was degassed under N_2 in an ice/water slurry for 20 minutes placed in an oil bath preheated 50 °C for 4 h. Polymerisation was quenched by exposure to air and cooling 20 °C. ^{1}H NMR spectroscopy was used to determine final monomer conversion and TEM was used to determine the copolymer morphology. A series of block copolymer nano-particles were synthesised by variation of the molar ratio of PEO_{113}-PETTC to $PQDMA_{125}$ and

the target degree of polymerisation of the PHPMA block at a fixed concentration of 20% solids to generate a phase diagram.

4.2.6 Synthesis of Core Cross-linked (poly(ethylene oxide)+poly([2-(methacryloyloxy)ethyl]trimethylammonium chloride))-(poly(2-hydroxypropyl methacrylate)-*stat*-poly(glycidyl methacrylate)) Copolymers Worms by RAFT Aqueous Dispersion Polymerisation of 2-Hydroxypropyl Methacrylate and Glycidyl methacrylate

In a typical protocol for the synthesis of cross-linked cationic worms (0.9 PEO_{113} + 0.1 $PQDMA_{125}$)-(P($HPMA_{160}$-*stat*-$GlyMA_{40}$)) at 20% solids: A 14ml sample vial was charged with $PQDMA_{125}$ macro-CTA (0.0801 g, 3.03 µmol), PEO_{113} macro-CTA (0.157 g, 27.3 µmol), VA-044 (3.30 mg, 10.2 µmol), HPMA (0.701 g, 4.86 mmol), GlyMA (0.173 g, 1.22 mmol) and deionized water (4.46 g) to afford a 20% w/w solution. The sealed vial was degassed under N_2 in an ice/water slurry for 20 minutes and placed in a preheated 50 °C oil bath for 4 h. Polymerisation was quenched by exposure to air and cooling 20 °C. TEM was used to determine a worm-like morphology. This worm-gel was diluted to 7.5% w/w by the addition of deionized water (9.28 g) and gently stirred for 24 h. (3-aminopropyl)triethoxysilane (0.269 g, 0.284 mL, 1.22 mmol, [PGlyMA]/[APTES] = 1) was added to the worm dispersion and stirred overnight. These core cross-linked cationic diblock copolymer worms were analysed by DLS and TEM to assess stability in methanolic and cetyltrimethylammonium bromide solutions.

4.2.7 Flocculation Study of Micron-sized or Nano-sized Silica Particles using Linear and Cross-Linked Cationic Block Copolymer Worms

In a typical flocculation experiment for a nominal adsorbed worm surface density of 4.8 mg m^{-2}, 2.0 mL of a 2.0 % w/w dispersion of 1.0 µm silica spheres at pH 9 was added dropwise to

2.0 mL of a 0.028 % w/w dispersion of either linear or core cross-linked cationic diblock copolymer worms at pH 9 and gently stirred for 24 h at 20 ºC. The initial polymer concentration was varied (while keeping $[silica]_0$ at 2.0 % w/w) to change the surface densities of the worms on the 1.0 µm silica surface. In addition, the flocculated dispersion was centrifuged at 6000 rpm for 60 min and any nanoparticles remaining in the aqueous supernatant were analysed by DLS and TEM. In separate experiments, 2.0 mL of 8% w/w of 4 µm silica dispersion was added to 2.0 mL of core cross-linked worm dispersions at pH 9. The resulting copolymer/silica dispersion was analysed by laser diffraction and SEM to assess its degree of flocculation. Similar flocculation experiments were performed on both 1 µm silica and 31 nm silica ($[silica]_0$ = 31 nm), using four high molecular weight commercial water-soluble polymers as flocculants: PEO, PA, PNVP and PDADMAC. The polymer concentration was varied to adjust the nominal adsorbed amount per unit surface area.

4.2.8 Surfactant Challenge Protocol

In a typical surfactant challenge, 1.0 mL of a pH 9, 0.20 % w/w aqueous dispersion of core cross-linked (0.9 PEO_{113} + 0.1 $PQDMA_{125}$)-P($HPMA_{160}$-*stat*-$GlyMA_{40}$) cationic worms was mixed with 1.0 mL of a 0.20 % w/w CTAB solution to give an aqueous solution containing 0.1% w/w copolymer and 0.1% w/w CTAB, followed by stirring for 24 h at 20 °C. The resulting copolymer/surfactant dispersion was analysed by DLS and TEM.

4.2.9 Copolymer Characterisation

^{1}H NMR Spectroscopy

All NMR spectra were recorded at 298 K using a 400 MHz Bruker AV3-HD spectrometer in CD_3OD or CD_2Cl_2. Sixty-four scans were averaged per spectrum. All chemical shifts are reported in ppm (δ).

THF Gel Permeation Chromatography

0.5% w/w copolymer solutions were prepared in THF using toluene (10 μL per mL) as the flow rate marker. GPC measurements were conducted using a THF eluent containing 2.0% v/v triethylamine and 0.05% w/v butylhydroxytoluene (BHT) at a 30 °C, flow rate of 1.0 mL min^{-1}. The GPC set-up comprised an Agilent PL guard column, two PLgel 5 μm Mixed C columns in series and a WellChrom K-2301 RI detector operating at 950 ± 30 nm. A series of poly(ethylene oxide) standards ranging from 1080 g mol^{-1} to 905,000 g mol^{-1} or ten near-monodisperse poly(methyl methacrylate) standards (M_p values from 1,280 g mol^{-1} to 330,000 g mol^{-1}) were used for column calibration and calculation of molecular weight data.

Aqueous Gel Permeation Chromatography

0.5 % w/w copolymer solutions were analysed in an acidic aqueous buffer (pH 2) containing 0.5 M acetic acid, 0.3 M NaH_2PO_4 and adjusted to pH 2 with concentrated HCl, at a flow rate of 1.0 ml min^{-1}. The GPC set-up comprised an Agilent 1260 Infinity series degasser and pump, an Agilent PL Aquagel-OH 30 8 μm column and an Agilent PL Aquagel-OH 20 5 μm column for PQDMA kinetic studies. This column set up was calibrated with PEO standards ranging from 400 g mol^{-1} to 134,300 g mol^{-1}. For analysis of the $PQDMA_{125}$ macro-CTA and its self-blocking experiment, the column set-up comprised of two Agilent PL Aquagel-OH 30 8 μm columns in series. This column set-up was calibrated with PEO standards from 1,080 g mol^{-1} to 905,000 g mol^{-1} and molecular weight data is calculated relative to these standards. In both cases, a refractive index detector was used at a flow rate of 1 mL min^{-1} and 30 °C.

Laser Diffraction

Laser diffraction studies were performed on a Malvern Mastersizer 3000 instrument was equipped with a Hydro EV dispersion unit and set at a stirring rate of 2000 rpm. A HeNe laser

operating at 633 nm and a solid-state blue laser operating at 466 nm were used to analyse each silica/polymer dispersion to assess the degree of flocculation.

Dynamic Light Scattering

All DLS measurements were recorded at 20 °C using a Malvern Instruments Zetasizer Nano series instrument equipped with a 4 mW 633 nm He−Ne laser and an avalanche photodiode. Aqueous electrophoresis measurements were conducted in the presence of 1 mM KCl. The dispersion pH was adjusted as required with either 1 M or 0.1 M HCl or KOH.

Helium Pycnometry

The solid-state density of the silica spheres was measured using a Micromeritics AccuPyc 1330 helium pycnometer at 20 °C.

Centrifugation

Copolymer/silica dispersions (1.5 mL) were centrifuged at 6000 rpm for 1 h using a Heraeus Biofuge Pico centrifuge. The aqueous supernatant was analysed by DLS, aqueous electrophoresis and TEM. The sedimented silica particles were redispersed and analysed by aqueous electrophoresis.

Transmission Electron Microscopy

Copper/palladium grids were surface-coated in-house to produce a thin film of amorphous carbon and then plasma glow-discharged for 20 seconds to give a hydrophilic surface. Freshly-prepared 0.1% w/v aqueous dispersions (10 μL) were onto the hydrophilic grid for 15 seconds, blotted to remove excess sample and then negatively stained with uranyl formate solution (0.75% w/v) for a further 15 seconds. Excess stain was removed by blotting and carefully dried

with a vacuum house. TEM grids were imaged using a FEI Tecnai Spirit 2 microscope fitted with an Orius SC1000B camera operating at 80 kV.

Scanning Electron Microscopy

Silica or copolymer/silica dispersions were placed on a glass slide and dried overnight, mounted onto SEM stubs using adhesive conducting pads and then gold-coated prior to analysis. Imaging was performed using an Inspect F microscope operating at 15 kV.

4.3 Results & Discussion

4.3.1 Synthesis of Macromolecular Chain Transfer Agents

The PEO_{113}-PETTC macro-CTA used in this work was synthesised in a similar fashion to that as described by Warren *et al.*,[49] see Scheme 4.1.

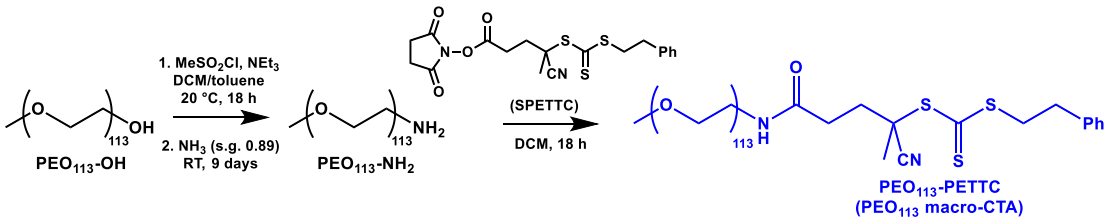

Scheme 4.1 Functional group conversion of PEO_{113}-OH to PEO_{113}-NH_2, followed by amidation with SPETTC to produce PEO_{113}-PETTC RAFT agent.[49]

A commercially available poly(ethylene oxide) monomethyl ether precursor (PEO_{113}-OH) was modified to give a mesylate adduct that was reacted with ammonia to produce a mono-aminated PEO_{113}-NH_2. The synthesis of the succinimide ester RAFT agent precursor, SPETTC, has been previously described in Chapter 2. The mono-aminated PEO_{113}-NH_2 was reacted with SPETTC to produce the desired PEO_{113}-PETTC macro-CTA. ^{1}H NMR studies indicated an end-group

functionality of 95% by comparison of the integration values of the aromatic signal at 7.2 – 7.4 ppm to that of the methylene protons at 2.9 – 3.0 ppm. UV spectroscopy analysis indicated end-group functionality 94%. THF GPC analysis indicated an M_n of 4,400 g mol^{-1} and a M_w / M_n = 1.08 vs. PEO standards (Figure 4.2).

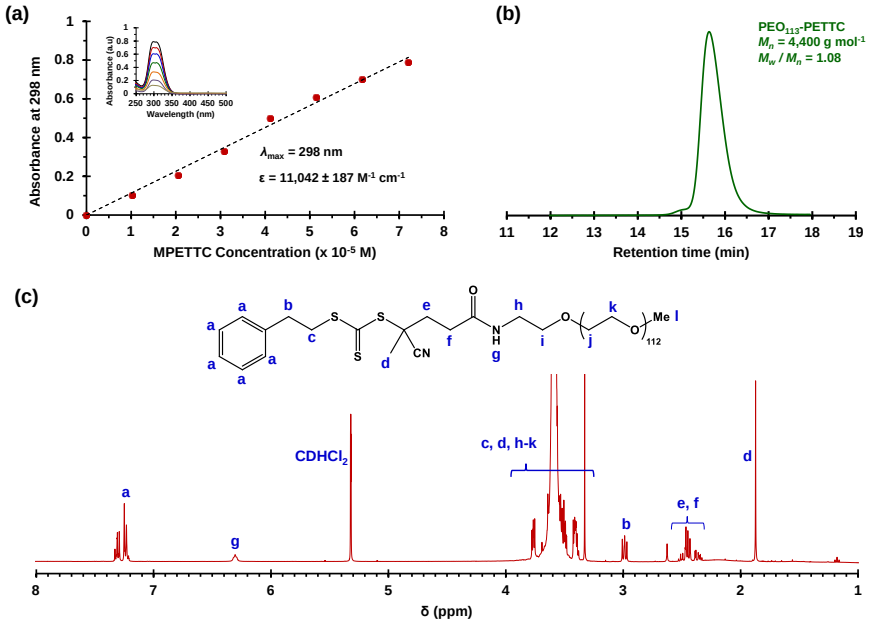

Figure 4.2(a) Beer-lambert plot for MPETTC RAFT agent in methanol, used to calculate the degree of functionality of PEO_{113}-PETTC macro-CTA. (b) THF GPC chromatogram obtained for PEO_{113}-PETTC macro-CTA. M_n and M_w / M_n are calculated against PEO standards. (c) Fully-assigned ^{1}H NMR spectra recorded in CD_2Cl_2 for PEO_{113}-PETTC macro-CTA to calculate the degree of amidation

2-(Methacryloyloxy)ethyl trimethylammonium chloride was selected as the electrolytic monomer in view of its pH-independent cationic character and commercial availability. The RAFT agent selected was MPETTC was prepared as described in Chapter 2. A kinetic study of the RAFT aqueous solution polymerisation of QDMA at 44 °C using MPETTC was undertaken at pH 4 (Figure 4.3).

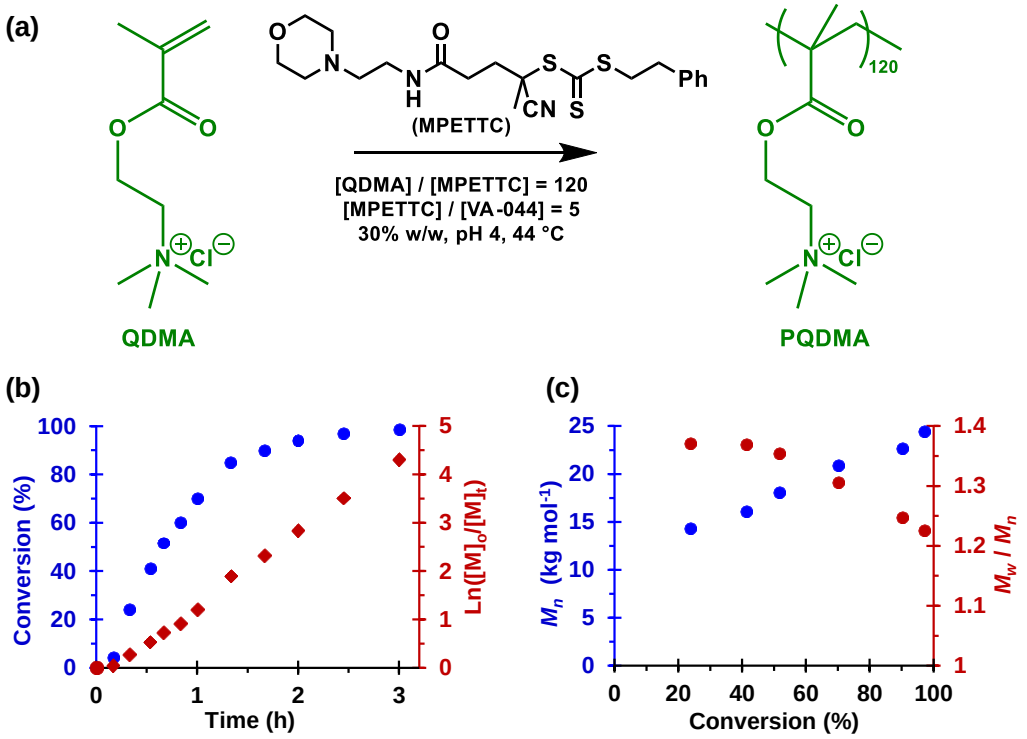

Figure 4.3 (a) Reaction scheme, (b) monomer conversion and Ln($[M]_0/[M]_t$) vs. time plot and (c) number-average molecular weight (M_n) and polydispersity (M_w / M_n) vs. monomer conversion plot for the RAFT aqueous solution polymerisation of QDMA using the RAFT agent MPETTC at pH 4, 30% w/w solids and 44 °C using a [MPETTC] / [VA-044] molar ratio of 5.0. The target PQDMA DP_n is 120. Monomer conversion was calculated by ^{1}H NMR spectroscopy by comparing the integrated aromatic peak at 7.2 - 7.4 ppm to that of the monomer vinyl signal at 6.2 ppm. M_n and M_w data were obtained by aqueous GPC analysis at pH 2 using a series of near mono-disperse PEO standards.

These conditions were selected to ensure protonation of the morpholine end-group of this RAFT agent and hence ensure its aqueous solubility. A DP_n of 120 was targeted at 30% w/w solids. Figure 4.3b shows the monomer conversion vs. time curve and corresponding semi-logarithmic plot, while Figure 4.3c shows the evolution in M_n and M_w / M_n with monomer conversion. After a brief induction period of around 10 min, the polymerisation proceeded at a relatively fast rate. More than 99 % QDMA conversion was obtained after 3 h. The linear evolution of molecular weight with monomer conversion indicated that this polymerisation has pseudo-living character

and proceeded under good RAFT control as expected. M_w / M_n values are reduced from 1.32 to less than 1.25 during the polymerisation. The non-zero y-intercept of 12.5 kg mol^{-1} is an experimental artefact that is attributed to inadequate resolution in the low molecular weight limit as a result of overlap between the polymer signal and low molecular species (monomer and/or CTA). A RAFT agent efficiency of 86 % was estimated using ^{1}H NMR spectroscopy by comparing the theoretical target PQDMA DP_n with the experimental DP_n obtained at the end of the kinetic study (after allowing for the final conversion). Under identical conditions, a large batch of PQDMA macro-CTA with a DP_n of 125 (Figure 4.4) was prepared. The mean PQDMA DP_n was calculated by comparison of the aromatic signals at 7.2 - 7.5 ppm with the polymer side-group peak at 3.4 – 4.2 ppm. Aqueous GPC analysis indicated an M_n = 31,800 g mol^{-1} and M_w / M_n = 1.19 relative to PEO standards.

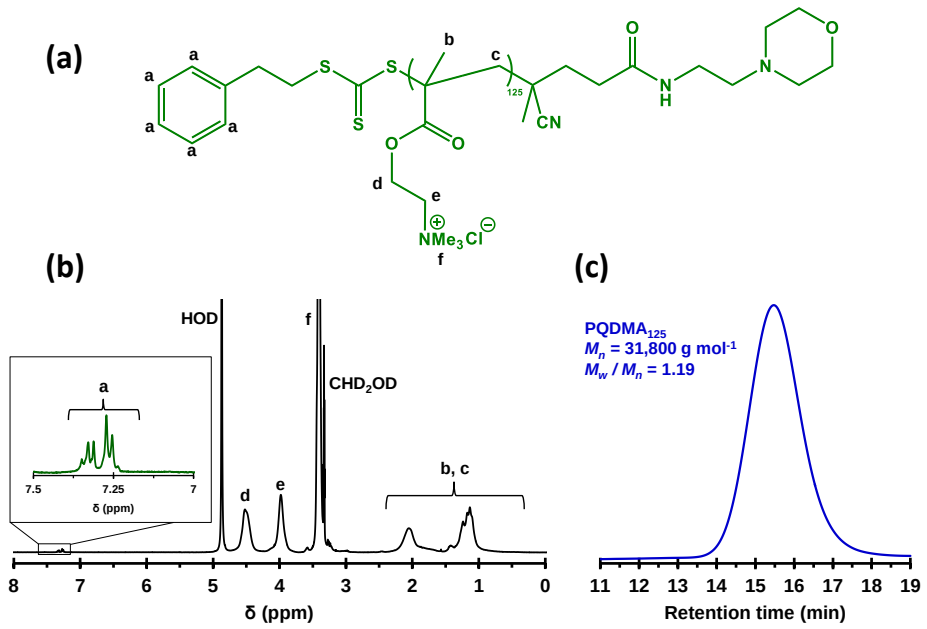

Figure 4.4 (a) Chemical structure and (b) partially assigned ^{1}H NMR spectrum recorded in CD_3OD for $PQDMA_{125}$ macro-CTA indicating the aromatic end-group and main QDMA signals. The mean PQDMA DP_n was calculated by comparison of the integrated aromatic signals at 7.2 – 7.5 ppm with those of the two methylene protons at 3.8 – 4.2 ppm. (c) Aqueous GPC chromatograms *vs.* PEO standards for $PQDMA_{125}$ macro-CTA.

4.3.2 Construction of ([1-*n*] PEO_{113} + *n* $PQDMA_{125}$)-$PHPMA_y$ Phase Diagram

A binary mixture of PEO_{113} and $PQDMA_{125}$ macro-CTAs was chain-extended with HPMA under RAFT aqueous dispersion polymerisation conditions to produce a range of linear cationic diblock copolymer nano-objects, see Scheme 4.2. (Table of data)

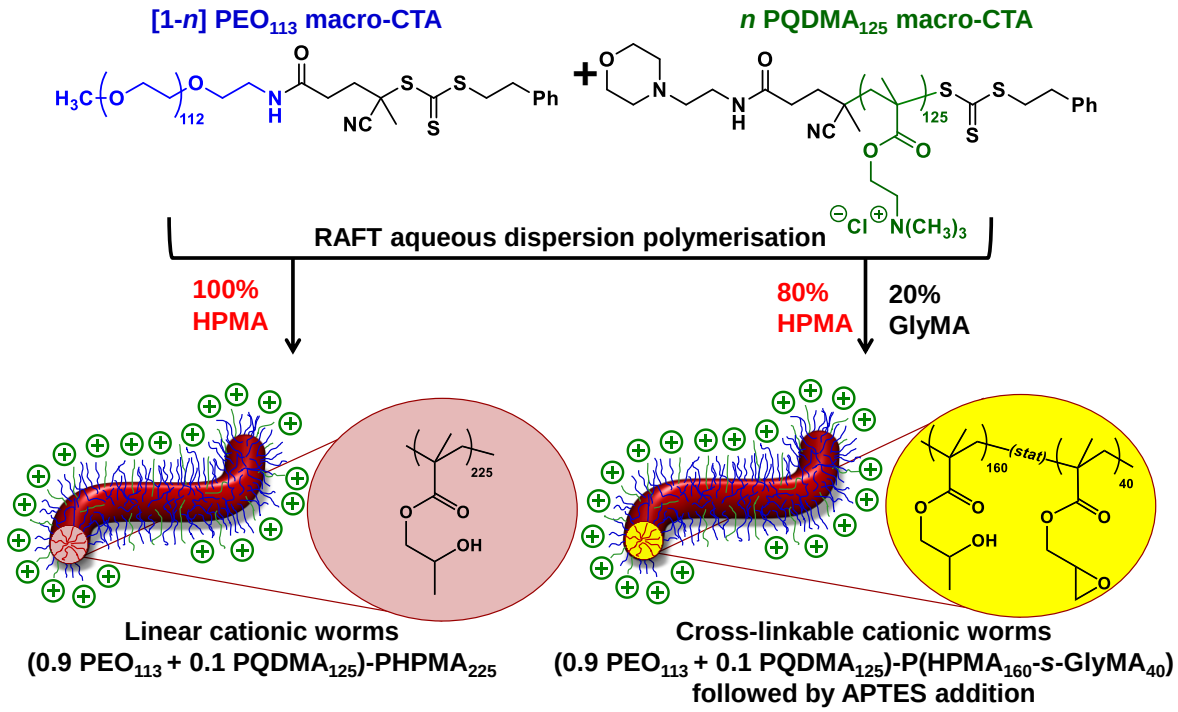

Scheme 4.2 The synthesis of either linear or core cross-linked cationic diblock copolymer worms was achieved *via* RAFT aqueous dispersion homopolymerisation of 2-hydroxypropyl methacrylate (HPMA) or statistical copolymerisation of HPMA with glycidyl methacrylate (GlyMA) using a binary mixture of poly(ethylene oxide) and poly(2-(methacryloyloxy)ethyl trimethylammonium chloride) macro-CTAs. Here, *n* represents the mol fraction of $PQDMA_{125}$ in the binary mixture of $PQDMA_{125}$ and PEO_{113} macro-CTAs.

All syntheses went to > 99% monomer conversion, as determined by ^{1}H NMR spectroscopy. Unfortunately, these linear cationic nanoparticles cannot be analysed by GPC because there is no suitable eluent that dissolves all three blocks (i.e. hydrophilic PEO_{113} and $PQDMA_{125}$ plus

the hydrophobic PHPMA). In separate experiments, both PEO_{113} and $PQDMA_{125}$ macro-CTAs were chain-extended to assess their blocking efficiency. PEO_{113} was chain-extended with 250 units of HPMA, and in this case the resulting diblock copolymer is amenable to GPC analysis.[49] In contrast, a self-blocking experiment was performed with the $PQDMA_{125}$ macro-CTA using 350 units of QDMA to target an overall DP_n of 475. THF and aqueous GPC analysis indicated high blocking efficiencies for both the PEO_{113} and $PQDMA_{125}$ macro-CTAs (Figure 4.5).

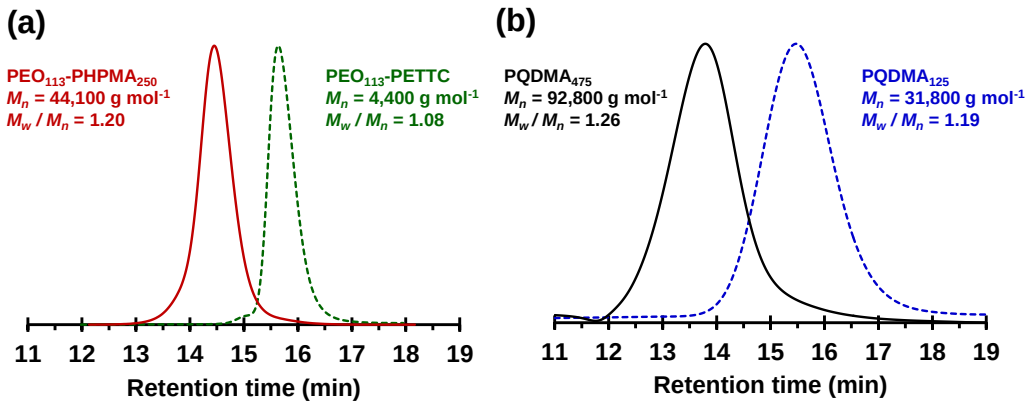

Figure 4.5 (a) THF GPC chromatogram (*vs*. PMMA calibration standards) obtained for PEO_{113}-$PHPMA_{250}$ diblock copolymer and PEO_{113} macro-CTA (green dotted line). (b) Aqueous GPC chromatogram (*vs*. PEO calibration standards) obtained at pH 2 after the self-blocking of $PQDMA_{125}$ macro-CTA (blue dotted line) with 350 units of QDMA monomer to prepare $PQDMA_{475}$.

A phase diagram was constructed at a constant copolymer concentration of 20% w/w solids (Figure 4.6) whereby the mol fraction (*n*) of the $PQDMA_{125}$ macro-CTA was systematically varied from 0 to 0.20 while targeting DP_ns of 150 to 600 for the PHPMA core-forming block. For all syntheses, the final HPMA conversion exceeded 99% and the final copolymer morphology was assigned by TEM studies. The general formula for this series of block copolymer nanoparticles is given by ([1-*n*] PEO_{113} + *n* $PQDMA_{125}$)-$PHPMA_y$

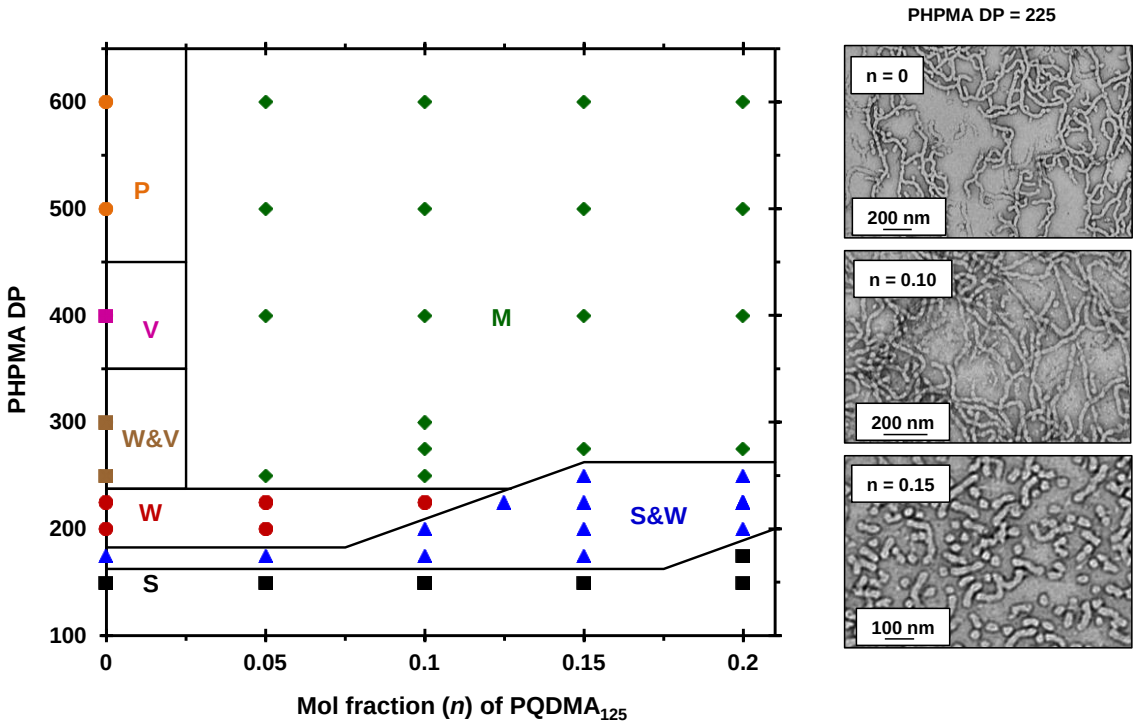

Figure 4.6 A phase diagram constructed for the RAFT aqueous dispersion polymerisation of HPMA at a fixed solids content of 20% w/w at 50 °C using a binary mixture of $PQDMA_{125}$ and PEO_{113} macro-CTAs. The general formula for this phase diagram is [(1-*n*) PEO_{113} + *n* $PQDMA_{125}$]-$PHPMA_y$, where *n* is the mol fraction of $PQDMA_{125}$ and y is the target PHPMA DP_n. In addition, three representative TEM images are shown for *n* values of 0, 0.10 and 0.15 at a fixed y value of 225. [S = spheres, W = worms, V = vesicles, P = precipitate and M = mixed phase].

To examine the effect of conferring cationic character on the diblock copolymer nanoparticles, a series of PEO_{113}-$PHPMA_y$ diblock copolymer PISA syntheses were performed as control experiments. A pure sphere phase was obtained when targeting PEO_{113}-$PHPMA_{150}$ while a mixed phase of spheres and worms was identified for PEO_{113}-$PHPMA_{175}$, which is in good agreement with previous work by Warren *et al.*[49] Free-standing worm gels were observed for PHPMA DP_ns of 220 to 225, with a mixed phase of worms and vesicles being observed for PHPMA DP_ns of 250 to 300. At a PHPMA DP_n of 400, a pure vesicle phase was identified, but precipitation occurred at a DP_n of 500. Addition of $PQDMA_{125}$ (*n* = 0.05) to such PISA syntheses has no discernible effect on the phase diagram when targeting PHPMA DP_ns of 225

or below. However, the worm/vesicle binary mixed phase and pure vesicle phase are no longer observed above this critical PHPMA DP_n. Instead, only rather ill-defined copolymer morphologies are obtained, such as mixed phases of worms and lamella-like sheets or mixtures of spheres, vesicles and tubular vesicles (Figure 4.7).

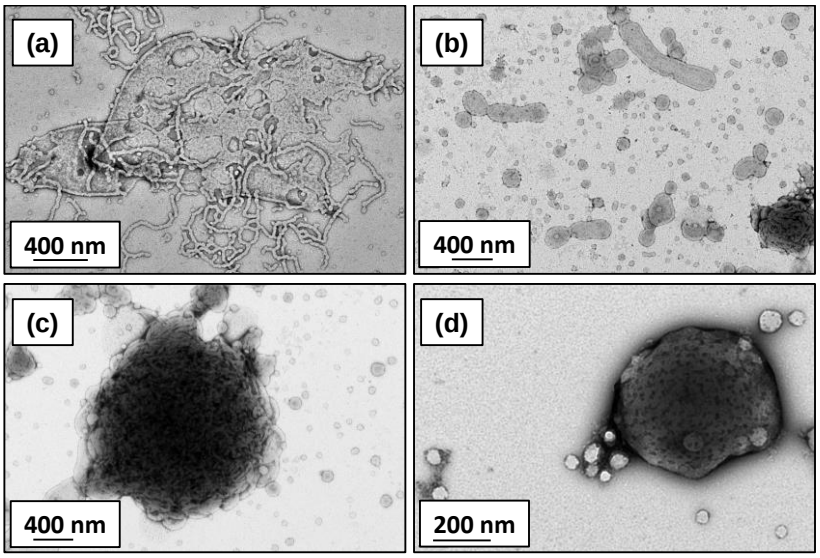

Figure 4.7 Representative TEM images obtained for a series of four diblock copolymer nanoparticles comprising (0.95 PEO_{113} + 0.05 $PQDMA_{125}$) – $PHPMA_y$ where (a) y = 250, (b) y = 400, (c) y = 500 and (d) y = 600.

However, precipitation does not occur at a PHPMA DP_n of 500 or 600 when $PQDMA_{125}$ is incorporated as a supplementary stabilizer block. Presumably, the polyelectrolytic character of this macro-CTA boosts the steric stabilization conferred by the non-ionic PEO_{113}, thus facilitating the formation of colloidally stable nano-objects. Increasing the $PQDMA_{125}$ mol fraction from n = 0.05 to n = 0.10 in this PISA formulation has a relatively modest effect on the phase diagram. The only discernible change is at a PHPMA DP_n of 200, where a sphere/worm mixed phase is observed, indicating narrowing of the worm phase space. A representative TEM image of linear (0.9 PEO_{113} + 0.1 $PQDMA_{125}$)-$PHPMA_{225}$ worms is shown in Figure 4.6. A pure worm phase is no longer observed on increasing n up to 0.125. This is consistent with more

recent work by Williams *et al.*,[47] who utilized PGMA, instead of PEO_{113} as a non-ionic stabilizer block, in combination with a $PQDMA_{95}$ macro-CTA to produce cationic thermoresponsive worm gels. Thus if a pure worm phase is desired, the maximum proportion of $PQDMA_{125}$ that can be incorporated into the present PISA formulation is n = 0.10. This constraint arises because the worm phase is relatively narrow, as reported previously.[47] Aqueous electrophoresis was used to characterize the cationic character of three pure diblock copolymer worms at a fixed PHPMA DP_n of 225 (see Figure 4.8).

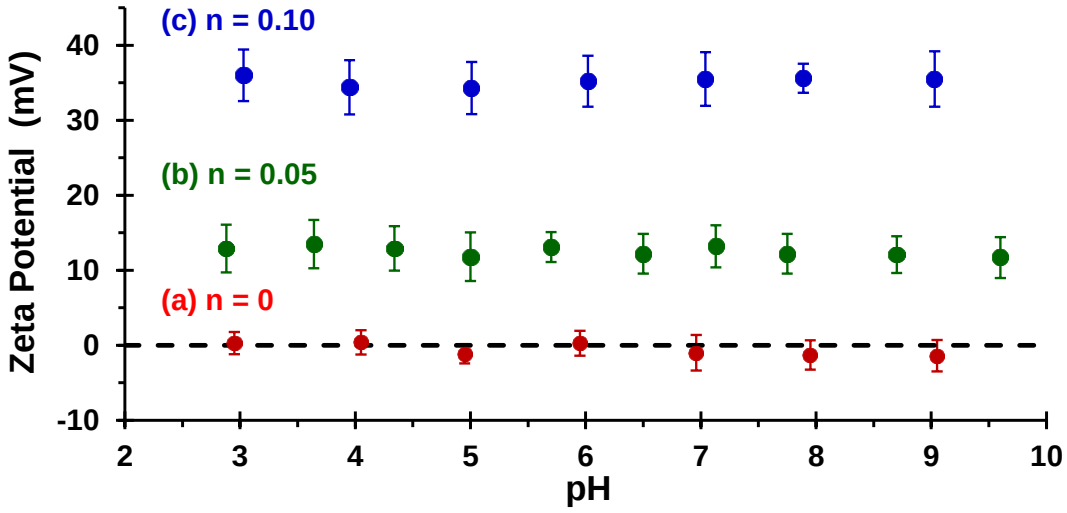

Figure 4.8 Zeta potential vs pH curves obtained for a series of [(1-*n*) PEO_{113} + *n* $PQDMA_{125}$]-$PHPMA_{225}$ linear diblock copolymer worms prepared at 20% w/w solids by RAFT aqueous dispersion polymerisation of HPMA at 50 °C. Here, (a) *n* = 0, (b) *n* = 0.05 and (c) *n* = 0.10. Zeta potentials were determined at 20 °C for 0.1% w/w copolymer dispersions in the presence of 1 mM KCl. Aqueous dispersion pH was adjusted using 0.1 M or 1 M HCl and error bars are equivalent to one standard deviation.

As expected, the PEO_{113}-$PHPMA_{225}$ copolymer worm control exhibited a zeta potential of approximately zero across the entire pH range studied. Introduction of $PQDMA_{125}$ into the stabilizer block (*n* = 0.05) led to initially weak cationic character, as indicated by a pH-independent zeta potential of approximately +13 mV. However, a relatively high zeta potential

of +35 mV was observed on doubling the mol fraction of $PQDMA_{125}$ (n = 0.10). Again, the block copolymer worms exhibited no discernible change over a wide pH range. In all cases, simultaneous DLS studies confirmed that there was no change in the 'sphere-equivalent' hydrodynamic diameter of 212 nm on varying the solution pH, suggesting that the original worm morphology was retained during these electrophoresis studies.

4.3.3 Covalent Cross-linking and Colloidal Stability of Cationic Diblock Copolymer Worms

Lovett *et al.* reported that 3-aminopropyl triethoxysilane (APTES) can be used to cross-link epoxy-functionalized worms *via* a post-polymerisation protocol.[75] Worm core cross-linking involves reaction of the epoxy groups on the GlyMA residues with APTES, with concomitant hydrolysis to form silanol groups which then condense with other silanol groups and/or secondary hydroxyl groups located on neighbouring HPMA residues (see Scheme 4.3).

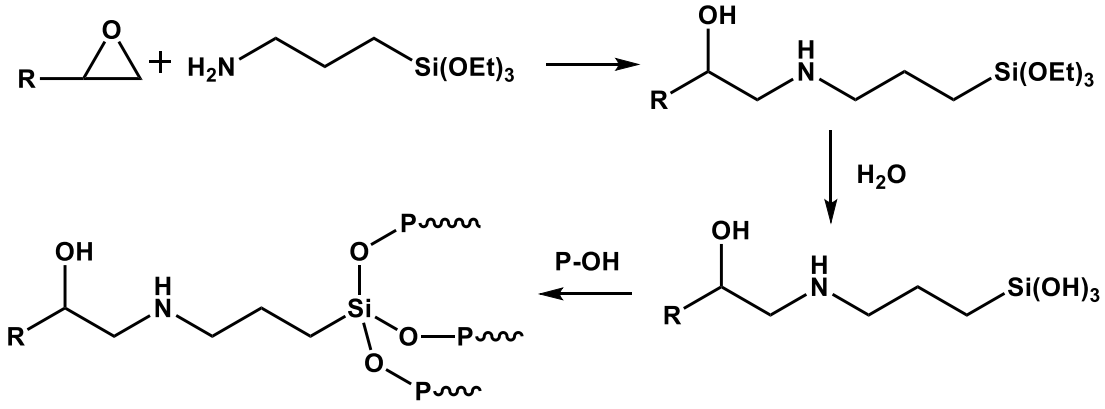

Scheme 4.3 Suggested cross-linking mechanism for the formation of core cross-linked cationic diblock copolymer worms. The epoxide groups on the PGlyMA residues are ring opened *via* nucleophilic attack of the APTES primary amine group. Simultaneously, the silanol groups hydrolyse and subsequently react with one another or the secondary hydroxyl groups of the PHPMA residues. These latter species are simply denoted by P-OH, where P stands for polymer.

These reactions lead to extensive cross-linking within the worm cores. ^{1}H NMR was used to monitor this complex cross-linking process and it was found that epoxide ring-opening and hydrolysis/condensation occurred on comparable time scales.[75] Such covalently-stabilised non-ionic worms remained colloidally stable in the presence of either excess methanol or anionic surfactant, whereas the linear precursor worms underwent rapid dissociation under the same conditions.[75] An increase in storage modulus (G') was found after core cross-linking, presumably due to an increase in the worm persistence length.[75] In view of these prior observations, it was decided to examine the PISA synthesis of core cross-linked cationic diblock copolymer worms and assess their colloidal stability in the presence of either methanol or a well-known cationic surfactant, cetyltrimethylammonium bromide (CTAB). The mol fraction of $PQDMA_{125}$ was fixed at 0.10 in order to maximize the cationic character of the copolymer nanoparticles while maintaining a pure worm phase. The PHPMA core-forming block was replaced with a statistical copolymer comprising 80 mol % PHPMA and 20 mol % GlyMA (see Scheme 4.2). However, introducing the GlyMA comonomer led to a subtle change in the phase diagram, with a mixed phase of worms and vesicles being observed instead of the desired pure worm phase when the total core DP_n is 225 (see Figure 4.9).

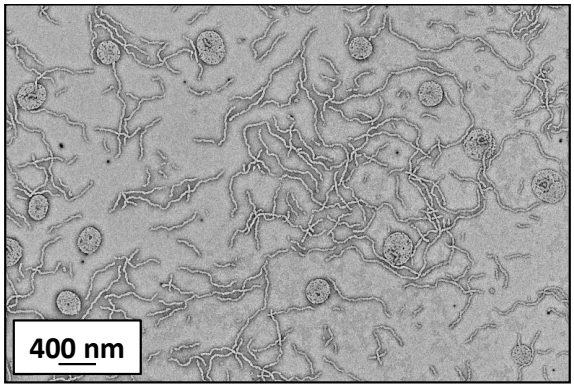

Figure 4.9 Representative TEM images of (0.9 PEO_{113} + 0.1 $PQDMA_{125}$)-(P($HPMA_{168}$-*stat*-$GlyMA_{42}$)) worm/vesicle mixed phase (total core DP_n = 225).

Thus the overall DP_n of the core-forming block was adjusted from 225 to 200 to compensate for the presence of the more hydrophobic GlyMA comonomer. A very high comonomer conversion (> 99%) was achieved to afford well-defined linear (0.9 PEO_{113} + 0.1 $PQDMA_{125}$)-P($HPMA_{160}$-*stat*-$GlyMA_{40}$) diblock copolymer worms. Unfortunately, PISA synthesis at 20% w/w solids produced a rather strong copolymer gel, which made APTES dissolution for post-polymerisation cross-linking somewhat problematic. Hence this worm gel was diluted to 7.5% w/w solids using deionised water prior to APTES addition ([PGlyMA] / [APTES] = 1), followed by gentle stirring for 24 h at room temperature. TEM studies confirmed no change in worm morphology after APTES addition (see Figure 4.10).

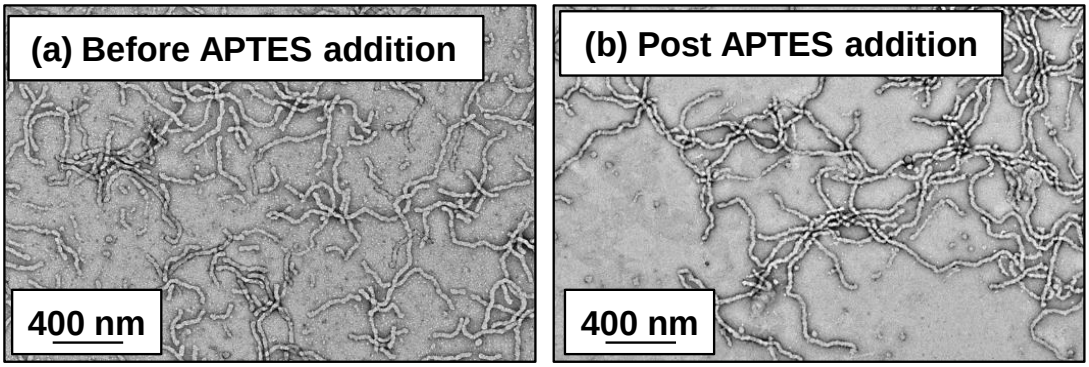

Figure 4.10 Representative TEM images recorded for 0.1% w/w copolymer worm dispersions at pH 9: (a) linear (0.9 PEO_{113} + 0.1 $PQDMA_{125}$)-P($HPMA_{160}$-*stat*-$GlyMA_{40}$) worms and (b) core cross-linked (0.9 PEO_{113} + 0.1 $PQDMA_{125}$)-P($HPMA_{160}$-*stat*-$GlyMA_{40}$) worms after APTES addition.

Chambon *et al.*[71] reported using DLS and TEM to assess the colloidal stability of block copolymer vesicles in the presence of various aqueous surfactant solutions. Herein the same approach is utilised to examine the colloidal stability of both linear and core cross-linked cationic worms (at 0.1% w/w) in the presence of either excess methanol or a 0.1% w/w CTAB solution. A 0.1% w/w CTAB solution corresponds to a concentration of 2.7 mM, which is above the critical micelle concentration for CTAB reported in the literature.[81, 82] Table 4.1 summarises

the intensity-average diameters, zeta potentials and the derived count rates obtained for linear and cross-linked cationic worms (i) dispersed in mildly alkaline aqueous solution (pH 9), (ii) in the presence of 0.1% w/w CTAB (also at pH 9) or (iii) as a methanolic solutions.

Table 4.1 Summary of the intensity-average diameters, zeta potential and derived count rate for linear (0.9 PEO_{113} + 0.1 $PQDMA_{125}$)-$PHPMA_{225}$ and core cross-linked (0.9 PEO_{113} + 0.1 $PQDMA_{125}$)-P($HPMA_{160}$-*stat*-$GlyMA_{40}$) cationic worms at either pH 9 or after serial dilution of the as-prepared worms using methanol or in the presence of 0.1% w/w cetyltrimethylammonium bromide. All dispersions were analysed at 0.1% w/w copolymer at 20 °C and in the presence of 1 mM KCl.

Worm type	Intensity-average diameter / nm (PDI)	Zeta potential / mV (1 SD)	DLS derived-count rate / kcps	Normalized Intensity
Cross-linked worms at pH 9	216 (0.244)	+34 (± 2)	6.0×10^4	100
Cross-linked worms in methanol	240 (0.239)	-	5.4×10^4	90
Cross-linked worms at pH 9 plus 0.1% CTAB	212 (0.292)	+33 (± 4)	5.9×10^4	97
Linear worms at pH 9	212 (0.292)	+35 (± 2)	5.9×10^4	100
Linear worms in methanol	78 (0.208)	-	1.4×10^2	0.2
Linear worms at pH 9 plus 0.1% CTAB	48 (0.762)	+38 (± 8)	9.3×10^2	1.6

It is important to note that the 'sphere-equivalent' hydrodynamic diameter reported by DLS does not correspond to either the mean worm length or the mean worm width. Notwithstanding this limitation, this sizing technique suggests that the dimensions of the linear and cross-linked worms at pH 9 are somewhat comparable. The linear worm dispersion diluted in methanol has a

very low normalized light scattering intensity, which suggests worm dissociation under these conditions. In contrast, the relatively high light scattering intensity observed for cross-linked worms in the same solvent indicates that the original vermicious morphology is preserved under these conditions. The slightly higher sphere-equivalent diameter for the cross-linked worms in methanol compared to the same worms in water (240 nm vs. 216 nm) most likely indicates some degree of worm swelling, which would also account for the modest (ca. 10%) reduction in the light scattering intensity. Thus successful cross-linking of the worm cores prevents molecular dissolution under these conditions. It is also useful to compare the linear and cross-linked worms exposed to the presence of 0.1% w/w CTAB. The relatively low normalised intensity observed for the former dispersion suggests near-molecular dissolution of the linear worms, whereas the high intensity clearly shows the cross-linked worms survive the CTAB challenge. Indeed, TEM studies of the corresponding dried dispersions confirm that the cross-linked worms survive exposure to 0.1 % w/w CTAB or dilution from 20 % w/w to 0.1% w/w solids using methanol co-solvent (see Figure 4.11).

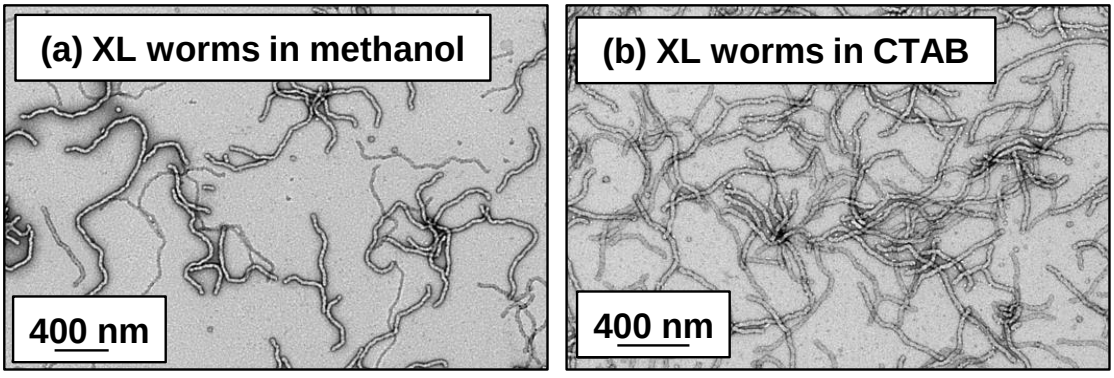

Figure 4.11 Representative TEM images obtained at pH 9 and 0.1% w/w for core cross-linked (0.9 PEO_{113} + 0.1 $PQDMA_{125}$)-P($HPMA_{160}$-*stat*-$GlyMA_{40}$) worms (a) diluted from 7.5% w/w copolymer to 0.1% w/w copolymer using methanol worms and (b) the same worms in the presence of 0.1% w/w CTAB. Abbreviations: XL = core cross-linked and CTAB = cetyltrimethylammonium bromide.

4.3.4 Flocculation of 1 µm Silica Particles

Bridging flocculation typically involves the adsorption of a high molecular weight water-soluble polymer onto two or more relatively small colloidal nanoparticles, which promotes their aggregation. For example, Solberg and Wågberg reported using high molecular weight polyacrylamide for the flocculation of 20 nm aqueous silica sols.[8] Other well-known flocculants include high molecular weight PEO or PNVP.[83, 84] Similarly, Mabire *et al*. found that cationic polyelectrolytes can act as highly effective flocculants for 125 nm anionic silica particles.[85] However, for the flocculation of much larger (micrometer-sized) particles, the bridging flocculation mechanism is likely to fail. This is because the markedly different length scales between the particles and the soluble polymer chains favour steric stabilization (i.e. the soluble polymer adsorbs onto and fully coats individual particles, see Figure 4.1). In the present Chapter, both linear and cross-linked cationic worms were evaluated as putative flocculants for micrometer-sized silica particles, with four high molecular weight water-soluble polymers being used as negative controls. In principle, core cross-linking should make the worm morphology much more robust. Moreover, stiffer worms should be obtained with greater mean persistence lengths, which should aid worm adsorption onto multiple silica particles. In initial experiments, zeta potential vs. pH curves were constructed for 0.1% w/w aqueous dispersions of linear worms, core cross-linked worms and 1.0 µm silica particles. A zeta potential of -69 mV was observed for these silica particles at pH 9, whereas the linear and cross-linked cationic worms had comparable zeta potentials of +35 mV and +34 mV, respectively (see Figure 4.12a). As expected, both worm dispersions exhibited pH-independent electrophoretic behaviour, whereas the zeta potential for the 1.0 µm silica particles gradually decreased to -20 mV at pH 2.8. Thus the flocculation study was performed at pH 9 in order to maximize the electrostatic interaction.

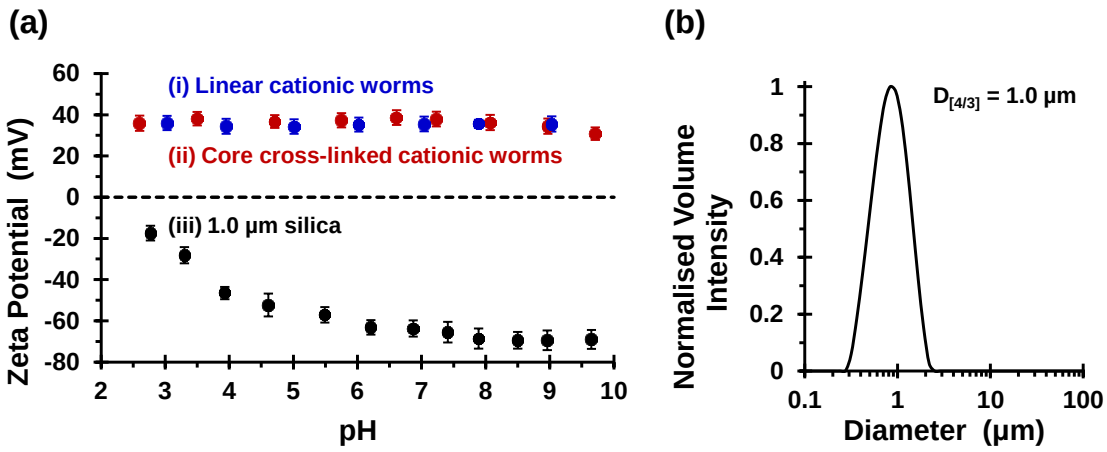

Figure 4.12 (a) Zeta potential vs. pH curves obtained for (i) linear (0.9 PEO_{113} + 0.1 $PQDMA_{125}$)-$PHPMA_{225}$ worms, (ii) core cross-linked (0.9 PEO_{113} + 0.1 $PQDMA_{125}$)-P($HPMA_{160}$-*stat*-$GlyMA_{40}$) worms and (iii) 1 µm silica particles. The linear worm data is reproduced from Figure 4.8 to enable direct comparison. Measurements were conducted at 20 °C on 0.1% w/w dispersions in the presence of 1 mM background KCl. The dispersion pH was adjusted by addition of either 1.0 M or 0.1 M HCl. (b) Volume-average laser diffraction particle size distributions obtained for pristine 1.0 µm silica spheres alone.

Furthermore, the bare micrometer-sized silica particles exhibit a volume-average diameter, $D_{[4/3]}$ of 1.0 µm, as judged by laser diffraction studies (see Figure 4.12b). All flocculation studies were conducted using 1.0 % w/w silica. The adsorbed amount (i.e. the worm mass per unit area of silica) was systematically varied in order to assess the effectiveness of the cationic worms as flocculants for the silica particles. The specific surface area, A_s, of these silica particles can be calculated using $A_s = 3/(\rho_{silica}.R)$, where ρ_{silica} and R are the density and mean radius of the silica particles, respectively. The solid-state density of the 1.0 µm diameter silica particles, ρ_{silica}, was found to be 2.03 g cm^{-3} by helium pycnometry. Using this density, A_s is estimated to be 2.9 m^2 g^{-1}. These silica particles were added to the cross-linked cationic worms at nominal adsorbed amounts of 0.1 mg m^{-2}, 2.1 mg m^{-2} and 4.8 mg m^{-2}. At a nominal adsorbed amount of 0.1 mg m^{-2}, laser diffraction studies indicated no significant change in $D_{[4/3]}$ for both the linear

and the cross-linked cationic worms, confirming that essentially no flocculation of 1.0 μm silica particles occurred under these conditions (see Figure 4.13a and b).

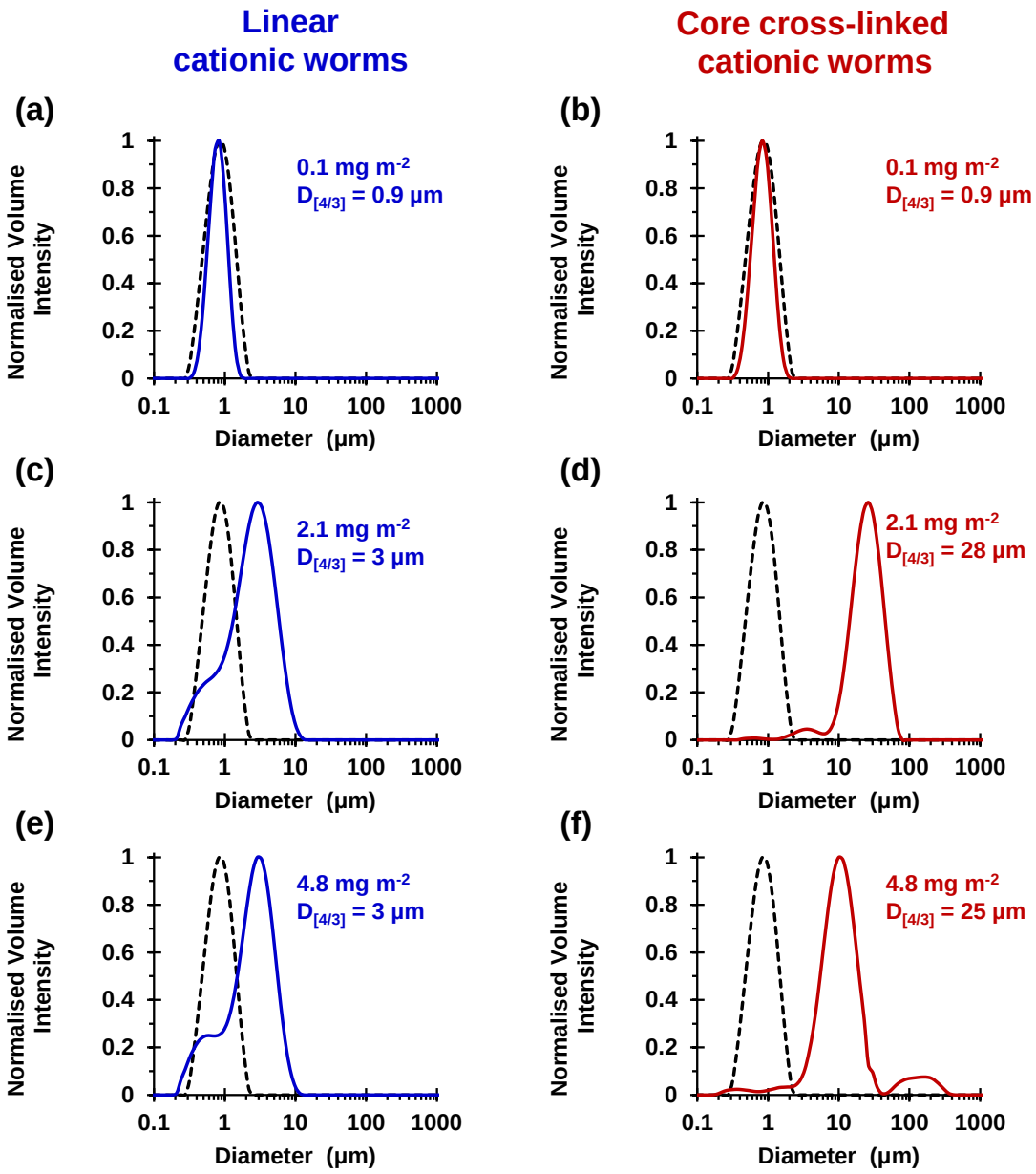

Figure 4.13 Volume-average particle size distributions obtained *via* laser diffraction for the attempted flocculation of 1.0 μm silica at pH 9 using either linear (0.9 PEO_{113} + 0.1 $PQDMA_{125}$)-$PHPMA_{225}$ worms (blue traces) or core cross-linked (0.9 PEO_{113} + 0.1 $PQDMA_{125}$)-P($HPMA_{160}$-*stat*-$GlyMA_{40}$) worms (red traces) at adsorbed amounts of (a, b) 0.1 mg m^{-2} (c, d) 2.1 mg m^{-2} and (e, f) 4.8 mg m^{-2}, respectively. The black dotted traces represent the volume-average particle size distribution obtained for the pristine 1.0 μm silica particles in the absence of any worms.

At a higher nominal adsorbed amount of 2.1 mg m^{-2}, laser diffraction indicated a $D_{[4/3]}$ of 3 μm for the linear cationic worms, suggesting only rather weak flocculation (see Figure 4.13c). However, the cross-linked cationic worms act as a highly effective flocculant, with a volume-average diameter of 28 μm being observed (see Figure 4.13d). Increasing the nominal adsorbed amount to 4.8 mg m^{-2} confirmed the superior flocculation performance of cross-linked worms compared to linear worms, with $D_{[4/3]}$ diameters of 25 μm and 3 μm being observed, respectively (compare Figure 4.13e and Figure 4.13f).

SEM studies were conducted on 1.0 μm silica particles before and after exposure to either linear or cross-linked cationic worms. The pristine 1.0 μm silica particles (Figure 4.14a) are spherical, uniform in size and have a smooth surface morphology. At a nominal adsorbed amount of 2.1 mg m^{-2}, SEM studies provide no evidence for the linear worms surviving electrostatic adsorption onto the silica surface (Figure 4.14b). Instead, only relatively small, pseudo-spherical structures can be observed. However, when cross-linked worms are used under the same conditions, intact adsorbed worms are clearly discernible at the silica particle surface (Figure 4.14c). Using a nominal adsorbed amount of 4.8 mg m^{-2} leads to similar observations, but higher surface coverage of the silica particles is achieved in each case (compare Figure 4.14b with Figure 4.14d and also Figure 4.14c with Figure 4.14e). Close inspection of Figure 4.14f indicates that some of the cross-linked cationic worms span between adjacent silica particles (see yellow arrows in Figure 4.14f). This provides direct evidence that the particle aggregation observed by laser diffraction is indeed the result of a bridging flocculation mechanism.

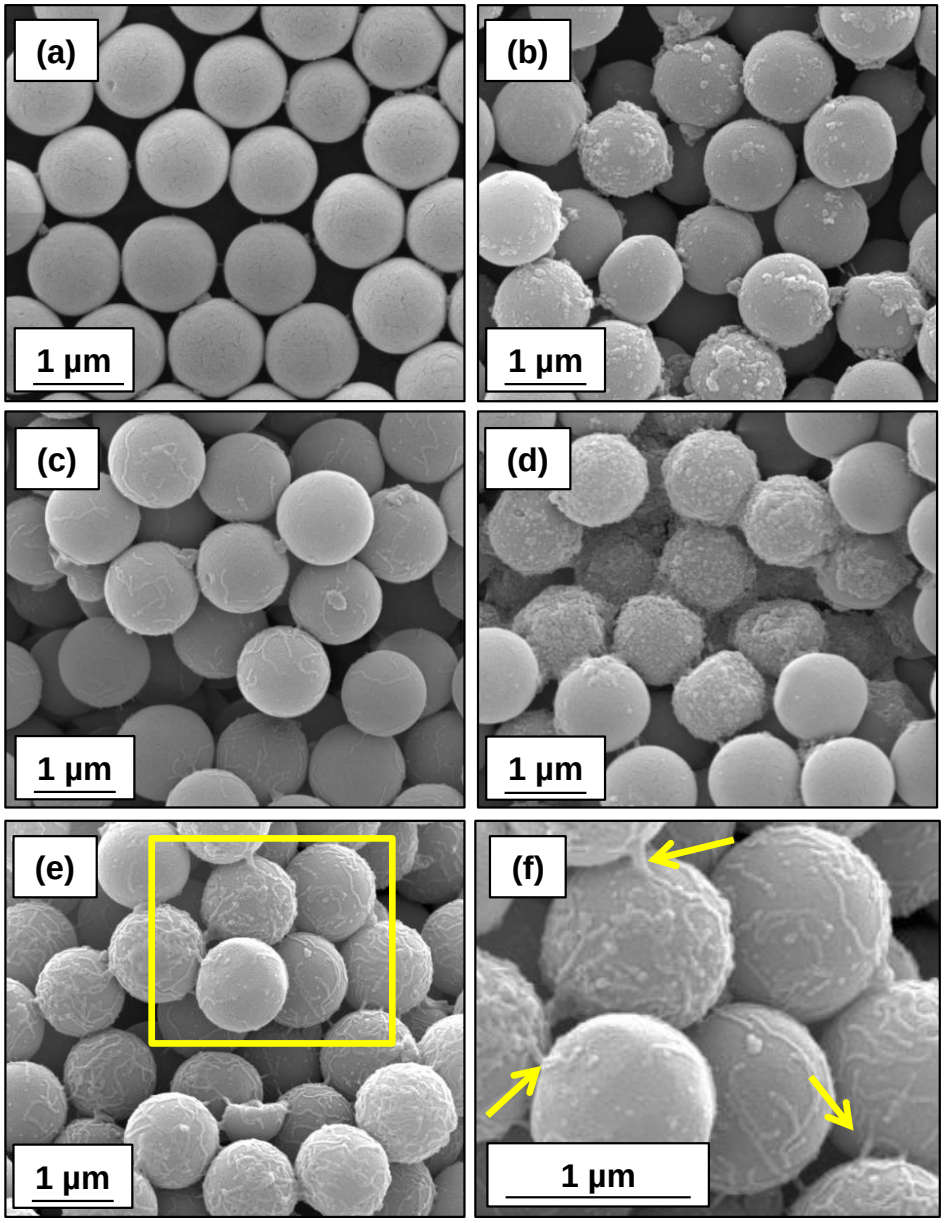

Figure 4.14 SEM images obtained for (a) pristine 1.0 µm silica spheres and the same spheres plus (b) linear cationic worms and (c) core cross-linked cationic worms at nominal adsorbed amounts of 2.1 mg m^{-2} respectively. Images shown in (d) and (e) correspond to 1.0 µm silica spheres in the presence of (d) linear cationic worms or (e) core cross-linked cationic worms at nominal adsorbed amounts of 4.8 mg m^{-2}. (f) A magnified section of (e) indicated by the yellow square in (e) confirming that core cross-linked cationic worms survive adsorption onto the 1.0 µm silica spheres and act as bridging flocculants. In each case worms were adsorbed onto the silica particles ([silica] = 1.0% w/w) at pH 9 followed by drying at 20 °C overnight.

Cross-linked worms are much more effective flocculants than linear worms because they are much more robust: covalent stabilization of the worm cores is essential to preserve the original copolymer morphology after electrostatic adsorption of the cationic worms onto the anionic silica particles. In striking contrast, the linear cationic worms break up following their adsorption onto the relatively massive silica particles to form two distinct populations of (mainly) non-ionic PEO_{113}-$PHPMA_{225}$ and (mainly) cationic $PQDMA_{125}$-$PHPMA_{225}$ nanoparticles, with each possessing a pseudo-spherical morphology (see Figure 4.15).

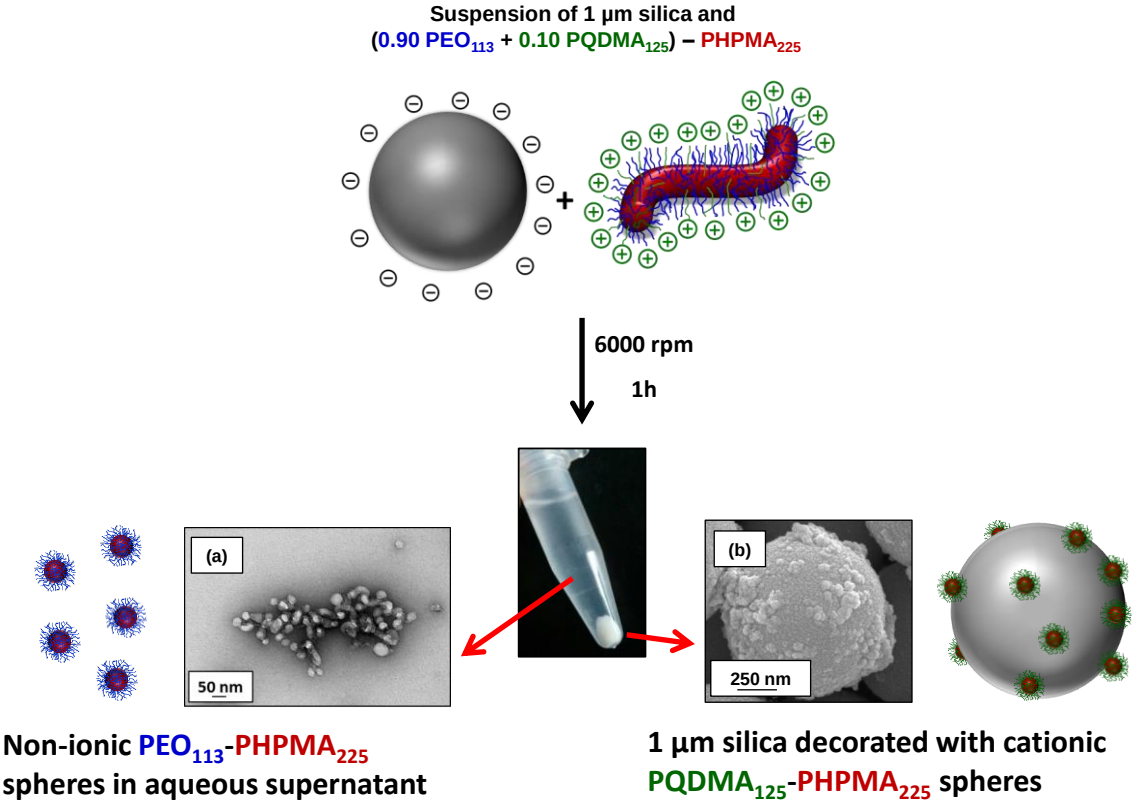

Figure 4.15 A suggested mechanism for the *in situ* break-up of linear (0.90 PEO_{113} + 0.10 $PQDMA_{125}$) – $PHPMA_{225}$ diblock copolymer worms upon addition to 1.0 µm silica spheres. Two distinct populations are formed of (a) (mainly) PEO_{113}-$PHPMA_{225}$ pseudo spheres in the supernatant and (b) (mainly) $PQDMA_{125}$-$PHPMA_{225}$ spheres adsorbed onto the 1.0 µm silica particles.

The weakly hydrophobic nature of the core-forming PHPMA block drives formation of the linear worms during PISA. However, this merely physical hydrophobic interaction is clearly insufficient to maintain the original morphology once these cationic worms adsorb onto the anionic silica particles. Image J software was used to assess worm dimensions from TEM images. Analysis of approximately 50 worms indicated a mean worm length, L_w, of 956 nm and a mean worm radius, r_w, of 15 nm. If the worm morphology is approximated to that a cylinder of volume V (where $V = \pi r_w^2 L_w$) and taking the worm density, ρ_w, to be that of the PHPMA core-forming block (1.15 g cm^{-3}), we estimate the mean mass, m, (where $m = \rho_w.V$) of a single worm to be 7.77 x 10^{-16} g. Hence the mass, M, of a single 1.0 μm silica particle is calculated using $M = \rho_{silica}.(4/3)\pi R^3$ (where R is the silica particle radius) to be 1.06 x 10^{-12} g, which is approximately 1,400 times greater than that of a single worm. Thus the linear cationic worms are simply unable to survive the strong torsional forces exerted on them by the much more massive silica particles during Brownian motion. Electrostatic interactions lead to strong adsorption of the cationic worms on the anionic silica particles, so the failure mechanism involves disruption of the physical van der Waals forces between the weakly hydrophobic PHPMA chains within the worm cores. In order to gain further mechanistic insight, an aqueous dispersion comprising a binary mixture of 1.0 μm silica particles plus linear copolymer worms prepared at a nominal adsorbed amount of 4.8 mg m^{-2} was centrifuged at 6 000 rpm for 1 h. After careful removal of the aqueous supernatant, the sedimented silica particles were redispersed in water at pH 9. Aqueous electrophoresis studies conducted at pH 9 indicated a zeta potential of only –17 mV, which is significantly lower than that of the original silica particles (see Figure 4.12). This suggests that the pseudo-spherical particles that remain on the surface of the silica particles (see Figure 4.14d) comprise mainly cationic $PQDMA_{125}$-$PHPMA_{225}$ chains. According to Semsarilar *et al.*, copolymer nanoparticles comprising mainly $PQDMA_{125}$-$PHPMA_{225}$ chains would be expected to form spheres, rather than worms.[79] In addition,

adsorption of non-ionic PEO_{113}-$PHPMA_{225}$ nanoparticles at the silica surface may also occur. However, DLS studies of the aqueous supernatant solution obtained after sedimentation of the silica particles indicated a mean hydrodynamic particle diameter of 85 nm (DLS polydispersity = 0.19), with aqueous electrophoresis studies indicating weakly negative zeta potential of -7 mV. TEM studies of this dried supernatant confirmed a pseudo-spherical morphology (see Figure 4.15a). Based on findings reported by Warren *et al.*, PEO_{113}-$PHPMA_{225}$ was expected to self-assemble to form worms in aqueous solution.[49] Inspecting Figure 4.6, this is indeed the case. However, for the highly dilute copolymer concentrations utilized in these flocculation studies, multiple sphere-sphere fusion (which is the critical first step for worm formation)[86] cannot occur, which leads to a kinetically-trapped spherical morphology. Thus there is strong experimental evidence to support the in situ disintegration of the linear cationic worms during their adsorption onto micrometer-sized silica particles, as summarised in Figure **4.15**. It is emphasised that this mechanism does not apply to the cross-linked cationic worms, since covalent stabilisation is sufficient to enable their survival after adsorption onto the relatively massive silica particles. This accounts for the marked difference in performance for these two putative bridging flocculants.

4.3.5 Flocculation of 4 µm Silica Particles

The flocculation performance of the cross-linked cationic worms was further examined by attempting flocculation of 4 µm silica particles at pH 9. At this pH, the silica spheres exhibit a zeta potential of -74 mV. Furthermore, laser diffraction studies confirm a volume-average diameter of $D_{[4/3]}$ = 4 µm with SEM studies indicating a spheres with a smooth surface morphology (Figure 4.16). Given that the A_s of these silica spheres is 0.72 m^2 g^{-1}, the final silica concentration was increased to 4.0 % w/w to maintain a constant silica surface area. No flocculation was observed when using nominal adsorbed amounts of 2.1 mg m^{-2} and 4.8 mg m^{-2},

which had been sufficient to flocculate the 1.0 µm silica particles. Thus, this parameter was increased to 88 mg m^{-2} (Figure 4.16).

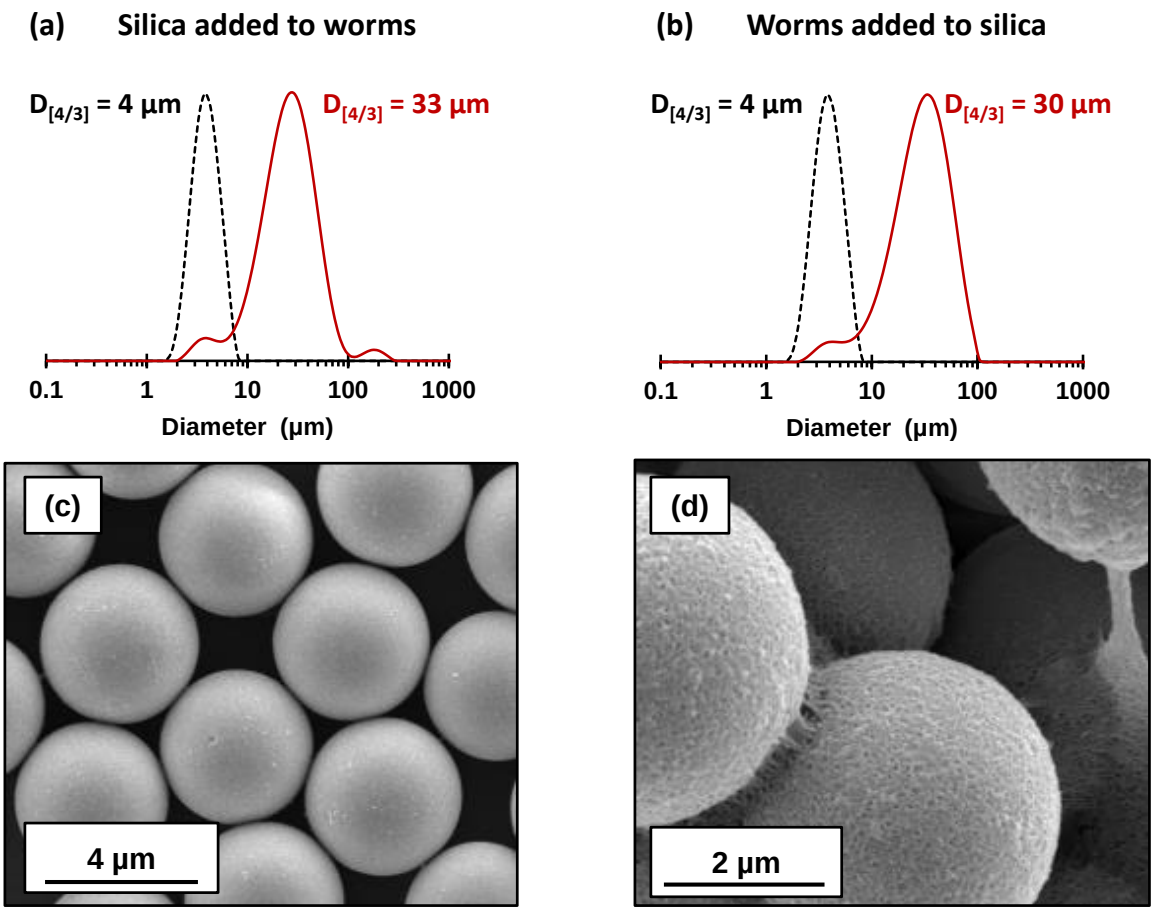

Figure 4.16 (a) and (b) Volume-average particle size distributions obtained *via* laser diffraction for pristine 4 µm silica particles (black dotted line) and the same particles in the presence of core cross-linked cationic (0.9 PEO_{113} + 0.1 $PQDMA_{125}$)-P($HPMA_{160}$-*stat*-$GlyMA_{40}$) worms adsorbed onto the 4 µm silica particles at a nominal adsorbed amount of 88 mg m^{-2}. (a) The silica spheres are added to the worms. (b) The worms are added to the silica spheres. Representative SEM images are shown for (c) pristine 4 µm silica particles and (d) the adsorbed cationic worms onto these silica particles. In this particular case, the silica was added to the worms.

Laser diffraction studies confirmed an increase in apparent volume-average diameter from 4 µm for the original silica particles up to 33 µm in the presence of the cross-linked cationic worms.

SEM studies indicated that these worms adsorb intact at the silica surface with relatively high surface coverage and readily identifiable worm bridges between adjacent silica particles. It is perhaps noteworthy that the 4.0 μm silica particles were always added to the cross-linked cationic worms. However, similarly strong flocculation was also observed if this order of addition was reversed (see Figure 4.16b).

4.3.6 Comparison with Commercial Flocculants

For comparative purposes, four high molecular weight commercial water-soluble polymers were examined as potential flocculants for the 1.0 μm silica particles at pH 9. These polymers were poly(ethylene oxide) (PEO; M_w = 4,000 kg mol^{-1}), polyacrylamide (PA; M_w = 6,000 kg mol^{-1}), poly(*N*-vinylpyrrolidone) (PNVP; M_w = 1,300 kg mol^{-1}) and poly(diallyldimethylammonium chloride) (PDADMAC; M_w = 500 kg mol^{-1}), see Table 4.2.

Table 4.2 Summary of the volume-average particle diameters obtained *via* laser diffraction after the attempted flocculation of a 1.0% w/w aqueous dispersion of 1.0 μm silica particles at pH 9 using four commercially available water-soluble polymers as putative flocculants. Abbreviations: PEO = poly(ethylene oxide), PA = polyacrylamide, PNVP = poly(*N*-vinylpyrrolidone) and PDADMAC = poly(diallyldimethylammonium chloride).

Commercial Polymer	M_w **(kg mol^{-1})**	**Volume-average diameter (μm) *via* laser diffraction using various adsorbed amounts of polymer per unit area of silica**			
		2.1 mg m^{-2}	**4.8 mg m^{-2}**	**17.2 mg m^{-2}**	**34.3 mg m^{-2}**
PEO	4,000	2	3	3	3
PA	6,000	1	1	1	3
PNVP	1,300	2	2	2	3
PDADMAC	500	1	1	1	3

Table 4.2 summarizes the apparent volume-average particle diameters of the silica particles obtained after addition of each of the four commercial polymers to 1.0 μm silica particles at pH 9 using nominal adsorbed amounts of 2.1 mg m^{-2}, 4.8 mg m^{-2}, 17.2 mg m^{-2} or 34.3 mg m^{-2}. Little or no flocculation was observed in all cases.

Table 4.3 Intensity-average diameters (nm) obtained by DLS for the attempted flocculation of 31 nm silica sols at pH 9 using four commercially available polymers. $[silica]_0$ = 0.05% w/w. Abbreviations: PEO = poly(ethylene oxide), PA = polyacrylamide, PNVP = poly(*N*-vinylpyrrolidone) and PDADMAC = poly(diallyldimethylammonium chloride)

Commercial Polymer	M_w (kg mol^{-1})	Intensity-average diameter (nm) obtained *via* laser diffraction using various adsorbed amounts of polymer per unit area of silica					
		0.6 mg m^{-2}	1.4 mg m^{-2}	2.6 mg m^{-2}	5.2 mg m^{-2}	7.7 mg m^{-2}	10.3 mg m^{-2}
PEO	4,000	57	60	76	81	78	84
PA	6,000	34	55	41	39	70	76
PNVP	1,300	52	57	60	59	66	66
PDADMAC	500	181	149	142	145	135	165

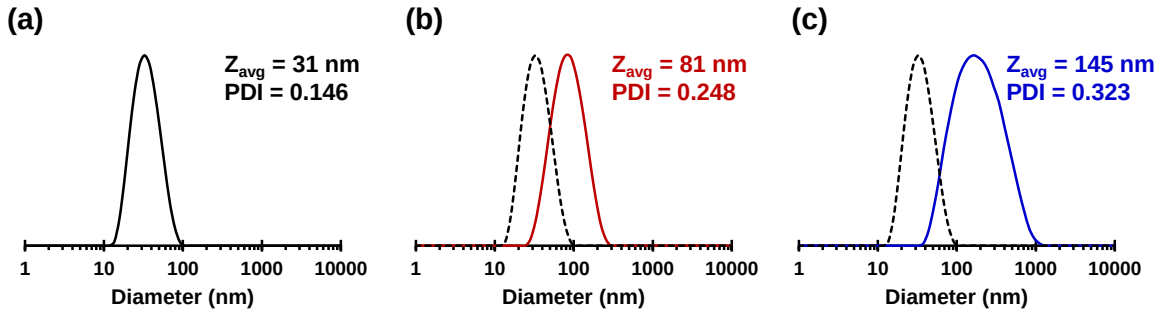

Figure 4.17 Intensity-average particle size distributions obtained *via* DLS for (a) Bindzil 2040 silica sols and these silica sols flocculated by (b) poly(ethylene oxide) and (c) poly(diallyldimethylammonium chloride) at a nominal adsorbed amount of 5.2 mg m^{-2}. $[silica]_0$ = 0.05% w/w.

However, when the same polymers were added to 31 nm anionic silica sols ($[silica]_0$ = 0.05% w/w), flocculation was observed in all cases (Table 4.3; Figure 4.17). In this case the length scales of the silica nanoparticles and the polymer coils are similar (tens of nm). These control experiments serve to illustrate the difficulty of aggregating micrometer-sized particles using conventional soluble polymeric flocculants. This highlights the exceptional performance of the cross-linked cationic worms revealed in this study: the mean contour length of these

highly anisotropic particles is comparable to the mean silica diameter which accounts for their 'superflocculant' behaviour.

4.4 Conclusions

In summary, chain extension of a binary mixture of PEO_{113} and $PQDMA_{125}$ macro-CTAs with HPMA using RAFT aqueous dispersion polymerisation at 20% w/w solids can be used to prepare diblock copolymer nano-objects. In particular, incorporation of 10 mol % $PQDMA_{125}$ while targeting an appropriate degree of polymerisation for the core-forming PHPMA block enables the formation of linear copolymer worms that remain highly cationic (+ 35 mV) across a wide pH range. Core cross-linked cationic worms were readily prepared using epoxy-amine chemistry via statistical copolymerisation of 20% mol GlyMA with HPMA, followed by addition of APTES. Extensive cross-linking occurs *via* reaction of the hydrolysed pendent silanol groups with the secondary alcohol groups on the HPMA residues and self-condensation reactions. Unlike the corresponding linear worms, these core cross-linked cationic worms can withstand the presence of either a cationic surfactant or methanol. Importantly, such cross-linked cationic worms are much more effective flocculants of highly anionic 1.0 μm silica particles at pH 9. In contrast, the linear cationic worms are much less effective flocculants, because they break up into (mainly) non-ionic and cationic block copolymer nanoparticle fragments. To benchmark the exceptional performance of the cross-linked cationic worms, a series of four high molecular weight commercial water-soluble polymers were also evaluated under the same conditions and found to be only weak flocculants for 1.0 μm silica particles. Finally, preliminary experiments confirmed that these cross-linked cationic worms can also flocculate 4 μm anionic silica particles at pH 9.

4.5 References

1. A. Swerin and L. Wågberg, *Nordic Pulp & Paper Research Journal*, 1994, **9**, 18.
2. R. Nicu, E. Bobu and J. Desbrieres, *Cellulose Chemistry and Technology*, 2011, **45**, 105.
3. M. S. Nasser and A. E. James, *Separation and Purification Technology*, 2006, **52**, 241.
4. S.-K. Kam and J. Gregory, *Water Research*, 2001, **35**, 3557.
5. B. Bolto and J. Gregory, *Water Research*, 2007, **41**, 2301.
6. M. Isik, A. M. Fernandes, K. Vijayakrishna, M. Paulis and D. Mecerreyes, *Polymer Chemistry*, 2016, **7**, 1668.
7. A. Bleier and E. D. Goddard, *Colloids and Surfaces*, 1980, **1**, 407.
8. D. Solberg and L. Wågberg, *Colloids and Surfaces A: Physicochemical and Engineering Aspect*, 2003, **219**, 161.
9. Y. Zhou, Y. Gan, E. J. Wanless, G. J. Jameson and G. V. Franks, *Langmuir*, 2008, **24**, 10920.
10. Y. Zhou and G. V. Franks, *Langmuir*, 2006, **22**, 6775.
11. M. Mende, S. Schwarz, G. Petzold and W. Jaeger, *Journal of Applied Polymer Science*, 2007, **103**, 3776.
12. C. Flood, T. Cosgrove, Y. Espidel, I. Howell and P. Revell, *Langmuir*, 2008, **24**, 7323.
13. S. Schwarz, K. Lunkwitz, B. Kessler, U. Spiegler, E. Killmann and W. Jaeger, *Colloids and Surfaces A: Physicochemical and Engineering Aspect*, 2000, **163**, 17.
14. V. H. Dao, N. R. Cameron and K. Saito, *Polymer Chemistry*, 2016, **7**, 11.
15. X. Wang, G. Guerin, H. Wang, Y. Wang, I. Manners and M. A. Winnik, *Science*, 2007, **317**, 644.
16. Y.-Y. Won, H. T. Davis and F. S. Bates, *Science*, 1999, **283**, 960.
17. H. Qiu, V. A. Du, M. A. Winnik and I. Manners, *Journal of the American Chemical Society*, 2013, **135**, 17739.
18. J. Massey, K. N. Power, I. Manners and M. A. Winnik, *Journal of the American Chemical Society*, 1998, **120**, 9533.
19. Y. Geng and D. E. Discher, *Journal of the American Chemical Society*, 2005, **127**, 12780.
20. Y.-Y. Won, K. Paso, H. T. Davis and F. S. Bates, *Journal of Physical Chemistry B*, 2001, **105**, 8302.
21. J. B. Gilroy, T. Gaedt, G. R. Whittell, L. Chabanne, J. M. Mitchels, R. M. Richardson, M. A. Winnik and I. Manners, *Nature Chemistry*, 2010, **2**, 566.
22. P. A. Rupar, L. Chabanne, M. A. Winnik and I. Manners, *Science*, 2012, **337**, 559.
23. N. Petzetakis, A. P. Dove and R. K. O'Reilly, *Chemical Science*, 2011, **2**, 955.
24. Y. Geng, P. Dalhaimer, S. Cai, R. Tsai, M. Tewari, T. Minko and D. E. Discher, *Nature Nanotechnology*, 2007, **2**, 249.
25. S. Cai, K. Vijayan, D. Cheng, E. M. Lima and D. E. Discher, *Pharmaceutical Research*, 2007, **24**, 2099.
26. A. H. Groschel, A. Walther, T. I. Lobling, F. H. Schacher, H. Schmalz and A. H. E. Muller, *Nature*, 2013, **503**, 247.
27. Y. Kang, A. Pitto-Barry, A. Maitland and R. K. O'Reilly, *Polymer Chemistry*, 2015, **6**, 4984.
28. A. O. Moughton and R. K. O'Reilly, *Chemical Communications*, 2010, **46**, 1091.
29. E. T. Garrett, Y. Pei and A. B. Lowe, *Polymer Chemistry*, 2016, **7**, 297.
30. Y. Pei, N. C. Dharsana and A. B. Lowe, *Australian Journal of Chemistry*, 2015, **68**, 939.

31. W. Zhang, F. D'Agosto, O. Boyron, J. Rieger and B. Charleux, *Macromolecules*, 2011, **44**, 7584.
32. J. Rieger, C. Grazon, B. Charleux, D. Alaimo and C. Jerome, *Journal of Polymer Science Part A: Polymer Chemistry*, 2009, **47**, 2373.
33. M. Dan, F. Huo, X. Xiao, Y. Su and W. Zhang, *Macromolecules*, 2014, **47**, 1360.
34. Z. Jia, V. A. Bobrin, N. P. Truong, M. Gillard and M. J. Monteiro, *Journal of the American Chemical Society*, 2014, **136**, 5824.
35. W.-J. Zhang, C.-Y. Hong and C.-Y. Pan, *Macromolecules*, 2014, **47**, 1664.
36. W. Zhao, G. Gody, S. Dong, P. B. Zetterlund and S. Perrier, *Polymer Chemistry*, 2014, **5**, 6990.
37. M. J. Derry, L. A. Fielding and S. P. Armes, *Polymer Chemistry*, 2015, **6**, 3054.
38. L. A. Fielding, M. J. Derry, V. Ladmiral, J. Rosselgong, A. M. Rodrigues, L. P. D. Ratcliffe, S. Sugihara and S. P. Armes, *Chemical Science*, 2013, **4**, 2081.
39. W. Cai, W. Wan, C. Hong, C. Huang and C. Pan, *Soft Matter*, 2010, **6**, 5554.
40. W. D. He, X. L. Sun, W. M. Wan and C. Y. Pan, *Macromolecules*, 2011, **44**, 3358.
41. S. Boisse, J. Rieger, K. Belal, A. Di-Cicco, P. Beaunier, M.-H. Li and B. Charleux, *Chemical Communications*, 2010, **46**, 1950.
42. S. Boisse, J. Rieger, G. Pembouong, P. Beaunier and B. Charleux, *Journal of Polymer Science Part A: Polymer Chemistry*, 2011, **49**, 3346.
43. X. Zhang, S. Boisse, W. Zhang, P. Beaunier, F. D'Agosto, J. Rieger and B. Charleux, *Macromolecules*, 2011, **44**, 4149.
44. W. Zhang, F. D'Agosto, O. Boyron, J. Rieger and B. Charleux, *Macromolecules*, 2012, **45**, 4075.
45. W. Zhang, F. D'Agosto, P.-Y. Dugas, J. Rieger and B. Charleux, *Polymer*, 2013, **54**, 2011.
46. M. Semsarilar, N. J. W. Penfold, E. R. Jones and S. P. Armes, *Polymer Chemistry*, 2015, **6**, 1751.
47. M. Williams, N. J. W. Penfold, J. R. Lovett, N. J. Warren, C. W. I. Douglas, N. Doroshenko, P. Verstraete, J. Smets and S. P. Armes, *Polymer Chemistry*, 2016, **7**, 3864.
48. V. J. Cunningham, A. M. Alswieleh, K. L. Thompson, M. Williams, G. J. Leggett, S. P. Armes and O. M. Musa, *Macromolecules*, 2014, **47**, 5613.
49. N. J. Warren, O. O. Mykhaylyk, D. Mahmood, A. J. Ryan and S. P. Armes, *Journal of the American Chemical Society*, 2014, **136**, 1023.
50. Q. Zhang and S. Zhu, *ACS Macro Letters*, 2015, **4**, 755.
51. B. Zhang, X. Yan, P. Alcouffe, A. Charlot, E. Fleury and J. Bernard, *ACS Macro Letters*, 2015, **4**, 1008.
52. M. J. Derry, L. A. Fielding and S. P. Armes, *Progress in Polymer Science*, 2016, **52**, 1.
53. N. J. Warren and S. P. Armes, *Journal of the American Chemical Society*, 2014, **136**, 10174.
54. C. J. Mable, N. J. Warren, K. L. Thompson, O. O. Mykhaylyk and S. P. Armes, *Chemical Science*, 2015, **6**, 6179.
55. P. Yang, L. P. D. Ratcliffe and S. P. Armes, *Macromolecules*, 2013, **46**, 8545.
56. A. Blanazs, R. Verber, O. O. Mykhaylyk, A. J. Ryan, J. Z. Heath, C. W. Douglas and S. P. Armes, *Journal of the American Chemical Society*, 2012, **134**, 9741.
57. R. Verber, A. Blanazs and S. P. Armes, *Soft Matter*, 2012, **8**, 9915.
58. K. A. Simon, N. J. Warren, B. Mosadegh, M. R. Mohammady, G. M. Whitesides and S. P. Armes, *Biomacromolecules*, 2015, **16**, 3952.
59. K. L. Thompson, C. J. Mable, A. Cockram, N. J. Warren, V. J. Cunningham, E. R. Jones, R. Verber and S. P. Armes, *Soft Matter*, 2014, **10**, 8615.

60. I. Canton, N. J. Warren, A. Chahal, K. Amps, A. Wood, R. Weightman, E. Wang, H. Moore and S. P. Armes, *ACS Central Science*, 2016, **2**, 65.
61. D. E. Mitchell, J. R. Lovett, S. P. Armes and M. I. Gibson, *Angewandte Chemie International Edition*, 2016, **55**, 2801.
62. J. R. Lovett, N. J. Warren, S. P. Armes, M. J. Smallridge and R. B. Cracknell, *Macromolecules*, 2016, **49**, 1016.
63. J. R. Lovett, N. J. Warren, L. P. D. Ratcliffe, M. K. Kocik and S. P. Armes, *Angewandte Chemie International Edition*, 2015, **54**, 1279.
64. N. J. W. Penfold, J. R. Lovett, P. Verstraete, J. Smets and S. P. Armes, *Polymer Chemistry*, 2017, **8**, 272.
65. N. J. W. Penfold, J. R. Lovett, N. J. Warren, P. Verstraete, J. Smets and S. P. Armes, *Polymer Chemistry*, 2016, **7**, 79.
66. Y. Pei, L. Thurairajah, O. R. Sugita and A. B. Lowe, *Macromolecules*, 2015, **48**, 236.
67. L. A. Fielding, J. A. Lane, M. J. Derry, O. O. Mykhaylyk and S. P. Armes, *Journal of the American Chemical Society*, 2014, **136**, 5790.
68. V. Bütün, A. B. Lowe, N. C. Billingham and S. P. Armes, *Journal of the American Chemical Society*, 1999, **121**, 4288.
69. R. K. O'Reilly, M. J. Joralemon, C. J. Hawker and K. L. Wooley, *Journal of Polymer Science Part A: Polymer Chemistry*, 2006, **44**, 5203.
70. A. Guo, G. Liu and J. Tao, *Macromolecules*, 1996, **29**, 2487.
71. P. Chambon, A. Blanazs, G. Battaglia and S. P. Armes, *Langmuir*, 2012, **28**, 1196.
72. M. J. Joralemon, R. K. O'Reilly, C. J. Hawker and K. L. Wooley, *Journal of the American Chemical Society*, 2005, **127**, 16892.
73. Q. Zhang, E. E. Remsen and K. L. Wooley, *Journal of the American Chemical Society*, 2000, **122**, 3642.
74. S. Liu, J. V. M. Weaver, Y. Tang, N. C. Billingham, S. P. Armes and K. Tribe, *Macromolecules*, 2002, **35**, 6121.
75. J. R. Lovett, L. P. D. Ratcliffe, N. J. Warren, S. P. Armes and B. R. Saunders, *Macromolecules*, 2016, **49**, 2928.
76. S. Sugihara, S. P. Armes, A. Blanazs and A. L. Lewis, *Soft Matter*, 2011, **7**, 10787.
77. A. E. Smith, X. Xu, T. U. Abell, S. E. Kirkland, R. M. Hensarling and C. L. McCormick, *Macromolecules*, 2009, **42**, 2958.
78. W. Shen, Y. Chang, G. Liu, H. Wang, A. Cao and Z. An, *Macromolecules*, 2011, **44**, 2524.
79. M. Semsarilar, V. Ladmiral, A. Blanazs and S. P. Armes, *Langmuir*, 2013, **29**, 7416.
80. M. Semsarilar, V. Ladmiral, A. Blanazs and S. P. Armes, *Langmuir*, 2012, **28**, 914.
81. S. A. Buckingham, C. J. Garvey and G. G. Warr, *Journal of Physical Chemistry*, 1993, **97**, 10236.
82. P. Ekwall, L. Mandell and P. Solyom, *Journal of Colloid and Interface Science*, 1971, **35**, 519.
83. N. L. McFarlane, N. J. Wagner, E. W. Kaler and M. L. Lynch, *Langmuir*, 2010, **26**, 13823.
84. F. Lafuma, K. Wong and B. Cabane, *Journal of Colloid and Interface Science*, 1991, **143**, 9.
85. F. Mabire, R. Audebert and C. Quivoron, *Journal of Colloid and Interface Science*, 1984, **97**, 120.
86. A. Blanazs, J. Madsen, G. Battaglia, A. J. Ryan and S. P. Armes, *Journal of the American Chemical Society*, 2011, **133**, 16581.

Chapter 5

Layer-by-Layer Self-Assembly of Charged Block Copolymer Worms onto Planar Surfaces

5.1 Introduction

Following seminal work by Decher and co-workers,[1-3] layer-by-layer (L-b-L) deposition of oppositely-charged polyelectrolytes has become an increasingly popular technique because it enables the convenient preparation of functional multilayers at planar surfaces or colloidal interfaces under exceptionally mild conditions (e.g. aqueous solution, neutral pH and ambient temperature).[4-8] In one embodiment, it simply involves alternately immersing the desired substrate into aqueous solutions of anionic and cationic polyelectrolytes, with intermediate washing steps (see Scheme 5.1).[9]

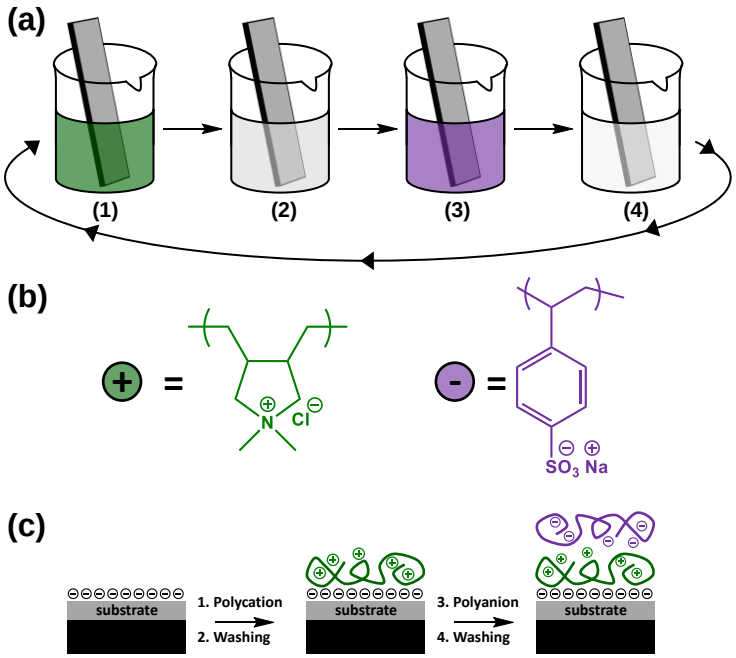

Scheme 5.1 (a) Schematic representation of the layer-by-layer deposition protocol used to prepare polyelectrolyte multilayers on a planar substrate. In this cartoon, the green beaker (1) represents an aqueous solution of cationic polyelectrolyte, beakers (2) and (4) indicate washing steps and the purple beaker (3) represents an aqueous solution of anionic polyelectrolyte. (b) Chemical structures of two commonly used polyelectrolytes: cationic poly(diallyldimethylammonium chloride) and anionic poly(sodium 4-styrene sulfonate).[4] (c) Schematic cartoon depicting the alternate deposition of these two polyelectrolytes onto an anionic substrate to build up polyelectrolyte bilayers (and, by extension, multilayers).

According to Bertrand *et al.*,[5] adsorption of a polyelectrolyte onto an oppositely-charged surface is driven by the gain in entropy as a result of release of small molecule counter-ions (e.g. Na^+ or Cl^- for the two polyelectrolytes shown in Scheme 5.1). Particularly strong adsorption is achieved in the absence of salt, which otherwise can screen the electrostatic interactions. Under such conditions, the adsorbed charged chains adopt a relatively flat conformation at the surface and the adsorbed amount, Γ, is relatively low (typically $\Gamma \sim 0.1 - 0.5$ mg m^{-2}). A wide range of thin films comprising polyelectrolyte multilayers (PEMs) have been prepared on planar substrates,[10-15] including antimicrobial surfaces.[16] However, the design of PEMs is not just restricted to polyelectrolytes. In principle, any charged species can be incorporated into a PEM. For instance, composite PEMs have been prepared by using polyelectrolytes in combination with oppositely-charged inorganic colloids[17-20] or biologically-active species such as enzymes,[21] DNA,[22-24] viruses[25, 26] or proteins.[27-29] Furthermore, the L-b-L protocol has been extended from flat surfaces to colloidal substrates[30-34] and even human red blood cells.[35, 36] PEM-modified surfaces have been evaluated for biomedical applications[9, 37, 38] but also for corrosion protection[39] or for the preparation of electrically conductive films. [40]

Of particular relevance to this thesis is the construction of composite PEMs comprising block copolymer micelles[41-43] and vesicles,[32] which have significantly larger dimensions than soluble polyelectrolytes. The literature also contains a few examples of composite PEMs comprising highly anisotropic particles such as cellulose nanocrystals,[44-47] microfibrillated cellulose[48] or mixtures of cellulose nanocrystals and single-walled carbon nanotubes.[49] As demonstrated within this thesis, RAFT-mediated PISA[50] offers a robust strategy for the rational design of highly anisotropic cationic diblock copolymer worms. Such vermicious particles are typically rather polydisperse in length (although Figg *et al.* have recently claimed to achieve better control over this parameter[51]) but have relatively well-defined worm widths (≈ 20 – 40 nm).

However, according to Semsarilar and co-workers, accessing highly charged worms directly in water can be problematic, because strong electrostatic repulsion between neighbouring polyelectrolytic stabiliser chains usually limits the copolymer morphology to kinetically-trapped spheres.[52, 53] As demonstrated in Chapter 4, diluting such lateral electrostatic interactions by incorporating a suitable non-ionic stabiliser can enable convenient access to either cationic or anionic diblock copolymer worms directly in the form of concentrated aqueous dispersions *via* aqueous PISA.[52-56] In principle, this should enable investigation of the L-b-L adsorption of oppositely-charged worms onto planar surfaces. It is well-known that polyelectrolyte chains behave as rigid rods in salt-free solutions.[57, 58] Hence, highly charged block copolymer worms should mimic the behaviour of individual polyelectrolyte chains in terms of their L-b-L behaviour. However, unlike molecularly-dissolved polyelectrolytes, it should be possible to image each layer of adsorbed worms *via* electron microscopy.

5.2 Experimental

5.2.1 Materials

[2-(Methacryloyloxy)ethyl] trimethylammonium chloride (QDMA, 80% w/w aqueous solution), monomethoxy poly(ethylene oxide) methyl ether (PEO, DP_n = 113), glycidyl methacrylate (GlyMA, 97%), potassium 3-sulfopropyl methacrylate (KSPMA, 98%), benzyl methacrylate (96%) *N*,*N*′-dicyclohexylcarbodiimide (DCC, 99%) and hydrogen peroxide (30% w/w aqueous solution) were purchased from Sigma Aldrich (UK) and used as received. 2-Hydroxypropyl methacrylate (HPMA; 97%), 3-mercaptopropyltriethoxysilane (MPTES, 95%), 4-(dimethylamino)pyridine (DMAP, 99%) and 4,4′-azobis(4-cyanovaleric acid) (ACVA, 98%) were purchased from Alfa Aesar (UK) and used as received. VA-044 was purchased from Wako Chemicals Ltd. Deuterated methanol (CD_3OD; D, 99.8%) and dichloromethane (CD_2Cl_2; D, 99.9%) were purchased from Cambridge Isotopes Laboratories Ltd. Dry dichloromethane was

obtained from an in-house Grubbs solvent purification system. All other solvents were purchased from either VWR International or Sigma Aldrich and were HPLC-grade quality. Deionised water was obtained from an Elgastat Option 3A water purification unit with a resistivity of 15 MΩ cm. Silicon wafers (Test grade, P(boron), 1-10 Ω cm) were purchased from PI-KEM and cleaned before use (see below).

5.2.2 Synthesis of Poly(ethylene oxide)-PETTC Macro-CTA

All glassware was dried in a 150 °C oven overnight and then flame-dried under vacuum prior to use. PETTC was synthesised as described in Chapter 2. A 1 L two-neck round-bottomed flask was charged with a magnetic stirrer bar, poly(ethylene oxide) monomethyl ether (PEO; M_n = 5000 g mol^{-1}, 39.9 g, 7.98 mmol) and toluene (ca. 800 mL) and this solution was subjected to azeotropic distillation under a stream of dry nitrogen to remove approximately 500 mL toluene. The flask was cooled to ≈ 0 °C prior to addition of anhydrous dichloromethane (ca. 300 mL) until the solution became clear. A 50 mL round-bottomed flask was charged with DMAP (97.5 mg, 0.789 mmol), PETTC (4.07 g, 12.0 mmol) and anhydrous dichloromethane (ca. 40 mL) then transferred into the PEO solution *via* cannula under a nitrogen atmosphere. A third 100 mL round-bottomed flask was charged with DCC (12.5 g, 60.6 mmol) and anhydrous dichloromethane (ca. 30 mL) then transferred into the reaction solution *via* cannula under a nitrogen atmosphere. The reaction solution was warmed to 20 °C, stirred for 20 h and then filtered to remove the insoluble dicyclohexylurea by-product. After concentrating the yellow solution *via* rotary evaporation under vacuum, the PEO_{113}-PETTC product was precipitated into excess diethyl ether (2 L), then dissolved in a minimum amount of dichloromethane (ca. 50 mL). This precipitation protocol was repeated a further three times and then the purified PEO_{113}-PETTC was dried in a vacuum oven at 30 °C (40.4 g, 95% yield). ^{1}H NMR studies indicated a mean degree of esterification of 95%. THF GPC studies indicated an

M_n of 5,500 g mol^{-1} and an M_w / M_n of 1.05 (vs a series of near-monodisperse PEO calibration standards).

5.2.3 RAFT Aqueous Dispersion Polymerisation of 2-Hydroxypropyl Methacrylate using a PEO_{113} Macro-CTA

A 14 mL vial was charged with a magnetic stirrer bar, HPMA (0.770 g, 5.34 mmol), PEO_{113}-PETTC macro-CTA (0.100 g, 17.79 µmol, target DP_n = 300), VA-044 (1.20 mg, 3.71 µmol, [PEO_{113}-PETTC] / [VA-044] molar ratio = 5.0) and water (7.83 g) to afford a 20% w/w pale yellow aqueous solution. The sealed vial was placed in ice-cold water, degassed with nitrogen for 30 min and then placed in a preheated oil bath set at 50 °C for 3 h. The HPMA polymerisation was quenched by exposure to air and cooling to 20 °C, yielding a free-flowing, milky-white dispersion. ^{1}H NMR studies indicated more than 99% HPMA conversion. THF GPC analysis indicated an M_n of 53,700 g mol^{-1} and a M_w / M_n of 1.21, expressed against a series of near-monodisperse poly(methyl methacrylate) calibration standards.

5.2.4 Synthesis of poly([2-(methacryloyloxy)ethyl] trimethylammonium chloride) Macro-CTA by RAFT Aqueous Solution Polymerisation

MPETTC RAFT agent was synthesised as described in Chapter 2. A 250 ml round-bottomed flask was charged with MPETTC (0.3413 g, 0.757 mmol) and ([2-(methacryloyloxy)ethyl] trimethylammonium chloride monomer (QDMA) (32.56 g of the as-supplied 80% aqueous solution, corresponding to 26.05 g QDMA monomer, 125 mmol, target DP_n = 165) and stirred for 10 min. Then 2,2'-azobis[2-(2-imidazolin-2-yl)propane]dihydrochloride (VA-044, 47.4 mg, 0.147 mmol) and water (55.79 g) were added to afford a 30% w/w cloudy-yellow solution. The pH was lowered to 4.0 by careful addition of 1 M HCl, the cloudy solution became transparent and was stirred for a further 5 min. The yellow solution was degassed under N_2 for 30 min while

the flask was immersed in an ice/water slurry. The sealed reaction vessel was immersed in a preheated oil bath set at 44 °C for 70 min. The polymerisation was quenched by exposure to air and cooling to room temperature. The QDMA conversion was calculated to be 75% by ^{1}H NMR. Purification and isolation of the polymer was achieved by precipitation into excess acetonitrile (3 x 500 mL), dissolution into deionised water, removal of residual acetonitrile under vacuum and then freeze-drying from water for 72 h to yield a yellow solid. ^{1}H NMR studies indicated a DP_n of 140 by comparing the integrated aromatic end-group signals at 7.1 – 7.4 ppm to that of the methacrylic backbone at 0.4 – 2.5 ppm, suggesting a RAFT agent efficiency of 87%. Aqueous GPC analysis (pH 2, 0.5 M acetic acid, 0.3 M NaH_2PO_4) of the purified $PQDMA_{140}$ macro-CTA indicated an M_n of 19,200 g mol^{-1} and an M_w / M_n of 1.26 against a series of near-monodisperse PEO calibration standards.

5.2.5 Chain Extension of $PQDMA_{140}$ Macro-CTA *via* RAFT Aqueous Solution Polymerisation of QDMA

A 14 mL vial was charged with a magnetic stirrer bar, QDMA (1.000 g of an 80% w/w aqueous solution, 0.800 g QDMA, 3.85 mmol), $PQDMA_{140}$ (1.000 g, 33.8 µmol, target DP_n = 115), VA-044 (2.20 mg, 7.85 µmol, [$PQDMA_{140}$] / [VA-044] molar ratio = 5.0) and water (2.333 g) to afford a 30% w/w pale yellow solution. The sealed vial was placed in ice-cold water, degassed using nitrogen for 30 min and then placed in a preheated oil bath set at 44 °C for 24 h. The QDMA polymerisation was quenched by exposure to air and cooling to 20 °C. ^{1}H NMR analysis indicated more than 99% QDMA conversion. Aqueous GPC analysis (pH 2, 0.5 M acetic acid, 0.3 M NaH_2PO_4) indicated an M_n of 34.4 kg mol^{-1} and an M_w / M_n of 1.17 against a series of near-monodisperse PEO calibration standards

5.2.6 Synthesis of Poly(potassium 3-sulfopropyl methacrylate) Macro-CTA by RAFT Solution Polymerisation in a Methanol/Water Mixture

PETTC was synthesised as described in Chapter 2. A 50 mL round-bottomed flask was charged with a magnetic stirrer bar, potassium 3-sulfopropyl methacrylate (KSPMA; 9.98 g, 40.4 mmol, target DP_n = 150), PETTC (91.5 mg, 0.270 mmol), ACVA (15.1 mg, 0.054 mmol, [PETTC] / [ACVA] molar ratio = 5.0). Methanol (17.0 g, 21.5 mL) and water (12.0 g) were added to afford a 25% w/w transparent yellow solution, which was then degassed under nitrogen for 30 min while immersing the flask in an ice/water slurry in order to minimise solvent evaporation. The sealed reaction vessel was then immersed in a preheated oil bath set at 70 °C for 3 h. The polymerisation was quenched by exposure to air and cooling to 20 °C, which resulted in the formation of a cloudy solution. ^{1}H NMR studies indicated a KSPMA monomer conversion of 69%. Methanol co-solvent was removed under vacuum using a rotary evaporator to afford a transparent yellow aqueous solution. Purification was achieved by precipitation into excess acetonitrile (250 mL), isolation *via* vacuum filtration, dissolution into a minimum amount of water then precipitated into excess acetonitrile (4 x 250 mL). The isolated purified PKSPMA was dissolved in water, residual acetonitrile was removed under vacuum, and then the aqueous PKSPMA solution was freeze-dried for 48 h to afford a pale yellow powder. ^{1}H NMR studies confirmed the absence of any KSPMA monomer and a DP_n of 111 was calculated by comparing the integrated aromatic end-group signals at 7.2–7.5 ppm with that of the oxymethylene proton signal assigned to the polymerised KSPMA residues at 3.7–4.3 ppm. This suggests a RAFT agent efficiency of 94%. Aqueous GPC analysis (pH 9.8, 0.2 M $NaNO_3$, 0.01 M NaH_2PO_4) of this $PKSPMA_{111}$ macro-CTA indicated an M_n of 19,200 g mol^{-1} and an M_w / M_n of 1.26 against a series of near-monodisperse PEO calibration standards.

5.2.7 Chain Extension of $PKSPMA_{111}$ Macro-CTA by RAFT Aqueous Solution Polymerisation of KSPMA

A 14 mL vial was charged with a magnetic stirrer bar, KSPMA (0.667 g, 2.70 mmol), $PKSPMA_{111}$ macro-CTA (0.3333 g, 12.0 μmol, target DP_n = 224), ACVA (0.70 mg, 2.38 μmol, [$PKSPMA_{111}$] / [ACVA] molar ratio = 5.0) and water (2.333 g) to afford a 30% w/w pale yellow solution. The sealed vial was placed in ice-cold water, degassed under nitrogen for 30 min and then placed in a preheated oil bath set at 70 °C for 24 h. The KSPMA polymerisation was quenched by exposure to air and cooling to 20 °C to afford a viscous, pale yellow solution. ^{1}H NMR studies confirmed more than 99% KSPMA conversion. Aqueous GPC analysis (pH 9.8, 0.2 M $NaNO_3$, 0.01 M NaH_2PO_4) indicated an M_n of 97,800 g mol^{-1} and an M_w / M_n of 1.22 against a series of near-monodisperse PEO calibration standards.

5.2.8 Synthesis of Core Cross-linked Cationic Copolymer Worms by RAFT Aqueous Dispersion Copolymerisation of 2-Hydroxypropyl Methacrylate and Glycidyl Methacrylate

A 14 ml sample vial was charged with a magnetic stirrer bar, $PQDMA_{140}$ macro-CTA (0.0700 g, 2.37 μmol), PEO_{113} macro-CTA (0.1267 g, 22.5 μmol), VA-044 (1.60 mg, 4.94 μmol), HPMA (0.4963 g, 3.42 mmol), GlyMA (0.1223 g, 0.86 mmol) and deionised water (3.2451 g) to afford a 20% w/w aqueous solution. The sealed vial was degassed under nitrogen in an ice-water slurry for 30 min and placed in a preheated oil bath at 50 °C for 4 h. This statistical copolymerisation was quenched by exposure to air followed by cooling to 20 °C. The cationic copolymer worm dispersion was diluted to 5.0 % w/w by adding deionised water and gently stirred for 24 h at 20 °C. Core cross-linking of these cationic worms was achieved at 20 °C by adding (3-mercaptopropyl)triethoxysilane (200 mg, 202 μL, 0.84 mmol, [GlyMA]/[MPTES] molar

ratio = 1.0) with continuous stirring for 48 h. These cross-linked cationic worms were characterised by aqueous electrophoresis, TEM and SEM.

5.2.9 Synthesis of Core Cross-linked Anionic Worms Copolymer Worms by RAFT Aqueous Dispersion Copolymerisation of 2-Hydroxypropyl methacrylate and Glycidyl methacrylate

A 14 ml sample vial was charged with a magnetic stirrer bar, $PKSPMA_{111}$ macro-CTA (0.0605 g, 2.35 µmol), PEO_{113} macro-CTA (0.1200 g, 21.4 µmol), VA-044 (1.50 mg, 4.64 µmol), HPMA (0.5746 g, 3.99 mmol), GlyMA (0.1298 g, 0.91 mmol) and deionised water (3.524 g) to afford a 20 % w/w aqueous solution. The sealed vial was immersed in an ice/water slurry bath and degassed under nitrogen for 30 min, before being placed in a preheated oil bath set at 50 °C for 4 h. The statistical copolymerisation was quenched by exposure to air and cooling to 20 °C. The aqueous copolymer worm dispersion was diluted to 5.0 % w/w using deionised water and gently stirred at 20 °C for 24 h. Core cross-linking of these anionic worms was achieved at 20 °C by addition of 3-mercaptopropyltriethoxysilane (0.2200 g, 222 µL, 0.92 mmol, [GlyMA]/[MPTES] molar ratio = 1.0) with continuous stirring for 48 h. These cross-linked anionic worms were by aqueous electrophoresis, TEM and SEM.

5.2.10 Synthesis of MePETTC-$PGMA_{58}$-$PBzMA_{500}$ Tracer Nanoparticles *via* RAFT Aqueous Emulsion Polymerisation of Benzyl methacrylate

The MePETTC-$PGMA_{58}$ macro-CTA synthesised in Chapter 2 was also used to prepare MePETTC-$PGMA_{58}$-$PBzMA_{500}$ nanoparticles *via* RAFT aqueous emulsion polymerisation of benzyl methacrylate (BzMA). A 50 mL round-bottomed flask was charged with a magnetic stirrer bar, BzMA (2.7500 g, 15.6 mmol), MePETTC-$PGMA_{58}$ macro-CTA (0.3000 g, 31.1 µmol, target DP_n = 500), VA-044 (2.10 mg, 7.70 µmol, [MePETTC-$PGMA_{58}$] / [VA-044]

molar ratio = 4.0) and water (27.50 g, affording a 10% w/w dispersion). The sealed flask was immersed in an ice bath, degassed *via* nitrogen bubbling for 30 min and then placed in a preheated oil bath set at 50 °C for 5 h. ^{1}H NMR analysis was performed in d_7-DMF and a BzMA conversion of 97% was calculated by comparing the integrated residual vinyl monomer signal at 6.3 ppm to the integrated aromatic signals at 7.3 – 7.9 ppm. DMF GPC studies indicated an M_n of 66,600 g mol^{-1} and an M_w / M_n of 1.31 against a series of near-monodisperse PMMA calibration standards, with no evidence for contamination with unreacted macro-CTA. These tracer particles were subsequently used for the determination of the surface zeta potential of silicon wafers.

5.2.11 Layer-by-Layer Deposition Protocol

Silicon wafers were cut into 4 mm x 5 mm rectangles (for surface zeta potential and SEM analysis) or 15 mm x 7 mm (rectangles for ellipsometric measurements) using glass cutter and placed into individual glass vials. Glassware and silicon wafers were cleaned by immersion in a 1:1 ethanol/water mixture with ultrasonication for 30 min, followed by sonication in deionised water for 30 min. Clean wafers were then immersed in acidic piranha solution, consisting of a 3:1 (v/v) mixture of H_2SO_4 and H_2O_2 (30% w/w) for 1 h. [**Warning:** Piranha solution is an extremely strong oxidising agent that heats spontaneously on mixing and is also known to detonate upon contract with organic materials]. After cooling to 20 °C, the wafers were washed ten times with deionised water. The wafers were then immersed in an RCA (Radio Corporation of America) solution (70% deionised water, 15% NH_3, 15% H_2O_2) and boiled for 1 h. Finally, the wafers were rinsed ten times with deionised water and placed in a 120 °C oven to dry overnight. Aqueous dispersions of either cationic or anionic worms were diluted to the desired copolymer concentration (typically 1.0 % w/w) at pH 7, and then a clean silicon wafer was dipped into such worm dispersions for the desired time-period at 20 °C. Afterwards, worm-

coated wafers were extensively washed with deionised water to remove excess worms and then dried using a nitrogen stream before being characterised by SEM, ellipsometry and surface zeta potential measurements.

5.2.12 Copolymer Characterisation

Aqueous Gel Permeation Chromatography

Aqueous GPC analysis of 0.50 % w/w copolymer solutions was performed using either an acidic or basic eluent. The cationic $PQDMA_{140}$ macro-CTA (and also the $PQDMA_{240}$ homopolymer obtaining from the self-blocking experiment) were analysed using an acidic aqueous buffer containing 0.3 M NaH_2PO_4, 0.5 M acetic acid and adjusted to pH 2 with concentrated HCl. The anionic $PKSPMA_{111}$ macro-CTA (and also the $PKSPMA_{335}$ homopolymer obtained after the self-blocking experiment) were analysed using a basic aqueous buffer containing 0.2 M $NaNO_3$ and 0.01 M NaH_2PO_4 and adjusted to pH 9.8 using NaOH. In both cases the GPC set-up comprised an Agilent 1260 Infinity series degasser and pump, an 8 µm Agilent PL Aquagel-OH 40 column and an 8 µm Agilent PL Aquagel-OH 30 column connected in series to a refractive index detector. The flow rate was 1.0 mL min^{-1} and the column oven was set at 30 °C. Calibration was achieved using a series of eight near-monodisperse poly(ethylene glycol) standards with M_p values ranging from 1,960 g mol^{-1} to 969,000 g mol^{-1}.

THF Gel Permeation Chromatography

The THF GPC set-up comprised an Agilent 1260 Infinity series degasser and pump, two Agilent PLgel 5 µn MIXED-C columns in series, a VWD detector operating at 298 nm and a refractive index detector. THF eluent contained triethylamine (2.0% w/w), butylhydroxytoluene (0.05% w/v). This set-up was operating at a flow rate of 1.0 mL min^{-1} and 30 °C. A series of either

seven poly(ethylene glycol) standards ranging from 238 g mol^{-1} to 86,200 g mol^{-1} or twelve near-monodisperse poly(methyl methacrylate) standards ranging from 800 g mol^{-1} to 2,200,000 g mol^{-1} were used for calibration.

Scanning Electron Microscopy

Both bare silicon wafers and worm-coated wafers were mounted onto SEM stubs using electrically conductive adhesive pads. The stubs were gold-coated for 2 min prior to analysis. SEM studies were performed using an Inspect F microscope operating at 5 kV.

DMF Gel Permeation Chromatography

Aqueous copolymer dispersions were freeze-dried overnight to obtain pale yellow powders. 0.50% w/w copolymer solutions were prepared in HPLC-grade DMF containing 10 mM LiBr and DMSO (1.0 % v/v) was used as a flow rate marker. GPC studies were conducted at 60 °C using a flow rate of 1.0 mL min^{-1}. The GPC set-up comprised an Agilent 1260 Infinity series degasser and pump, a Agilent PL-gel guard column, two Agilent PL-gel Mixed-C columns and a refractive index detector. Sixteen near-monodisperse poly(methyl methacrylate) standards ranging from M_p = 645 g mol^{-1} to 2,480,000 g mol^{-1} were used for calibration.

Transmission Electron Microscopy

Copper/palladium grids were surface-coated in-house to produce a thin film of amorphous carbon and then plasma glow-discharged for 20 seconds to give a hydrophilic surface. A 10 μL droplet of the freshly-prepared 0.1% w/v aqueous copolymer dispersion was placed on the hydrophilic grid for 15 seconds, blotted to remove excess sample and then negatively stained with uranyl formate solution (0.75% w/v; 10 μL) for a further 15 seconds. Excess stain was removed by blotting and each grid was carefully dried with a vacuum house. TEM studies were

performed using a FEI Tecnai Spirit 2 microscope equipped with an Orius SC1000B camera operating at 80 kV.

^{1}H NMR Spectroscopy

All NMR spectra were recorded in either CD_3OD or CD_2Cl_2 at 298 K using a 400 MHz Bruker AV3-HD spectrometer. Sixty-four scans were averaged per spectrum. All chemical shifts are reported in ppm (δ).

Ellipsometry

Dry ellipsometry measurements were performed on bare silicon wafers or worm-coated silicon wafers in air and at room temperature using a J. A. Woollman M2000 V ellipsometer at a fixed angle of incidence of 70° to the sample surface normal. Measurements were conducted from λ = 370 – 1000 nm and obtained ellipsometry parameters Ψ and Δ were fitted to a three layer model consisting of a silicon substrate, a native oxide layer and Cauchy layer (equation 5.1). Data analysis and modelling were performed using Woollam CompleteEase software which fits values of Ψ and Δ calculated from this three-layer model to the experimentally measured values.

$$n(\lambda) = A_n + \frac{B_n}{\lambda^2} + \frac{C_n}{\lambda^4} \qquad \textbf{5.1}$$

Dynamic Light Scattering

All DLS measurements were recorded at a copolymer concentration of 0.1% w/w and at 20 °C using a Malvern Instruments Zetasizer Nano series instrument equipped with a 4 mW 633 nm He−Ne laser and an avalanche photodiode. Scattered light was detected at 173°. Aqueous electrophoresis measurements were conducted in the presence of 1 mM KCl. The dispersion pH

was adjusted as required with either 1 M or 0.1 M HCl or KOH. Zeta potentials were calculated using the Henry equation using the Smoluchowski approximation.

Laser Doppler Electrophoresis (Surface Zeta Potential) Measurements

Surface zeta potentials were calculated for both bare and worm-coated silicon wafers *via* laser Doppler electrophoresis measurements using a Malvern Surface Zeta Potential ZEN1020 cell. Clean or worm-coated silicon wafers (4 mm x 5 mm) were attached to the sample holder using ethyl cyanoacrylate 'superglue' (Gorilla Super Glue, Gorilla Glue Europe A/S) and the wafer-loaded sample holder was placed into a Malvern ZEN 1020 dip cell. The Zetasizer was set to detect forward-scattered light at an angle of 13° with the attenuator adjusted to position eleven (100% laser transmission). The voltage was selected to be automatic (typically 10 V was selected). The dip cell was placed in a cuvette containing 1.0 mL of 0.0025 % w/w MePETTC-$PGMA_{58}$-$PBzMA_{500}$ spherical nanoparticles in the presence of 1 mM KCl at 25 °C. This nanoparticle concentration was selected to give an optimal derived count rate of 500 kcps when the attenuator was set to 11.[59] The instrument was set up to perform five slow-field reversal measurements at four distances from the sample surface (125 μm, 250 μm, 375 μm and 500 μm), with each measurement comprising 15 sub-runs and 1 min between measurements. Lastly, three fast-field reversal measurements were performed at a distance of 1000 μm from the sample surface to calculate the electro-osmotic mobility of the tracer nanoparticles. In this case, each measurement consisted of 100 sub-runs with an interval of 20 s between each measurement. Zeta potentials were calculated using the Henry equation using the Smoluchowski approximation.

5.3 Results and Discussion

5.3.1 Synthesis of Macromolecular Chain Transfer Agents

The use of PEO macro-CTAs as stabiliser blocks for PISA syntheses has dramatically grown over the past few years.[60-67] However, the PEO_{113} macro-CTA synthesis *via* amidation (as described in Chapter 4) is undesirable because of its relatively long reaction time. In the present Chapter, a new PEO_{113} macro-CTA is prepared *via* esterification of monomethoxy poly(ethylene oxide) methyl ether using PETTC (see Scheme 5.2), as described by Tan and co-workers.[61] This synthesis route reduces the total synthesis time from approximately two weeks to just three days.

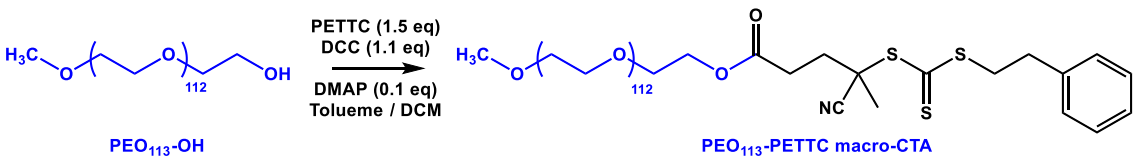

Scheme 5.2. Esterification of monomethoxy poly(ethylene oxide) methyl ether using PETTC to produce the PEO_{113}-PETTC macro-CTA.

^{1}H NMR analysis indicated a mean degree of esterification of 95% by comparing the integrated signals associated with the aromatic end-groups at 7.2–7.5 ppm with the PEO backbone signals at 3.1 – 4.6 ppm (Figure 5.1a). THF GPC analysis indicated an M_n of 5,500 g mol^{-1} and an M_w / M_n of 1.05 against a series of near-monodisperse PEO calibration standards (Figure 5.1b). A $PQDMA_{140}$ macro-CTA was synthesised by RAFT aqueous solution polymerisation using MPETTC as the RAFT agent (see Figure 4.3 in Chapter 4). ^{1}H NMR was used to calculate a DP_n of 140 by comparing the integrated aromatic signals at 7.2 – 7.5 ppm against those assigned

to the methacrylic backbone at 0.5 – 2.5 ppm. Aqueous GPC studies Figure 5.2 indicated an M_n of 19,200 g mol^{-1} and an M_w / M_n of 1.26 (expressed relative to PEO calibration standards).

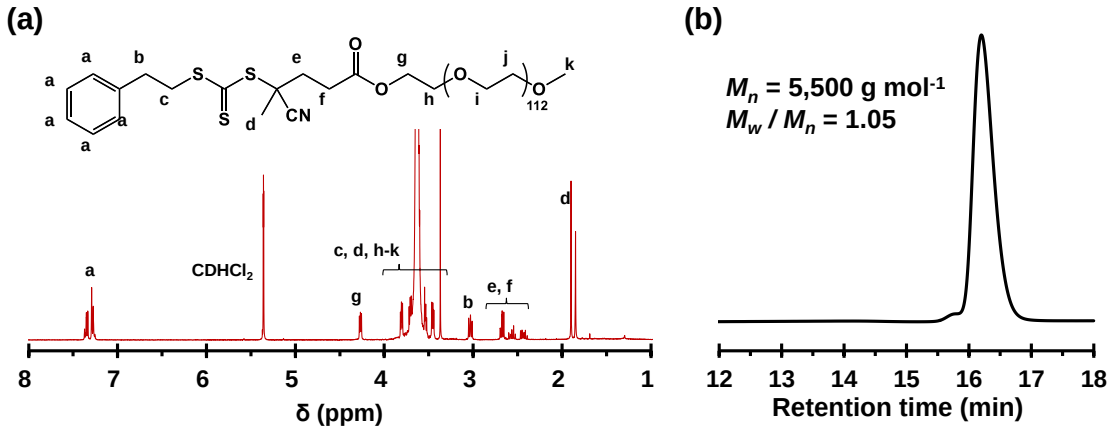

Figure 5.1 (a) Assigned ^{1}H NMR spectrum recorded in CD_2Cl_2 and (b) THF GPC chromatogram obtained for PEO_{113} macro-CTA. Molecular weight data are expressed relative to PEO standards.

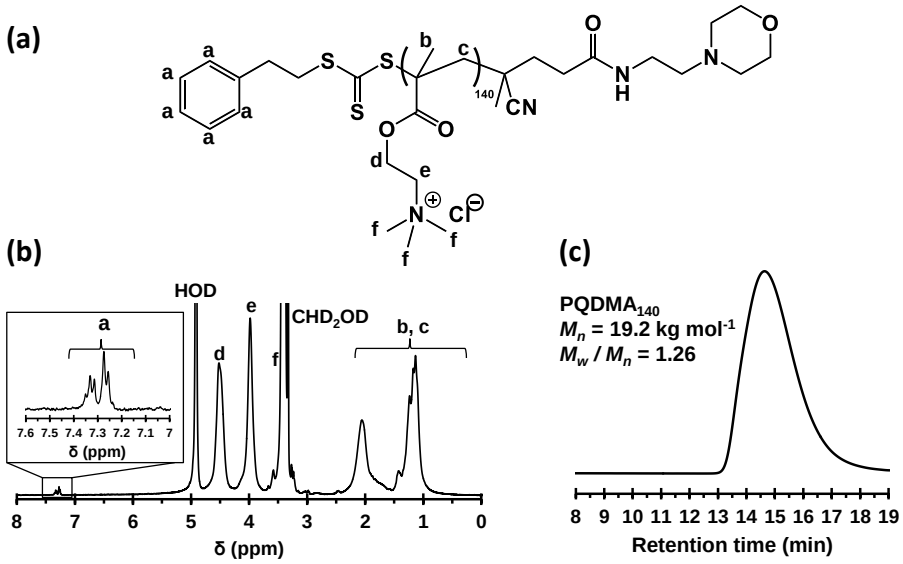

Figure 5.2 (a) Chemical structure of the cationic $PQDMA_{140}$ macro-CTA used in this study. (b) Partially assigned ^{1}H NMR spectrum recorded in CD_3OD and (c) corresponding aqueous GPC chromatogram obtained at pH 2 (data expressed relative to PEO calibration standards).

KSPMA was selected as the anionic monomer because Semsarilar *et al.*[52] had previously reported the preparation of highly anionic PKSPMA-based block copolymer nanoparticles *via* RAFT aqueous dispersion polymerisation of HPMA. Accordingly, a PKSPMA macro-CTA was synthesised by RAFT solution polymerisation in a 13:7 v/v methanol/water mixture using PETTC as a RAFT agent (see Scheme 5.3). A 13:7 v/v methanol/water solvent composition was selected to ensure full solubility of all reagents at both 20 °C and 70 °C. A DP_n of 150 was targeted using a [PETTC] / [ACVA] molar ratio of 5.0.

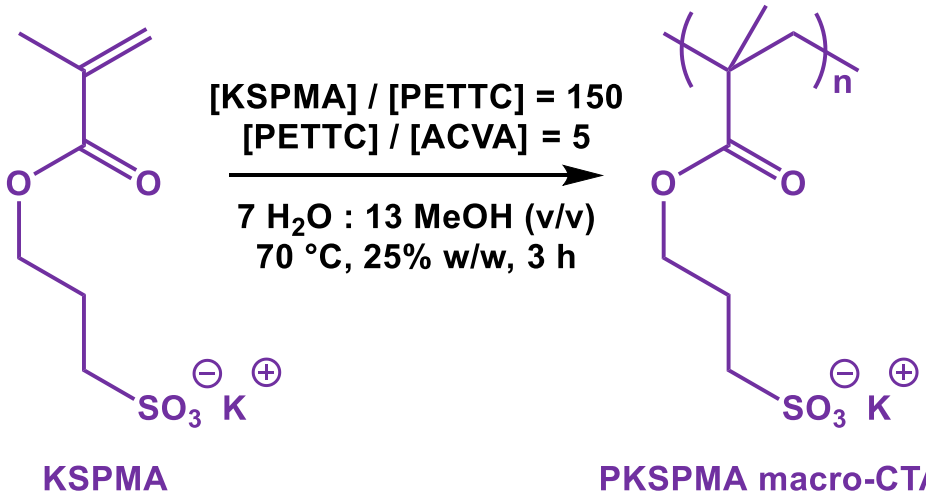

Scheme 5.3 Reaction scheme for the synthesis of a poly(potassium 3-sulfopropyl methacrylate) macro-CTA by RAFT solution polymerisation of KSPMA in a 13:7 v/v methanol / water mixture at 70 °C targeting a DP_n of 150.

^{1}H NMR studies confirmed that a KSPMA conversion of 69% was achieved after heating for 3 h at 70 °C. The purified PKSPMA macro-CTA had a DP_n of 111, as judged by comparing the integrated aromatic signals at 7.2 – 7.5 ppm to that of the oxymethylene proton signal at 4.0 – 4.2 ppm (see Figure 5.3a and b). Aqueous GPC studies at pH 9.8 indicated an M_n of 28,700 g mol^{-1} and an M_w / M_n of 1.15 relative to PEO standards (see Figure 5.3c).

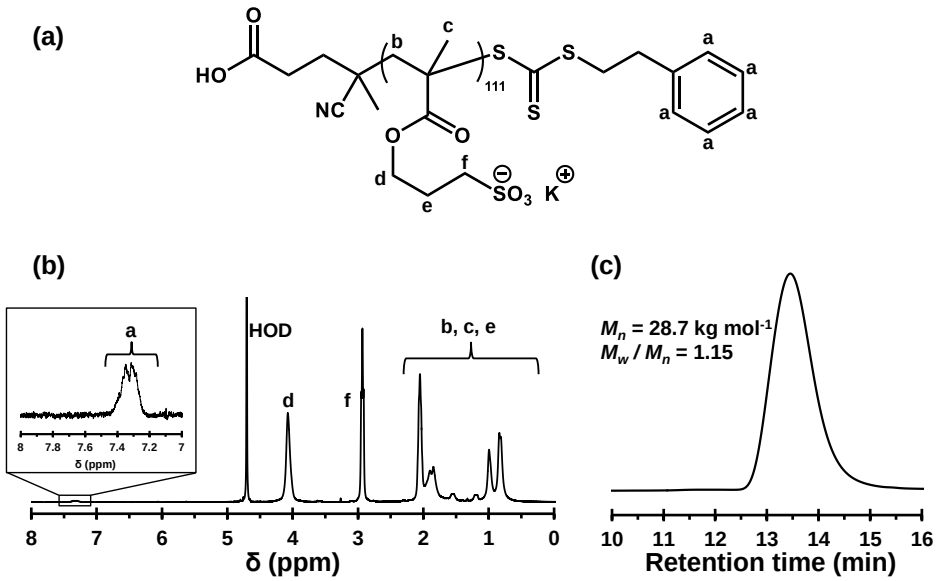

Figure 5.3 (a) Chemical structure of the $PKSPMA_{111}$ macro-CTA used in this study. (b) Partially assigned ^1H NMR spectrum recorded in D_2O and (c) corresponding aqueous GPC chromatogram obtained at pH 9.8 (data expressed relative to PEO calibration standards).

Unfortunately, there is no common GPC eluent that dissolves all four of the constituent (co)polymers that make up the polyelectrolytic worms reported in this Chapter. In view of this problem, experiments were performed to investigate the living character and blocking efficiency of the three macro-CTAs. Thus the PEO_{113} macro-CTA was chain-extended with 300 units of HPMA *via* RAFT aqueous dispersion polymerisation at 10 % w/w solids to yield diblock copolymer vesicles.[64] The final HPMA conversion was determined to be more than 99% by ^1H NMR spectroscopy. THF GPC analysis indicated an M_n of 53,700 g mol^{-1}, an M_w / M_n of 1.21 and a relatively high blocking efficiency for the PEO_{113} macro-CTA (see Figure 5.4a). The cationic $PQDMA_{140}$ and anionic $PKSPMA_{111}$ macro-CTAs were subjected to self-blocking experiments *via* RAFT aqueous solution polymerisation of either QDMA or KSPMA respectively to yield well-defined $PQDMA_{255}$ and $PKSPMA_{335}$ homopolymers at 30% w/w solids. In both cases, final monomer conversions exceeded 99% as judged by ^1H NMR spectroscopy and aqueous GPC analyses indicated high blocking efficiencies in each case.

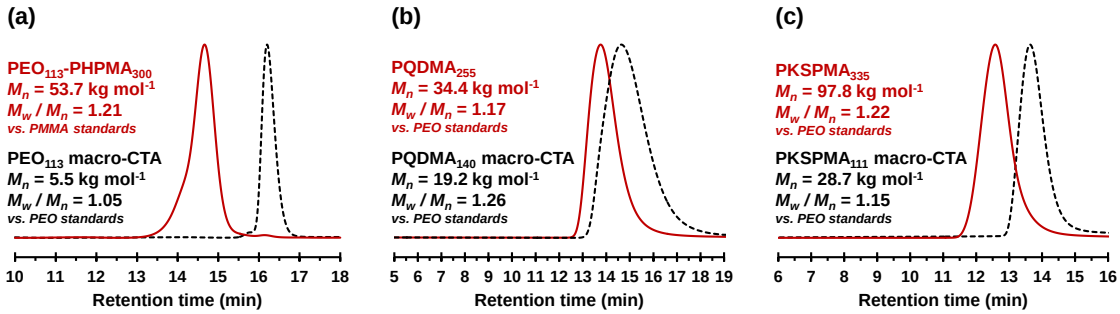

Figure 5.4 (a) THF GPC chromatograms (vs. PMMA standards) obtained for a PEO_{113}-$PHPMA_{300}$ diblock copolymer prepared *via* RAFT aqueous dispersion polymerisation of HPMA and the corresponding PEO_{113} macro-CTA precursor. (b) and (c) Aqueous GPC chromatograms (vs. PEO standards) obtained for $PQDMA_{225}$ and $PKSPMA_{335}$ homopolymers prepared by self-blocking experiments *via* RAFT aqueous solution polymerisation using $PQDMA_{140}$ or $PKSPMA_{111}$ macro-CTAs, respectively.

5.3.2 Synthesis and Characterisation of Core Cross-linked Polyelectrolytic Worms

As described in Chapter 4, core cross-linking of cationic block copolymer worms is essential for retention of the original worm morphology following adsorption onto colloidal silica spheres. Without such covalent stabilisation, the strong torsional forces exerted on the worms by the micrometer-sized silica particles are much greater than the weak hydrophobic forces holding the linear worms together, thus resulting in worm dissociation. In contrast, this Chapter is focused on the layer-by-layer deposition of polyelectrolytic worms onto *planar* silica surfaces. Nevertheless, core cross-linking was considered desirable to maximise the mean persistence length of the charged worms (cf. the 'rigid rod' nature of polyelectrolytes in the absence of any salt),[57, 58] as well as to prevent potential loss of the worm morphology after adsorption. Thus polyelectrolytic block copolymer worms were prepared using similar protocols as those described in Chapter 4: RAFT statistical copolymerisation of HPMA and GlyMA was conducted using a binary mixture of a non-ionic (PEO_{113}) and polyelectrolytic (either $PQDMA_{140}$ or $PKSPMA_{111}$) macro-CTAs, as outlined in Scheme 5.4.

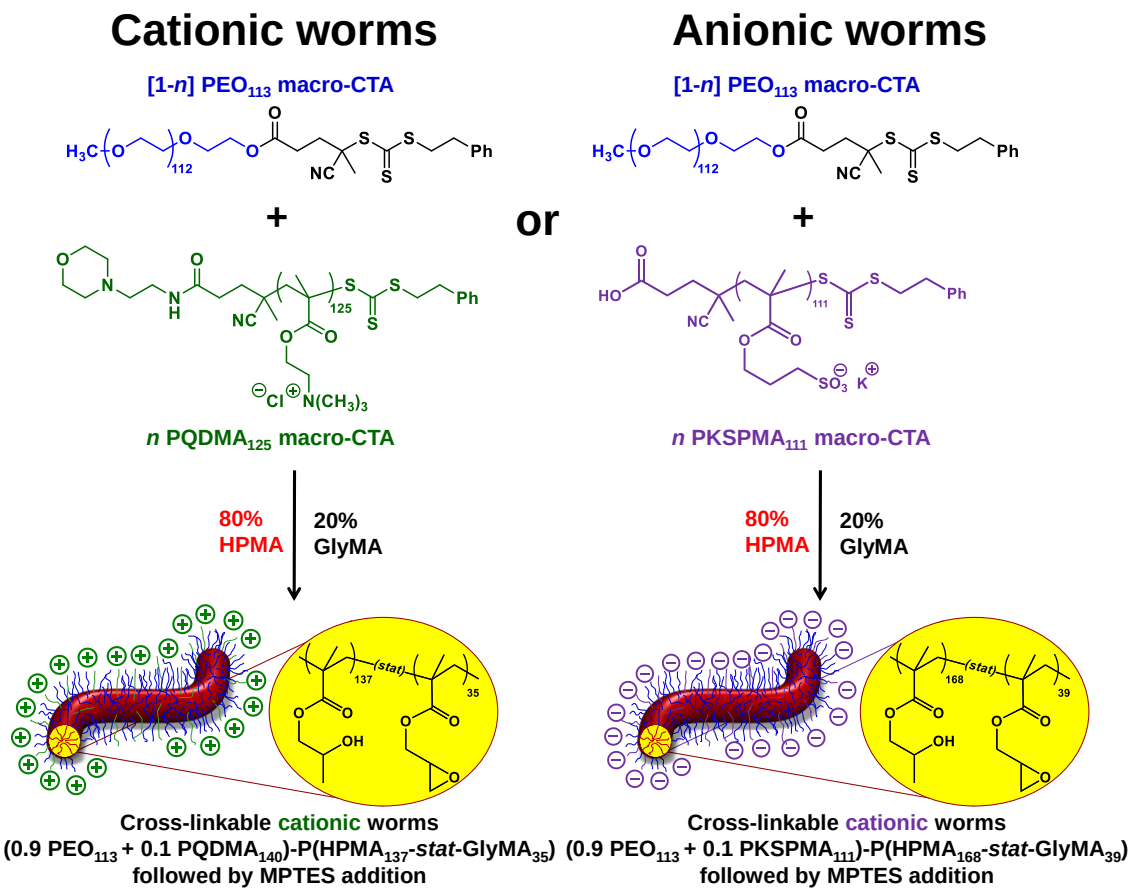

Scheme 5.4 Schematic representation of the synthesis of either cationic or anionic cross-linked block copolymer worms *via* RAFT aqueous copolymerisation of 2-hydroxypropyl methacrylate and glycidyl methacrylate using a binary mixture of PEO_{113} macro-CTA with either a cationic $PQDMA_{140}$ macro-CTA or an anionic $PKSPMA_{111}$ macro-CTA. Here, *n* represents the mol fraction of the polyelectrolyte macro-CTA. For brevity, P, Q and K denote the PEO, PQDMA and PKSPMA stabiliser blocks, respectively and H and Gly refer to the HPMA and GlyMA comonomers within the core-forming blocks.

In both cases the core-forming block comprised 80 mol % HPMA and 20 mol % GlyMA. A series of scouting experiments were conducted to identify the precise diblock copolymer compositions required to access well-defined cationic (0.9 PEO_{113} + 0.1 $PQDMA_{140}$)-P($HPMA_{137}$-*stat*-$GlyMA_{35}$) worms and anionic (0.9 PEO_{113} + 0.1 $PKSPMA_{111}$)-P($HPMA_{168}$-*stat*-$GlyMA_{39}$) worms, respectively. Cross-linking of the worm cores is achieved by ring-

opening of the epoxy groups in the GlyMA residues using 3-mercaptopropyltriethoxysilane (MPTES), as opposed to the APTES reagent used in Chapter 4. This epoxy-thiol reaction occurs with simultaneous hydrolysis/condensation of the pendent triethoxysilane groups with themselves and also with the secondary hydroxyl groups located on neighbouring HPMA residues. The primary amine functionality of APTES is potentially undesirable in this context: secondary amines are formed when this reagent reacts with epoxy groups which could potentially reduce the negative surface charge on the anionic worms. In contrast, epoxy-thiol chemistry only produces neutral species and hence does not confer cationic character. Prior to MPTES addition (using a [GlyMA] / [MPTES] molar ratio of 1.0), the worm gels were diluted to 5.0 % w/w using deionised water. MPTES was then added and the worm dispersions were stirred at 20 °C for 24 h. TEM analysis of the core cross-linked polyelectrolytic nanoparticles was performed to confirm that the original worm morphology was preserved (see Figure 5.5).

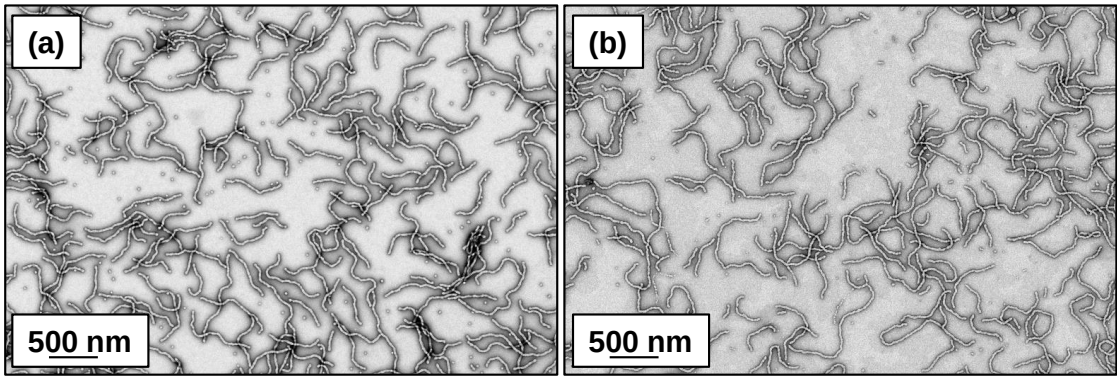

Figure 5.5 Representative TEM images obtained for (a) cationic (0.9 PEO_{113} + 0.1 $PQDMA_{140}$)-P($HPMA_{137}$-*stat*-$GlyMA_{35}$) and (b) anionic (0.9 PEO_{113} + 0.1 $PKSPMA_{111}$)-P($HPMA_{168}$-*stat*-$GlyMA_{39}$) worms after core cross-linking in each case using MPTES.

ImageJ analysis of core cross-linked cationic and anionic worms TEM images indicated a mean thickness of 27 ± 3 nm and 31± 5 nm, respectively. The thickness was calculated from 50 measurements, constituting from five width measurements recorded equally spaced across

the worm length for ten worms. Aqueous electrophoresis studies were conducted on 0.1% w/w aqueous dispersions of core cross-linked polyelectrolytic worms from pH 9.5 to pH 3 in the presence of 1 mM KCl. As expected, the core cross-linked cationic worms exhibited positive zeta potentials of approximately +41 mV across this pH range (see Figure 5.6). Similarly, the core cross-linked anionic worms exhibited a pH-independent zeta potential of around –39 mV (see Figure 5.6).

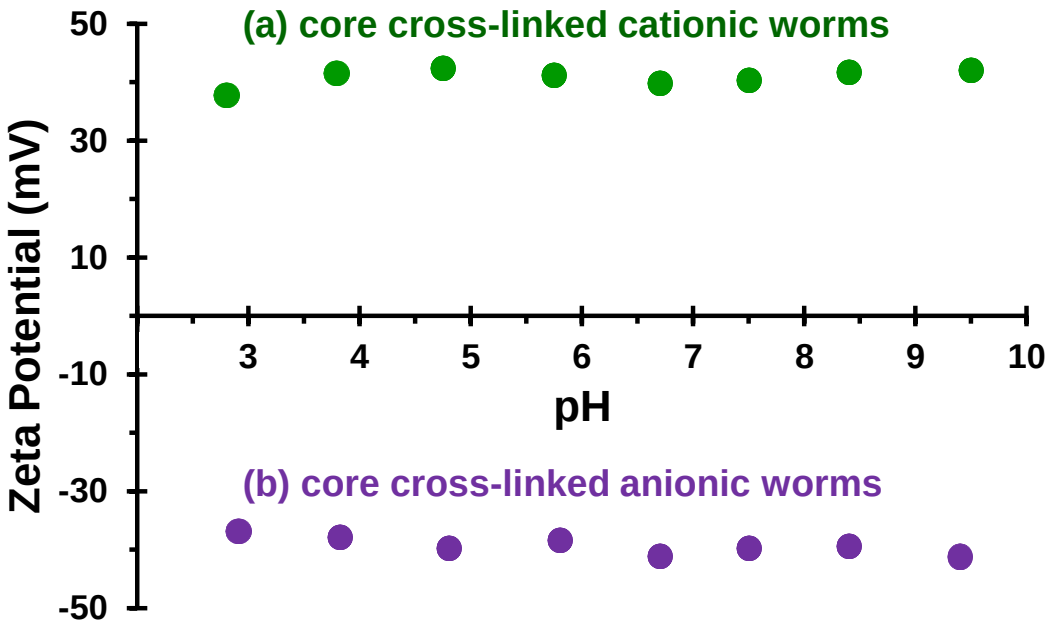

Figure 5.6 Zeta potential *vs.* pH curves constructed for (a) cationic (0.9 PEO_{113} + 0.1 $PQDMA_{140}$)-P($HPMA_{137}$-*stat*-$GlyMA_{35}$) core cross-linked worms and (b) anionic (0.9 PEO_{113} + 0.1 $PKSPMA_{111}$)-P($HPMA_{168}$-*stat*-$GlyMA_{39}$) core cross-linked worms. Zeta potentials were determined at 20 °C for 0.1% w/w copolymer dispersions in the presence of 1 mM KCl. The aqueous dispersion pH was adjusted using 0.1 M or 1 M HCl.

5.3.3 Adsorption of Core Cross-Linked Cationic Worms onto Planar Silicon Wafers

The kinetics of adsorption of cationic cross-linked worms onto anionic planar silicon wafers at pH 5 was investigated. In these experiments, silicon wafers were dipped into a 1.0 % w/w aqueous dispersion of cationic cross-linked worms at an arbitrary pH of pH 5 for various time intervals, washed with deionised water and then dried under a stream of nitrogen gas. SEM images of the dried wafers were obtained to visualise the adsorbed cationic worms on the wafer surface. However, an interesting observation was made in initial experiments: worm coverage was not uniform across the whole wafer. A significantly higher surface coverage was frequently observed along the wafer edge (see Figure 5.7a and b), which in principle might be a drying protocol artefact. However, similar observations were also made when drying the wafers in a 25 °C oven overnight (see Figure 5.7c and 5.7d) without nitrogen blowing. Thus this phenomenon may be related to the so-called 'coffee ring' effect often observed following evaporation of water from an aqueous dispersion of nanoparticles.[68-70] Interestingly, Decher *et al.* reported very similar observations during the alternate adsorption of anionic and cationic polyelectrolytes onto planar silicon wafers.[3] The kinetics of adsorption for cationic cross-linked worms on an anionic silicon wafer was quantified using ImageJ software to analyse SEM images recorded at various time points. Only the central section of each wafer was analysed, thus ignoring any edge effects. Ten SEM images were recorded for each time point at the same magnification (25,000 x), hence the total surface area analysed is approximately 900 μm^2 per time point. Representative SEM images obtained for wafers dipped into a 1.0 % w/w aqueous dispersion of (0.9 PEO_{113} + 0.1 $PQDMA_{140}$)-P($HPMA_{137}$-*stat*-$GlyMA_{35}$) cationic cross-linked worms at pH 5 for various time periods are shown in Figure 5.8. As expected, the cationic cross-linked worms retained their morphology after adsorption onto the silicon wafers.

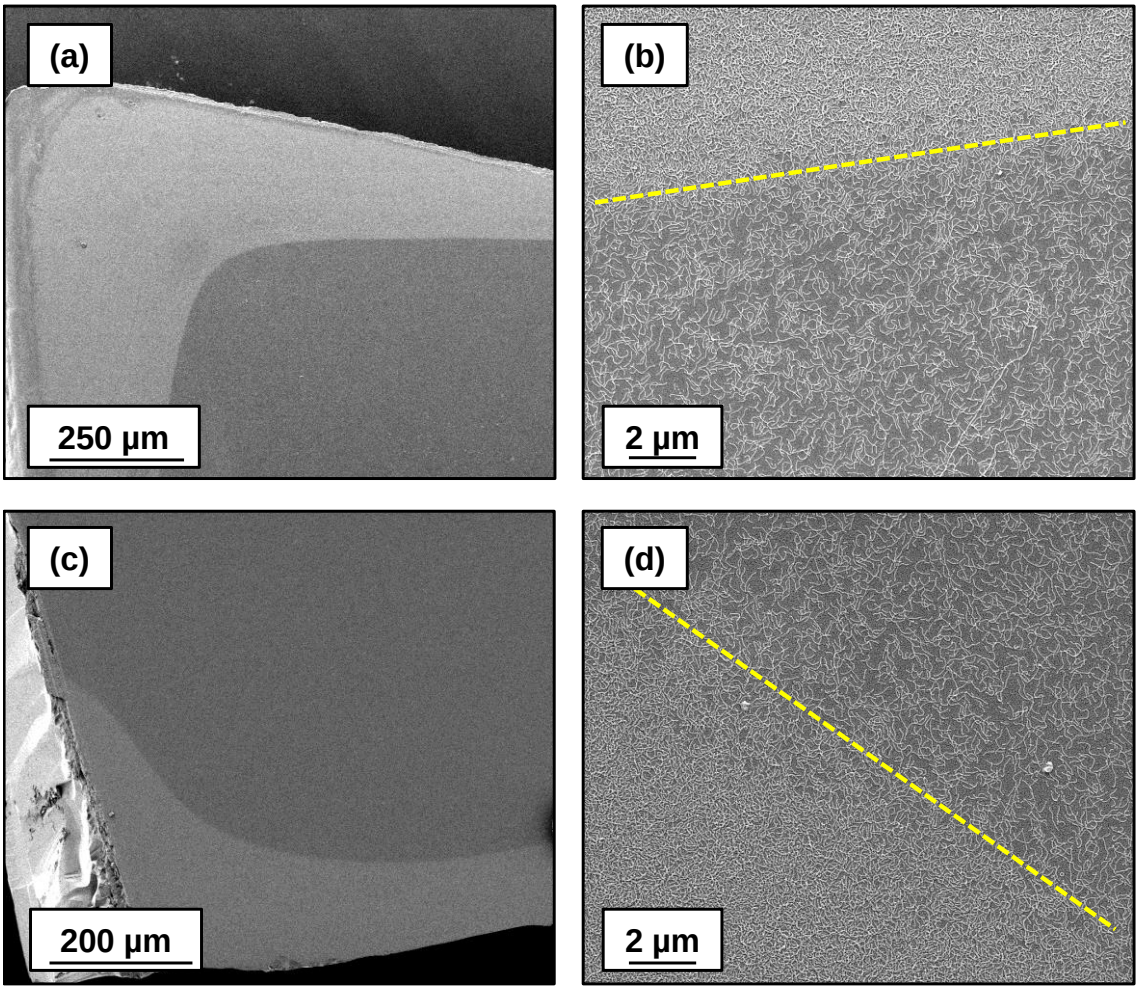

Figure 5.7 Representative SEM images obtained after dipping an anionic planar silicon wafer into a 1.0 % w/w aqueous dispersion of (0.9 PEO_{113} + 0.1 $PQDMA_{140}$)-P($HPMA_{137}$-*stat*-$GlyMA_{35}$) cationic cross-linked worms at pH 5 for 20 min at 20 °C in the absence of any added salt. For (a) and (b), wafers were dried under a nitrogen gas stream. However, for (c) and (d) wafers were dried in a 25 °C oven overnight. The dashed yellow line indicates the well-defined boundary between the densely-covered wafer edges and the less densely-coated central section of the wafer.

The kinetics of electrostatic adsorption of these worms is remarkably fast, with a surface coverage of approximately 16% obtained within just 2 s under the stated conditions (1.0 % w/w copolymer worms at 20 °C). No further increase in worm surface coverage occurs on extending the adsorption time up to 2 min or 10 min (see Figure 5.9 below).

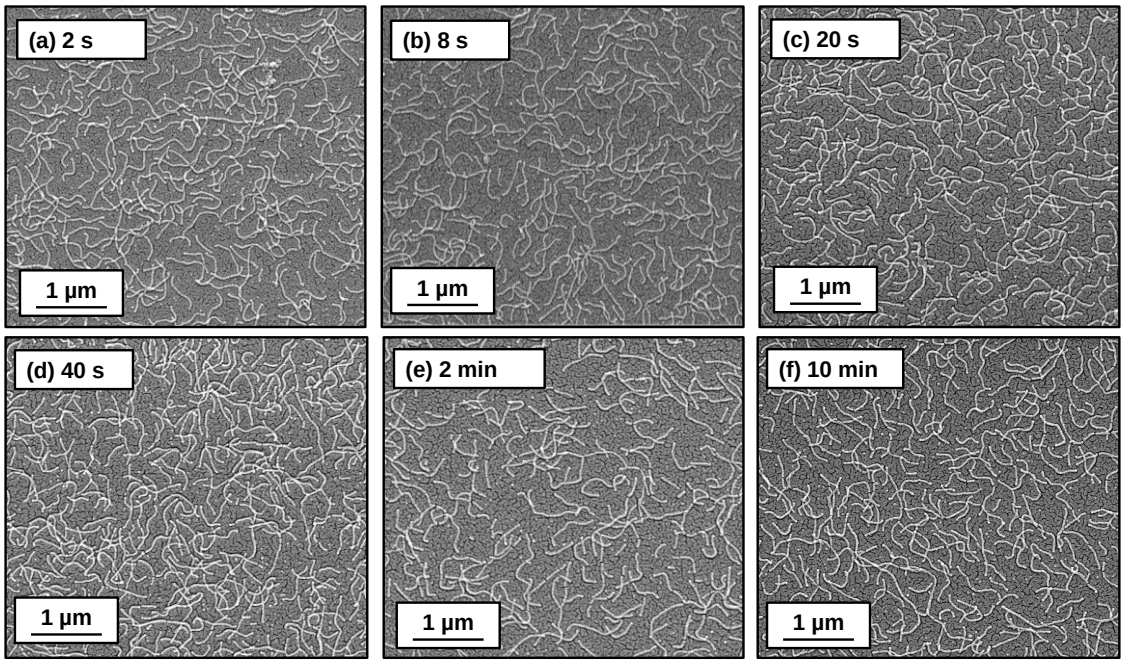

Figure 5.8 Representative SEM images obtained after dipping an anionic planar silicon wafer into a 1.0 % w/w aqueous dispersion of (0.9 PEO_{113} + 0.1 $PQDMA_{140}$)-P($HPMA_{137}$-*stat*-$GlyMA_{35}$) cationic cross-linked worms at pH 5 for (a) 2 s, (b) 8 s, (c) 20 s, (d) 40 s, (e) 2 min and (d) 10 min. Adsorption conditions: pH 5, no added salt, 20 °C.

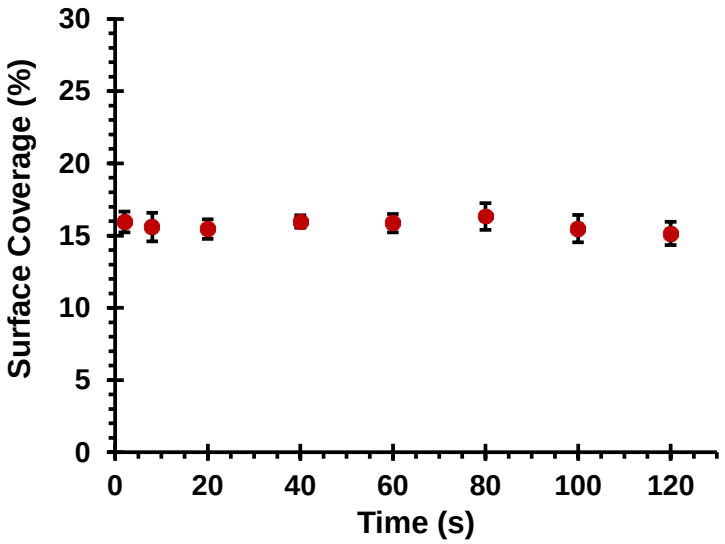

Figure 5.9 Surface coverage vs. adsorption time plot, indicating the remarkably rapid adsorption of a 1.0 % w/w aqueous dispersion of cationic cross-linked worms at pH 5 onto the surface of a clean anionic silicon wafer at 20 °C. Surface coverages were determined using ImageJ software threshold analysis to analyse ten silicon wafers per time point; the total surface area analysed per time point is approximately 900 μm^2.

An important control experiment was performed to demonstrate that the observed rapid worm adsorption was actually the result of electrostatic interactions, rather than merely sedimentation under gravity. A clean silicon wafer (manipulated using tweezers) was immersed into a 1.0% w/w aqueous dispersion of cationic worms at pH 5 for either 20 s or 60 s with its anionic surface facing upside down. SEM analysis of the dried wafers indicated a near-identical surface coverage of approximately 16% for both time periods (see Figure 5.10).

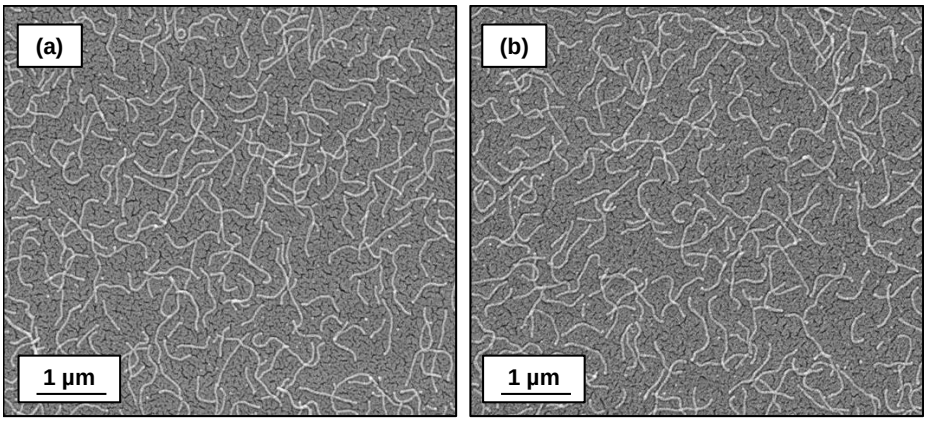

Figure 5.10 Representative SEM images obtained after dipping an anionic silicon wafer facing upside down into a 1.0 % w/w aqueous dispersion of (0.9 PEO_{113} + 0.1 $PQDMA_{140}$)-P($HPMA_{137}$-*stat*-$GlyMA_{35}$) cationic cross-linked worms for either (a) 20 s or (b) 60 s. Importantly, the silicon surface wafer orientation does not appear to affect either the worm adsorption kinetics or the final surface coverage. Adsorption conditions: pH 5, no added salt, 20 °C

Ellipsometry is an established technique for determining the thickness of thin films.[71] It has been widely applied to characterise both polymer brushes[72-75] and layer-by-layer systems.[23, 48, 76] It is a model-dependent technique that assumes a uniform thickness for the adsorbed layer (slab model). This is not strictly the case for these adsorbed multilayers of oppositely-charged worms, particularly at lower surface coverages. Nevertheless, ellipsometry is expected to provide complementary information to SEM analysis and perhaps offer greater reliability for thicker worm layers, where determining the fractional surface coverage by digital image analysis

becomes increasing subjective. Furthermore, the ellipsometer beam projected dimensions are 8 mm x 3 mm thus the surface area analysed by ellipsometry (24 mm^2) is far greater than that analysed by SEM (900 μm^2). Ellipsometry parameters Ψ and Δ were collected from 370 to 1000 nm. Firstly, analysis of a clean silicon wafer indicated a mean native oxide thickness of 1.97 nm. The mean-square error (MSE) of this measurement is very low at 1.4, which validates the data fit for the experimental Ψ and Δ values against the native oxide model within the CompleteEase modelling software. MSE values of less than 2 indicate very good fits to the model used.[77] Secondly, the kinetics of cationic worm adsorption onto a clean silicon wafer (1.0% w/w, pH 5, 20 °C, no added salt) was monitored *via* ellipsometry to determine the dry worm layer thickness. The Cauchy model (see equation 5.1) uses three Cauchy parameters (A_n, B_n and C_n) to describe the λ dependence of the refractive index (n) of an optically transparent material. A_n is a dimensionless parameter describing the refractive index of the material such that as λ tends to infinity, then $n(\lambda)$ tends to A_n. The constants B_n and C_n are parameters that characterise the non-linear relationship between the refractive index and λ. Figure 5.11a shows the fitted Ψ and Δ data after adsorption of 1.0 % w/w core cross-linked cationic worms onto the anionic silicon surface for 2 min at pH 5 without added salt. In this case, the refractive index of the surface is not known, but this value must lie between 1.00 and 1.50 as the surface comprises an anionic silicon wafer, block copolymer cationic worms and air voids within the adsorbed worm layer. Thus all three Cauchy parameters were fitted to the data, enabling a mean worm layer thickness of 8.9 nm to be calculated. The excellent fit provided by the experimental Ψ and Δ data to the Cauchy model was validated by a relatively low MSE of 1.29 when $A_n = 1.257$ (Figure 5.11b). The latter value is reasonable because the adsorbed worms form a non-uniform patchy layer, rather than a homogeneous thin film. Since these cationic worms exhibit a mean worm width of 27 ± 3 nm and a surface coverage of $\approx$ 16% as judged by ImageJ threshold analysis, an ellipsometric worm layer thickness of 8.9 nm seems to be physically realistic.

Similar worm layer thicknesses of 6.0 nm, 6.6 nm and 6.5 nm were also determined by ellipsometry when anionic silicon wafers were dipped into the cationic worm dispersion for 2 s, 20 s and 40 s, which confirms the remarkably fast kinetics of adsorption of these worms onto the silicon surface. Furthermore, when an inverted bare anionic silicon wafer is immersed into the worm dispersion, the same mean worm layer thickness is observed. This suggests that purely electrostatic interactions, rather than gravitational sedimentation, is the primary driving force for worm adsorption. Thus worm adsorption is essentially complete within a few seconds under the stated conditions.

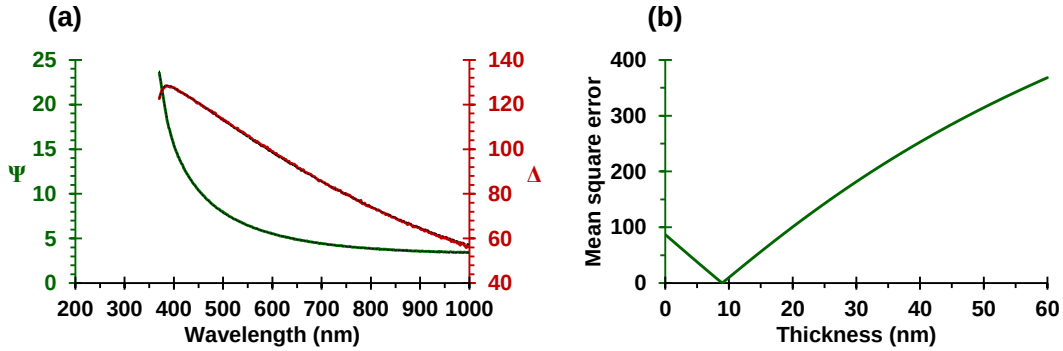

Figure 5.11 (a) Plots of the fitted ellipsometric parameters Ψ (red line) and Δ (green line) to λ using the Cauchy model (black dotted line) for the deposition of cationic cross-linked worms onto an anionic silicon wafer (layer 1). (b) Mean-square error against thickness plot to validate the fit of Ψ and Δ to the model. Adsorption conditions: 1.0% w/w worms, 2 min, pH 5, no salt, 20 °C.

5.3.4 Layer-by-layer deposition of Polyelectrolytic Worms onto Silicon Wafers

Formation of polyelectrolytic worm multilayers was achieved by successive adsorption of oppositely-charged worms onto a clean anionic silicon wafer. The adsorption conditions were fixed at an arbitrary time of 2 min, pH 5, no added salt and an aqueous copolymer worm concentration of 1.0% w/w. SEM, ellipsometry and surface zeta potential studies were performed for each successive layer. The results obtained from each technique are discussed in turn below. Representative SEM images obtained for layers 1-9 are shown in Figure 5.12.

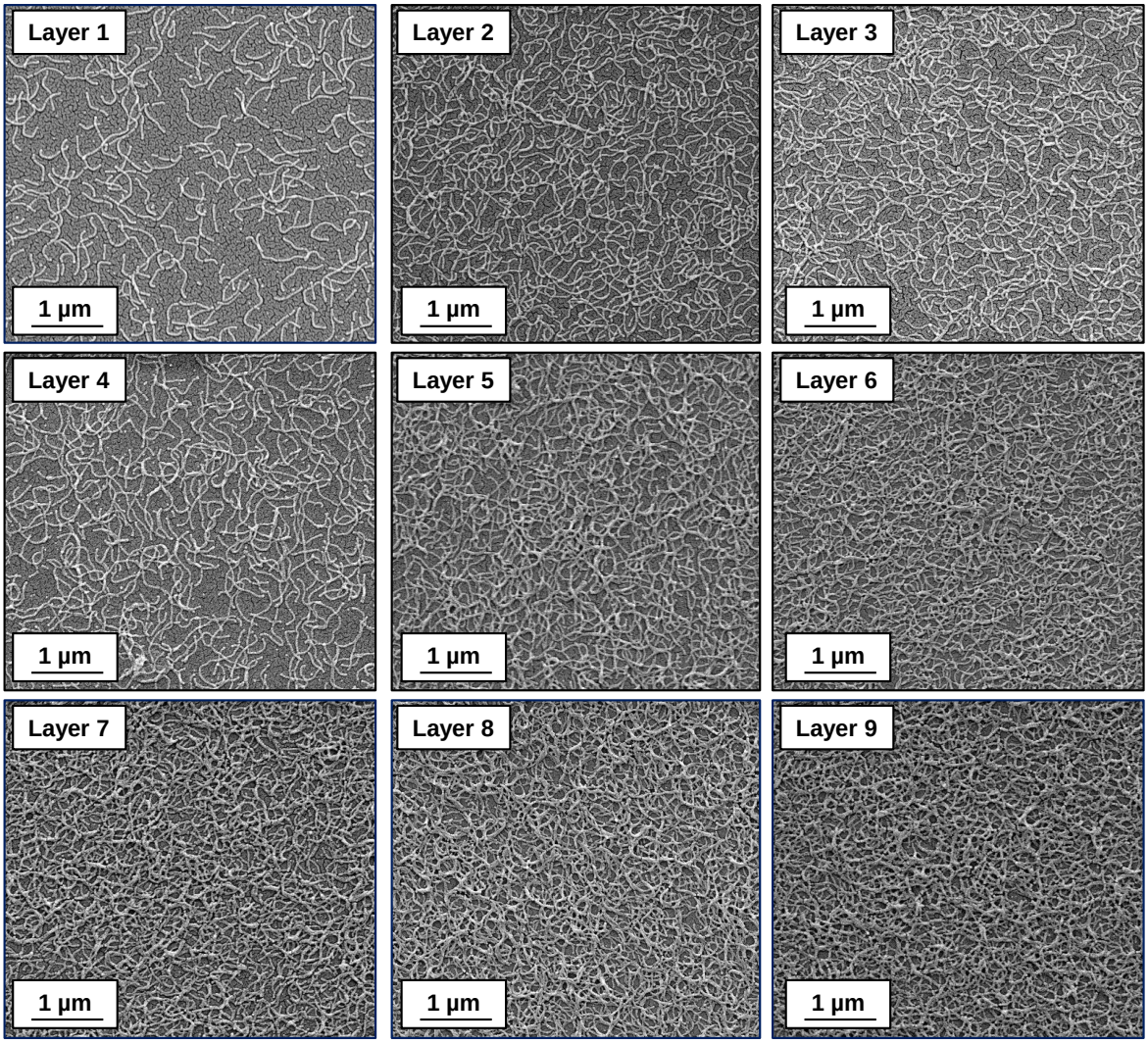

Figure 5.12 Representative SEM images obtained for the gradual build-up of worm multilayers obtained via layer-by-layer deposition of alternately cationic and anionic cross-linked worms onto a planar anionic silicon wafer. Odd layer numbers correspond to the adsorption of cationic worms and even layer numbers correspond to the adsorption of anionic worms. Adsorption conditions: 1.0 % w/w aqueous worm dispersions, pH 5, 20 °C, time allowed for the adsorption of each layer = 2 min.

Visual inspection of these images suggests an increase in surface coverage with layer number, indicative of the formation of polyelectrolytic worm multilayers. Threshold analysis using ImageJ software was performed to estimate the increase in surface coverage for each successive

worm layer. Adsorption of cationic worms to form the first adsorbed layer only results in a surface coverage of approximately 16% (see Figure 5.9). Formation of a further four consecutive worm layers results in an approximate increase in surface coverage of 4% per layer (see Figure 5.13). Digital image analysis of the corresponding SEM images is fairly straightforward for layers 1 to 5 because it is relatively easy to judge an appropriate threshold cut off as green background dots can be seen on the silicon wafer surface (see Figure 5.14a and Figure 5.14b). Increasing the layer number results in a higher surface coverage. However, it becomes increasingly problematic to judge the appropriate threshold limit to apply when assessing surface coverage. For example, the two threshold cut-off limits indicated in Figure 5.14c and Figure 5.14d both appear to be reasonable choices, even though the corresponding worm surface coverages differ significantly. Thus the experimental uncertainty in the surface coverage rises as the number of worm layers is increased.

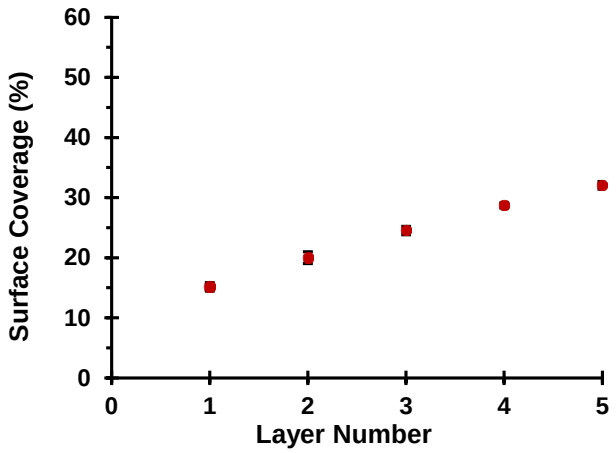

Figure 5.13 Relationship between surface coverage of a planar silicon wafer and layer number for the consecutive deposition of six layers of (0.9 PEO_{113} + 0.1 $PQDMA_{140}$)-P($HPMA_{137}$-*stat*-$GlyMA_{35}$) cationic cross-linked worms (layers 1, 3 and 5) and (0.9 PEO_{113} + 0.1 $PKSPMA_{111}$)-P($HPMA_{168}$-*stat*-$GlyMA_{39}$) anionic cross-linked worms (layers 2, 4 and 6). Surface coverages were determined using ImageJ software threshold analysis to analyse ten silicon wafers per time point; total surface area analysed per time point is approximately 900 μm^2. Adsorption conditions used for each worm layer: pH 5, 20 °C, no added salt, 2 min per adsorption event.

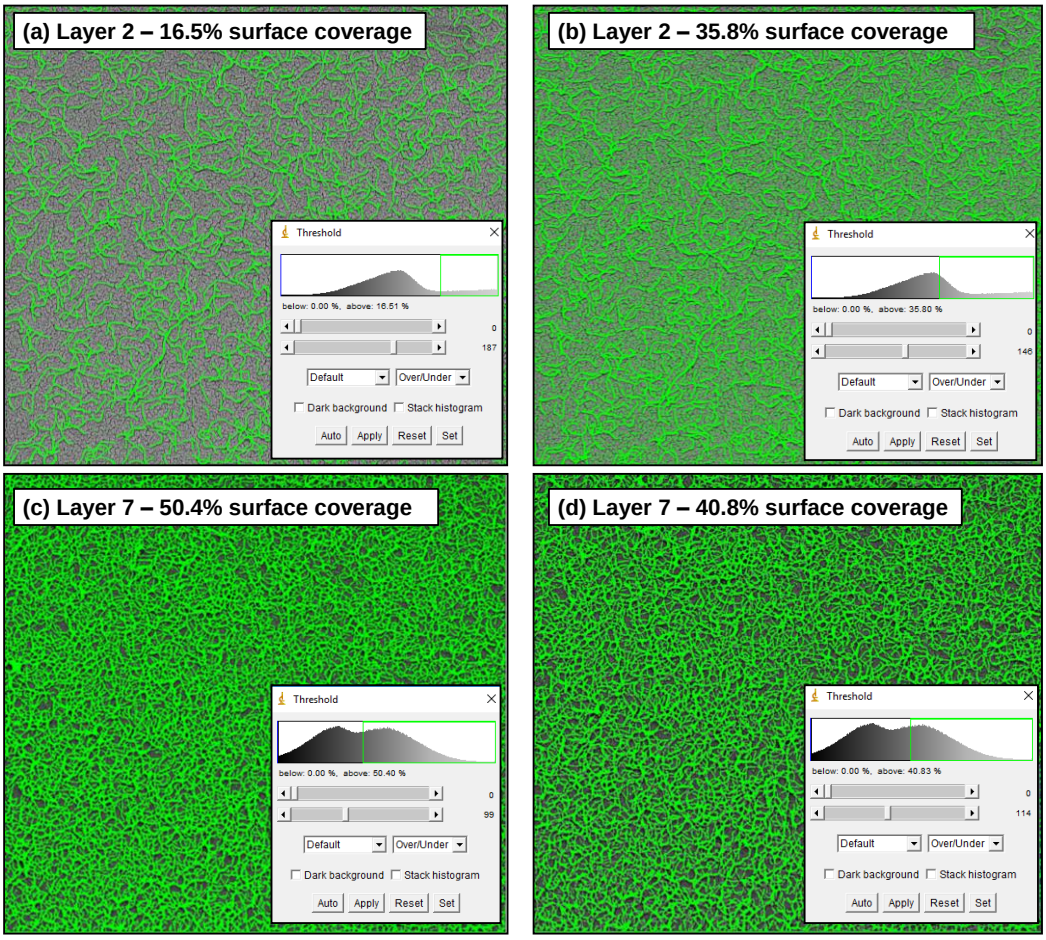

Figure 5.14 Representative ImageJ threshold analyses of SEM images obtained for layer 2 demonstrating (a) an appropriate choice of threshold cut off corresponding to 16% surface coverage and (b) the overestimation of surface coverage (36%) that occurs when the threshold cut off is set too high. Digital image analysis becomes increasingly problematic for larger numbers of adsorbed worm layers. Representative threshold analyses applied to images recorded for seven worm layers are shown in (c) and (d) to illustrate this cut off problem; both threshold values appear reasonable by visual inspection yet they result in a significantly different in surface coverages.

In view of this problem, ellipsometric measurements were also undertaken to assess the extent of worm adsorption. As described earlier, the Cauchy equation provides an appropriate model. The experimental Ψ and Δ data were fitted using the three Cauchy parameters (A_n, B_n and C_n). The relationship between dry layer thickness and worm layer number is shown in Figure 5.15. According to the literature, the L-b-L deposition of strong (water-soluble) polyelectrolyte chains

onto a planar surface is typically characterised by a linear increase in film thickness with layer number.[8, 78] However, non-linear (exponential) growth in film thickness has been reported in some cases when using weak polyelectrolytes. This has been attributed to either film roughness effects and/or the 'in-and-out' diffusion of at least one of the two polyelectrolytes throughout the film.[8, 79] For example, Yuan and Li prepared relatively thick nanoporous films *via* L-b-L assembly using poly(ethylene imine) (PEI) and poly(acrylic acid) (PAA).[80] SEM studies were performed to assess the nanoporous nature of such L-b-L films (see Figure 5.16). Importantly, basic conditions (pH 9.5) were employed for PEI adsorption, whereas acidic solutions (pH 2.9) were utilised for PAA adsorption. This approach reduces the charge density on these two weak polyelectrolytes. Interestingly, increasing the PEI/PAA charge density by adjusting the solution pH suppressed the exponential film growth. Furthermore, Podsiadlo and co-workers reported exponential growth for multilayer films composed of PEI, PAA and inorganic sheets of sodium montmorillonite.[79]

In the present Chapter, non-linear film growth is observed for the successive deposition of ten layers of oppositely-charged worms onto a silicon surface (Figure 5.15). Two growth regimes are observed. For layers 1 to 5 there is a linear increase in dry film thickness with layer number, with each layer contributing an additional mean thickness of 3 nm. SEM images recorded for layers 1 to 5 (compare Figure 5.12 and Figure 5.16) reveal the build-up of a relatively rough nanoporous film with a comparable structure to that reported by Yuan and Li.[80] Presumably, the rigidity and much longer contour lengths of these cross-linked polyelectrolytic worms leads to greater surface roughness, which accounts for the non-linear growth observed over the whole layer range. On the other hand, it seems rather unlikely that the 'in-and-out' diffusion mechanism proposed to account for the enhanced adsorption of water-soluble weak polyelectrolytes is applicable to the present study.

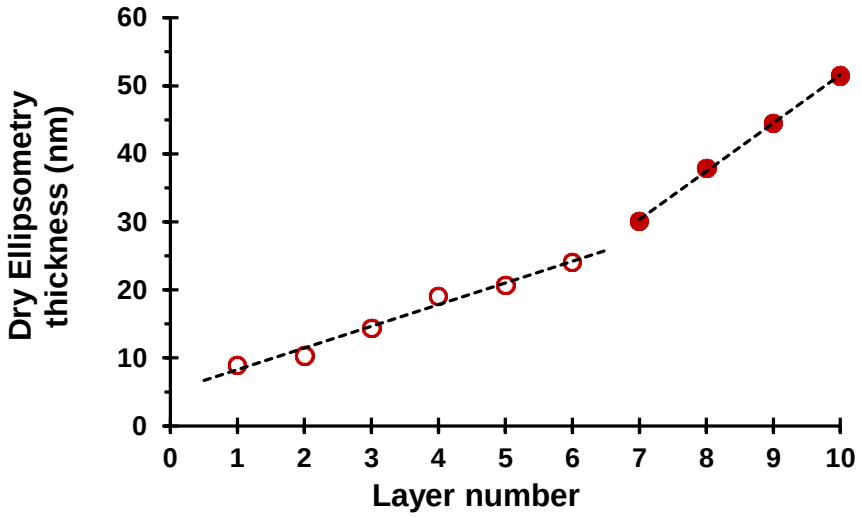

Figure 5.15 Relationship between the dry ellipsometric thickness of adsorbed worm layers and layer number for the consecutive deposition of ten layers of (0.9 PEO_{113} + 0.1 $PQDMA_{140}$)-P($HPMA_{137}$-*stat*-$GlyMA_{35}$) cationic cross-linked worms (layers 1, 3, 5, 7 and 9) and (0.9 PEO_{113} + 0.1 $PKSPMA_{111}$)-P($HPMA_{168}$-*stat*-$GlyMA_{39}$) anionic cross-linked worms (layers 2, 4, 6, 8 and 10). Conditions used for each worm layer: pH 5, 20 °C, no added salt, 2 min per adsorption event.

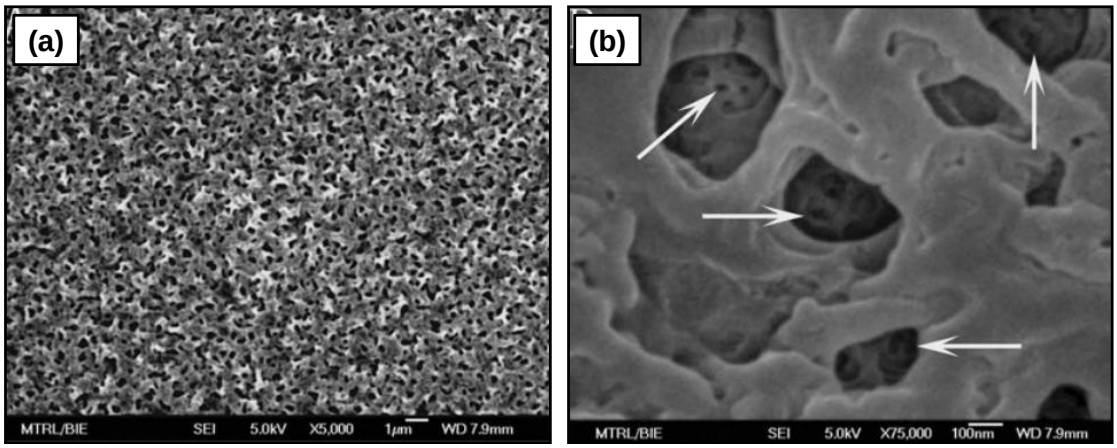

Figure 5.16 (a) Low magnification and (b) high magnification SEM images of self-assembled nanoporous polyelectrolyte multilayers comprising poly(ethylene imine) and poly(acrylic acid). Figure reproduced with permission from ref. [80].

A clear change in gradient is observed after adsorption of the first six worm layers (cumulative layer thickness ~ 24 nm), for which the mean increment in layer thickness is 3 nm. Thereafter, each successive worm layer contributes an additional 7 nm to the overall layer thickness.

Although higher surface coverages and thicker adsorbed layers are observed with increasing layer number, neither SEM nor ellipsometry can distinguish between the cationic and anionic worms adsorbed at the wafer surface. However, reversal of surface charge with increasing layer number would be expected for the successive adsorption of oppositely-charged worms. Historically, various techniques have been used to determine the surface zeta potential, including streaming potential measurements[81] and capillary flow.[82, 83] Streaming potential measurements require the sample to be sealed within a sample chamber so that greater than ambient pressures (typically a few atmospheres) can be applied. Capillary flow studies require careful sealing of the sample to the optical part of a capillary which is not always possible for small surfaces or surfaces with significant roughness.[84] Furthermore, tracer particles are required which, depending on the capillary orientation, can sediment onto the sample surface.[85] In 2012, Corbett *et al*.[84] reported a new, convenient method for determining the surface zeta potential. This new approach requires no sealing, so relatively fragile surfaces can be measured. Furthermore, the sample surface is inverted so tracer particles cannot sediment onto the surface during measurement, thus minimising sample contamination. An Uzgiris[86] dip cell is used in conjunction with a standard Malvern Zetasizer Nano instrument (Figure 5.17). To calculate the surface zeta potential, the motion of non-adsorbing tracer particles dispersed in aqueous electrolyte and subjected to an electric field is monitored *via* phase analysis light scattering.[84] Thus no modification of a conventional Malvern Zetasizer Nanosizer instrument is required.[87]

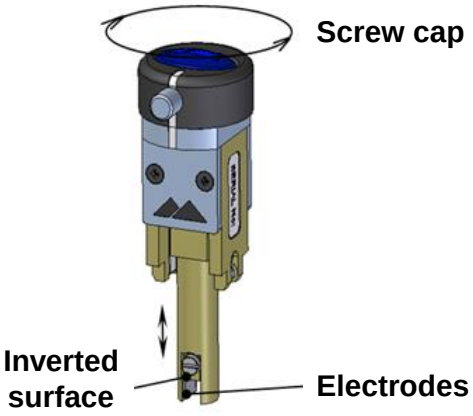

Figure 5.17 Diagram of the a Malvern ZEN1020 Surface Zeta Potential Dip Cell indicating the location of the inverted sample surface under testing, the electrodes and the screw cap that allows for micrometer adjustments to be made.[84, 87]

First, four slow field reversal (SFR) measurements of the tracer particles are performed at fixed displacements of 125 μm, 250 μm, 375 μm and 500 μm from the sample surface. Under SFR conditions, the electrophoretic (E_p) and electroosmotic (E_o) contributions to the apparent zeta potential of the tracer particles are calculated. Then an independent fast field reversal (FFR) measurement is undertaken at a displacement of 1000 μm from the sample surface, where the E_p contribution is the dominant term. The zeta potential *vs* displacement data is the plotted for the tracer particles and the surface zeta potential is calculated from the negative intercept of the linear plot for the SFR measurements plus the E_p value for the FFR measurement (see equation 5.2.)

$$\zeta_{surface} = -intercept + \zeta_{Ep} \qquad \textbf{5.2}$$

One parameter that requires careful consideration in such experiments is selection of appropriate tracer particles. The sole role of the tracer particles is to scatter light: chemical functionality or

surface chemistry does not affect their performance. However, it is essential that the tracer particles must not interact with the sample surface. Typical tracer particles reported in the literature include either sterically-stabilised polystyrene latexes[59] or a food-grade milk substitute (Coffee Compliment).[84] However, in both cases such tracer particles possess non-negligible surface charge at pH 5. This is clearly problematic for the present worm multilayer study, because universal tracer particles that are suitable for both anionic and cationic surfaces are desired. Cationic tracer particles would be prone to electrostatic adsorption onto an anionic surface and *vice versa*. Thus non-ionic spherical nanoparticles exhibiting zero surface charge at pH 5 are required to ensure no interaction with either type of worm layer. Alswieleh *et al.*[88] have recently reported that sterically-stabilised latexes prepared using a zwitterionic macromonomer can be used as tracer particles to determine surface zeta potentials for zwitterionic polymer brushes grown from silicon wafers. However, such bespoke latexes require a four-step synthesis.[89] On the other hand, a recently reported PISA formulation for non-ionic PGMA-PBzMA nanoparticles reported by Cunningham *et al.* offers a relatively straightforward and convenient route on non-ionic tracer nanoparticles.[90] Thus, the MePETTC-PGMA$_{58}$ macro-CTA prepared in Chapter 2 was chain-extended with BzMA (target DP$_n$ = 500) at 10% w/w solids using a RAFT aqueous emulsion formulation (see Scheme 5.5).

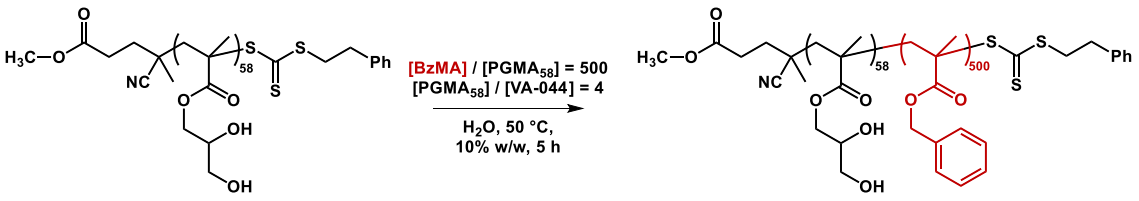

Scheme 5.5. Reaction scheme for the RAFT aqueous emulsion polymerisation of BzMA using a MePETTC-PGMA$_{58}$ macro-CTA to prepare non-ionic MePETTC-PGMA$_{58}$-PBzMA$_{500}$ nanoparticles. Such nanoparticles serve as a non-adsorbing tracer for the surface zeta potential measurements presented in this Chapter.

^{1}H NMR spectroscopy studies confirmed a monomer conversion of 97% after 5 h at 50 °C (Figure 5.18a). DMF GPC studies confirmed a high blocking efficiency for the MePETTC-$PGMA_{58}$ macro-CTA and indicated an M_n of 66,600 g mol^{-1} and an M_w / M_n of 1.31 (using a series of near-monodisperse PMMA calibration standards) for the $PGMA_{58}$-$PBzMA_{485}$ copolymer chains (Figure 5.18b).

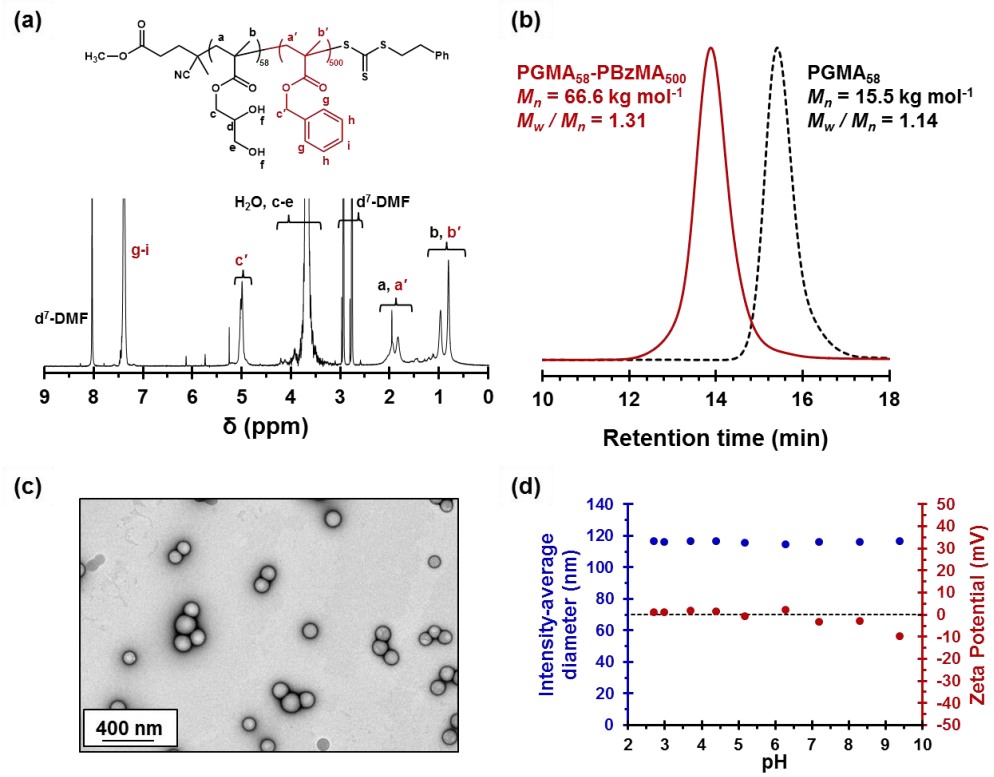

Figure 5.18. (a) Assigned ^{1}H NMR spectrum recorded in d_7-DMF obtained for a freeze-dried sample of MePETTC-$PGMA_{58}$-$PBzMA_{500}$ diblock copolymer. (b) DMF GPC chromatograms (calibrated using a series of near-monodisperse PMMA standards) recorded for the MePETTC-$PGMA_{58}$ macro-CTA precursor and the MePETTC-$PGMA_{58}$-$PBzMA_{500}$ diblock copolymer. (c) Representative TEM image obtained for a dried 0.10% w/w aqueous dispersion of MePETTC-$PGMA_{58}$-$PBzMA_{500}$ nanoparticles, confirming their spherical morphology and relatively narrow particle size distribution. (d) Intensity-average diameter *vs* pH and zeta potential *vs* pH curves obtained for MePETTC-$PGMA_{58}$-$PBzMA_{500}$ diblock copolymer nanoparticles. Measurements were recorded using a 0.10% w/w aqueous dispersion in the presence of 1 mM KCl. The dispersion pH was adjusted using either 0.1 M or 1 M HCl.

Furthermore, TEM analysis of the dried dilute aqueous dispersion confirmed a well-defined spherical morphology (Figure 5.18c). DLS and aqueous electrophoresis studies were performed to examine the effect of varying the solution pH on both the intensity-average particle diameter and zeta potential (Figure 5.18d). As expected, these spherical nanoparticles exhibit pH-independent behaviour: their intensity-average diameter (approximately 120 nm) and zeta potential (around 0 mV) remain constant across a wide pH range.

Corbett *et al.*[84] reported that a relatively low derived count rate of 250 – 500 kcps is required for SZP analysis. For the MePETTC-PGMA$_{58}$-PBzMA$_{500}$ nanoparticles, this corresponds to a concentration of 0.0025% w/w when the attenuator is set to position 11 (100% light transmittance). All surface zeta potentials were determined at pH 5 using 1 mM KCl as background electrolyte. Two control experiments were performed to demonstrate that these tracer particles were indeed suitable for surface zeta potential measurements. Firstly, a clean anionic silicon wafer was analysed at pH 5. The zeta potential *vs* displacement plot obtained for the tracer nanoparticles and the raw phase data are shown in Figure 5.19. Figure 5.19a displays the phase plots obtained for SFR measurements at four displacements and the FFR measurement made at 1000 μm. High signal-to-noise ratios were obtained in all cases, indicating the expected Doppler shift for the non-ionic tracer nanoparticles. From these phase data, the tracer nanoparticle zeta potential was plotted against displacement (Figure 5.19b) and used to calculate the surface zeta potential using equation 5.2. The surface zeta potential for a clean bare anionic silicon wafer is calculated to be -53 ± 4 mV at pH 5 in the presence of 1 mM KCl. This value is comparable to literature data obtained *via* streaming potential measurements under the same conditions.[91]

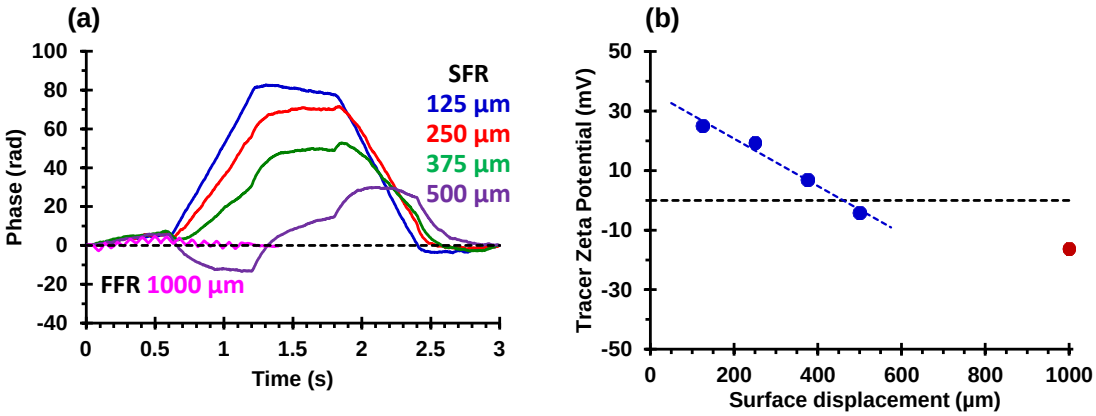

Figure 5.19 (a) Raw phase plot obtained for a clean bare anionic planar silicon wafer illustrating the expected Doppler shift when using non-ionic MePETTC-PGMA$_{58}$-PBzMA$_{500}$ nanoparticles as a tracer. Slow field reversal (SFR) measurements were performed at displacements of 125 µm, 250 µm, 375 µm and 500 µm from the surface of the silicon wafer. A fast field reversal (FFR) measurement was performed at a displacement of 1000 µm from the surface of the silicon wafer. (b) From these phase data, the tracer nanoparticle zeta potential is plotted against displacement and the surface zeta potential is calculated using Equation 5.2. All measurements were performed at 25 °C with a Malvern ZEN1020 Surface Zeta Potential Dip Cell using a 0.0025% w/w aqueous dispersion of MePETTC-PGMA$_{58}$-PBzMA$_{500}$ nanoparticles as a non-adsorbing tracer to determine surface zeta potentials at pH 5 in the presence of 1 mM KCl.

The same surface zeta potential studies were performed on a worm-coated silicon wafer (layer 1) after immersion of a clean bare anionic silicon wafer into a 1.0% w/w aqueous dispersion of cationic cross-linked worms for 2 min at pH 5. Figure 5.20a depicts the phase plots obtained for SFR measurements at four displacements and also the FFR measurement made at 1000 µm for this cationic worm-coated wafer. In this case, the sign of the phase plot has changed, indicating surface charge reversal as the original anionic silicon wafer is converted into a cationic worm-coated silicon wafer. A surface zeta potential of +22 ± 1 mV is calculated from this phase data set. These experiments also confirm that the MePETTC-PGMA$_{58}$-PBzMA$_{500}$ spheres are appropriate tracer nanoparticles for both cationic and anionic substrates. Surface zeta potential measurements were performed on subsequent worm multilayer films (see Figure 5.21).

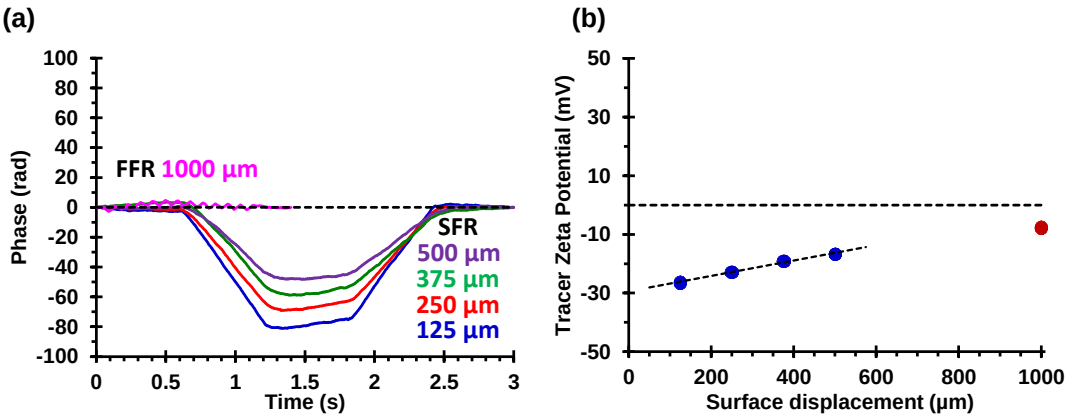

Figure 5.20 (a) Raw phase plot obtained after immersing a clean anionic silicon wafer into an aqueous dispersion of cationic worms (layer 1) illustrating the expected Doppler shift for MePETTC-PGMA$_{58}$-PBzMA$_{500}$ non-ionic tracer nanoparticles. Note the change in sign for this phase data set compared to that shown in Figure 5.18, indicating surface charge reversal. Slow field reversal (SFR) measurements were performed at displacements of 125 µm, 250 µm, 375 µm and 500 µm from the surface of the worm-coated silicon wafer. A fast field reversal (FFR) measurement was performed at a displacement of 1000 µm from the surface of the silicon wafer. (b) Relationship between tracer particle zeta potential and displacement used to calculate the surface zeta potential *via* Equation 5.2. All measurements were performed at 25 °C with a Malvern ZEN1020 Surface Zeta Potential Dip Cell using a 0.0025% w/w aqueous dispersion of MePETTC-PGMA$_{58}$-PBzMA$_{500}$ nanoparticles as a non-adsorbing tracer to determine surface zeta potentials at pH 5 in the presence of 1 mM KCl.

As previously mentioned, the initial clean anionic silicon wafer (layer 0) exhibits a surface zeta potential of -53 ± 4 mV at pH 5. Surface charge reversal is observed after deposition of the first worm layer (layer 1) to give a surface zeta potential of +22 ± 1 mV. Adsorption of anionic worms (layer 2) onto this cationic worm layer again results in surface charge reversal, giving a surface zeta potential of -30 ± 2 mV. The successive adsorption of oppositely-charged worms results in successive surface charge reversal, as expected.[92] Thus these surface zeta potential measurements confirm sequential deposition of cationic and anionic worms onto an anionic planar silicon wafer and are consistent with the corresponding SEM and ellipsometric data.

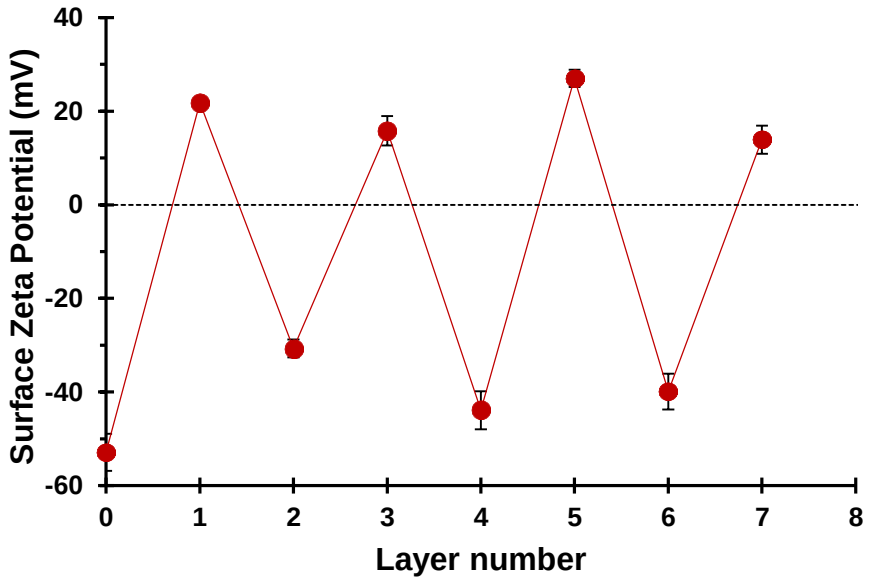

Figure 5.21 Variation in surface zeta potential with worm layer number for the sequential adsorption of cationic and anionic cross-linked worms onto a planar anionic silicon wafer. Odd layer numbers correspond to the adsorption of cationic worms, whereas an even layer number corresponds to the adsorption of anionic worms. All measurements were performed at 25 °C with a Malvern ZEN1020 Surface Zeta Potential Dip Cell using a 0.0025% w/w aqueous dispersion of MePETTC-PGMA$_{58}$-PBzMA$_{500}$ nanoparticles as a non-adsorbing tracer to determine surface zeta potentials at pH 5 in the presence of 1 mM KCl.

5.4 Conclusions

RAFT-mediated PISA can be used to prepare either cationic or anionic block copolymer worms *via* RAFT aqueous dispersion polymerisation using a judicious binary mixture of a non-ionic (PEO) and a polyelectrolytic (PQDMA or PKSPMA) stabiliser macro-CTA. Both types of worms contain reactive epoxy groups located within their core-forming blocks, which enables their covalent stabilisation on the addition of MPTES. Kinetic studies indicate that the electrostatic adsorption of cationic worms from aqueous solution onto a clean bare anionic planar silicon wafer is complete within a few seconds at 20 °C, although the final surface coverage achieved for this first layer is only 16% as determined by ImageJ analysis. The

successive layer-by-layer deposition of the cationic and anionic polyelectrolytic worms onto a planar anionic silicon wafer was investigated at pH 5. SEM analysis confirms the gradual build-up of worm multilayers, but assessing the fractional surface coverage via digital image analysis becomes somewhat subjective after the first few worm layers. Ellipsometric studies confirm that the worm layer thickness initially increases linearly with layer number, as expected. However, a second adsorption regime corresponding to a steeper linear gradient is observed after the sixth worm layer. According to the literature, this latter regime may be the result of a surface roughness effect for these relatively large rigid worms. Surface zeta potential studies using bespoke non-ionic tracer nanoparticles confirm that surface charge reversal occurs on addition of each successive worm layer. These worms are a useful mimic for understanding the adsorption behaviour of soluble 'rigid rod' polyelectrolytes, since their longer length scales facilitates direct visualisation *via* electron microscopy.

5.5 References

1. G. Decher and J. D. Hong, *Makromol. Chem., Macromol. Symp.*, 1991, **46**, 321.
2. G. Decher and J. D. Hong, *Berichte der Bunsen-Gesellschaft*, 1991, **95**, 1430.
3. G. Decher, J. D. Hong and J. Schmitt, *Thin Solid Films*, 1992, **210-211**, 831.
4. G. Decher, *Science*, 1997, **277**, 1232.
5. P. Bertrand, A. Jonas, A. Laschewsky and R. Legras, *Macromolecular Rapid Communications*, 2000, **21**, 319.
6. S. T. Dubas, T. R. Farhat and J. B. Schlenoff, *Journal of the American Chemical Society*, 2001, **123**, 5368.
7. J. B. Schlenoff, S. T. Dubas and T. Farhat, *Langmuir*, 2000, **16**, 9968.
8. J. Borges and J. F. Mano, *Chemical Reviews*, 2014, **114**, 8883.
9. P. T. Hammond, *Advance Materials*, 2004, **16**, 1271.
10. S. S. Shiratori and M. F. Rubner, *Macromolecules*, 2000, **33**, 4213.
11. J. D. Mendelsohn, C. J. Barrett, V. V. Chan, A. J. Pal, A. M. Mayes and M. F. Rubner, *Langmuir*, 2000, **16**, 5017.
12. S. T. Dubas and J. B. Schlenoff, *Macromolecules*, 1999, **32**, 8153.
13. S. T. Dubas and J. B. Schlenoff, *Macromolecules*, 2001, **34**, 3736.
14. B. Schwarz and M. Schoenhoff, *Langmuir*, 2002, **18**, 2964.
15. K. Glinel, A. Moussa, A. M. Jonas and A. Laschewsky, *Langmuir*, 2002, **18**, 1408.
16. J. A. Lichter, K. J. Van Vliet and M. F. Rubner, *Macromolecules*, 2009, **42**, 8573.

17. B. V. Parakhonskiy, A. M. Yashchenok, M. Konrad and A. G. Skirtach, *Advances in Colloid and Interface science*, 2014, **207**, 253.
18. N. A. Kotov, I. Dekany and J. H. Fendler, *Journal of Physical Chemistry*, 1995, **99**, 13065.
19. Y. Lvov, K. Ariga, M. Onda, I. Ichinose and T. Kunitake, *Langmuir*, 1997, **13**, 6195.
20. K. Ariga, Y. Lvov, M. Onda, I. Ichinose and T. Kunitake, *Chemistry Letters*, 1997, **26**, 125.
21. G. Decher, M. Eckle, J. Schmitt and B. Struth, *Current Opinion in Colloid & Interface Science*, 1998, **3**, 32.
22. Y. Lvov, G. Decher and G. Sukhorukov, *Macromolecules*, 1993, **26**, 5396.
23. J. Blacklock, T. K. Sievers, H. Handa, Y.-Z. You, D. Oupicky, G. Mao and H. Mohwald, *Journal of Physical Chemistry B*, 2010, **114**, 5283.
24. K. Ren, J. Ji and J. Shen, *Biomaterials*, 2006, **27**, 1152.
25. Y. Lvov, H. Haas, G. Decher, H. Moehwald, A. Mikhailov, B. Mtchedlishvily, E. Morgunova and B. Vainshtein, *Langmuir*, 1994, **10**, 4232.
26. P. J. Yoo, K. T. Nam, J. Qi, S.-K. Lee, J. Park, A. M. Belcher and P. T. Hammond, *Nature Materials*, 2006, **5**, 234.
27. G. Ladam, C. Gergely, B. Senger, G. Decher, J.-C. Voegel, P. Schaaf and F. J. G. Cuisinier, *Biomacromolecules*, 2000, **1**, 674.
28. F. Caruso and H. Möhwald, *Journal of the American Chemical Society*, 1999, **121**, 6039.
29. Y. Lvov, K. Ariga, I. Ichinose and T. Kunitake, *Journal of the American Chemical Society*, 1995, **117**, 6117.
30. G. B. Sukhorukov, E. Donath, H. Lichtenfeld, E. Knippel, M. Knippel, A. Budde and H. Möhwald, *Colloids and Surfaces A: Physicochemical and Engineering Aspects*, 1998, **137**, 253.
31. A. A. Antipov and G. B. Sukhorukov, *Advances in Colloid and Interface science*, 2004, **111**, 49.
32. M. Coustet, J. Irigoyen, T. A. Garcia, R. A. Murray, G. Romero, M. Susana Cortizo, W. Knoll, O. Azzaroni and S. E. Moya, *Journal of Colloid and Interface Science*, 2014, **421**, 132.
33. J. Rao, H. Zhang, S. Gaan and S. Salentinig, *Macromolecules*, 2016, **49**, 5978.
34. T. Addison, O. J. Cayre, S. Biggs, S. P. Armes and D. York, *Langmuir*, 2008, **24**, 13328.
35. I. Estrela-Lopis, S. Leporatti, E. Typlt, D. Clemens and E. Donath, *Langmuir*, 2007, **23**, 7209.
36. O. Kreft, R. Georgieva, H. Bäumler, M. Steup, B. Müller-Röber, G. B. Sukhorukov and H. Möhwald, *Macromolecular Rapid Communications*, 2006, **27**, 435.
37. T. Boudou, T. Crouzier, K. Ren, G. Blin and C. Picart, *Advanced Materials*, 2010, **22**, 441.
38. A. G. Skirtach, A. M. Yashchenok and H. Moehwald, *Chemical Communications*, 2011, **47**, 12736.
39. D. V. Andreeva, E. V. Skorb and D. G. Shchukin, *ACS Applied Materials and Interfaces*, 2010, **2**, 1954.
40. Y. Li, S. Chen, M. Wu and J. Sun, *Advanced Materials*, 2012, **24**, 4578.
41. L. Xu, Z. Zhu and S. A. Sukhishvili, *Langmuir*, 2011, **27**, 409.
42. B.-S. Kim, S. W. Park and P. T. Hammond, *ACS Nano*, 2008, **2**, 386.
43. P. M. Nguyen, N. S. Zacharia, E. Verploegen and P. T. Hammond, *Chemistry of Materials*, 2007, **19**, 5524.
44. C. Moreau, N. Beury, N. Delorme and B. Cathala, *Langmuir*, 2012, **28**, 10425.

45. E. D. Cranston and D. G. Gray, *Colloids and Surfaces A: Physicochemical and Engineering Aspect*, 2008, **325**, 44.
46. E. D. Cranston, D. G. Gray and M. W. Rutland, *Langmuir*, 2010, **26**, 17190.
47. E. D. Cranston and D. G. Gray, *Biomacromolecules*, 2006, **7**, 2522.
48. L. Wagberg, G. Decher, M. Norgren, T. Lindstrom, M. Ankerfors and K. Axnas, *Langmuir*, 2008, **24**, 784.
49. C. Olivier, C. Moreau, P. Bertoncini, H. Bizot, O. Chauvet and B. Cathala, *Langmuir*, 2012, **28**, 12463.
50. N. J. Warren and S. P. Armes, *Journal of the American Chemical Society*, 2014, **136**, 10174.
51. C. A. Figg, R. N. Carmean, K. C. Bentz, S. Mukherjee, D. A. Savin and B. S. Sumerlin, *Macromolecules*, 2017, **50**, 935.
52. M. Semsarilar, V. Ladmiral, A. Blanazs and S. P. Armes, *Langmuir*, 2012, **28**, 914.
53. M. Semsarilar, V. Ladmiral, A. Blanazs and S. P. Armes, *Langmuir*, 2013, **29**, 7416.
54. M. Williams, N. J. W. Penfold, J. R. Lovett, N. J. Warren, C. W. I. Douglas, N. Doroshenko, P. Verstraete, J. Smets and S. P. Armes, *Polymer Chemistry*, 2016, **7**, 3864.
55. M. Williams, N. J. W. Penfold and S. P. Armes, *Polymer Chemistry*, 2016, **7**, 384.
56. N. J. W. Penfold, Y. Ning, P. Verstraete, J. Smets and S. P. Armes, *Chemical Science*, 2016, **7**, 6894.
57. C. Holm, M. Rehahn, W. Oppermann and M. Ballauff, *Advances in Polymer Science*, 2004, **166**, 1.
58. M. J. Stevens and K. Kremer, *Journal of Chemical Physics*, 1995, **103**, 1669.
59. T. E. Thomas, S. A. Aani, D. L. Oatley-Radcliffe, P. M. Williams and N. Hilal, *Journal of Membrane Science*, 2017, **523**, 524.
60. L. D. Blackman, K. E. B. Doncom, M. I. Gibson and R. K. O'Reilly, *Polymer Chemistry*, 2017, **8**, 2860.
61. J. Tan, H. Sun, M. Yu, B. S. Sumerlin and L. Zhang, *ACS Macro Letters*, 2015, **4**, 1249.
62. J. Tan, Y. Bai, X. Zhang and L. Zhang, *Polymer Chemistry*, 2016, **7**, 2372.
63. J. Yeow, J. Xu and C. Boyer, *ACS Macro Letters*, 2015, **4**, 984.
64. N. J. Warren, O. O. Mykhaylyk, D. Mahmood, A. J. Ryan and S. P. Armes, *Journal of the American Chemical Society*, 2014, **136**, 1023.
65. K. Ren and J. Perez-Mercader, *Polymer Chemistry*, 2017, **8**, 3548.
66. B. Yuan, X. He, Y. Qu, C. Gao, E. Eiser and W. Zhang, *Polymer Chemistry*, 2017, **8**, 2173.
67. J. Rieger, F. Stoffelbach, C. Bui, D. Alaimo, C. Jerome and B. Charleux, *Macromolecules*, 2008, **41**, 4065.
68. R. D. Deegan, O. Bakajin, T. F. Dupont, G. Huber, S. R. Nagel and T. A. Witten, *Nature*, 1997, **389**, 827.
69. X. Shen, C.-M. Ho and T.-S. Wong, *Journal of Physical Chemistry B*, 2010, **114**, 5269.
70. T. P. Bigioni, X.-M. Lin, T. T. Nguyen, E. I. Corwin, T. A. Witten and H. M. Jaeger, *Nature Materials*, 2006, **5**, 265.
71. J. L. Keddie, *Current Opinion in Colloid & Interface Science*, 2001, **6**, 102.
72. A. Rastogi, M. Y. Paik, M. Tanaka and C. K. Ober, *ACS Nano*, 2010, **4**, 771.
73. S. Edmondson, C.-D. Vo, S. P. Armes and G.-F. Unali, *Macromolecules*, 2007, **40**, 5271.
74. A. M. Granville, S. G. Boyes, B. Akgun, M. D. Foster and W. J. Brittain, *Macromolecules*, 2004, **37**, 2790.
75. M. P. Weir, S. Y. Heriot, S. J. Martin, A. J. Parnell, S. A. Holt, J. R. P. Webster and R. A. L. Jones, *Langmuir*, 2011, **27**, 11000.

76. S. Edmondson, C.-D. Vo, S. P. Armes, G.-F. Unali and M. P. Weir, *Langmuir*, 2008, **24**, 7208.
77. S. Edmondson, N. T. Nguyen, A. L. Lewis and S. P. Armes, *Langmuir*, 2010, **26**, 7216.
78. G. Decher and J. Schmitt, *Progress in Colloid and Polymer Science*, 1992, **89**, 160.
79. P. Podsiadlo, M. Michel, J. Lee, E. Verploegen, N. W. S. Kam, V. Ball, J. Lee, Y. Qi, A. J. Hart, P. T. Hammond and N. A. Kotov, *Nano Letters*, 2008, **8**, 1762.
80. W. Yuan and C. M. Li, *Chemical Communications*, 2010, **46**, 9161.
81. C. Werner, H. Körber, R. Zimmermann, S. Dukhin and H.-J. Jacobasch, *Journal of Colloid and Interface Science*, 1998, **208**, 329.
82. C. J. Evenhuis, R. M. Guijt, M. Macka, P. J. Marriott and P. R. Haddad, *Electrophoresis*, 2006, **27**, 672.
83. M. Kosmulski and E. Matijevic, *Langmuir*, 1992, **8**, 1060.
84. J. C. W. Corbett, F. McNeil-Watson, R. O. Jack and M. Howarth, *Colloids and Surfaces A: Physicochemical and Engineering Aspects*, 2012, **396**, 169.
85. A. Doren, J. Lemaitre and P. G. Rouxhet, *Journal of Colloid and Interface Science*, 1989, **130**, 146.
86. E. E. Uzgiris, *Advances in Colloid and Interface science*, 1981, **14**, 75.
87. I. M. Tucker, J. C. W. Corbett, J. Fatkin, R. O. Jack, M. Kaszuba, B. MacCreath and F. McNeil-Watson, *Current Opinion in Colloid & Interface Science*, 2015, **20**, 215.
88. A. M. Alswieleh, N. Cheng, I. Canton, B. Ustbas, X. Xue, V. Ladmiral, S. Xia, R. E. Ducker, O. El Zubir, M. L. Cartron, C. N. Hunter, G. J. Leggett and S. P. Armes, *Journal of the American Chemical Society*, 2014, **136**, 9404.
89. K. L. Thompson, I. Bannister, S. P. Armes and A. L. Lewis, *Langmuir*, 2010, **26**, 4693.
90. V. J. Cunningham, A. M. Alswieleh, K. L. Thompson, M. Williams, G. J. Leggett, S. P. Armes and O. M. Musa, *Macromolecules*, 2014, **47**, 5613.
91. P. J. Scales, F. Grieser, T. W. Healy, L. R. White and D. Y. C. Chan, *Langmuir*, 1992, **8**, 965.
92. C. Picart, P. Lavalle, P. Hubert, F. J. G. Cuisinier, G. Decher, P. Schaaf and J. C. Voegel, *Langmuir*, 2001, **17**, 7414.

Chapter 6

Conclusions and Outlook

The current era is a particularly exciting time to be researching synthetic polymer chemistry. The synthetic toolbox available to polymer chemists has dramatically evolved over the last twenty years, particularly due to the invention of pseudo-living radical polymerisation techniques such as ATRP[1, 2] and RAFT.[3] It is now relatively straightforward for polymer chemists (and even non-specialists) to prepare tailor-made functional copolymers with complex architectures. Moreover, it is now feasible to prepare functional block copolymer nanoparticles *via* RAFT-mediated PISA formulations. Copolymer concentrations are typically 10-30% w/w solids, which are typically two orders of magnitude higher than traditional post-polymerisation processing techniques. Numerous block copolymer formulations have been reported by various academic groups,[4-7] but of particular relevance to this thesis are PGMA-PHPMA block copolymer worm gels, which have been shown to have various potential biomedical applications. For example, Blanazs *et al.* demonstrated that PGMA-PHPMA worm gels can be used as a sterilisable medium *via* cold ultrafiltration.[8] Furthermore, such PGMA-PHPMA worm gels are synthetic mimics of naturally-occurring mucins, with comparable levels of hydroxyl functionality and gel strength. Taking advantage of this similarity, Canton *et al.* recently demonstrated that such PGMA-PHPMA worm gels can act as a storage medium for either pluripotent human stem cell colonies or human embryos at 37 °C.[9] Stasis was observed in both cases, thus PGMA-PHPMA worm gels can in principle be used as a transportation medium for the global delivery of human stem cells. Furthermore, Mitchell *et al.* recently produced the first solvent-free, fully-synthetic formulation for the cryopreservation of red blood cells.[10] Each of the above examples relies on a thermally-induced reversible worm-to-sphere morphology transition for their application. A second important attribute is the ability to prepare high-quality transparent gels *via* direct dissolution of the freeze-dried copolymer powder in cold water.

Lovett and co-workers reported that a change in dispersion pH can induce a morphology transition for PGMA-PHPMA block copolymer worms and vesicles, prepared using a

carboxylic acid functionalised RAFT agent.[11, 12] In the first half of this thesis, similar block copolymer worms and vesicles were prepared using a new morpholine-functionalised RAFT agent (MPETTC) at pH 7.0 – 7.5. The morpholine groups are located at the end of each PGMA stabiliser chain, thus residing at the nanoparticle periphery. Protonation of the morpholine group results in an increase in the effective volume fraction of the PGMA block, thus inducing a morphology transition. For example, acidification of MPETTC-PGMA$_{50}$-PHPMA$_{140}$ worm gels initially at pH 7 results in a worm-to-sphere transition with concomitant degelation at pH 3. Returning to pH 7 results in worm reformation, with the original gel strength regained. Furthermore, if the analogous MPETTC-PGMA$_{43}$-PHPMA$_{y}$ copolymer vesicles are similarly acidified, a vesicle-to-worm transition only occurs for a certain DP$_n$ range (y = 190 – 200). Unfortunately, returning to pH 7 resulted in syneresis rather than initial vesicle reformation. When the PHPMA DP$_n$ is too long, the pH-responsive behaviour conferred by the protonated morpholine end-group is lost, although surface cationic charge is still acquired. However, cooling these unresponsive cationic vesicles did result in a change in nanoparticle morphology, to either spheres or sphere/worm mixed phase.

In was envisaged that such morpholine-terminated vesicles might be used as drug delivery vehicles. Encapsulation of model cargos such as 12 nm silica nanoparticles or bovine serum album (BSA) protein within PGMA-PHPMA vesicles has been demonstrated very recently by Mable and co-workers[13, 14] and Deng *et al.*[15] The encapsulated cargo is released by disintegration of the vesicle morphology: by either cooling to 0 °C for 30 min[13, 14] or by selective binding of 3-aminophenylboronic acid to the cis-diol groups of the PGMA stabiliser chains.[15] However, the stimulus-responsive nature of such vesicles must occur at physiologically relevant salt concentrations (≈ 140 mM) to be relevant for biomedical applications. Unfortunately, the pH-responsive behaviour of both MPETTC-PGMA-PHPMA worms and vesicles prepared in this thesis is suppressed in the presence of 100 mM KCl.

Furthermore, the solution acidity required to induce a morphology change (pH 3) is too acidic relative to the extra-cellular matrix pH associated with cancer cells (pH 5.5). In principle, this pH mismatch could be addressed by the addition of more basic groups on either the R group or both the R and Z groups of the RAFT agent. An alternative method could be to introduce a small amount of an amine-functionalised methacrylate into the stabiliser block, such as 2-(*N*-morpholine ethyl) methacrylate. This could be achieved *via* statistical copolymerisation with GMA or *via* a binary macro-CTA approach.[16, 17] If pH-responsive behaviour of PGMA-PHPMA vesicles could be achieved at around pH 5-6 in the presence of 140 mM salt then such vesicles could be examined as potential vehicles for the delivery of therapeutic agents.

In the second half of this thesis, polyelectrolytic block copolymer worms were prepared *via* the RAFT aqueous dispersion polymerisation of HPMA, using a binary mixture of a non-ionic PEO macro-CTA and either a cationic PQDMA or anionic PKSPMA macro-CTA. Furthermore, core cross-linked worms were conveniently prepared using a slightly modified PISA protocol by incorporating a small amount (20 mol%) of GlyMA comonomer into the core-forming block, followed by addition of a cross-linking agent (APTES or MPTES).[18] In Chapter 4, both linear and cross-linked cationic worms were evaluated as a new type of superflocculant for micron-sized silica particles. It was found that core cross-linking is a prerequisite for efficient particle flocculation. Linear cationic worms comprising weakly hydrophobic, PHPMA cores simply dissociated after adsorption onto the silica particles due to the strong torsional forces exerted by Brownian motion of the relatively massive silica particles. However, covalent stabilisation reinforces the worms and the cross-linked worms remain intact on the silica surface and so act as effective bridging flocculants. In principle, core cross-linking of the worms may not be necessary. Replacing PHPMA with a strongly hydrophobic core-forming block (such as PBzMA) may prevent worm break-up. However, the direct preparation of cationic worms in water with a PBzMA core would be problematic. Typically, RAFT aqueous emulsion

polymerisation generates kinetically-trapped spheres even when higher order morphologies would be expected.[6, 19] Nevertheless, Charleux and co-workers[20-22] and recently Cockram *et al.*[23] have shown that non-spherical morphologies can be obtained *via* RAFT aqueous emulsion polymerisation. It is currently believed that subtle differences in aqueous monomer solubility may play a vital role in accessing worms and vesicles.[23]

In principle, preparing PQDMA-PBzMA nanoparticles in methanol may facilitate access to higher order morphologies. The dielectric constant of methanol is less than water, thus reducing the effective lateral electrostatic repulsion of the neighbouring PQDMA chains. Furthermore, BzMA monomer is soluble in methanol while the resulting PBzMA polymer is insoluble. Thus chain extension of PQDMA with BzMA should proceed *via* RAFT alcoholic dispersion polymerisation, which would increase likelihood of accessing worms. If a pure phase of cationic PQDMA-PBzMA worms could be prepared then it would be very interesting to compare the flocculation ability of such linear cationic worms to the core linked cationic worms described in Chapters 4 and 5.

Recently, Thompson *et al* demonstrated that PGMA-PHPMA worms are more effective Pickering emulsifiers of oil-in-water emulsions than their corresponding spherical micelles.[24] However, core cross-linking was necessary to prevent particle break-up during the high shear homogenisation step. In 2006, Fujii *et al.*[25] reported that surfactant-free, sub-micrometer-sized polystyrene latex particles can be used as long-term effective foam stabilisers. Furthermore, foams prepared using cationic latex particles suffered less collapse over time compared to neutral latex particles, presumably as a result of the stronger adsorption at the anionic air/water interface. Thus it would be interesting to investigate if cationic worms prepared *via* RAFT-mediated PISA are more effective foam stabilisers than their corresponding cationic spheres. In addition, it would be prudent to investigate if cross-linking is beneficial in this context

The successive deposition of oppositely-charged, cross-linked worms onto a planar surface *via* a L-b-L protocol was demonstrated in Chapter 5. These worms mimic the rigid rod behaviour of polyelectrolyte chains in salt-free solutions.[26] The worms adsorb onto the silicon wafers and at a remarkably rapid rate, with a constant surface coverage (for the first layer) observed within 20 seconds. The dimensions of these worms enable their direct visualisation *via* electron microscopy, unlike the soluble polyelectrolyte chains. On the other hand, it is virtually impossible to distinguish between cationic and anionic worms due to their similar dimensions Surface zeta potential measurements confirmed charge reversal after deposition of each new worm layer. The build-up of worm multilayers was confirmed by both SEM and ellipsometry studies but two regimes were observed which maybe the result of surface roughness effects for these relatively large rigid worms. In principle, the L-b-L deposition of other particle morphologies onto planar surfaces should be straightforward. It would be worth investigating whether charged spherical spheres or vesicles exhibit similar deposition rates and surface coverages compared to these polyelectrolytic worms. Furthermore, hybrid multilayers of worms with spheres or vesicles could also be prepared.

6.1 References

1. J.-S. Wang and K. Matyjaszewski, *Journal of the American Chemical Society*, 1995, **117**, 5614.
2. M. Kato, M. Kamigaito, M. Sawamoto and T. Higashimura, *Macromolecules*, 1995, **28**, 1721.
3. J. Chiefari, Y. K. Chong, F. Ercole, J. Krstina, J. Jeffery, T. P. T. Le, R. T. A. Mayadunne, G. F. Meijs, C. L. Moad, G. Moad, E. Rizzardo and S. H. Thang, *Macromolecules*, 1998, **31**, 5559.
4. N. J. Warren and S. P. Armes, *Journal of the American Chemical Society*, 2014, **136**, 10174.
5. M. J. Derry, L. A. Fielding and S. P. Armes, *Progress in Polymer Science*, 2016, **52**, 1.
6. S. L. Canning, G. N. Smith and S. P. Armes, *Macromolecules*, 2016, **49**, 1985.
7. Y. Pei, A. B. Lowe and P. J. Roth, *Macromolecular Rapid Communications*, 2017, **38**, 1600528.

8. A. Blanazs, R. Verber, O. O. Mykhaylyk, A. J. Ryan, J. Z. Heath, C. W. Douglas and S. P. Armes, *Journal of the American Chemical Society*, 2012, **134**, 9741.
9. I. Canton, N. J. Warren, A. Chahal, K. Amps, A. Wood, R. Weightman, E. Wang, H. Moore and S. P. Armes, *ACS Central Science*, 2016, **2**, 65.
10. D. E. Mitchell, J. R. Lovett, S. P. Armes and M. I. Gibson, *Angewandte Chemie International Edition*, 2016, **55**, 2801.
11. J. R. Lovett, N. J. Warren, L. P. D. Ratcliffe, M. K. Kocik and S. P. Armes, *Angewandte Chemie International Edition*, 2015, **54**, 1279.
12. J. R. Lovett, N. J. Warren, S. P. Armes, M. J. Smallridge and R. B. Cracknell, *Macromolecules*, 2016, **49**, 1016.
13. C. J. Mable, M. J. Derry, K. L. Thompson, L. A. Fielding, O. O. Mykhaylyk and S. P. Armes, *Macromolecules*, 2017, **50**, 4465.
14. C. J. Mable, R. R. Gibson, S. Prevost, B. E. McKenzie, O. O. Mykhaylyk and S. P. Armes, *Journal of the American Chemical Society*, 2015, **137**, 16098.
15. R. Deng, M. J. Derry, C. J. Mable, Y. Ning and S. P. Armes, *Journal of the American Chemical Society*, 2017, **139**, 7616.
16. M. Semsarilar, V. Ladmiral, A. Blanazs and S. P. Armes, *Langmuir*, 2012, **28**, 914.
17. M. Semsarilar, V. Ladmiral, A. Blanazs and S. P. Armes, *Langmuir*, 2013, **29**, 7416.
18. J. R. Lovett, L. P. D. Ratcliffe, N. J. Warren, S. P. Armes and B. R. Saunders, *Macromolecules*, 2016, **49**, 2928.
19. V. J. Cunningham, A. M. Alswieleh, K. L. Thompson, M. Williams, G. J. Leggett, S. P. Armes and O. M. Musa, *Macromolecules*, 2014, **47**, 5613.
20. X. Zhang, S. Boisse, W. Zhang, P. Beaunier, F. D'Agosto, J. Rieger and B. Charleux, *Macromolecules*, 2011, **44**, 4149.
21. S. Boisse, J. Rieger, K. Belal, A. Di-Cicco, P. Beaunier, M.-H. Li and B. Charleux, *Chemical Communications*, 2010, **46**, 1950.
22. S. Boisse, J. Rieger, G. Pembouong, P. Beaunier and B. Charleux, *Journal of Polymer Science Part A: Polymer Chemistry*, 2011, **49**, 3346.
23. A. A. Cockram, T. J. Neal, M. J. Derry, O. O. Mykhaylyk, N. S. J. Williams, M. W. Murray, S. N. Emmett and S. P. Armes, *Macromolecules*, 2017, **50**, 796.
24. K. L. Thompson, C. J. Mable, A. Cockram, N. J. Warren, V. J. Cunningham, E. R. Jones, R. Verber and S. P. Armes, *Soft Matter*, 2014, **10**, 8615.
25. S. Fujii, P. D. Iddon, A. J. Ryan and S. P. Armes, *Langmuir*, 2006, **22**, 7512.
26. C. Holm, M. Rehahn, W. Oppermann and M. Ballauff, *Advances in Polymer Science*, 2004, **166**, 1.